The enhancement of percutaneous absorption by nonionic surfactants

French, Edward James

Award date:
1991

Awarding institution:
University of Bath

THE ENHANCEMENT OF PERCUTANEOUS ABSORPTION BY NONIONIC SURFACTANTS

submitted by

Edward James French BSc

for the degree of Doctor of Philosophy

of the University of Bath

1991

This research has been carried out at the School of Pharmacy and Pharmacology of the University of Bath under the supervision of Dr C.W. Pouton

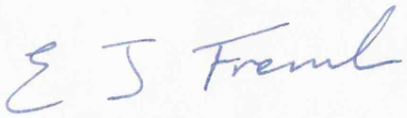

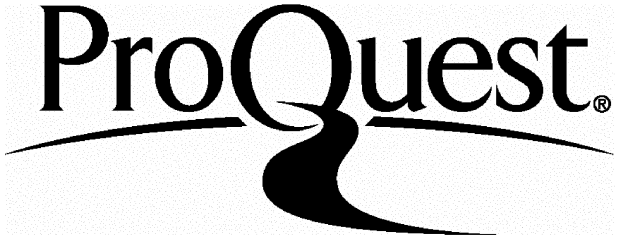

To My Parents

SUMMARY

The effect of a homologous series of pure dodecyl ether ethoxylate surfactants on the absorption of steroids through porcine skin has been determined. The effect of the same series of surfactants upon the fluidity of model lipid bilayers was investigated by a variety of physical techniques in an attempt to correlate lipid bilayer fluidity with skin penetration enhancement.

The introduction includes a review of the use of nonionic surfactants as enhancers of percutaneous absorption and of the proposed mechanisms of action of skin penetration enhancers. The experimental work is divided into four sections. In the first section the fluidisation of lipid bilayers was studied by differential scanning calorimetery (DSC). This work showed $C_{12}E_3$ to be the most potent fluidiser of lipid bilayers. This compound also reduced the lipid melting temperature in both extracted skin lipids and whole stratum corneum. In the second section using a variety of fluorescent membrane probes it was shown that molecules with low ethoxy content $C_{12}E_2$-$C_{12}E_4$ fluidised the lipid bilayer core whilst the more hydrophilic molecules $C_{12}E_5$-$C_{12}E_7$ fluidised the bilayer headgroup region. In the third section the more hydrophilic molecules were found to be the most potent fluidisers when studied by electron spin resonance spectroscopy. By use of this method lipid bilayer fluidisation by surfactants was also observed in whole stratum corneum. In the final section *in-vitro* skin permeation studies showed $C_{12}E_3$ to be the most potent penetration enhancer for both polar and nonpolar steroids. The more hydrophilic surfactants were relatively more potent enhancers for polar steroids.

The findings of these four experimental sections have been correlated and discussed in relation to mechanisms of permeation enhancement. The data suggests different modes of action for the enhancement of polar and nonpolar permeants and highlights the link between lipid bilayer fluidisation and penetration enhancement.

ACKNOWLEDGEMENTS

I would like to express my deepest gratitude to Dr. Colin Pouton for the guidance and encouragement he has given throughout this work.

I would like to thank my industrial supervisor Dr. Gerry Steele of Fisons Pharmaceuticals plc for his input into this project. Thanks must by made to various people who have aided me with technical aspects of this work, notably, Mike Walker for his demonstration of skin permeation experiments and Kevin Smith for running the GC-MS analyses. The help given to me by Megan Hughes-Jones in typing this thesis is greatly appreciated. I would like to all thank my collegues and friends in the School of Pharmacy and Pharmacology for the support they have given me over the last four years and also Helen for her warmth and constant encouragement.

The financial aid of the S.E.R.C. and Fisons Pharmaceuticals plc over the first two years of this work is greatfully acknowledged.

TABLE OF CONTENTS

CHAPTER 1

INTRODUCTION

1.1 Transdermal Drug Delivery

The skin has become recognised as a feasible and important route for the delivery of systemically acting drugs. There are many potential advantages of transdermal drug delivery over oral dosing, especially if the drug is administered from a transdermal drug delivery system (TDS) which controls the rate of delivery (1).

A number of TDS systems are already marketed for the delivery of nitroglycerin (Deponit^{R}), oestradiol (Estraderm^{R}), Scopolomine (Transderm^{R}-Scop) and Clonidine (Catapres-TTS^{R}). These systems are in the form of small adhesive patches. The effective rate of drug delivery from these systems is however not controlled by the TDS but by the rate of percutaneous absorption of the drug. This highlights one of the main problems associated with the transdermal route. The skin has a low permeability for most drug compounds, therefore the transdermal route can at present only be used for very potent drugs that have the right physiochemical characteristics for absorption through the skin. This limits the range of drugs at present suitable for these systems. For controlled transdermal delivery of drugs the permeability of the skin for the drug needs to be higher than is needed for successful therapy; the rate of drug delivery can then be retarded by the TDS giving device controlled administration (2). Before discussing potential ways of achieving increased drug penetration through the skin a brief review will be given of the relevant aspects of skin structure and current views on the mechanisms of percutaneous absorption.

1.2 The Structure of Mammalian Skin

1.2.1 Skin Physiology

The skin is a multilayered organ which is highly complex in its nature. Macroscopically two distinct layers are apparent, the outer epidermis and the underlying dermis. Below the dermis lies the fatty subcutaneous tissue. The skin also contains various appendages such as hair follicles, sweat, sebaceous and eccrine

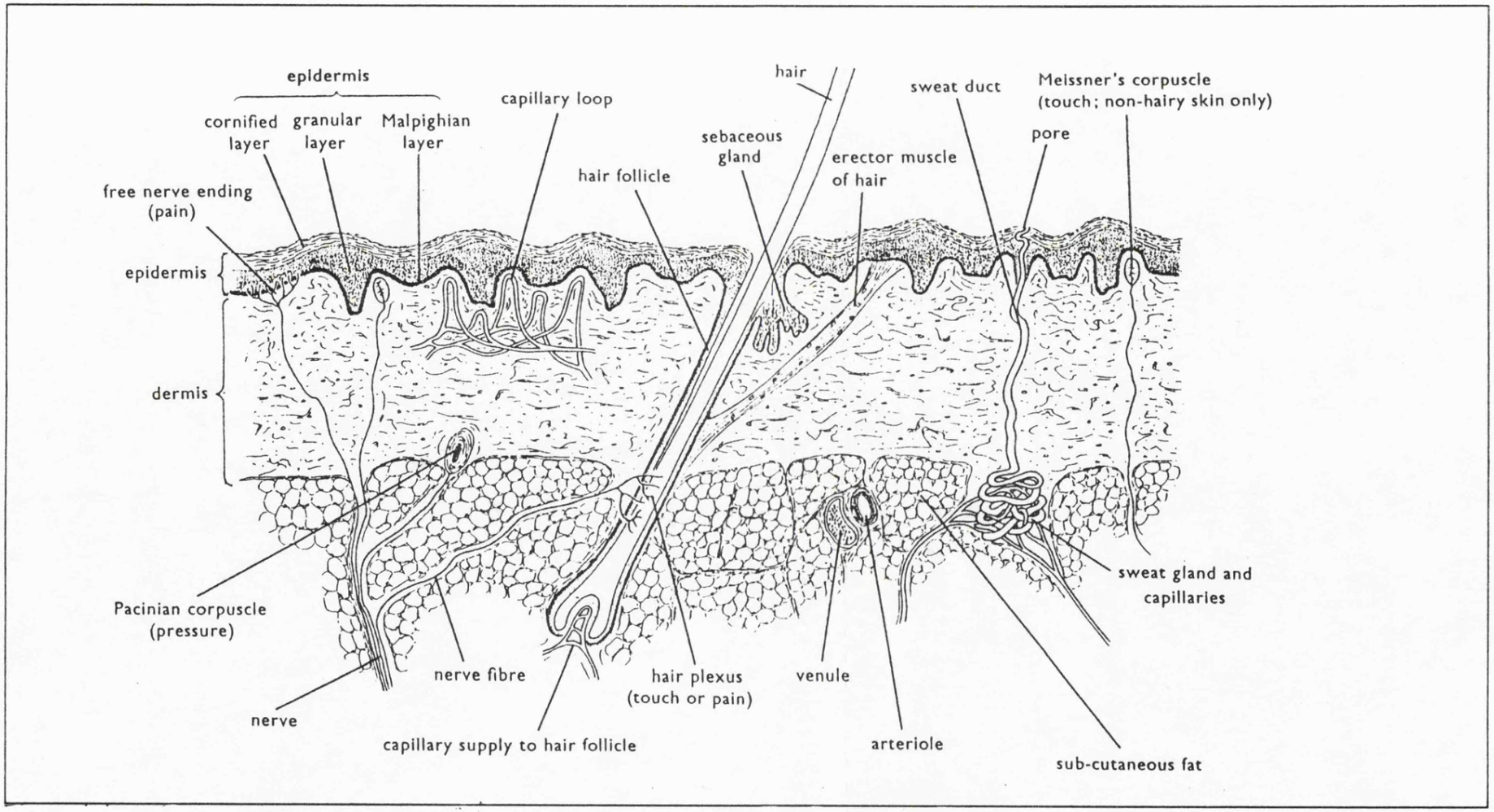

Figure 1.1 A diagramatic representation of the structure of mammalian skin in cross section

glands. The structure of mammalian skin is shown schematically in transverse section in Figure 1.1. The structure of the layers of the skin will now be described in more detail.

The dermis is approximately 3 to 5mm thick and so makes up the bulk of the skin (3). It consists of a matrix of connective tissue of fibrous proteins such as collagen and elastin. This network is embedded in an amorphous ground substance of which mucopolysaccharide makes up approximately 20% of the mass (4). These structural aspects makes the dermis very hydrophilic. The dermis contains the skin's blood supply, nerves and lymphatic systems. The vascular capillary network extends to just below the epidermis and provides a large surface area for exchange of materials between local tissue and the blood (5).

The epidermis is structurally far more complex than the underlying dermis and can itself be split into several layers. The epidermis can range between 0.06 - 0.8mm in thickness depending upon the body site and species (6). Functionally the epidermis comprises of the viable epidermis and the dead horny layer, the stratum corneum. The viable epidermis undergoes continuous differentiation as the cells rise to the skin surface. The cells change from metabolically active dividing cells in the stratum germivation, which is closest to the dermis, into flattened, dead, keratinized cells of the outermost layer the stratum corneum (7).

1.2.2 The Stratum Corneum

The stratum corneum is a highly specialized structure. It consists of layers of organised, flattened, keratinized dead cells. Over most areas of the body there are approximately 10-15 layers of such cells (8) producing an average thickness of about 10μm. These cells are embedded in a continuous matrix of multilamellar, extracellular, lipid bilayers, the structure and composition of which is unique to the stratum corneum (9,10). In recent years these lipids have been extensively studied and characterised. These investigations have shown that the stratum corneum lipids consist mainly of nonpolar lipid species of which up to 50% are ceramides. The

other lipid classes identified as major components in these studies were cholesterol, free fatty acids, triglycerides and cholesterol sulphate (11-15). A high proportion of ceramides and free fatty acids have been shown to contain long unsaturated acyl chains up to C_{30} in length (14,15). These lipids form broad bilayers which have a high degree of crystallinity in their structure (16,17).

1.2.3 The Barrier Function of Skin

It has long been known that the skin's various layers were not equally permeable (18). Through a series of initiative deductions from observations of diseased and damaged skin and elegant biophysical experiments it was deduced that the main barrier to the permeability of the skin lay in the stratum corneum (18,19). The stratum corneum is not uniform throughout its depth. It has therefore been suggested that the lowest regions of the stratum corneum known as the stratum lucidium or compactum may be the greatest barrier to permeation by polar molecules (20). It has further more been shown that the key to this impermeability of the stratum corneum is the intercellular lipid lamellae. As described above (1.2.2) these are present as broad crystalline bilayers of saturated lipids which provide a good barrier to diffusion (21-23).

1.3 Percutaneous Absorption

1.3.1 Routes of Penetration

When a penetrant molecule comes into contact with the skin it has two potential routes of penetration across the barrier layer. One is by the transappendageal route, that is down sweat ducts or hair follicles. The second route is by penetrating through the continuous stratum corneum. The transappendageal route has become known as the "shunt" diffusion pathway and is considered comparatively unimportant due to the relatively low surface area occupied by the structures involved (24). An exception to this is the diffusion of large polar molecules where this may be the only route available. Two pathways have been

proposed for the diffusion of molecules through the stratum corneum, the transcellular and the intercellular routes (24). These are shown on the schematic of the stratum corneum in Figure 1.2. It was suggested by Scheuplein and Blank (18) that as the lipid channels provide only a small fraction of the total volume of the stratum corneum most of the diffusion would be transcellular. More recent evidence has however shown that the intercellular channels may be far larger than first thought and epidermal lipid composition greatly affects permeation rates (25), thus implicating the intercellular route as a major pathway across the stratum corneum. By use of electron microscopy combined with autoradiography the permeation of compounds through the stratum corneum has been visualised (26-28). In these studies it was found that the majority of the permeant compounds accumulated in the intercellular spaces suggesting percutaneous absorption occurs primarily through the intercellular channels. The authors proposed that lipid soluble molecules would pass down the centre of the lipid bilayers whilst hydrophillic molecules would diffuse along water channels present between the polar headgroups of the bilayers.

1.3.2 The Kinetics of Percutaneous Absorption

If it is assumed that the stratum corneum is the major barrier to penetration of the skin (see 1.2.3) and the viable epidermis and dermis act as a perfect sink for any permeant (29), then the rate of percutaneous absorption will be limited by the permeability of the stratum corneum. There has been no reported evidence for active transport of permeants across the stratum corneum, penetration is thought to occur by passive diffusion. The permeation of drug molecules through the skin can be represented by Fick's first law of diffusion:-

$$J = \frac{DKc}{h} \qquad \text{Equation 1.1}$$

where J is the rate of transfer per unit area of membrane surface per unit time (the flux), h is the membrane thickness, c is the concentration of the drug applied to the

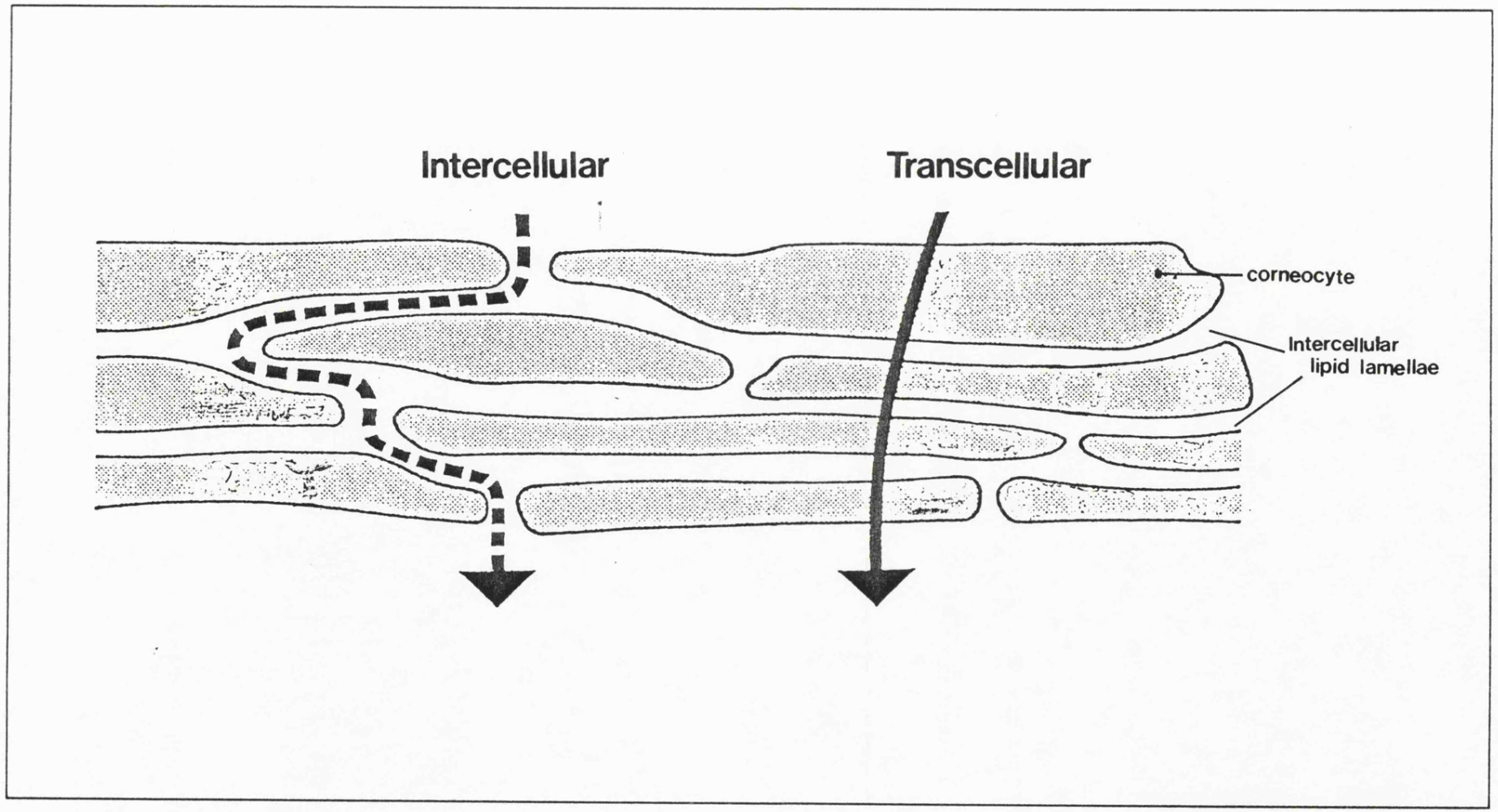

Figure 1.2 Possible pathways for the diffusion of a molecule through the stratum corneum.

skin, K is the membrane/vehicle partition coefficient and D is the diffusion coefficient of the drug in the membrane. From this equation it can be seen that the rate of flux can be increased by decreasing the thickness of the barrier layer or increasing either the concentration, the diffusion coefficient or the membrane/vehicle partition coefficient.

Commonly in studies of percutaneous absorption the cumulative amount of drug permeating the skin per unit area of membrane, M, is plotted as a function of time. These are known as Barrer plots. From the linear portion of this plot pseudosteady state flux values and rate constants can be obtained. A typical Barrer plot is shown for simple zero order flux in Figure 1.3. The lag time (3), may be obtained by extrapolation of the linear portion of the graph to the time axis.

1.4 Methods of studying Percutaneous Absorption

1.4.1 *In-Vivo* Techniques

In order to truly assess the percutaneous absorption of a drug into a living animal the permeation of that compound should ideally be determined in that species. However, particularly with man this approach is often fraught with experimental and ethical difficulties.

There are several methods of studying percutaneous absorption *in-vivo*. One commonly used approach is to use an indirect method by measuring radioactivity in excreta following topical application of the labelled compounds. This technique has been used by Feldmann and Maibach (30,31) to study the percutaneous penetration of radiolabelled compounds in man. In these studies the total radioactivity excreted in the urine was measured. This method has the problem that the drug may be metabolised in crossing the viable tissues. The body's organs may bind or store much of the absorbed drug and there are other routes of excretion. In order to try to correct for this the authors determined the amount of radioactivity excreted in the urine following parenteral administration of a bolus of drug. Even with this correction the method has its limitations and the interpretation of this type of data

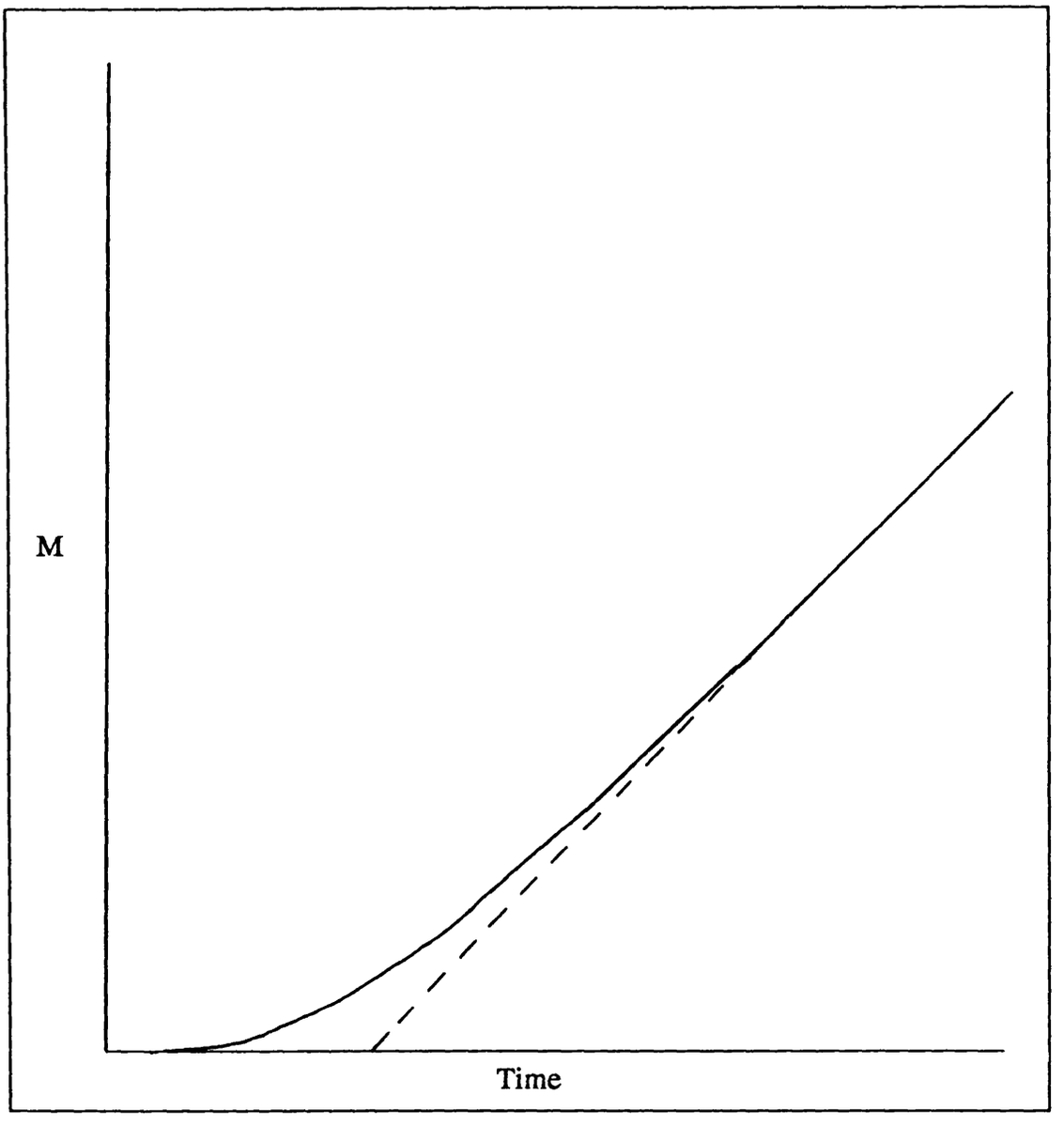

Figure 1.3 A Barrer plot for the diffusion of drug through the stratum corneum. M is the cumulative mass of drug that has permeated the skin per unit area.

should be made carefully. The indirect method described above has also been used in many animal studies of percutaneous absorption (32,33). In these experiments measurements of both CO_2 and fecal excretion can be obtained by use of a metabolic cage.

Another method of analysis of percutaneously absorbed substances is the determination of plasma concentration of the drug over a period of time. The area under the curve can be used as a measure of the amount of drug absorbed. This again can be carried out using radiolabelled drugs or substances that are easily assayed using chromatographic techniques. This method again suffers with problems due to drug metabolism and storage of the drug by the organs in the body.

An alternative approach in determining *in-vivo* percutaneous absorption is the surface recovery method. In this technique a drug dose is applied as a formulation and after a period of time the amount remaining on the skin surface is determined. It is assumed that the difference between the amount of drug applied and the amount recovered is the amount absorbed. This method has a problem in the fact that you can never be sure all the drug has been recovered. Also, drug may partition into the stratum corneum but may never be systemically absorbed, remaining in the corneum until it is sloughed off. This drug would not be accounted for by the surface recovery method leading to an over estimation of drug absorption.

The use of the biological or pharmacological response produced by the drug is another way of estimating the extent of percutaneous absorption. A good example of this is the vasoconstrictor test for steroids. Application of many steroids to the skin induce vacoconstriction of the superficial arteries and so causes blanching of the skin. This effect has been used as an assay for topical steroids since the early 1960's (34). This test has since been updated and standardised (3). However, in many cases it is still based on a subjective assessment of degree of palor of the skin by eye, which may lead to large variation between investigations.

1.4.2 *In-vitro* Techniques

In-vivo studies would be expected to produce the best clinically relevant data, however *in-vivo* studies are expensive, suffer from ethical problems and can not be used to provide percutaneous absorption data for highly toxic compounds. With these aspects in mind many studies of percutaneous absorption are carried out *in-vitro* on excised human or animal skin.

The basis of *in-vitro* absorption studies is that the major barrier layer of the skin lies primarily in the stratum corneum. As this is composed of nonliving tissue and diffusion through it is a passive process (see 1.2.3 and 1.3.2) the rate of absorption *in-vivo* and *in-vitro* should be the same over a short time course before the excised skin decays. *In-vitro* studies are very simple compared with *in-vivo* work. They can therefore be carried out with less effort and in a greater number than *in-vivo* experiments, so are popular with many investigators.

Early *in-vitro* studies involved vertically mounted two chamber diffusion cells in which drug was applied in solution on one side of the membrane and the same solvent minus drug placed on the other side of the membrane (35). This technique however causes excessive hydration of the skin. The vertical cell has now largely been replaced by a horizontal cell with receptor fluid below the skin and the upper chamber (above the stratum corneum surface) left open to ambient conditions. These cells can be either static cells as described by Franz (36) or of a flow-through design (37).

In all *in-vitro* experiments care must be taken with drugs of low aqueous solubility. Lipophilic drugs may not partition from the stratum corneum into the aqueous viable epidermis or dermis. *In-vivo* the drug would be cleared from this site by the circulation. Also, if the drug has a higher solubility in the skin than the receptor phase then it will be unfavourable for the drug to partition into the receptor fluid. In both of these situations an artificial barrier will be created, the permeant will not be detected and a low estimate of percutaneous absorption will be obtained. The permeation rate *in-vitro* can thus be greatly affected by the receptor fluid

especially for lipophilic compounds (38-40). Sink conditions must be available for the penetrating drug without the barrier properties of the skin being affected.

1.4.3 Animal Models for Human Skin

It is not always possible to obtain a reliable source of consistent human skin to carry out large numbers of permeability experiments which would be needed for structure activity studies. To get around this problem various animal models have been used in both *in-vivo* and *in-vitro* studies. Commonly the data from these studies are extrapolated to the human case. However, the validity of these extrapolations will depend upon the animal species used. There have been several studies carried out which compare the permeability of various animal skins to that of human skin. These have been carried out both *in-vivo* and *in-vitro*.

Bartek *et al* (41) compared the permeability of rat, rabbit, pig and human skins to six radiolabelled compounds *in-vivo*. The authors found that the permeability of the skin decreased in the following order, rabbit, rat, pig and man. The skin of the miniature swine had by far the closest permeability to that of human skin. Bronaugh *et al* (42) compared the percutaneous absorption of several substances through selected animal skins to that through human skin using an *in-vitro* technique. The relative permeability of the skins examined was dependent upon the permeant. For all compounds pig skin was observed as a better model for human skin. Similarly Marzulli *et al* (43) found that the skin of the weanling pig had the closest permeability to human amongst a range of common laboratory animals including chimpanzee and monkey to a series of chemical warfare agents. In a review of these studies Wester and Maibach (44) concluded that the animals most predictive of percutaneous absorption in man are the monkey and the pig. *In-vitro* studies (45,46) show whole rat skin to be a good model for human skin with polar molecules but not for lipophilic substances. This has been put down to the dermis acting as an artificial barrier to absorption. The use of epidermal membranes was suggested as a way around this. In a more recent study by the

same group porcine epidermal membranes were considered to be a better model for human skin (47).

1.4.3.2 Porcine Skin as a Model for Human Skin

In many of the studies cited in the previous section it was shown that porcine skin was a relatively good model for human skin in terms of its permeability characteristics. There has also been evidence that suggests that porcine skin is structurally similar to human skin. Bronaugh *et al* (42) found that porcine and human skin have the same hair follicle density, whereas that of the rat was 26 times greater. Pig skin was however, measured as having a stratum corneum 15 times thicker than man.

The barrier properties of the skin have been shown to be associated with the intercellular lipids of the stratum corneum (see 1.2.3). In particular the long acyl chain ceramides are implicated in the barrier function. Detailed analysis of these lipids from both human and porcine skin have shown that the glycosphingolipids and ceramides present in the stratum corneum of both species are very similar in structure and composition (48). It has recently been shown using a small angle x-ray scattering that the diffraction patterns obtained from the extracellular lipid lamellae of human and porcine stratum corneum are very similar, demonstrating good structural parity, whilst those from mouse skin are different (49).

1.5 Permeation Enhancement

1.5.1 Penetration Enhancers

At the start of this chapter it was stated that percutaneous absorption is hampered as a means of drug delivery by the impermeability of the skin, in particular the stratum corneum. One approach to overcome this and open up the route for the delivery of many drugs is to employ the use of chemical penetration enhancers. These can be defined as molecules which partition into the stratum corneum and interact with its constituents decreasing the resistance of the skin to

percutaneous absorption. The ideal characteristics of a penetration enhancer were listed by Barry (3). A condensed form of this list is given below. It is a very unlikely any single compound could have all of this spectrum of properties.

Ideal properties of a chemical penetration enhancer:

1. The enhancer should be pharmacologically and chemically inert.
2. The material should not be toxic, allergenic or irritating.
3. The onset of action of the enhancer should be immediate and reversible. The integrity of the skins barrier function being completely returned when the enhancer is removed.
4. The material should be a good solvent for drugs.
5. The material should be cosmetically acceptable.
6. The materials should be relatively cheap.

Many compounds have been investigated for permeation enhancing activity. There have also been compounds specifically synthesised for use as penetration enhancers. These compounds can be seen to fall into one or both of two categories, the solvents and the surfactants. There are a few compounds such as urea which do not fall into either of these groups. Before looking at these compounds and their effectiveness a brief review will be given of the current theories of the mechanisms of action of chemical penetration enhancers.

1.5.2 Mechanisms of Action of Penetration Enhancers.

Although there have been many studies involving chemical penetration enhancers their exact mechanisms of action are yet to be fully elucidated. The different types of enhancer would be expected to have different modes of action upon the skin, this is also likely to vary from drug to drug. A brief review will be given of some of the current theories of permeation enhancement i.e. how enhancers affect the stratum corneum and it's permeability.

The permeation of a compound through the skin can be described mathematically by Ficks 1st Law of Diffusion (see 1.3.2). Looking at this equation it can be seen that there are two possible ways in which enhancers can act in the skin to increase drug flux. If the enhancer is a good solvent for the drug when it penetrates into the skin it may act as a cosolvent for the permeant in the skin. This will increase the stratum corneum: vehicle partition coefficient for the drug and thus increase the flux through the skin. The other way enhancers may act is to decrease the resistance in the barrier layer to diffusion of the drug. This will increase the diffusion coefficient of the permeant and hence its rate of absorption.

The highly structured, intercellular lipid lamellae are known to play a major role in the barrier function of the stratum corneum (1.2.3). By the use of differential scanning calorimetry (DSC) and Fourier transform infrared spectroscopy (FTIR) increases in skin permeation rates have been correlated to increased lipid fluidity in the stratum corneum (50-53). Fluidisation of the lipids apparently decreases the diffusional resistance of the membranes. This is the suggested major mechanism of action of many known penetration enhancers such as Azone, oleic acid and decamethyl sulphoxide (DCMS) which are thought to penetrate into the lipid bilayers, disrupt their packing and so increase lipid fluidity (50). This action would be expected to increase the permeation of hydrophobic compounds, but will also affect polar penetrants which at sometime in their passage through the stratum corneum will have to cross lipid bilayers (28).

Polar drugs are suspected as permeating the stratum corneum principly via aqueous regions between the lipid bilayer headgroups (see 1.3.1). Hydration of the skin would swell these areas and allow increased flux of drug along these channels. Enhancers may also act in these regions by increasing hydration disrupting the packing of bound water in the hydration spheres around the lipid headgroups, or replacing this water. This would allow increased diffusion of polar permeants (28).

Many enhancers such as DCMS and sodium lauryl sulphate and urea may interact with the keratin of the stratum corneum allowing increased permeation through or around the corneocytes and reducing possible drug binding sites (54). Many compounds will also have effects in the topical vehicle increasing the thermodynamic activity or the bioavailability of the drug, thereby increasing permeation rates. Although this is observed as penetration enhancement there is no action on the skin and so does not fit the criteria as defined in 1.5.1. It is thought that most enhancers will act by a combination of the above suggested mechanisms.

1.5.3 Solvents as Penetration Enhancers

There are many compounds that have been investigated for penetration enhancing activity that can be regarded as solvents. Water is the most simple of these compounds and one which complies with many of the criteria stated above (see 1.5.1). Hydration of the stratum corneum, usually achieved by occlusion of the skin surface, generally causes a large increase in the permeability of the skin. These effects have been demonstrated for many permeants, both *in-vivo* (55) and *in-vitro* (56). Lipid removing solvents such as chloroform: methanol mixtures and hexane cause dramatic increases in skin permeability but these effects are irreversible and inflict damage upon the skin (57). These cannot be seen to be suitable for use as penetration enhancers. Dimethyl sulphoxide (DMSO) has been known for many years to increase the percutaneous absorption of various chemicals in a reversible fashion (3). It is unlikely however, that a clinical application will be found for DMSO due to potential toxicological problems. Other solvents used as enhancers include ethanol (53) and propylene glycol which is known to enhance the permeation of steroids (58). Propylene glycol also displays a synergistic action when used with other penetration enhancers such as 1-dodecyl azacycloheptan-2-one, Azone (59).

1.5.4 Surfactants as Penetration Enhancers

1.5.4.1 Classification of Surfactants

Molecules which have an amphipathic nature, i.e. they possess both hydrophilic and hydrophobic groups, will often display surface activity. The hydrophobic portion of surfactants usually consists of alkyl or acyl chains. The hydrophilic 'head' group may be charged or uncharged. The classification of surfactants into three major groups is based upon the charge of the headgroup. Thus, surfactants can be anionic (e.g. sodium dodecyl sulphate), cationic (e.g. cetyltriacetyl ammonium bromide) or nonionic, where the polar headgroup is normally a polyoxyethylene chain (e.g., nonylphenol ether polyethoxylate).

1.5.4.2 Ionic Surfactants as Penetration Enhancers

A number of anionic and cationic surfactants have been shown to act as enhancers of percutaneous absorption (60). The activity of these surfactants may be due to their ability to interact with and possibly extract the skin lipids. Anionic surfactants are also known to interact strongly with the protein in the stratum corneum. However, both anionic and cationic surfactants are unlikely to find a use in transdermal drug delivery as enhancers of permeation as both are reputed as having irritation potential (61).

1.5.4.3 Nonionic Surfactants as Penetration Enhancers

1.5.4.3.1 Structure of Nonionic Surfactants

Nonionic surfactants are known to be the least irritating to the skin of the three classes of surfactant and as such, have the greatest potential for use as enhancers. Although there are many types of nonionic surfactants the majority of studies has been limited to four principle series. These are the polysorbates, esters or partial esters of sorbitol condensed to ethylene oxide chains; polyoxyethylene alkyl ethers and esters, polyoxyethylene alkylphenols and poloxamers

(polyoxyethylene polyoxypropylene copolymers). The generalised structues of each of these types of surfactants are given in Figure 1.4.

1.5.4.3.2 The Effect of Nonionic Surfactants on Percutaneous Absorption

In order to exert an effect in the skin the surfactant must first itself penetrate into the stratum corneum. The rate of penetration of polyoxyethylene surfactants into the skin is generally quite low, although some possess a greater intrinsic rate of permeation than their anionic counterparts (62). There are many variables which will affect the extent of permeation of the surfactant and hence its potency as an enhancer. The vehicle used to deliver the drug and enhancer to the skin surface will affect the partitioning behaviour of the enhancer and possibly the physical characteristics of the skin. The degree of enhancing activity is also strongly dependent upon the surfactant structure and concentration (60,63). Therefore, attempts to correlate data from different sources proves to be very difficult with each investigator using different systems and a variety of different anatomical sites of application and animal species (11,44). Surfactants have been shown to enhance, retard or have no effect upon skin permeability. This is dependent upon how they are used and in what concentration (60).

The polysorbates have been shown to increase percutaneous absorption in several studies. Polysorbates 20, 40, 60 and 80, when present in low concentrations $<0.5\%$ $^{v}/_{v}$ caused increased flux of both hydrocortisone and lidocaine through hairless mouse skin from a propan-2-ol/H_2O vehicle (64-66). When used in conjugation with propylene glycol (PG) the extent of enhancement was increased significantly suggesting some synergism between the PG and the surfactants. Polysorbates have been shown to increase the permeation of salicylic acid, sodium salicylate and flufenamic acid through rabbit skin, *in-vivo* from white petroleum bases containing 5 or 10% DMSO (67,68), as with PG, some synergism was observed between DMSO and the surfactant. Polysorbate 80 increased the permeation of chloramphenicol through hairless mouse skin (69), whilst Mezei and

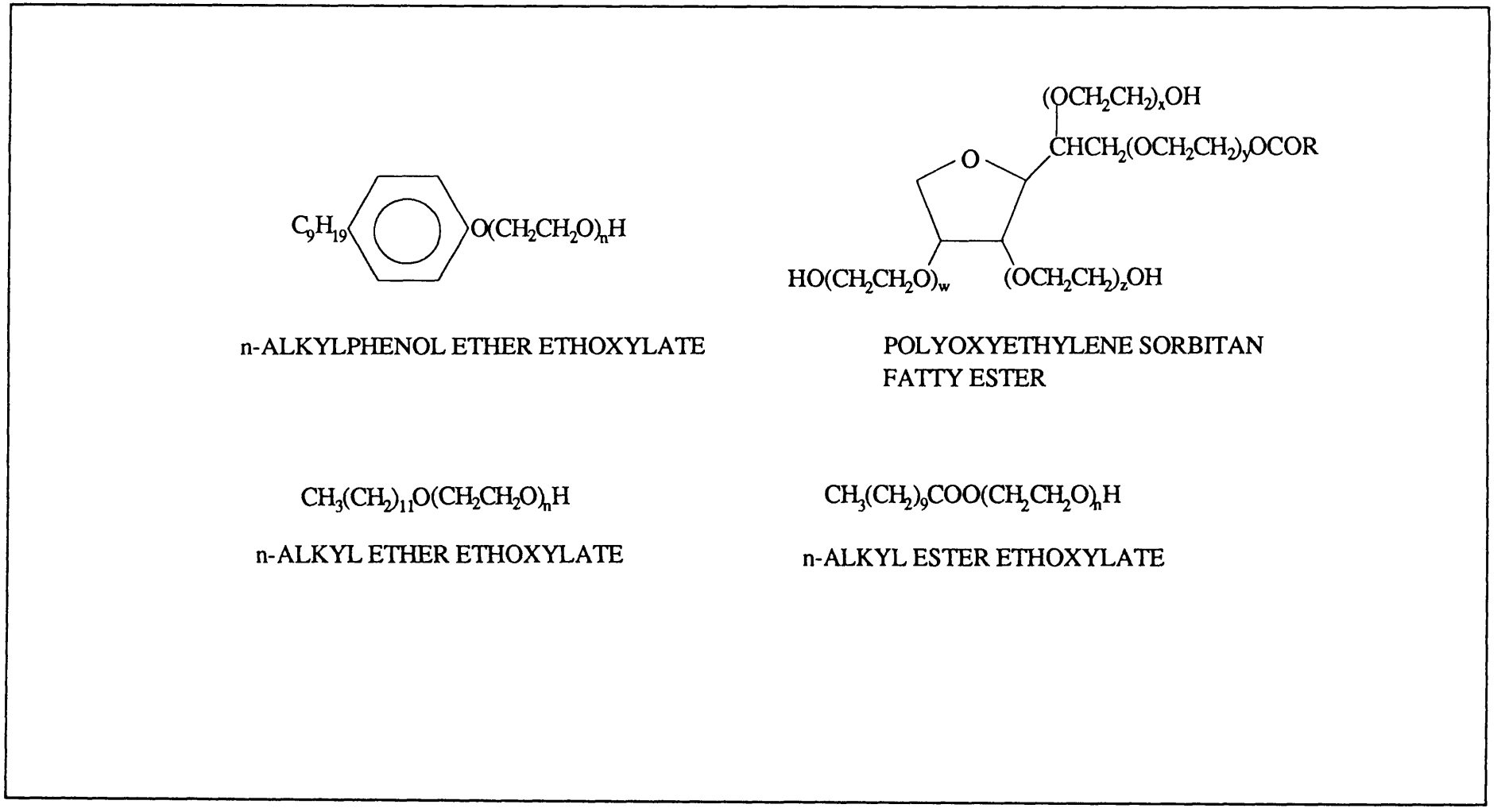

Figure 1.4 Chemical structures of a range of nonionic surfactants investigated as potential pentration enhancers

Ryan (70) observed that polysorbate 85 increased the transepidermal water loss from excised rabbit skin. All these studies show the polysorbates affect the skin's barrier layer, however, polysorbate 20 had no effect on the absorption of naloxone through human skin (71) and similarly polysorbate 60 had little effect on the permeation of naproxen through rat, rabbit or human skin (72). From these studies it was not possible to form any definite quantitative structure-activity relationships for the polysorbates as permeation enhancers.

Polyoxyethylene aryl ethers are known to have potent membrane disrupting activity and are widely used as solubilising agents for membrane bound enzymes (73). Despite this there is little evidence to show these surfactants will act as enhancers of percutaneous absorption. Walters *et al* (74) found that the rate of skin permeation of methyl nicotinate across mouse skin was unaltered by both octyl and nonylphenol decaethoxylates. The aryl ethers can also retard the percutaneous absorption of compounds. Dalvi and Zatz (75) observed that micellar concentrations of nonylphenol pentadecaethoxylate considerably reduced the permeation of benzocaine through hairless mouse skin. It has been reported elsewhere that the damage potential upon the skin from anionic surfactants is reduced by the presence of long ethoxy chain acyl ethers (76). The nonionic surfactant presumably reduces the absorption of the ionic surfactant.

As with the other classes of surfactants there are conflicting reports about the poloxamers. Members of the poloxamer series had little effect on the flux of naloxone through human cadaver skin *in-vitro* (71). However, poloaxamers 231 and 182 significantly increased the flux of salicylic acid and sodium salicylate through rabbit skin (67).

Polyoxyethylene alkyl ethers and esters have been shown to enhance the percutaneous absorption of many compounds and appear to be the most potent enhancers amongst the nonionic surfactant classes. The efficacy of these surfactants was very structure dependent and several structure activity studies have been carried out. Walters *et al* (74,77) studied the effect of a wide range of alkyl ether

ethoxylates, which varied in both alkyl and ethylene oxide chain lengths, upon the permeation of methyl nicotinate through hairless mouse skin in two chambered diffusion cells. They found that the surfactants with a linear alkyl chain length greater than C_8 and ethoxy chain length of less than E_{14} significantly increased the permeation of methyl nicotinate. Maximum enhancement was achieved with Brij 36T ($C_{12}E_{10}$) followed by Brij 96 ($C_{18}{=}E_{10}$), Brij 56 ($C_{16}E_{10}$) and Brij 52 ($C_{16}E_6$). The effectiveness of Brij 36T as an enhancer upon the permeation of both hexyl and methyl nicotinate has been noted by other investigators (78,79). In a study of the effects of fifteen nonionics on the permeation of sodium salicylate and salicylic acid through rabbit skin *in-vitro* significant enhancement was obtained with Brij 30 ($C_{12}E_4$) and $C_{18}{=}E_2$ (63). $C_{18}E_2$ was also shown to be a good enhancer for flufenamic acid in the same test conditions (68). The flux of naloxone was enhanced by lauryl alcohol ($C_{12}E_0$), and $C_{12}E_4$ but $C_{12}E_{20}$ had little effect (71). Also in this latter study it was observed that the dodecyl (C_{12}) chain was often the optimum alkyl chain length for enhancement with both nonionic and ionic surfactants. Other work showed $C_{18}{=}E_5$ to enhance the permeation of nitroglycerin (80) and that $C_{12}E_2$ enhanced the flux of both theophylline and adenosine *in-vitro* (81). As discussed earlier it is difficult to correlate these data due to differences in experimental procedures between studies.

Azone was synthesized for use as a permeation enhancer. It can be regarded as a fairly lipophilic nonionic surfactant. Azone is reported as having very good enhancing activity with a number of compounds such as narcotic analgesics (82), 5-flurouracil (83) and anxiolytics (84).

1.5.4.2.3 The Effect of Nonionic Surfactants on other Biological Membranes

The skin can be regarded as a very complex biological membrane. If it is assumed that the barrier function of the skin is related to the structuring of the intercellular lipid bilayers then the effects that compounds have on other natural or synthetic lipid bilayers may indicate their potential as skin permeation enhancers.

Nonionic surfactants are known to interact strongly with membranes and several structure-activity studies have been undertaken to find the optimum physiochemical characteristics for surfactant membrane activity. In a study upon the mobility of the protozoan *Tetrahymena elliotti*, Baillie *et al* (85) observed that with octyl and nonylphenol based surfactants, as the ethoxy chain length increased the surfactant potency upon the membrane decreased. A similar observation was made for the alkyl ether ethoxylates where the most potent effects amongst all the surfactants studied were seen with $C_{12}E_4$. The polysorbates investigated were far less effective. Structure-activity relationships similar to those described above for the alkylphenol ether ethoxylates were obtained with similar surfactants by Gadd and Curtis-Prior (86) working on spermatozoon membranes and Levin (87) who studied effects on rat vaginal membranes.

In a review of the interactions of alkyl and aryl polyoxyethylene ethers Florence *et al* (63) concluded that optimum biological activity was often obtained with a C_{12} hydrocarbon chain. The ability of this chain to penetrate membranes and the depth of penetration will be affected by the ethoxy chain length. For many of the investigations reviewed an ethoxy chain length $< E_{12}$ gave the most active surfactant.

1.6 Objectives of this Work

A quantitative structure-activity study will be made of the membrane fluidising activity of a homogogous series of pure dodecyl ether ethoxylates $C_{12}E_0$-$C_{12}E_8$. These surfactants are all of single ethoxy chain length and so differ from the polydisperse surfactants used in many other studies of this type. Distearoylphosphatidylcholine (DSPC) liposomes contain bilayers of structured lipid. These will be used as a simple model of the intercellular lipid lamellae of the stratum corneum in order to investigate bilayer fluidisation by the nonionic surfactants. Physical changes in the bilayers will be quantitatively assessed by differential scanning calorimetry (DSC), fluorescence polarisation spectroscopy (FPS) and electron spin resonance (ESR). The effects of the surfactants upon

extracted skin lipids and whole stratum corneum will be made using DSC and ESR. Finally, penetration enhancement studies on the permeation of both polar and nonpolar steroids through porcine skin *in-vitro* will be carried out using the same series of surfactants. Attempts will be made to correlate the permeation data to the physical fluidisation studies. This will hopefully lead to further insight into the mechanisms of permeation enhancement by nonionic surfactants.

CHAPTER 2

MATERIALS

2.1 Acquisition and Storage of Porcine and Human Skin

Whole porcine ears were obtained from a local abatoir within 15 minutes of slaughter. The ears were washed with copious cold tap water and blotted dry. The whole skin from the back of the ear was carefully dissected and peeled away from the ear cartilage. The skin was laid flat and the hair carefully shaved from the skin before rewashing the skin with cold tap water. The skin was blotted dry and pressed flat, stratum corneum uppermost onto aluminium foil. The samples were then sealed into plastic bags and stored frozen at -20°C until required.

Whole human cadaver abdominal skin was obtained from autopsy. Samples were from caucasian subjects in the age range 30-70 years old. Upon receipt of the samples the subcutaneous fat was removed by blunt dissection. The skin was then stored flat on aluminium foil at -20°C as described above.

2.2 Water and Buffers

2.2.1 Distilled Water

Distilled water used in experimental protocols and for the preparation of buffers was freshly distilled from an all glass apparatus.

2.2.2 Phosphates Buffered Saline (PBS) pH 7.4

Phosphate buffered saline pH 7.4 was prepared using the formula stated below. All buffer salts used were of reagent grade obtained from BDH chemicals Ltd (Poole, UK) and were used in their anhydrous form.

KH_2PO_4	1.36g
Na_2HPO_4	6.90g
NaCl	4.59g
Distilled water	to 1000ml

Prior to finally making up to volume the pH of the buffer was adjusted to exactly pH 7.4 with 0.02M NaOH.

2.2.3 Borate Buffer pH 8.8

Clark and Lubs (88) borate buffer was used in the ESR studies, the formula for which is given below:

Solution A 0.1M boric acid in 0.1M KCl

H_3BO_3	6.2g
KCl	7.46g
Distilled water	to 1000ml

Solution B 0.1N NaOH

Final Solution

Solution A	50ml
Solution B	to pH 8.8, approx 16.3ml.
Distilled water	to 100ml

2.3 Glassware

2.3.1 Standards and Suppliers

Whenever possible grade A volumetric flasks and glass pipettes were used. The 1.5 and 4.5ml vials used in many experiments were obtained from Chromacol (London, UK).

2.3.2 Cleaning of Glassware

The glass vials were supplied acid washed and so were used without further cleaning. For the physical measurements of lipid bilayer fluidisation by nonionic surfactants it was important to avoid contamination from other detergents. The glassware used was therefore routinely soaked in chromic acid for >4 hours, usually overnight, before being thoroughly rinsed with distilled water. At least 10

changes of distilled water were used. The glassware was then oven dried before use.

2.4 Nonionic Surfactants

Two types of nonionic surfactants were used in these studies, aryl ether ethoxylates based upon nonylphenol and alkyl ether ethoxylates based upon either decanol or dodecanol. All surfactants were used as supplied.

2.4.1 Nonylphenyl Ether Ethoxylates

The nonylphenyl ether ethoxylates used in this study were polydisperse, each surfactant contained a mixture of ethylene oxide chain lengths. These surfactants will be refered to as NPX, where X is the average number of ethylene oxide groups condensed to the nonylphenol moiety as stated by the manufacturer. The general surfactant structure is shown in Figure 1.4 In order to obtain a large range for a homologous series of these surfactants it was necessary to obtain samples from greater than one supplier. The supplier and the surfactant trade names are given in Table 2.1.

2.4.2 Alkyl Ether Ethoxylates

The alkyl ether ethoxylates used during this study were based on either decanol or dodecanol, these will be refered to as $C_{10}E_n$ or $C_{12}E_n$ respectively where n = the number of ethoxy groups condensed to the straight chain alcohol as stated by the supplier. For the Brij series surfactants n refers to an average ethoxy chain length. The general structure of these surfactants is shown in Figure 1.4.

The decyl ether ethoxylates $C_{10}E_3$-$C_{10}E_6$ and the dodecyl ether ethoxylates $C_{12}E_1$-$C_{12}E_8$ were obtained from the Nikkol Chemical Company (Tokyo, Japan) Dodecanol $C_{12}E_0$ was from BDH Chemicals Ltd (Poole, UK) and was stated as having 99% purity. Brij 30 nominally $C_{12}E_4$ was obtained from ICI Speciality Chemicals (Leatherhead, UK). One sample of Brij 36T ($C_{12}E_{10}$) was obtained from

Nominal Name	Trade Name	Supplier	Ethoxy Chain Length[a]
NPO	Nonylphenol	1	-
NP1	Ethylan NP1	2	1.33±0.2
NP2	Dowfax 9N2	3	1.98±0.15
NP4	a)Synperonic NP4 b)Dowfax 9N4	4 3	4.11±0.31 3.96±0.27
NP5	a)Synperonic NP5 b)Dowfax 9N5	4 3	5.07±0.18 4.96±0.26
NP6	a)Arkopal N060 b)Dowfax 9N6	5 3	5.47±0.42 6.00±0.23
NP7	Dowfax 9N7	3	7.10±0.31
NP8	Arkopal N-080	5	8.15±0.35
NP9	Ethylan BCP	2	9.23±0.48
NP10	a)Arkopal N-100 b)Dowfax 9N10	5 3	9.93±0.24 11.00±0.47
NP11	Arkopal N-110	5	10.88±0.24
NP12	Dowfax 9N12	3	12.97±0.38
NP15	Arkopal N-150	5	14.56±0.26

Table 2.1 Suppliers, trade names and calculated average ethoxy chain lengths of the nonylphenyl surfactants

[a] Determined by ^{1}H-NMR (mean±range, n=2)

Key to suppliers

1. Aldrich Chemical Company (Gillingham U.K.)
2. Lambro Chemical Company (Eccles, UK)
3. The Dow Chemical Company (Hounslow, UK)
4. CargoFleet Chemical Company Ltd (Stockton,UK)
5. Hoechst UK Ltd. (Hounslow, UK)

The Sigma Chemical Company (Poole, UK), the second sample was a gift from Fisons Pharmaceuticals (Loughborough, UK).

2.4.3 Methods of Analysis of Surfactants

To determine the chemical purity and the average ethoxy content of the polydisperse surfactants each sample was analysed by gas chromatography - mass spectrometry (GC-MS) and ^1H NMR. In addition to this the melting points of the Nikkol dodecyl ether ethoxylates were determined by differential scanning calorimetry (DSC).

2.4.3.1 Gas Chromatography - Mass Spectrometery (GC-MS)

The surfactants were dissolved in HPLC grade ethyl acetate to produce solutions of 1mg ml^{-1} concentration. These were run on a Hewlett Packard HP59970C gas chromatograph with mass selective detection using the following GC run parameters:

Column	HP1
Initial oven temperature	55°C
Time at Initial temperature	0.50min
Ramp rate	15°Cmin^{-1}
Final temperature	280°C
Time at final temperature	up to 30 min^{-1}
Injection volume	2μl

The GC chromatographs and mass spectrometer fractionation spectra were analysed on the Hewlett Packard software supplied. Where possible the library of stored spectra supplied with the software was used to identify components.

2.4.3.2 Proton NMR

The technique of analysis of polyethoxylated aryl and alkyl ether nonionic surfactants was adapted from methods used by other investigators (89-91). Samples of surfactant as 20-40 $^{w}/v$ solutions in $CDC1_3$ were analysed on a Jeol GX270 FT spectrometer operating at 270 MHz using tetramethylsilane (TMS) as an NMR reference point. The spectra and integrals obtained were an accumulation of 64 scans.

2.4.3.3. Determination of Melting Points by DSC

The principles of differential scanning calorimetry and techniques of analysis of DSC traces are described in Chapter 3 of this thesis. For the analysis of surfactants, 5mg sample of pure surfactant was accurately weighed into hermetically sealed DSC pans. The samples were then scanned over a standard heating run between -20 and 80°C at 5°C min^{-1} on a Dupont 910 DSC with 9900 thermal analyser. The DSC had been previously calibrated with distilled water and indium (see 3.2.8). The surfactant melting temperatures (T_m) were obtained directly from the traces produced.

2.4.4 Results of Surfactant Analyses

2.4.4.1 GC MS

2.4.4.1.1 Nonylphenyl Ether Ethoxylates

The nonylphenyl based surfactants produced complex chromatographs. The mass spectra taken from these peaks was used for peak identification and this was aided by searching for expected molecular ions. Figure 2.1 shows the GC chromatographs for NP0, NP2 and NP4. Complex groups of peaks eluted after various times up to 25 minutes. The probable identity of these peaks was determined by molecular ion searches and is given in Table 2.2. Nonyl phenol, NP0, was found to be multicomponent. This was most likely due to the presence of isomers of the alkyl chain on the phenol group. The uni-, di-, tri-,and

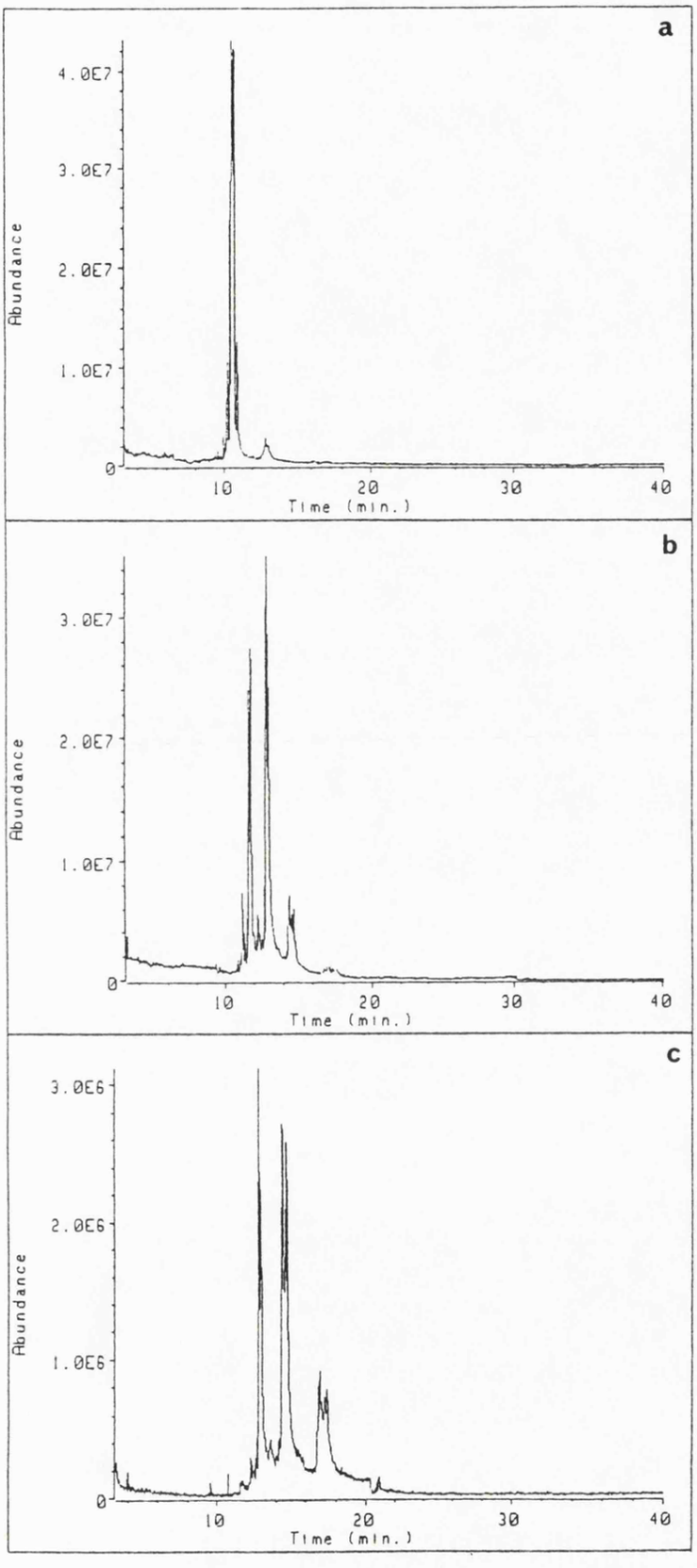

Figure 2.1 Typical GC chromatographs for three nonylphenol ether ethoxylates.

a) NP0 b) NP2 c) NP4.

Elution time (min)	Largest ion	Peak identity
10.15-11.2	220	NP0
11.6-11.9	264	NP1
12.7-13.3	308	NP2
14.1-14.8	352	NP3
16.7-17.6	396	NP4
20.8-22.2	440	NP5

Table 2.2 Peak elution times, the largest detected ion and suspected peak identity for nonylphenyl ether ethoxylates analysed by GC-MS.

tetraethoxylated compounds were also multicomponent presumably due to the same reason. From the data obtained it can be seen that NP2 contained NP1-NP3 and traces of NP4. However, above NP4/5 poor elution from the column and sample tailing prevented detailed analysis of these and higher molecular weight surfactants.

2.4.4.1.2 Alkyl Ether Ethoxylates

The dodecyl ether ethoxylate surfactants $C_{12}E_0$-$C_{12}E_8$ all produced single peaks on the GC chromatograph. The trace shown in Figure 2.2 is for $C_{12}E_5$, similar chromatographs were obtained for the other surfactants of the series. As the molecular weight of the surfactant increased so did the elution time for the compound. This lead to some tailing of the peaks and caused them to become broader and flattened. The elution times of the surfactants $C_{12}E_0$-$C_{12}E_8$ are given in Table 2.3.

The mass spectra observed were in parity with results obtained by McDonald and Robinson (89) who worked with similar compounds. Molecular ions were identified for all surfactants. Other peaks were consistant with the loss of $-CH_2$ and $-CH_2CH_2O$ units or multiples there of, i.e. peaks at M-14, M-28, M-44, M-88 etc. Dodecanol $C_{12}E_0$ and $C_{12}E_1$ produced mass spectra which were homologous with those stored for these compounds in the software of the computer further comfirming the identity of the peaks.

The GC chromatograph for Brij 30 was far more complex and showed the surfactant to be polydisperse (Figure 2.3). From the analyses of the pure Nikkol surfactants it was possible to identify many of the peaks on the Brij chromatographs. Components were identified corresponding to $C_{12}E_0$-$C_{12}E_5$, however, it was thought that due to tailing higher ethoxylated surfactants may have not been detected. A sample was therefore analysed using a faster temperature ramp rate. From the resulting chromatograph $C_{12}E_6$ and $C_{12}E_7$ were also detected. A set of peaks of slighty lower retention time were observed shadowing those of the dodecyl ethoxylates. These were believed to be due to ethoxylates of another alkyl chain length, possibly decanol.

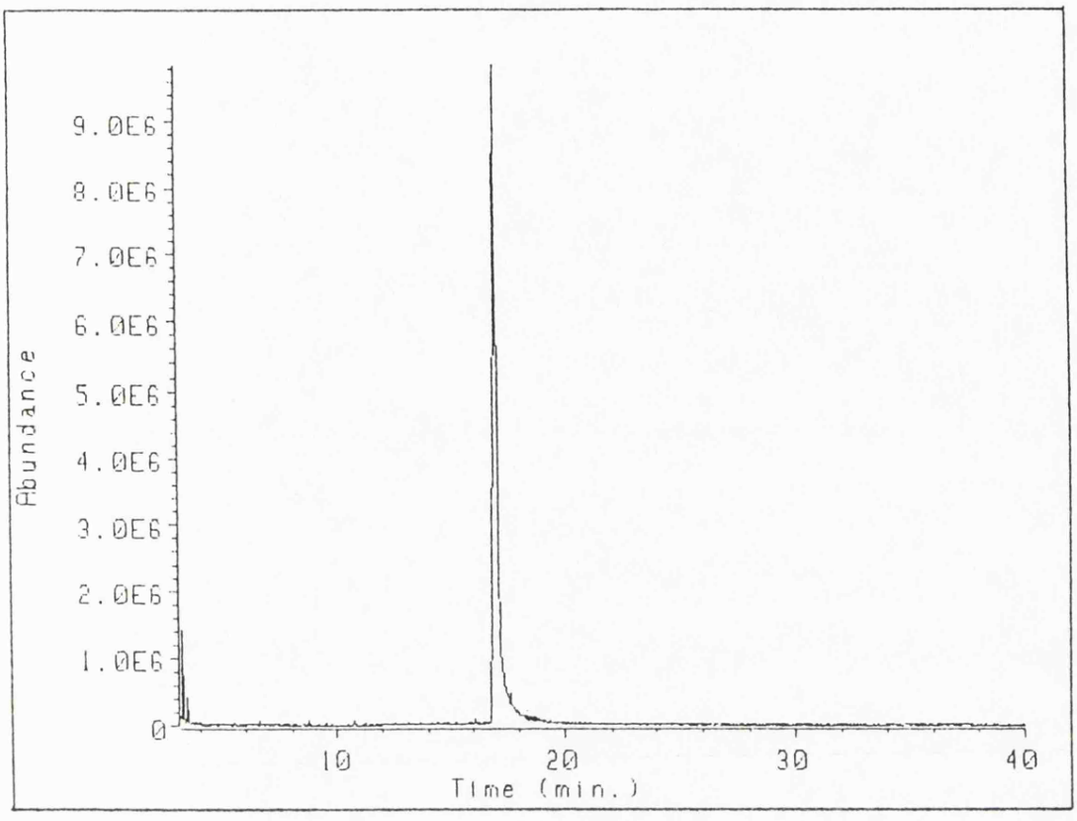

Figure 2.2 GC chromatograph for the Nikkol dodecyl ether ethoxylate, $C_{12}E_5$.

Surfactant	Molecular weight	Elution time (min)
$C_{12}E_0$	186	9.18
$C_{12}E_1$	230	10.55
$C_{12}E_2$	274	11.76
$C_{12}E_3$	318	12.92
$C_{12}E_4$	362	14.54
$C_{12}E_5$	406	17.06
$C_{12}E_6$	450	21.43
$C_{12}E_7$	494	28.76
$C_{12}E_8$	538	32.22

Table 2.3 The molecular weights and GC elution times of the dodecyl ether ethoxylate surfactants.

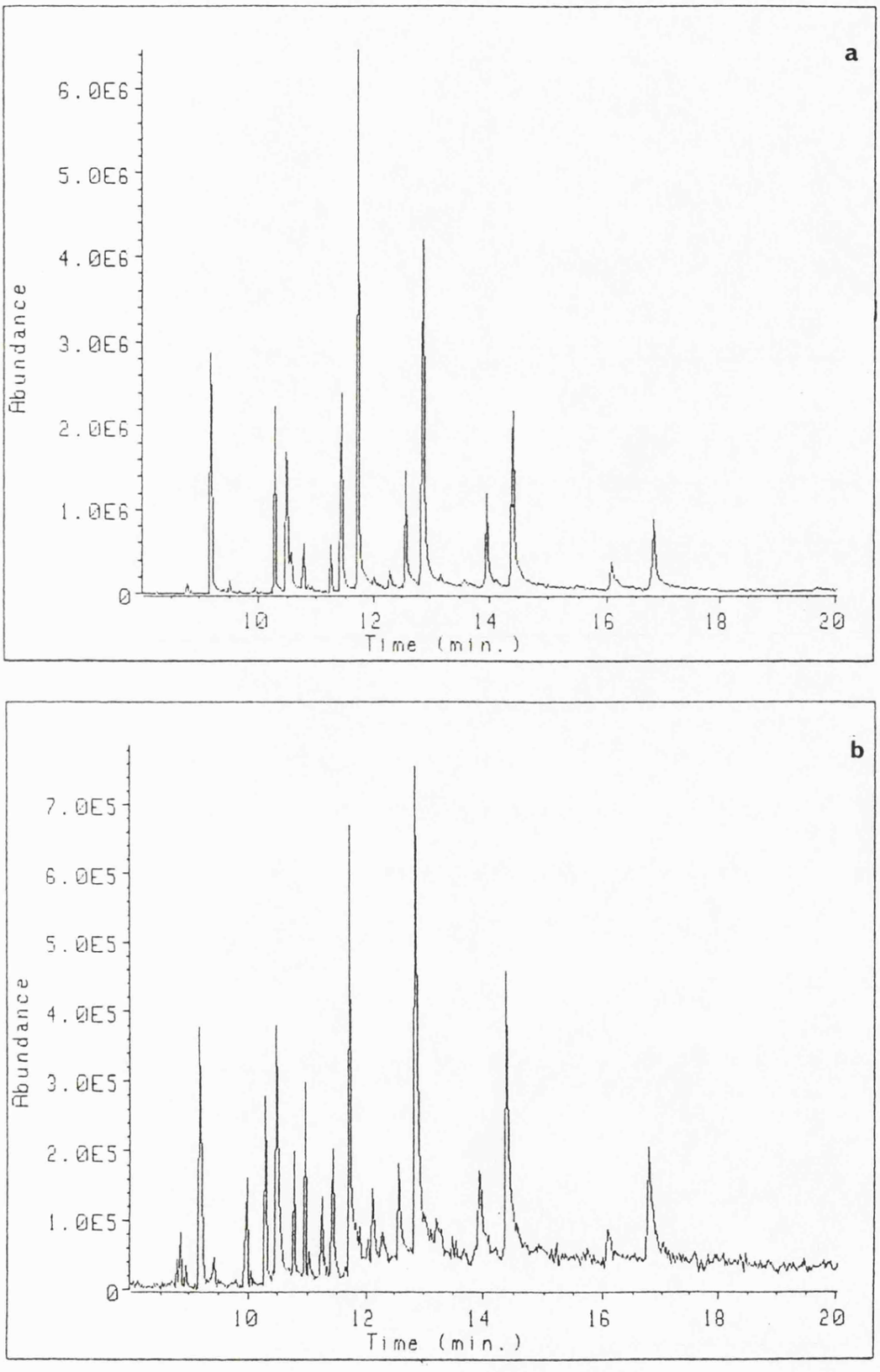

Figure 2.3 GC chromatographs for a) Brij 30 b) Brij 36T.

The chromatographs for the two samples of Brij 36T were even more complex than that for Brij 30. The chromatograph for the Fisons donated sample is shown in Figure 2.3. Surfactants in the range $C_{12}E_0$-$C_{12}E_8$ were identified. There were also many other peaks presumably due to other alkyl chain length alcohol ethoxylates. The Sigma sample had fewer peaks of low retention time and more between 18-24 minutes. As with Brij 30 runs using higher ramp rates were used to attempt to resolve longer ethoxylate peaks, however, no compound larger than $C_{12}E_9$ was detected.

2.4.4.1.3 Azone

The GC chromatograph for Azone showed a single peak that eluted after 11.1 minutes. This demonstrated that the sample was pure. Azone is of similar molecular weight to $C_{12}E_2$ and its elution time indicated that it of a similar polarity to these surfactants. The mass spectrum was typical of a compound of its type.

2.4.4.2. Proton NMR

2.4.4.2.1 Nonylphenyl Ether Etholylates

Figure 2.4 shows a typical ^1H NMR spectrum for an alkylphenol ether ethoxylate, in this case NP5. There were three well separated groups of lines in the spectrum. The lowest field group (6.8-7.3 ppm) was due to protons on the aromatic ring. The middle grouping (3.5-4.3 ppm) was from the protons of the ethylene oxide chain. The proton of the terminal hydroxyl was observed slightly upfield from this (3.3 ppm). The complex high field grouping (0.4-1.8 ppm) was from the protons of the alkyl side chain. Similar spectra were observed for alkyphenol ether ethoxylates by Flanagan *et al* (90) and Crutchfield *et al* (91).

Printed above the spectrum is the integrals for each group of lines; each step is a quantitative measure of the number of protons giving rise to the signal. Since it is known that the total aromatic signal came from four protons (2x2) the average number of protons in the ethoxy chain can be measured by proportional height. The

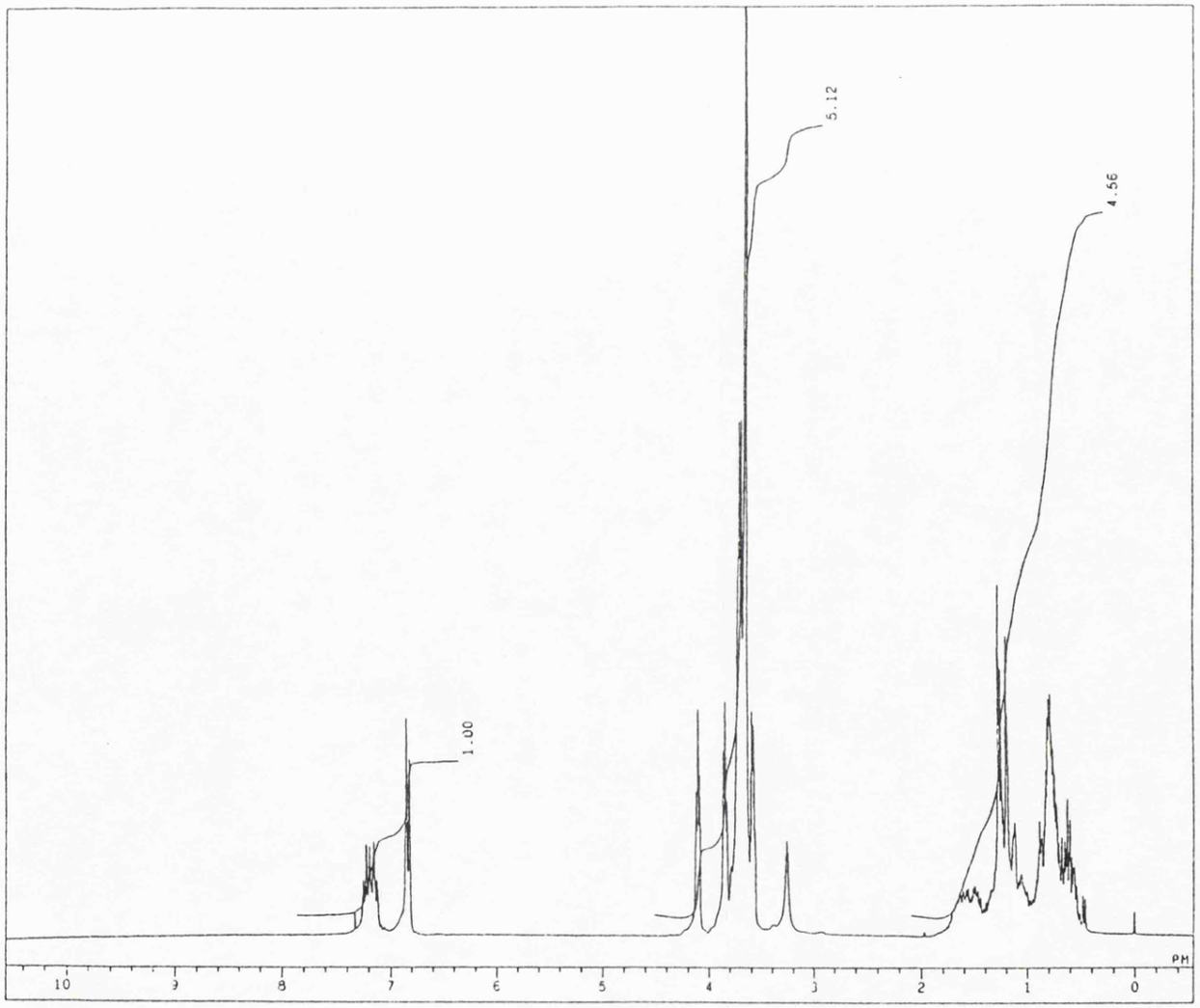

Figure 2.4 ^{1}H-NMR spectrum for the nonylphenol ether ethoxylate, NP5.

average number of ethoxy groups in the chain was then calculated by dividing this by four.

The average ethoxy chain length was determined, by the above method for the series of surfactants NP1-NP15. The results of these analyses are given as mean±range, n=2, in Table 2.1. The alkyl chain length or conformation was not determined as it was deemed to be too complex.

2.4.4.2.2 Alkyl Ether Ethoxylates

Figure 2.5 shows a typical ^1H NMR spectrum for an alkyl ether ethoxylate, in this case $C_{12}E_5$. There were two groups of lines in the spectrum. The low field peak (3.4-3.8 ppm) was due to the protons of the ethoxy chain and the $-CH_2$ group of the alkyl chain next to the oxygen. The terminal hydroxyl was slightly upfield from this peak (3.25 ppm). The other group of lines at a higher field (0.8-1.2 ppm) was due to the protons of the alkyl chain. The three protons of the terminal methyl group ($-CH_3$) can be clearly identified at the high field end of the group (0.8 ppm). Similar spectra were obtained for other alkyl ether ethoxylates by Flanagan *et al* (90) and McDonald and Robinson (89).

As with the alkylphenol ether ethoxylates the number of protons in the ethoxy chain was calculated by measuring the height of their integral relative to the height produced by a known number of protons; in this case the three of the terminal methyl group of the alkyl chain. In a similar fashion the length of the alkyl chain can also be calculated. The average ethoxy and alkyl chain lengths for Brij 30 and Brij 36T are given in Table 2.4. For the Brij surfactants the results are mean±SD, n=5. For all the Nikkol surfactants $C_{12}E_1$-$C_{12}E_8$ and $C_{10}E_3$-$C_{10}E_6$ both alkyl and ethoxy chain lengths were as stated by the supplier.

2.4.4.3 Melting Points Determined By DSC

All the dodecyl ether ethoxylates, $C_{12}E_0$-$C_{12}E_8$ gave a sharp melting endotherm typical of a pure, single component compound. The melting points of

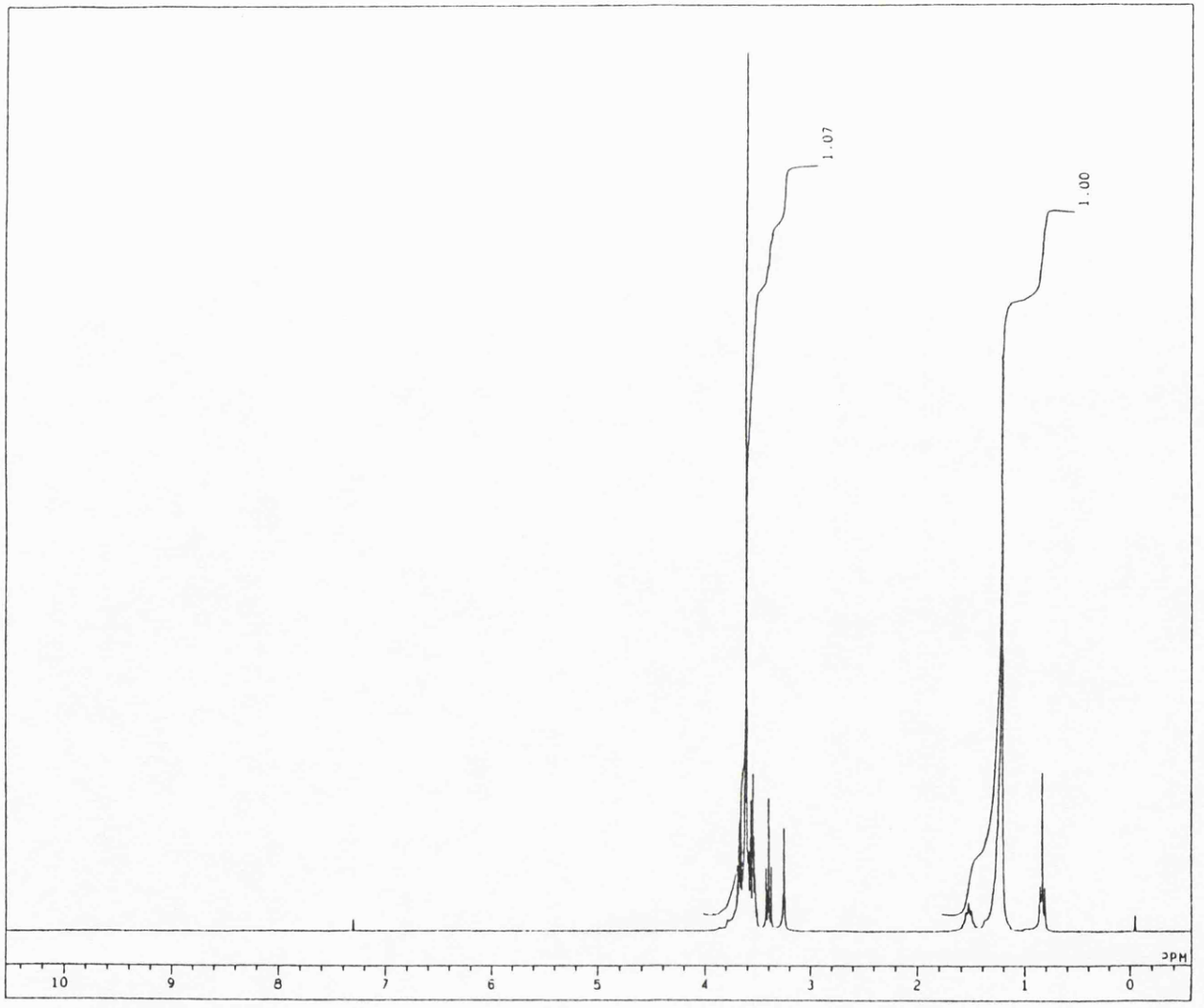

Figure 2.5 ^{1}H-NMR spectrum for the Nikkol dodecyl ether ethoxylate, $C_{12}E_5$.

Surfactant	Alkyl Chain[a]	Ethoxy Chain[a]	No. of Peaks[b]	Range[c]
Brij 30	12.3±0.21	4.06±0.34	14	E_0-E_7
Brij 36T[1]	12.9±0.28	7.85±0.54	31	E_0-E_9
Brij 36T[2]	12.15±0.45	9.27±0.28	18	E_0-E_9

Table 2.4 Alkyl and ethoxy chain lengths of Brij surfactants determined by ^{1}H NMR and the surfactant purity determined by GC-MS.

a determined by ^{1}H NMR (mean±SD, n=5)

b number of major peaks on GC chromatograph

c range of surfactant components identified by GC-MS

1 sample from Fisons

2 sample from Sigma

the surfactants are shown plotted as a function of ethylene oxide chain length of the molecule in Figure 2.6. Looking across the series of surfactants from $C_{12}E_0$-$C_{12}E_8$ the melting temperature decreased form $C_{12}E_0$-$C_{12}E_3$, a minimum was observed with $C_{12}E_3$. From $C_{12}E_3$-$C_{12}E_8$ as the ethoxy chain length of the surfactant increased so did the melting point of the surfactant.

2.4.5 Conclusions

2.4.5.1 Nonylphenyl Ether Ethoxylates

From the results obtained from both the ^{1}H-NMR and the GC-MS analyses it can be seen that the nonylphenyl based surfactants were complex mixtures of surfactants being polydisperse in both ethylene oxide chain length and in the isomeric form of the nonyl chain. The ^{1}H-NMR analyses showed the average ethoxy chain length of all the surfactants to be close to that stated by the supplier in general $< \pm 0.5$ ethoxy units. By use of GC-MS it was possible to show the polydispersity of the surfactants but this power of this technique was restricted to low molecular weight compounds.

2.4.5.2 Alkyl Ether Ethoxylates

The Nikkol supplied decyl and dodceyl ether ethoxylates were all shown to be pure and of the ethoxy chain length stated by the supplier. It would be expected that as the molecular weight of the surfactants increased that the melting points of the surfactants would also increase, however, from $C_{12}E_0$-$C_{12}E_3$ the melting point decreased. This may indicate that over this range surfactants the crystalline packing of the molecules in the solid state decreased.

The Brij surfactants were shown to be polydisperse both in ethoxy and alkyl chain length. The average ethoxy chain length of the sample of Brij 30 was close the value stated by the supplier, however, that was not the case for the samples of Brij 36T. The sample obtained from Sigma had an average ethoxy chain length of 9.27 ± 0.28, whilst that of the sample donated by Fisons was 7.85 ± 0.54 over two

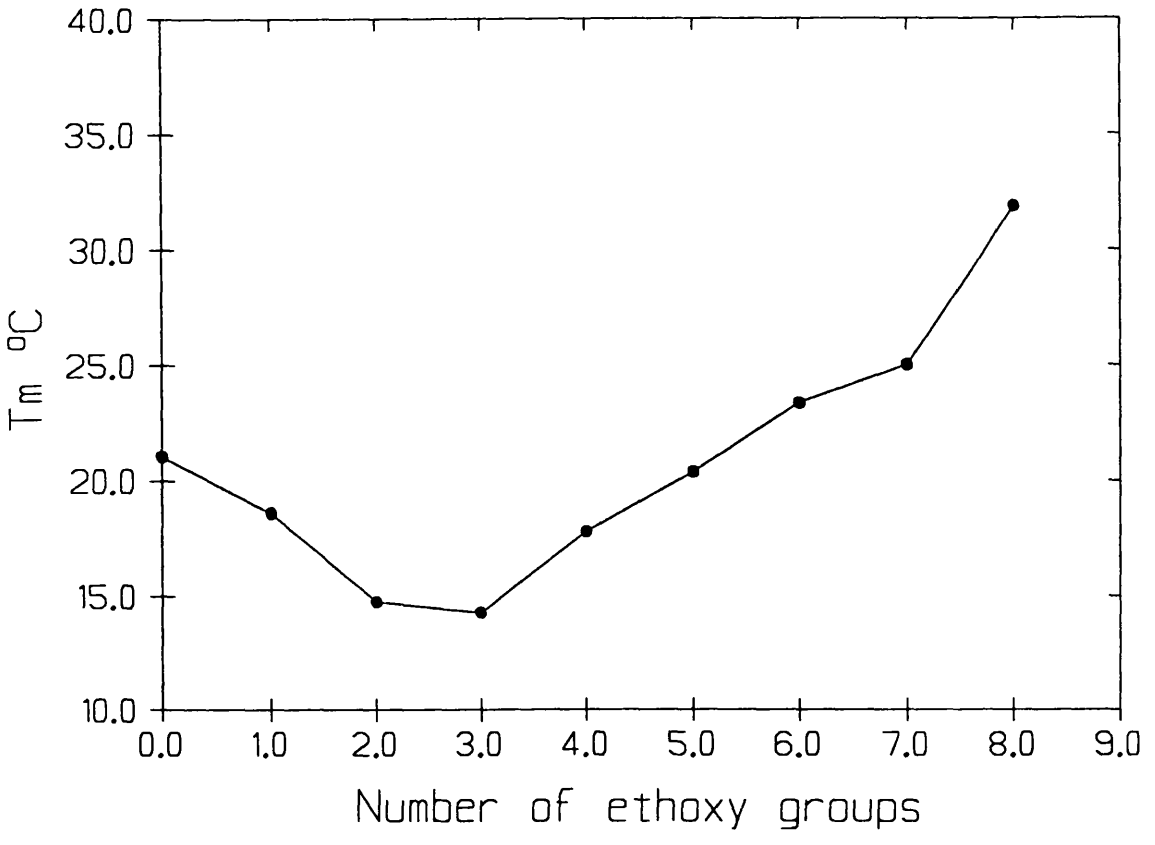

Figure 2.6 The melting points of the dodecyl ether ethoxylates, as determined by DSC, plotted as a function of surfactant ethoxy chain length.

ethoxy groups less than the stated $C_{12}E_{10}$. This difference between the two samples was verified by their GC chromatographs.

2.5 Materials used in the DSC Studies

Distearoylphosphatidylcholine (DSPC) stated as >99% purity was obtained from Sigma (Poole, UK). The DSPC was shown to be chromatographically pure and produced a single spot when analysed by thin layer chromatography (silica gel G; solvent: chloroform:methanol 2:1). The DSPC was used without further purification.

The chloroform used in these studies was freshly distilled from an all glass distillation apparatus prior to use to remove any contaminants. Trypsin used in the preparation of stratum corneum was bovine type III trypsin prepared from bovine pancreas, this was obtained from Sigma (Poole, UK). 1-dodecyl-aza-cycloheptan-2-one (Azone^R) was kindly donated by Fisons Pharmaceuticals (Loughborough, UK). This was shown to be pure when analysed by GC-MS. Hexane, methanol, KCl, $CuSO_4$ and absolute ethanol were of reagent grade and obtained from BDH Chemicals Ltd (Poole, UK). These were used as supplied.

2.6 Materials used in the FPS Studies

DSPC, chloroform and Azone were as described above (2.5). Four fluorescent membrane probes were used in the FPS study. Cis-parinaric acid (cis-pna), and 8-anilino-1-naphthalene sulphonic acid (ANS) were obtained from Sigma (Poole, UK). The cis-pna was stored in absolute ethanol, under helium, at -80°C to prevent oxidation. Perylene and 1,6-diphenylhexatriene (DPH) were obtained from Aldrich (Gillingham, UK). These were used as supplied. The chemical structures of all four probes are shown in Figure 2.7. Glycogen and 2,6-di-t-butyl-4 methyl phenol (BHT) were both obtained from Sigma (Poole, UK). The acetone used was of HPLC grade. Tetrahydrofuran (THF) and absolute ethanol were of reagent

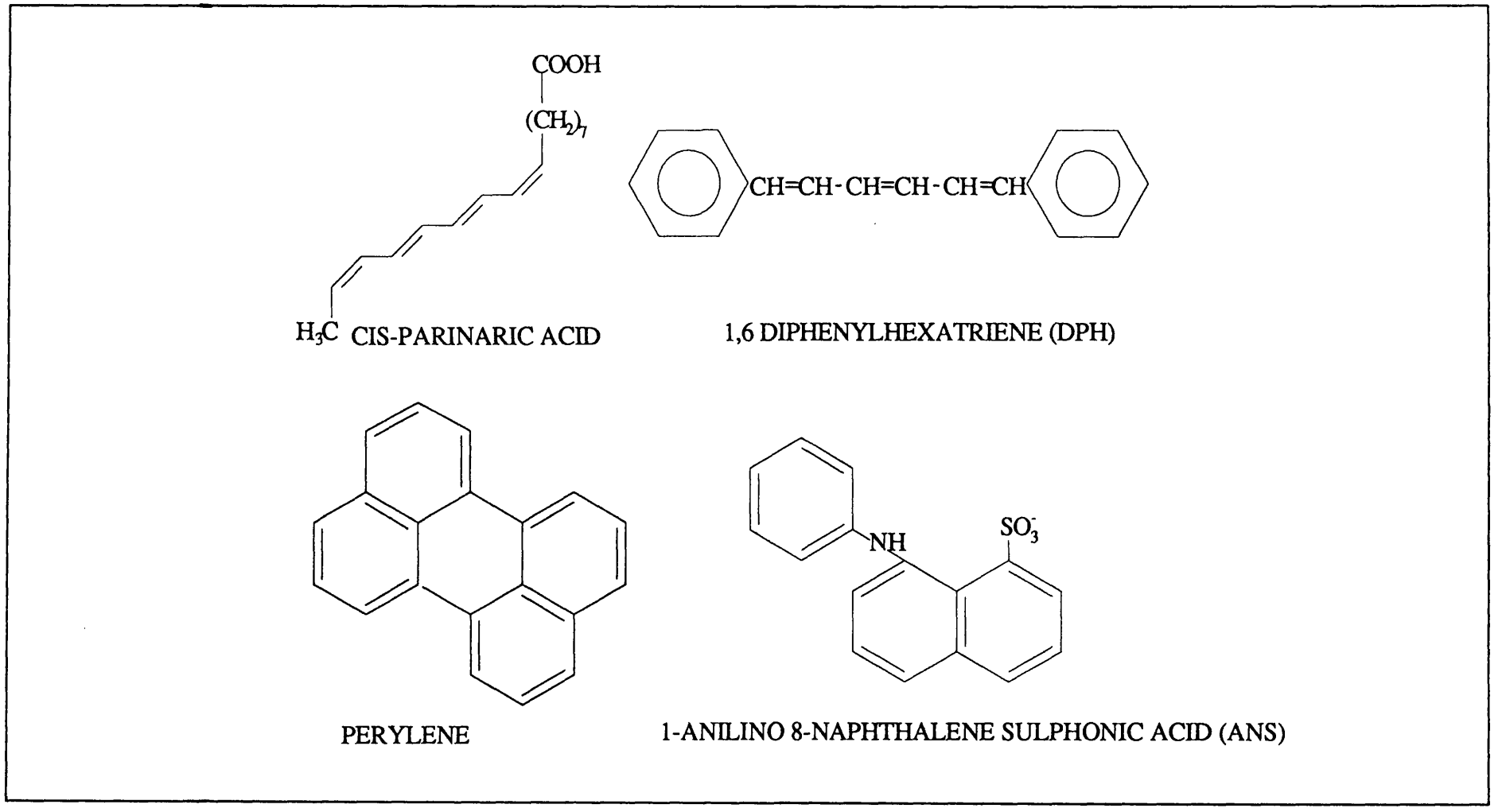

Figure 2.7 Chemical structures of the fluorescent probes cis-pna, DPH, perylene and ANS.

grade. All three were obtained from BDH Chemicals Ltd (Poole, UK). All these solvents were used as supplied.

2.7 Materials used in the ESR Studies

DSPC, chloroform, acetone and ethanol were as described above. The spin probe, 5-doxyl stearic acid (5-DS) was obtained from Sigma (Poole, UK) and this was stored in absolute ethanol under helium at -80°C. The silica quartz capillary tubing used to make the sample tubes was obtained from Jencons Scientific (Leighton Buzzard, UK).

2.8 Materials used in the Permeation Studies

The ^{14}C-hydrocortisone, ^{14}C-oestradiol, ^{14}C-progesterone and ^{14}C-oestrone used as permeants in these studies were obtained from Amersham International plc (Amersham, UK). The structures of these steroids is shown in Figure 2.8. The steroids were all labelled at the four position in the steroidal ring, as shown by the asterisk. All had specific activities of 2.07GBq mmol^{-1} (56mCi mmol^{-1}) and were stated as having radiochemical purities between 99.7 and 99.9 percent. The steroids were stored at -20°C and used without further purification. Unlabelled steroids were obtained from Sigma (Poole, UK) and used as supplied. The steroids were prepared as solutions in acetone. A ratio of hot to cold steroid of 1:200 was used for all four compounds. Optiphase^{R} scintillation fluid was from Pharmacia (Uppsala, Sweden). The glass diffusion cells, underwater magnetic stirrers and stir bars were all kindly donated by Fisons Pharmaceuticals (Loughborough, UK).

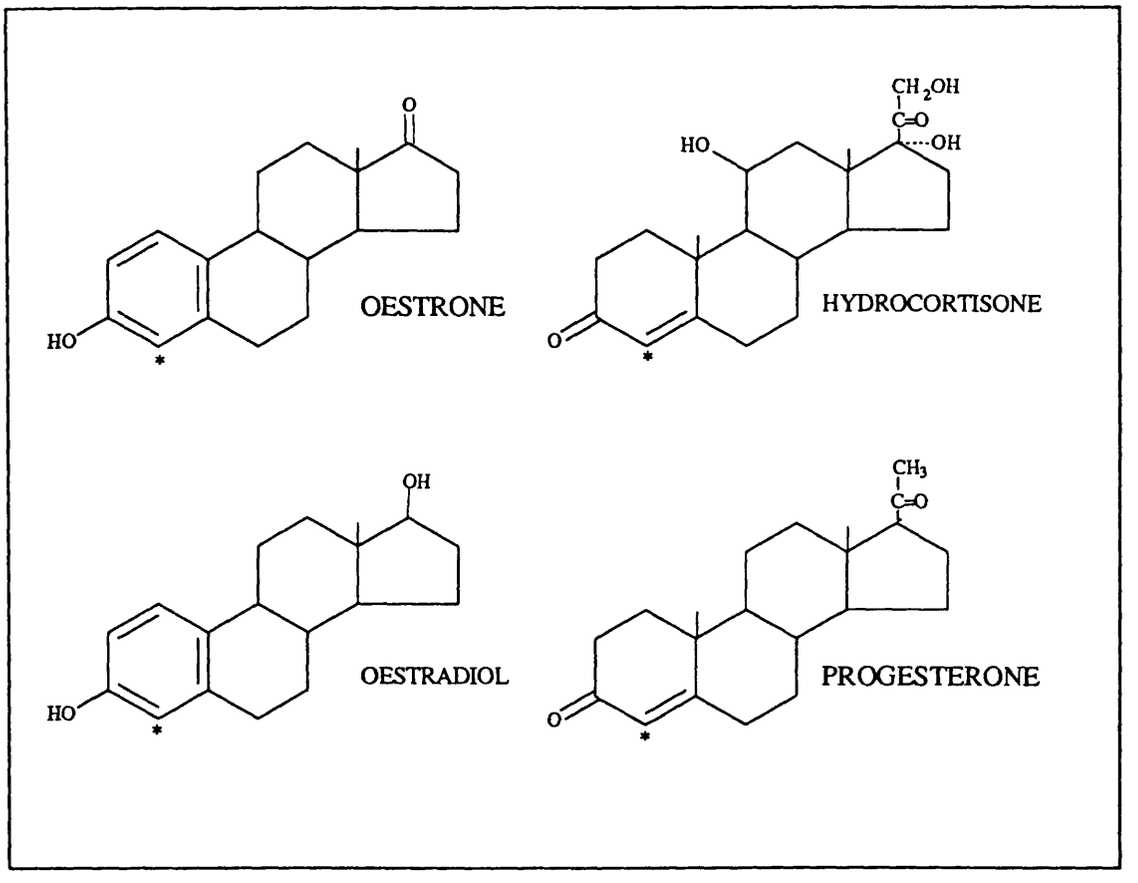

Figure 2.8 Chemical structures of the four radiolabelled ^{14}C-steriods used in the skin permeation studies. The position of the ^{14}C label is shown by an asterisk.

CHAPTER 3

MEASUREMENT OF LIPID BILAYER FLUIDISATION BY DIFFERENTIAL SCANNING CALORIMETRY

3.1. INTRODUCTION

3.1.1 Principles of Differential Scanning Calorimetry (DSC)

DSC is used mainly for the study of physical transitions. It is a basic thermal analysis technique which can be defined as "a technique in which the difference in energy input into a substance and a reference material is measured as a function of temperature whilst the substance and reference material are subjected to the same controlled temperature programme" (92). Typical DSC equipment is illustrated schematically in Figure 3.1. Sample and reference are heated at identical predetermined rates. In the event of a transition occurring thermal energy (power) is added or subtracted from the sample or reference in order to maintain isothermal conditions. The differential energy is equivalent to the energy absorbed or evolved in the particular transition (93).

3.1.2 DSC of Biological Membranes

Historically DSC has been used to study the thermally-induced transition from a relatively ordered gel-crystalline state at lower temperatures to a relatively disordered fluid liquid-crystalline state at higher temperatures in model lipid bilayers and biological membranes (94). This thermotropic transition can, for pure lipids be viewed as a simple two state, first order, endothermic process (95).

A typical DSC trace for such a transition is shown in Figure 3.2. From such a transition profile a number of important parameters can be determined directly. The phase transition temperature, denoted T_m, is the temperature at which the excess specific heat required for the transition reaches a maximum. The peak area is equal to the enthalpy of the transition (ΔH_{cal}) and can be determined by integration of the peak when the calorimeter has been calibrated with a known standard. The sharpness of the transition is often expressed as the width, in degrees Kelvin, at half peak height ($\Delta T_{1/2}$). This value may range from 0.2K for very pure synthetic lipids (96) to as much as 15-20K for biological membranes (97).

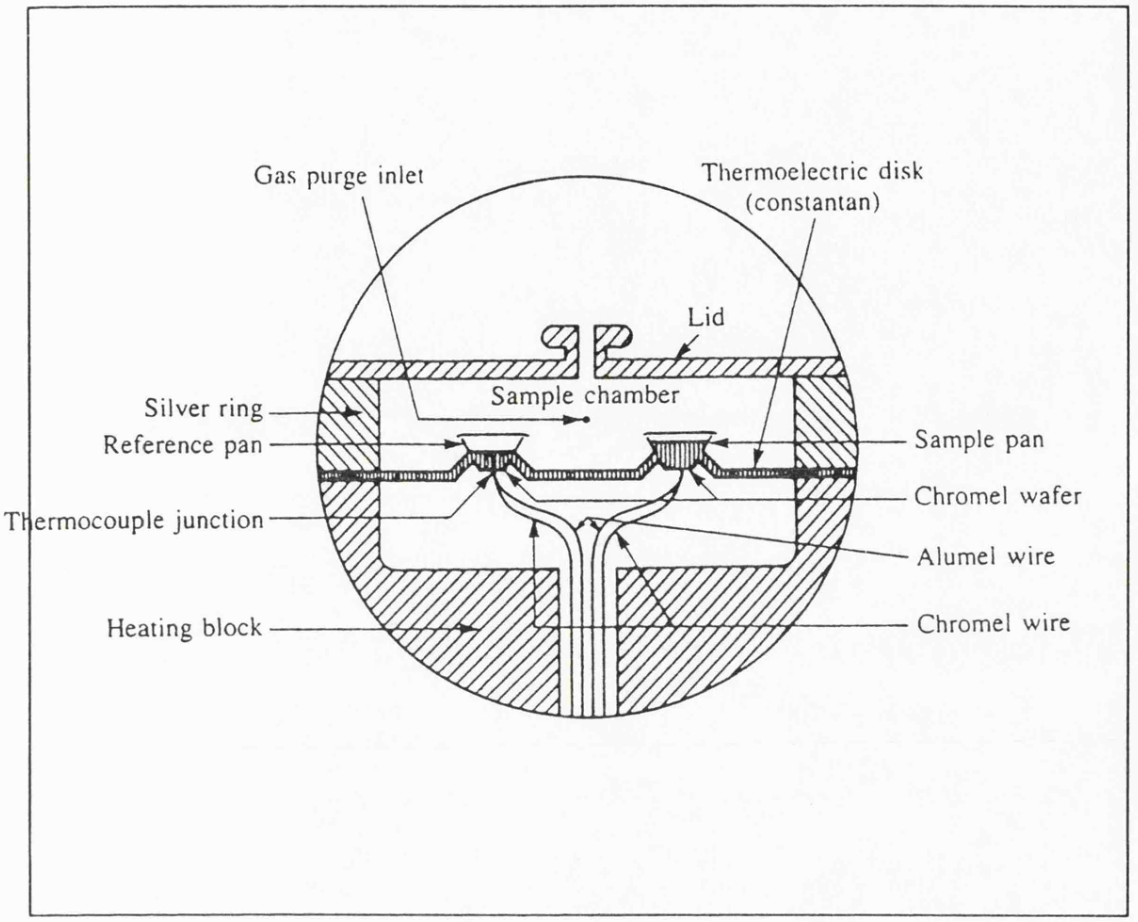

Figure 3.1 The arrangement of the heaters and temperature sensors in a typical DSC apparatus.

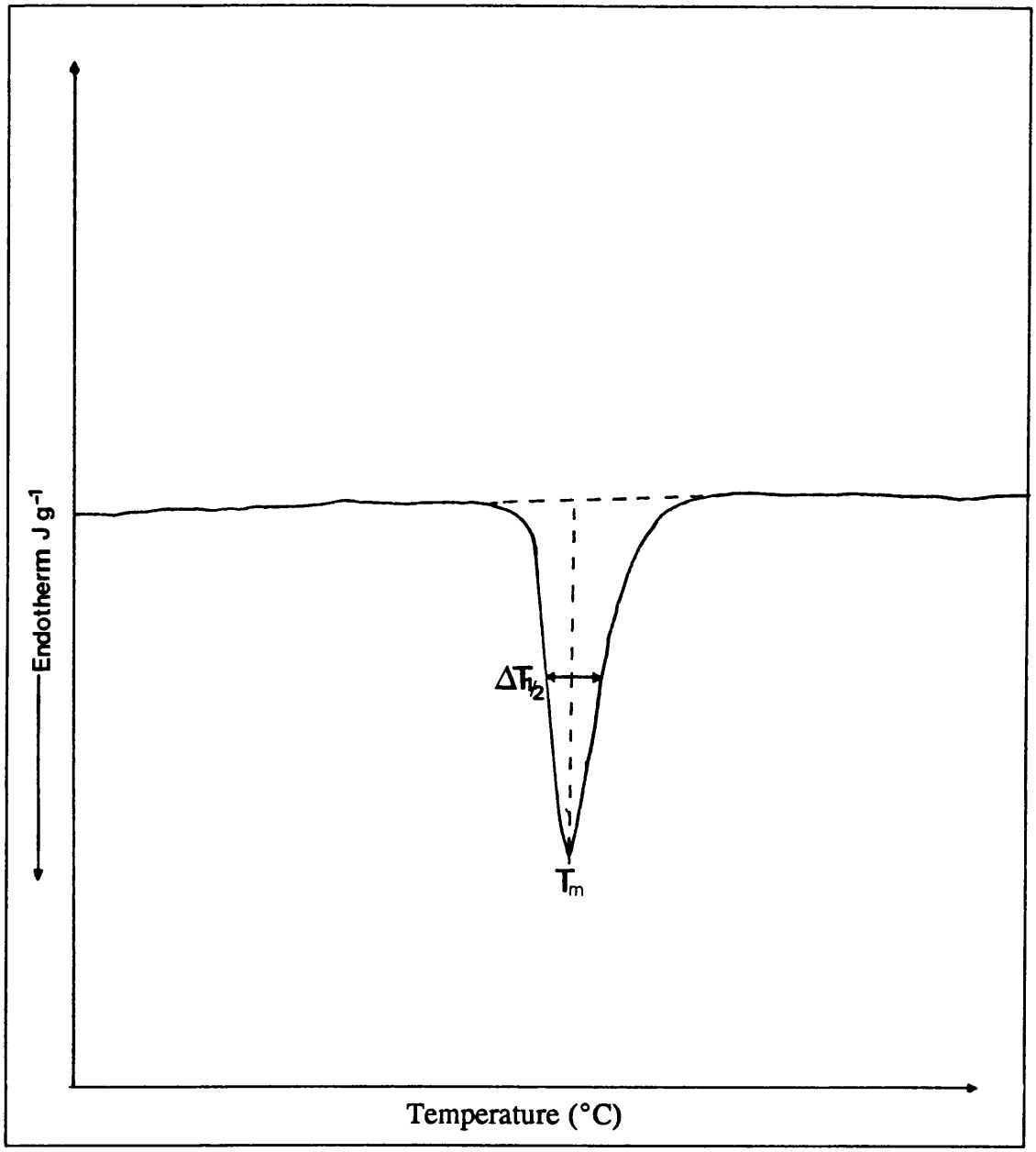

Figure 3.2 Typical DSC trace of a first order melt endotherm showing the transition midpoint temperature (T_m) and the peak width at half peak height ($\Delta T_{½}$).

From these measurements more complex information can be obtained. The Van't Hoff enthalpy (ΔH_{VH}) can be determined from the relationship.

$$\Delta H_{VH} = 4RT_m^2/\Delta T_{1/2} \qquad (95)$$

where R = Universal Gas Constant

$\Delta T_{1/2}$ and T_m are in Kelvin.

The cooperative unit (CU) of the transition expressed as a number of molecules can be calculated from the ratio $\Delta H_{VH}/\Delta H_{cal}$. The CU is a measure of the degree of intermolecular cooperation between phospholipid molecules in a bilayer. For a completely cooperative first order transition of a pure substance the CU should approach infinity, while for a non-cooperative process the value should approach unity. (94)

Early work with DSC by Chapman and co-workers (98) and Hinz and Sturtevant (96) produced valuable information concerning the thermotropic phase transitions of single chain length 1,2-diacylphosphatidylcholines and phosphatidyl ethanolamines. This work showed T_m, $\Delta T_{1/2}$ and ΔH_{cal} to be dependent upon head group type, hydrocarbon chain length and degree of unsaturation. Further investigations concentrated upon transitions involving mixtures of diacyl lecithins of homogeneous chain length (99-101) heterogeneous chain length (102), and the addition of "foreign" molecules such as surfactants (103) and proteins (104) to membranes.

Addition of other lipids and foreign molecules to artificial membranes causes a widening of $\Delta T_{1/2}$ and an alteration in T_m, the degree of effect is highly dependent on the concentration and structure of molecules added to the membranes (103). Natural cell membranes produce far more complex transitions involving many lipid-lipid and lipid-protein interactions (104).

3.1.3 DSC of Stratum Corneum

There have been several recent reports of thermal analyses of stratum corneum. Van Duzee (105) studied isolated human stratum corneum. He found four endothermic transitions with peak midpoints at 40, 75, 85 and 107°C. These results were later confirmed and substantiated by Golden *et al* (106), Goodman and Barry (107) and Knutson *et al* (52). However in these studies the presence of the lowest temperature transition (38-40°C) was variable.

The endothermic peaks can be assigned to thermal transitions of various parts of the stratum corneum. The highest temperature transition (107°C) is due to the thermal denaturation of intracellular keratin. The transition at 85°C is lipid-associated and is thought to be connected with membrane protein-intercellular lipid complexes (108) although this suggestion has been debated (50,106). The transition at 75°C has been assigned to the gel-liquid crystalline phase transition of the intercellular lipids. The lowest temperature broad transition at 40°C is also lipid associated being either a structural rearrangement or melting of sebaceous lipid (50).

Studies have also been carried out using the stratum corneum of other mammalian species. A pattern of transitions similar to human stratum corneum were found by investigators studying neonatal mouse tissue (109), hairless mouse tissue (52) and porcine stratum corneum (110) but with variations in the transition temperature.

Transdermal penetration enhancers have been shown to alter both the T_m and ΔH_{cal} of the lipid transitions of the stratum corneum (107,111). The extent of these effects was correlated to the potency of the chemicals as penetration enhancers which suggests their site of action is centred in the stratum corneum lipids (50,111).

3.2 METHODS

3.2.1 Preparation of Liposomes

DSPC multilamellar liposomes were formed by an adaption of the method of Bangham (112). 100μl of DSPC stock solution, usually 100mg ml^{-1}, in chloroform were pipetted into clean 1.5ml glass screwtop vials. The chloroform was blown off using a stream of dry nitrogen gas whilst the vial was rotated by hand. This produced a thin film of lipid on the inner surface of the vial. The vials were then placed under high vacuum overnight to remove any residual solvent. Phosphate buffered saline (PBS) pH 7.4 was added to the samples, usually 100μl, and the vials sealed. The vials were then heated to 65°C, which is above the transition temperature of DSPC, for 30 minutes and whilst hot mixed on a bench vortex mixer for 30 seconds. The heating and vortexing procedure was then repeated as above.

The samples were then usually stored at 4°C overnight before thermal analysis. The liposomes were stable for at least 6 days at 4°C, no significant change in thermal characteristics were observed over that time period (Table 3.1).

3.2.2 Incorporation of Surfactant into the Liposomes

Two methods of preparing mixed lipid-surfactant vesicles were investigated. Either the phospholipid and surfactant were codeposited from chloroform to produce a mixed film in the vials prior to hydration, or the surfactant was added as a solution or suspension in buffer to a lipid film for hydration of the lipid.

There were no significant differences in the thermal behaviour between vesicles produced by either method (t-test, $p > 0.05$) except in the case of the low HLB surfactant NP2 which was insoluble in water (Table 3.2). This was probably due to the difficulty in preparing homogeneous suspensions of the low HLB surfactants. For subsequent studies the codeposition method was adopted as standard.

For all experiments involving the Nikkol dodecyl ethoxylate surfactants the mass of surfactant added to the DSPC was calculated on a molar basis. This approach was used for some of the nonylphenyl experiments using a molecular

Time of storage	T_m(°C)	$\Delta T_{1/2}$(°C)	ΔH_{cal}
<1	54.54±0.26	1.47±0.08	46.85±0.47
4	54.39±0.17	1.33±0.22	46.26±0.32
24	54.15±0.04	1.41±0.34	47.42±0.61
48	54.27±0.09	1.30±0.11	47.66±0.51
96	54.29±0.18	1.28±0.26	46.16±0.31
144	54.14±0.10	1.18±0.06	45.98±0.17

Table 3.1 The effect of storage at 4°C upon the thermal characteristics of DSPC liposomes (mean±S.D., n=3)

.

	Surfactant codeposited			Surfactant added in solution		
Surfactant	T_m (°C)	$\Delta T_{1/2}$ (°C)	ΔH_{cal}	T_m (°C)	$\Delta T_{1/2}$ (°C)	ΔH_{cal}
NP2	48.80±0.09	5.57±0.86	38.21±9.7	52.92±0.5	3.02±0.08	41.18±4.7
NP4	49.28±0.76	4.86±0.05	49.28±3.6	50.01±0.87	4.9±0.66	54.81±8.7
NP6	51.79±0.41	4.76±0.12	29.58±6.7	51.64±0.53	4.43±0.32	35.17±7.1
NP8	53.39±0.17	2.57±0.06	49.60±3.2	53.76±0.85	1.95±0.64	38.20±6.4
NP10	53.23±0.63	2.52±0.31	32.29±4.1	53.65±0.14	2.52±0.18	28.19±2.6
NP12	53.17±0.08	2.46±0.27	34.87±2.6	53.29±0.38	2.14±0.74	33.89±6.1
NP15	54.17±0.37	2.38±0.55	28.05±4.6	54.43±0.12	2.86±0.89	26.94±5.2

Table 3.2 The effect of the method of addition of surfactant upon the thermal characteristics of DSPC/surfactant mixed vesicles.

weight average. In other cases the surfactant present was calculated as a percent weight in final volume.

3.2.3 Thermal Analysis of Liposomes

For thermal analysis approximately 10mg of liposome or liposome/surfactant suspension was pipetted into preweighed DSC pans. The pans were hermetically sealed and reweighed.

3.2.4 Preparation of Stratum Corneum

Porcine skin from the back of the ear and human abdominal skin were obtained and stored as described (2.1). Both skin types were subjected to the same preparative methods for the isolation of stratum corneum.

Subcutaneous fat was removed by dissection with a #12 scalpel. The whole epidermis was seperated from the dermis by the method of Kligman and Christophers (113). Whole skin was immersed in distilled water at 60 ± 1°C for 60 seconds. The epidermis was then gently scraped and pealed from the dermis with the aid of a pair of curved forceps. The epidermis was then placed, stratum corneum up, on filter paper soaked in 0.05% trypsin solution in pH 7.4 PBS. This was sealed into a petri dish and incubated overnight at 37°C. Following incubation the stratum corneum was washed by gentle vortex mixing three times in distilled water. The dermal side was gently brushed with cotton buds to remove any adhering epidermal cells. The seperated stratum corneum was then dried on stainless steel racks under vacuum and subsequently stored desiccated over silica gel at -20°C until required.

3.2.5 Thermal Analysis of Stratum Corneum

Dry stratum corneum was cut into pieces of approximately 4mg and accurately weighed. Some samples were then washed for 20 seconds in hexane at 0°C to remove surface lipids (105). The samples were allowed to rehydrate for 24 hours at ambient temperature (18-20°C) over a saturated aqueous solution of

$CuSO_4$, a relative humidity of 98% (114). This procedure was carried out in a glass desiccator fitted with an electric fan to circulate the humid air.

For samples treated with surfactant 0.4mg of surfactant was deposited onto the stratum corneum surface from 30μl of absolute ethanol prior to rehydration. Control samples were prepared with 30μl of ethanol only.

The hydrated stratum corneum was folded into preweighed aluminium DSC pans which were hermetically sealed and reweighed. From the stratum corneum weights before and after hydration the percentage hydration by mass was calculated. At least four sample controls were prepared for each treatment.

3.2.6 Extraction of Skin Lipids

Total stratum corneum lipids were extracted by a method adapted from Bligh and Dyer (115). Whole stratum corneum was prepared and stored as previously described (3.2.4). For lipid extraction the samples were weighed, cut into small pieces with dissecting scissors, and put in a clean glass 100ml beaker. The stratum corneum was then covered with extraction solvent (2:1 methanol:chloroform) 1ml for every 25mg dry tissue, and homogenised for 3-4 minutes with a Ultra-Turrax homogeniser (Janke+Kunkel, Germany) at medium speed. The extraction was covered (Nescofilm) and allowed to stand at room temperature for 1 hour before rehomogenisation. The extract was filtered through Whatman #1 filter paper on a Buchner funnel under low vacuum. The beaker was rinsed with chloroform and the washings passed through the same filter paper. 0.1M KCl was added to the filtrate to produce a two phase system. A solution of KCl was used rather than distilled water to force cholesterol sulphate into the organic phase (10). The extracts were then centrifuged at 3200 rpm for 15 minutes (MSE Chilspin) in clean glass centrifuge tubes. The upper aqueous phase was decanted and discarded and the lower organic layers pooled into a clean 100ml round botton flask. The chloroform was removed on a rotary evaporator below 40°C to leave a lipid film. This was taken up in a small volume of chloroform and transferred to a clean, dry

preweighed glass vial. The chloroform was removed under a stream of dry nitrogen and finally high vacuum. The vial was reweighed and stoppered. The lipids were stored under nitrogen at -80°C until required.

3.2.7 Thermal Analysis of Extracted Skin Lipids

The hydration of extracted skin lipids and skin lipid/surfactant mixtures was carried out by one of the following two methods:

(1) The extracted skin lipids and lipid-surfactant mixtures were hydrated as for DSPC liposomes (see 3.2.1).

(2) About 5mg of lipids were deposited, or lipid-surfactant mixtures codeposited, from chloroform directly into preweighed DSC pans, the chloroform was removed under vacuum. The pans were weighed then rehydrated at 98% humidity (see 3.2.5) for 48hr. The pans were then hermetically sealed, reweighed and percentage water content calculated. At least two samples were produced for each treatment.

3.2.8 Calibration of the Dupont 910 DSC

The Dupont 910 DSC was calibrated with reference materials to produce accurate measurements of transition temperatures (temperature calibration) and for enthalpy calculations (cell constant calibration). The unit was calibrated prior to each set of experiments under the conditions of the experimental run, and recalibrated before any change in experimental conditions, heating rate, purge gas flow or sample pan type.

The cell constant was calculated from the melting transition of pure indium metal (ΔH° = 28.4 J g^{-1}). A two point temperature calibration was carried out with pure glass distilled water (T_m = 0.0°C) and indium metal (Tm = 156.6°C).

Sample type	Temperature range (°C)
DSPC liposomes	0-75
Extracted lipids	0-85
Stratum corneum	0-140

Table 3.3 Temperature ranges used for the various sample types analysed by DSC.

3.2.9 Thermal Analysis Run Parameters

All samples were run on a Dupont 910 DSC attached to a Dupont 9900 thermal analyser unit. The samples were run in hermetically sealed pans against an empty pan as reference. The DSC head was continually purged with dry nitrogen gas. Each sample was analysed at a heating rate of 5°C min^{-1} over the temperature ranges detailed in Table 3.3.

3.2.10 Treatment of Data

The phase transition midpoint (T_m) and transition enthapy (ΔH_{cal}) were obtained using the Dupont software. H_{cal} is expressed as kJ per mole of lipid for the phospholipids and J per gram dry weight of extracted lipid and stratum corneum. The phase transition width ($\Delta T_{1/2}$) was measured directly from the DSC traces. Figures quoted are mean$\pm$standard deviation (n=4) unless otherwise stated.

3.3 RESULTS

3.3.1 Accuracy and Reproducibility of Results

The T_m value obtained for runs of the same sample was reproducible to <0.1°C. The intersample variation of a duplicate pair was slightly greater but generally reproducible to <0.2°C. $\Delta T_{1/2}$ values were measured directly from hard copies of DSC traces. Errors due to measurement and line thickness were minimal (0.05°C). $\Delta T_{1/2}$ values were normally reproducible to <0.2°C.

ΔH_{cal} values were highly dependent upon both accurate sample weighing and baseline calculation. Variation in baseline placement resulted in estimates different by up to 15% of the endotherm, the differences being greater for wide, flat transitions. All samples were weighed on a four figure balance so that for a 10mg sample there may have been errors up to 5% of the total weight.

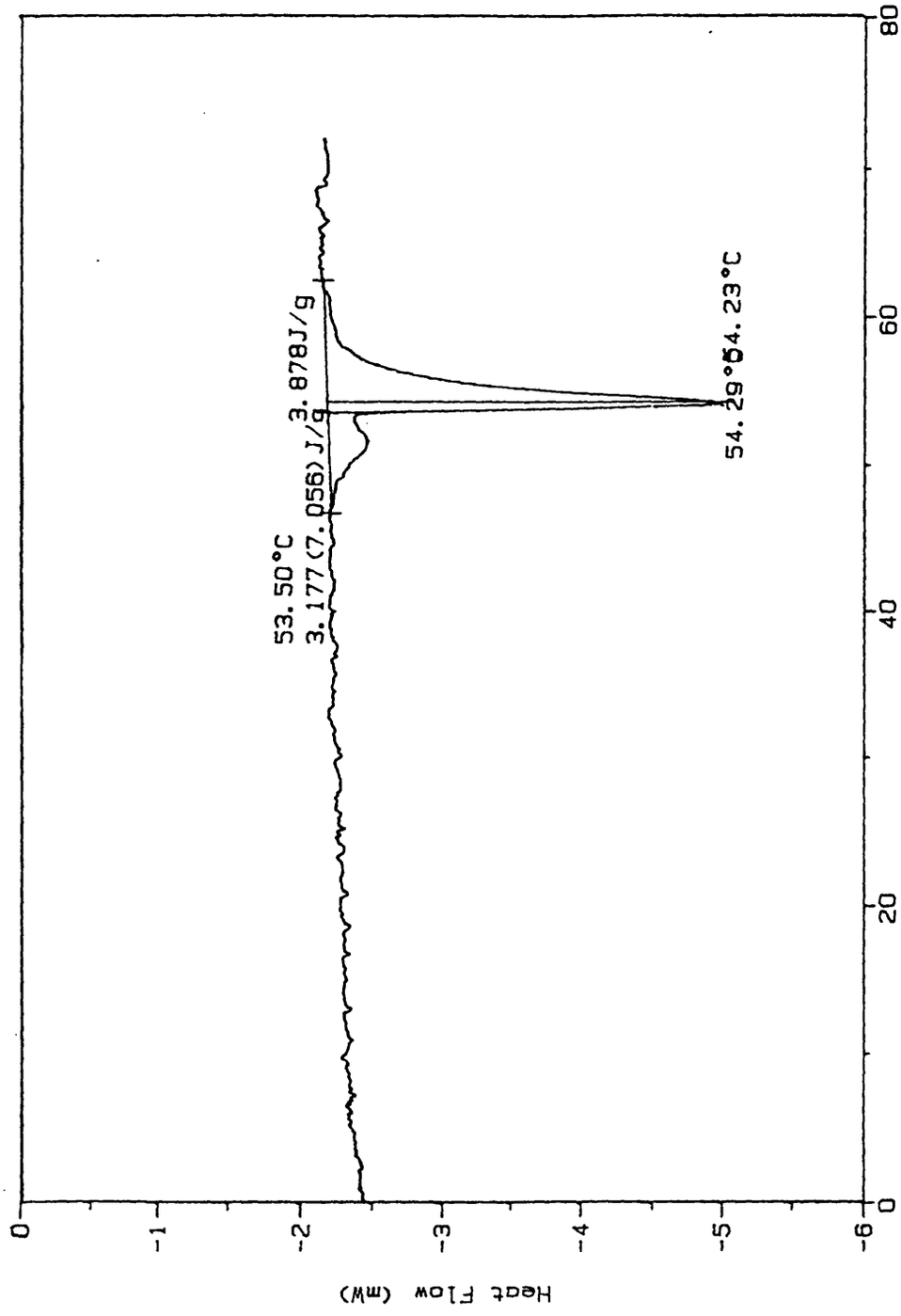

Figure 3.3 Typical DSC heating curve for pure DSPC liposomes.

3.3.2 Pure DSPC Liposomes

A typical heating curve for pure DSPC liposomes is shown in Figure 3.3. A sharp gel to liquid crystalline phase transition was observed with a T_m of 54.34±0.37°C (n=27), a $\Delta T_{1/2}$ of 1.51±0.23°C (n=27) and a peak enthalpy (ΔH_{cal}) of 44.69±10.18 kJ mole^{-1} (n=27). From these values the cooperative unit (CU) was calculated to be 53±28 molecules. A smaller broad pretransition was noted at 51.51±0.24°C with a ΔH_{cal} of 4.3KJ mole^{-1}.

3.3.3 Effect of Nonylphenyl Ether Ethoxylates

Addition of nonylphenyl ether ethoxylates to DSPC liposomes lowered T_m, increased $\Delta T_{1/2}$ and in some cases decreased ΔH_{cal} of the gel to liquid-crystalline phase transition. These effects were both structure and concentration dependent.

Figure 3.4 shows the effect of addition of increasing mole fraction NP6 upon the DSPC gel to liquid-crystalline phase transition. At a concentration of 1.6 mole% NP6 (0.1% $^{w}/_{v}$) there was no significant change to the main transition peak, but the pretransition disappeared. Below this concentration this effect was not seen and the transition profile was as for pure DSPC. As the mole fraction of NP6 increased the transition peak flattened and became broader up to 70 mole% NP6 whereafter the transition became sharper. This is shown by a plot of $\Delta T_{1/2}$ against mole fraction NP6 (Figure 3.5).

The T_m decreased linearly over the concentration range 0-70 mole% NP6 to a value of 41.81°C (Figure 3.6). An increase of concentration to 83 mole % NP6 caused T_m to reduce to 34.93°C, further increases in NP6 concentration did not further reduce T_m. There was no change in transition ΔH_{cal} with addition of NP6 to DSPC liposomes.

Addition of NP10 to DSPC liposomes also caused reduction in T_m and an increase in $\Delta T_{1/2}$ but the extent of the effects was lower than for NP6 and plateaued at a lower concentration with respect to NP6 (Figures 3.5, 3.6). NP10 did cause a

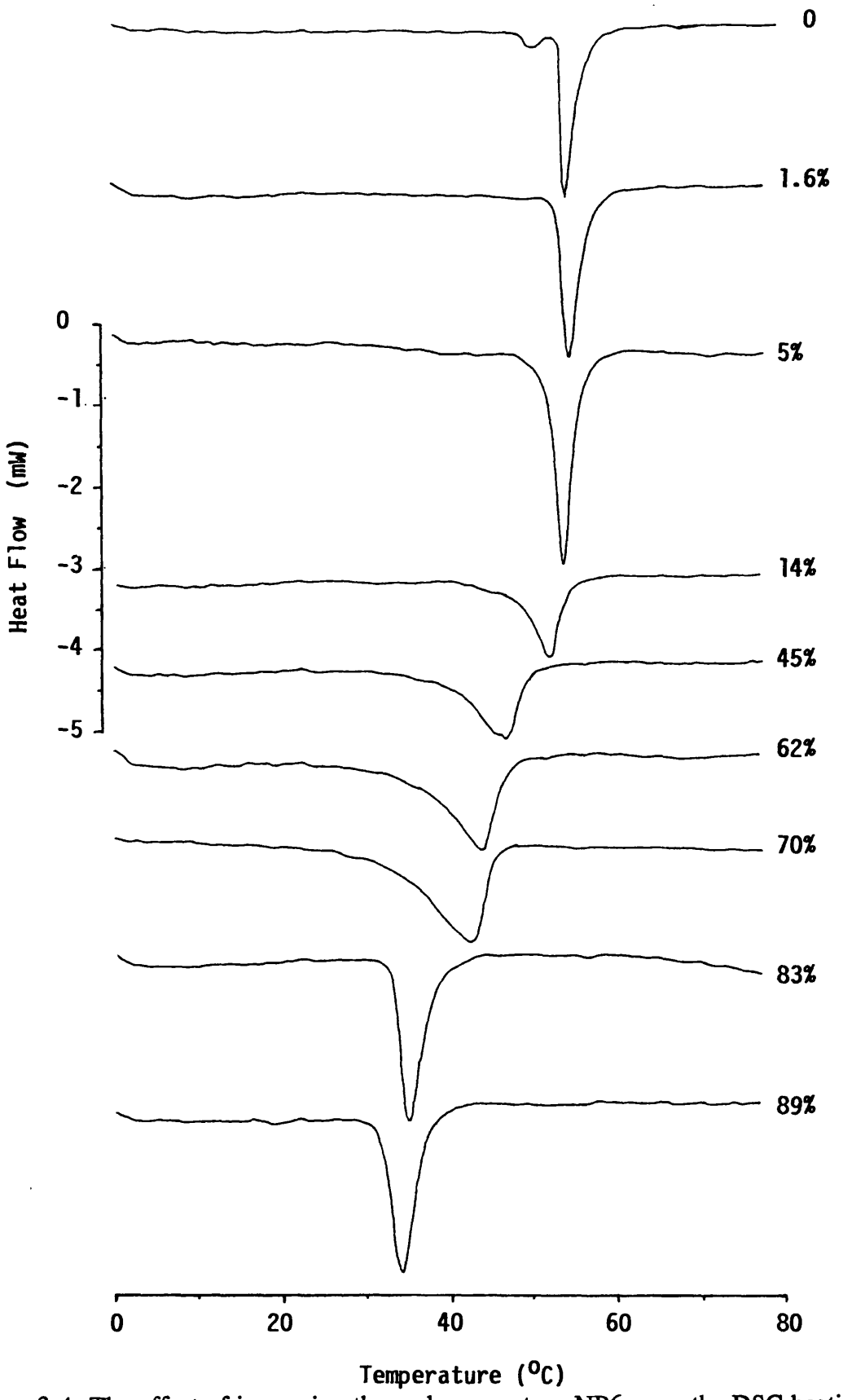

Figure 3.4 The effect of increasing the mole percentage NP6 upon the DSC heating curves for DSPC/NP6 mixed vesicles.

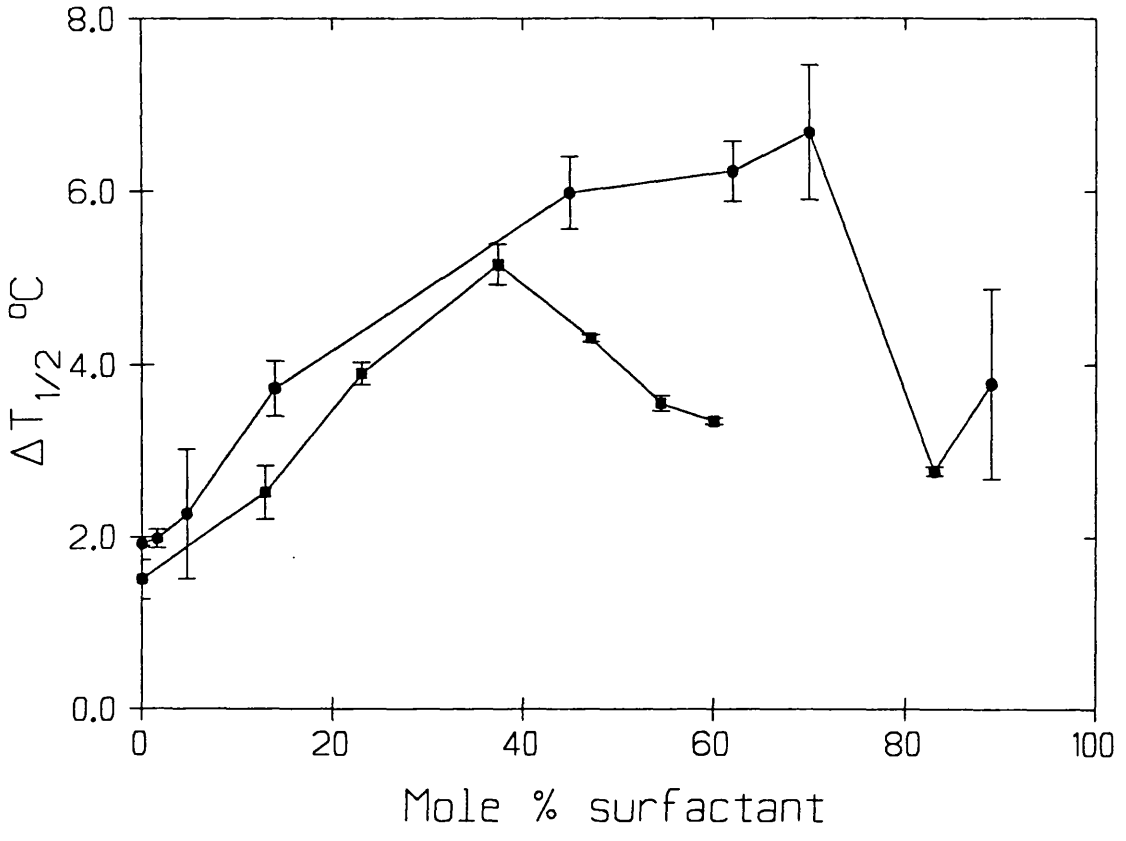

Figure 3.5 The effect of increasing mole percentage surfactant upon the value of $\Delta T_{1/2}$ for the DSPC gel-liquid crystalline phase transition. NP6 (●), NP10 (■) Mean±SD, n=4.

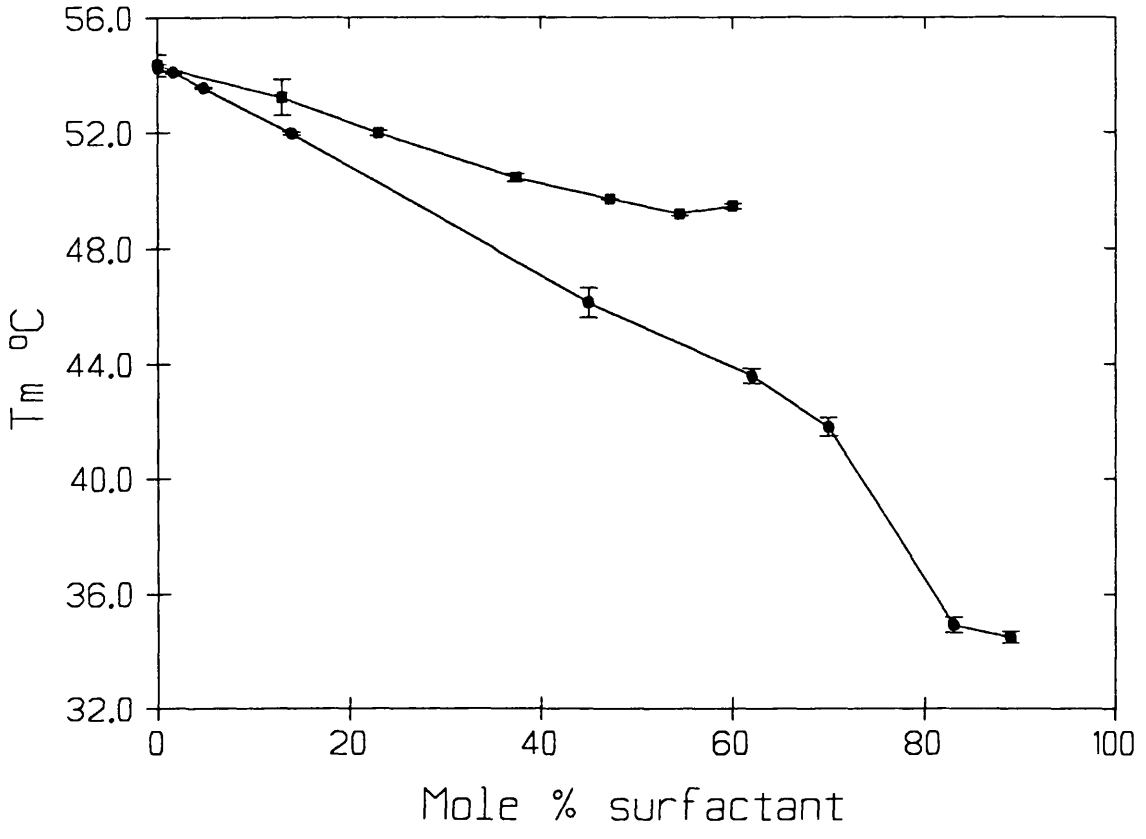

Figure 3.6 The effect of increasing mole percentage surfactant upon the value of T_m for the DSPC gel-liquid crystalline phase transition. NP6 (●), NP10 (■) Mean±SD, n=4.

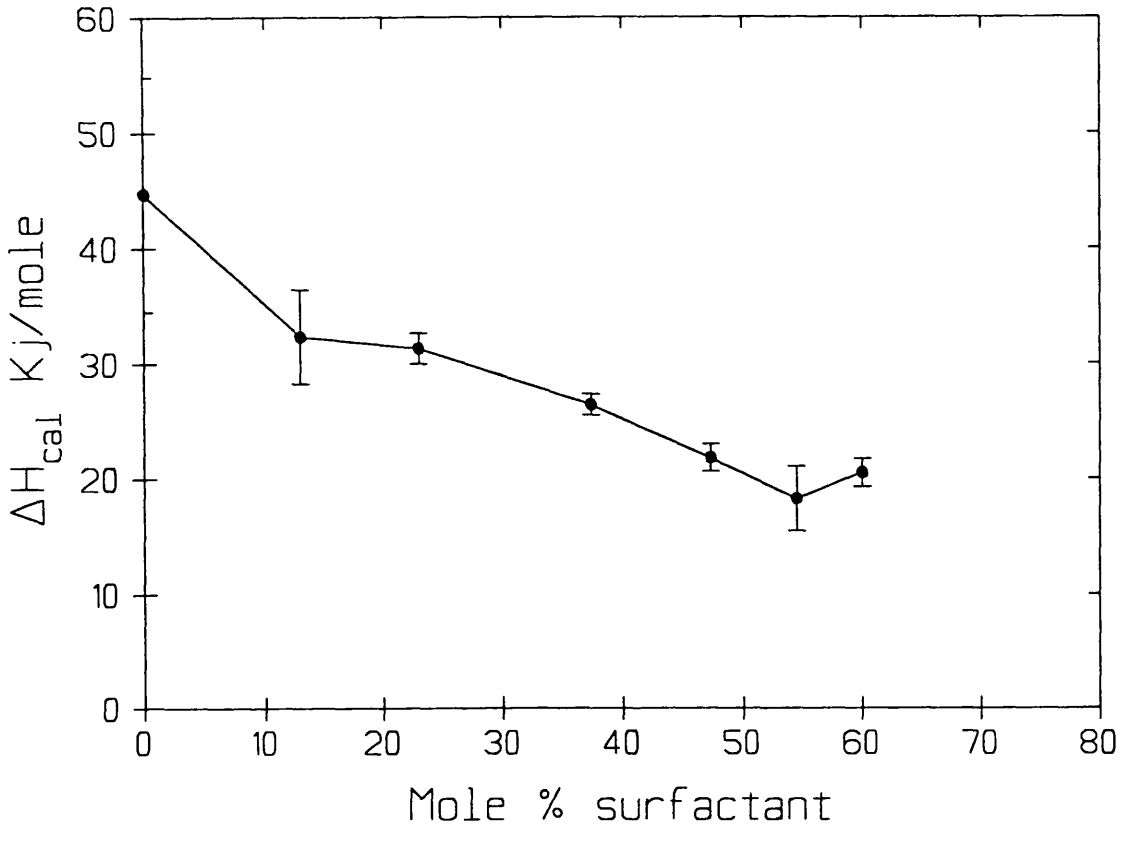

Figure 3.7 The effect of increasing mole percentage NP10 upon the value of ΔH_{cal} for the DSPC gel-liquid crystalline phase transition. Mean$\pm$SD, n=4.

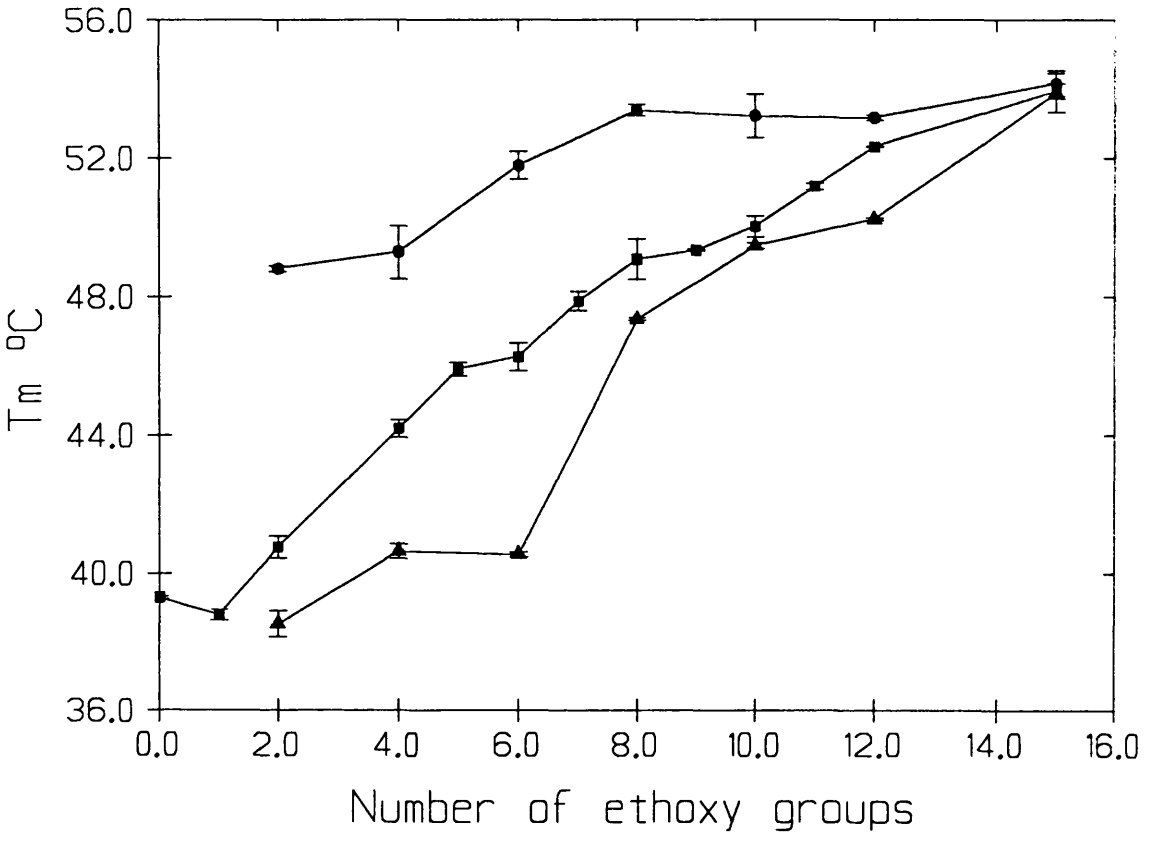

Figure 3.8 T_m values for the gel-liquid crystalline phase transition of DSPC/NPX mixed vesicles plotted as a function of surfactant ethoxy chain length. 1% (●), 5% (■) and 10% (▲) $^{w}/_{v}$ surfactant. Mean±SD, n=4.

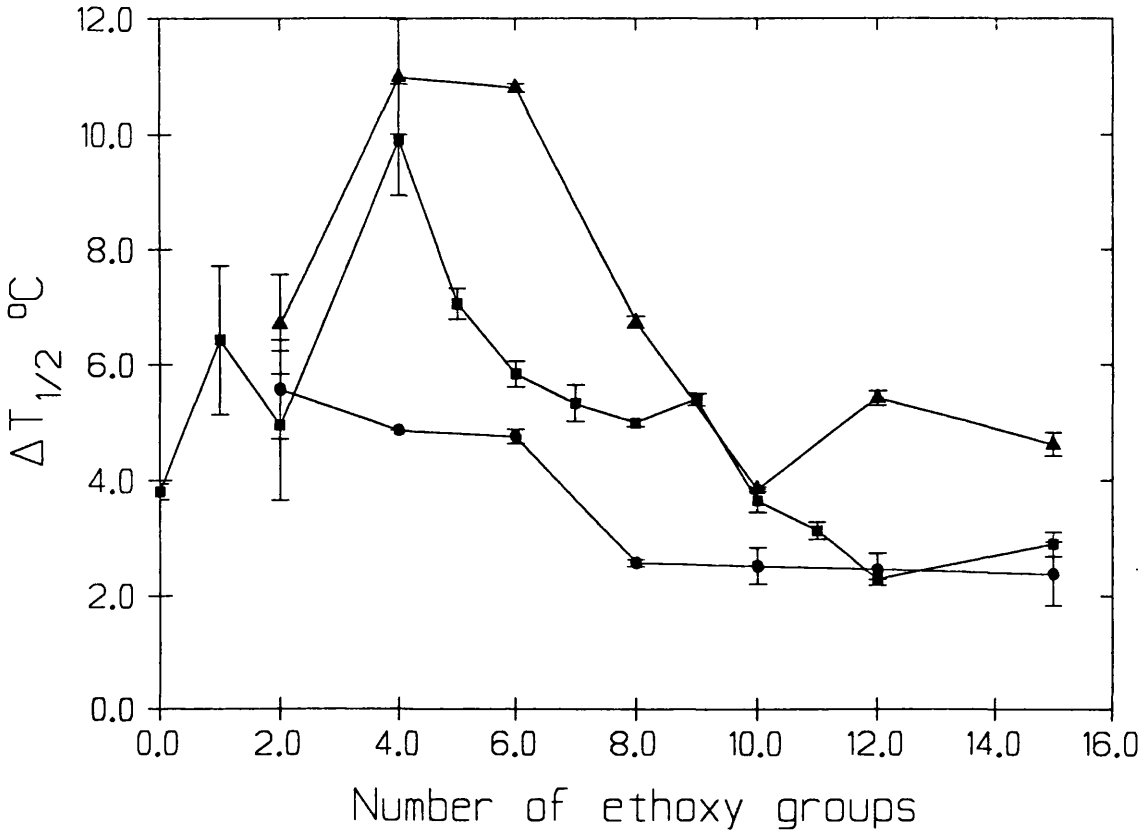

Figure 3.9 $\Delta T_{1/2}$ values for the gel-liquid crystalline phase transition of DSPC/NPX mixed vesicles plotted as a function of surfactant ethoxy chain length. 1% (●), 5% (■) and 10% (▲) $^{w}/_{v}$ surfactant. Mean±SD, n=4.

concentration dependent reduction of apparent ΔH_{cal} which decreases from 44.69 kJ mole^{-1} for pure DSPC to 18.25 kJ mole^{-1} DSPC at 54 mole% NP10 (Figure. 3.7).

The effect of the series of nonylphenyl ether ethoxylates NP0-NP15 upon the T_m of DSPC liposomes at concentrations of 1% and 10%($^{W}/_{V}$) surfactant (constant DSPC concentration) is shown in Figure 3.8. At all three concentrations the lower ethoxy content members of the series were more potent at reducing T_m. At the higher concentrations, 5 and 10%, this relationship was much more pronounced. NP15 had little effect upon T_m even at 10% whereas NP2 caused a 5.4°C reduction in T_m at 1%($^{W}/_{V}$) and a 15.4°C reduction in T_m at 10% concentration.

A similar trend was observed for the increase in $\Delta T_{1/2}$ of the phase transition (Figure 3.9). Across the range the lower HLB surfactants produced far broader transitions than the more hydrophilic surfactants which had little effect on the phase transition. No significant trends were observed in the transition enthalpies.

3.3.4 Effect of Dodecyl Ether Ethoxylates

The lowering of the T_m of the gel-liquid-crystalline phase transition of DSPC liposomes with inclusion of increasing concentrations of $C_{12}E_3$, $C_{12}E_5$ and $C_{12}E_7$ is shown in Figure 3.10. The 3 surfactants caused similar decreases in T_m up to concentration of 10 mole% surfactant. Above this concentration the curves diverged. The $C_{12}E_7$ curve flattened off to a minimum T_m of about 47°C for concentrations of 40 mole% $C_{12}E_7$ and above. A similar shaped curve was produced for $C_{12}E_5$ when a constant T_m of about 42°C occurred for 50 mole% $C_{12}E_3$ and above. For $C_{12}E_3$ a constant T_m of about 34.5°C was reached with the addition of 66 Mole% surfactant and above.

Increases in $\Delta T_{1/2}$ values for the phase transition with the incorporation of $C_{12}E_3$, $C_{12}E_5$ and $C_{12}E_7$ corresponded to decreases in T_m (Figure 3.11) except that the plateaus in $\Delta T_{1/2}$ increase were reached at lower concentrations than those for T_m decrease.

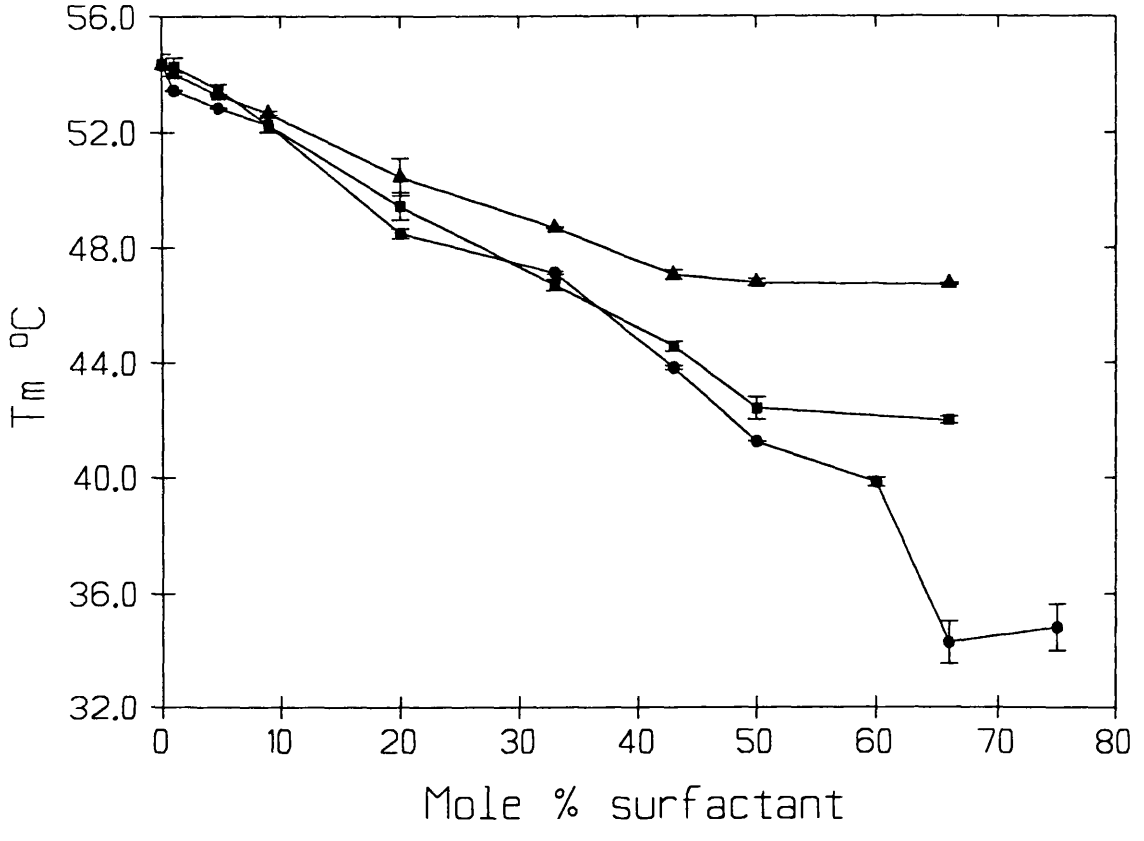

Figure 3.10 The effect of increasing mole percentage surfactant upon the value of T_m for the gel-liquid crystalline phase transition in DSPC/$C_{12}E_n$ mixed vesicles. $C_{12}E_3$ (●), $C_{12}E_5$ (■), $C_{12}E_7$ (▲). Mean±SD, n=4.

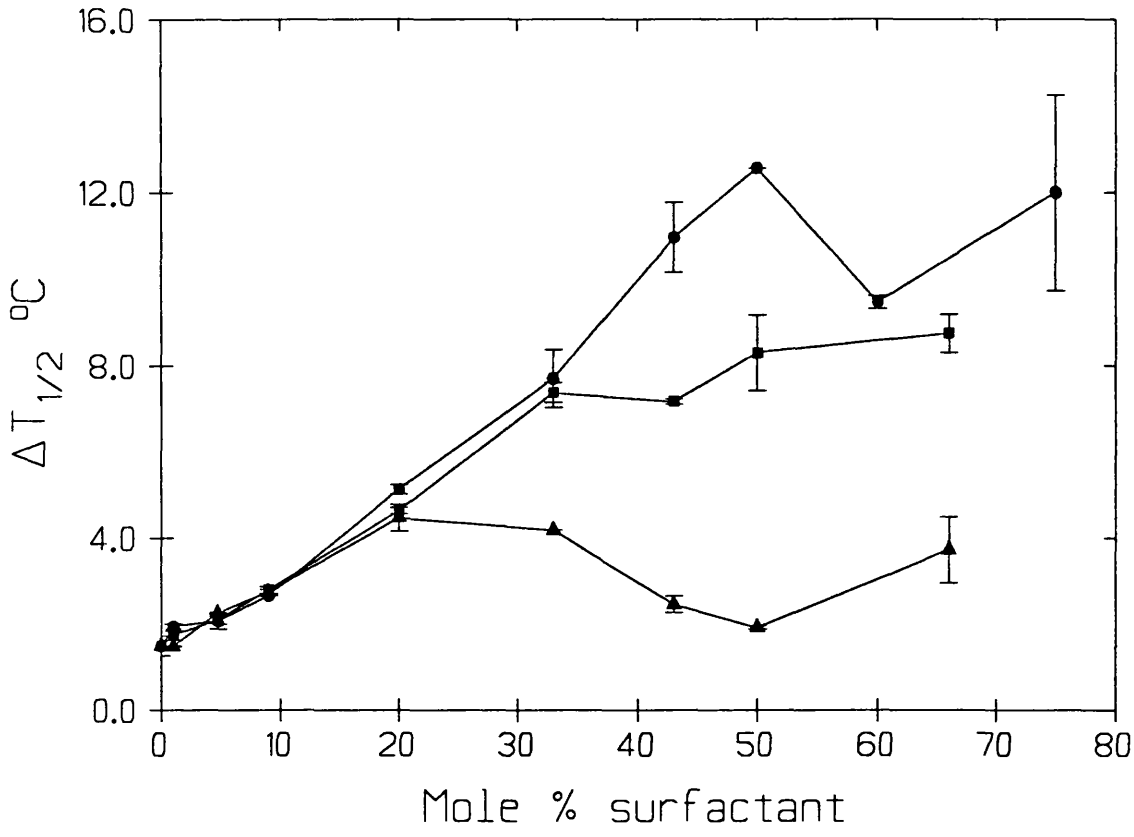

Figure 3.11 The effect of increasing mole percentage surfactant upon the value of $\Delta T_{1/2}$ for the gel-liquid crystalline phase transition in DSPC/$C_{12}E_n$ mixed vesicles. $C_{12}E_3$ (●), $C_{12}E_5$ (■), $C_{12}E_7$ (▲). Mean±SD, n=4.

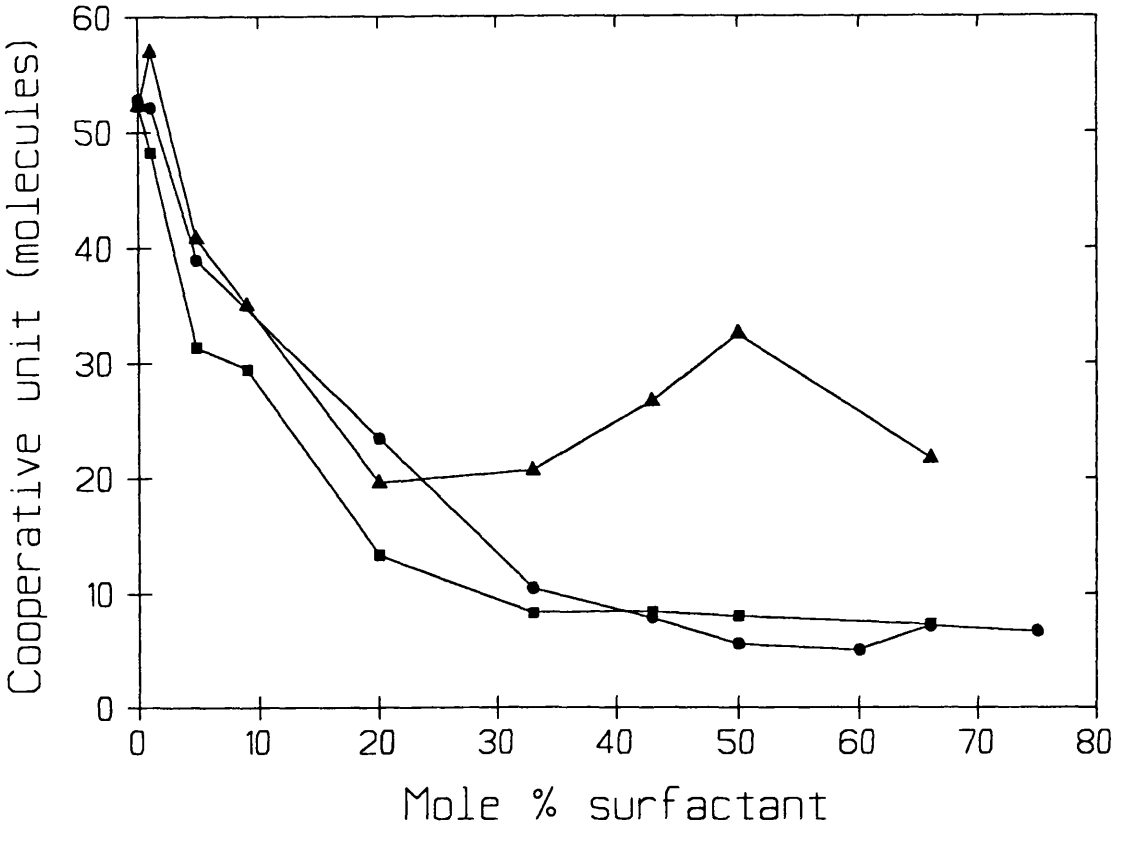

Figure 3.12 The effect of increasing mole percentage surfactant upon the value of the cooperative unit for the gel-liquid crystalline phase transition in DSPC/$C_{12}E_n$ mixed vesicles. $C_{12}E_3$ (●), $C_{12}E_5$ (■), $C_{12}E_7$ (▲). Mean values.

The cooperative unit of the phase transition was calculated for increasing concentrations of $C_{12}E_3$, $C_{12}E_5$ and $C_{12}E_7$ (Figure 3.12). Both $C_{12}E_3$ and $C_{12}E_5$ caused a rapid decrease in the size of the CU between 0 and 30 mole% surfactant when a minimum value was reached. Above this point further increases in concentration produced no charge in the CU. With $C_{12}E_7$ the size of the calculated CU was a complex function of surfactant concentration. A decrease was observed up to 20 mole% $C_{12}E_7$ where a minimum was reached. Increases in concentration above this value caused an increase in size of the calculated size of the CU followed by a decrease above 50 mole% surfactant.

The DSC heating profiles of pure DSPC and DSPC/surfactant vesicles incorporating the surfactant range $C_{12}E_0$-$C_{12}E_8$ at 50 mole% surfactant concentration, (1:1 molar ratio) are shown in Figure 3.13. Dodecyl alcohol, $C_{12}E_0$, removed the pretransition but had little effect upon the main transition. As the ethoxy content of the surfactant increased from $C_{12}E_0$-$C_{12}E_3$ there was an increase in the reduction of Tm and broadening of $\Delta T_{1/2}$. As ethoxy chain length increased further, $C_{12}E_3$-$C_{12}E_8$, this trend was reversed; the reduction in Tm and increase in $\Delta T_{1/2}$ becoming smaller. T_m and $\Delta T_{1/2}$ values are presented graphically as a function of surfactant ethoxy chain length in Figures 3.14 and 3.15 respectively. Mixed micelles containing either $C_{12}E_5$ or $C_{12}E_6$ showed biphasic melting transitions with two peak maxima (Figure 3.13). In Figure 3.14 the higher of the two T_m values were plotted. Figures 3.14 and 3.15 also show the effect of the same surfactant series, $C_{12}E_0$-$C_{12}E_8$, upon DSPC phase transition T_m and $\Delta T_{1/2}$ at a 1:0.1 lipid to surfactant molar ratio (9 mole% surfactant). No relationship could be deduced between surfactant ethoxy chain length and transition enthalpy.

The size of the cooperative unit of the transition is shown as a function of surfactant ethoxy chain length in Figure 3.16 at 9 and 50 mole% surfactant. No clear relationship can be seen on 9 mole% surfactant but at 50 mole% the reduction in the size of the CU followed the same trend across the series as for the reduction in T_m and increase in $\Delta T_{1/2}$.

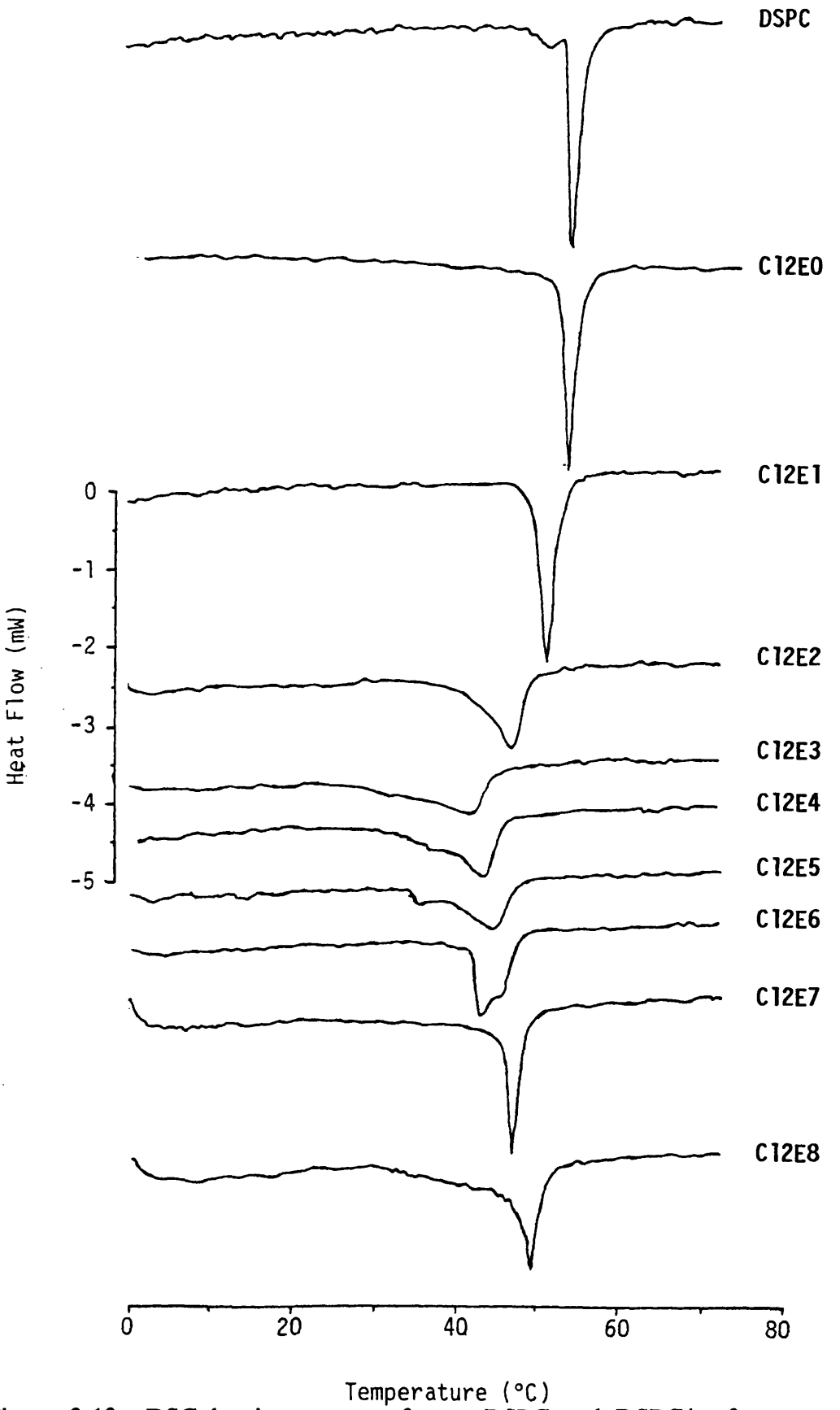

Figure 3.13 DSC heating curves of pure DSPC and DSPC/surfactant vesicles incorperating $C_{12}E_0$-$C_{12}E_8$ at 50 mole% surfactant.

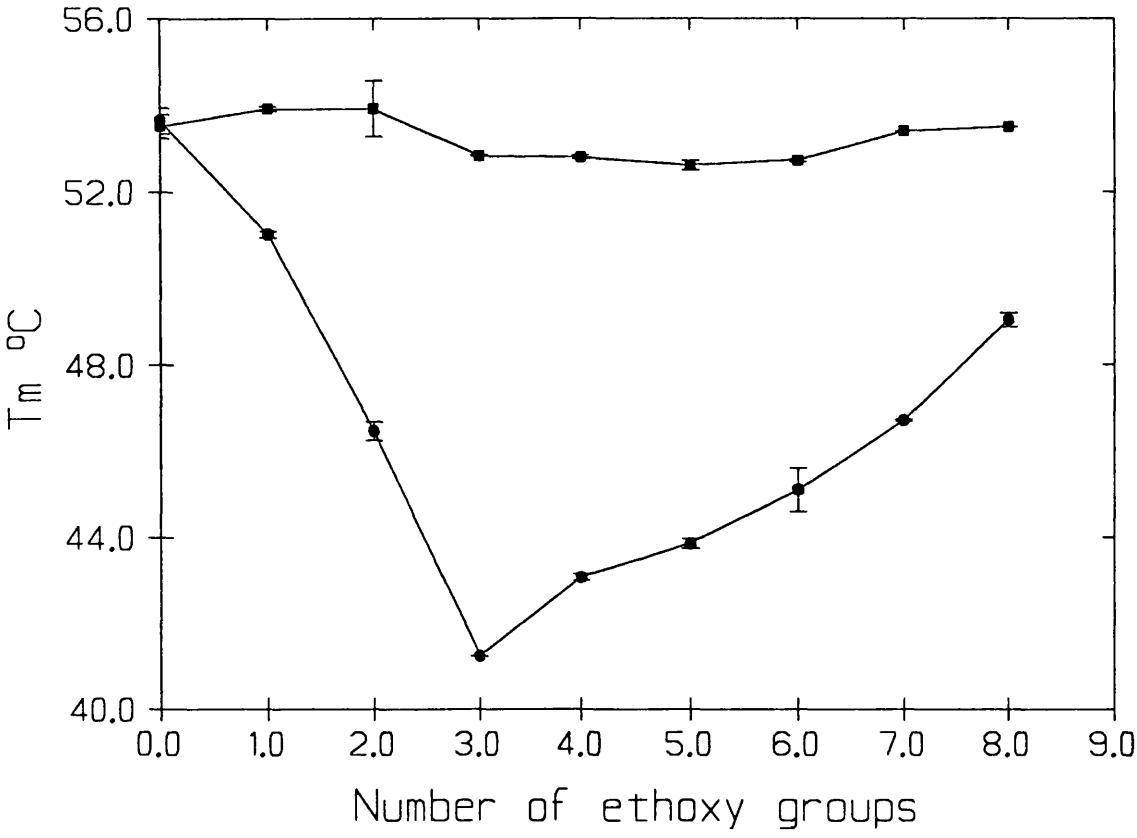

Figure 3.14 T_m values for the gel-liquid crystalline phase transition of DSPC/$C_{12}E_n$ mixed vesicles plotted as a function of surfactant ethoxy chain length. 9 (■), and 50 (●) mole% surfactant. Mean±SD, n=4.

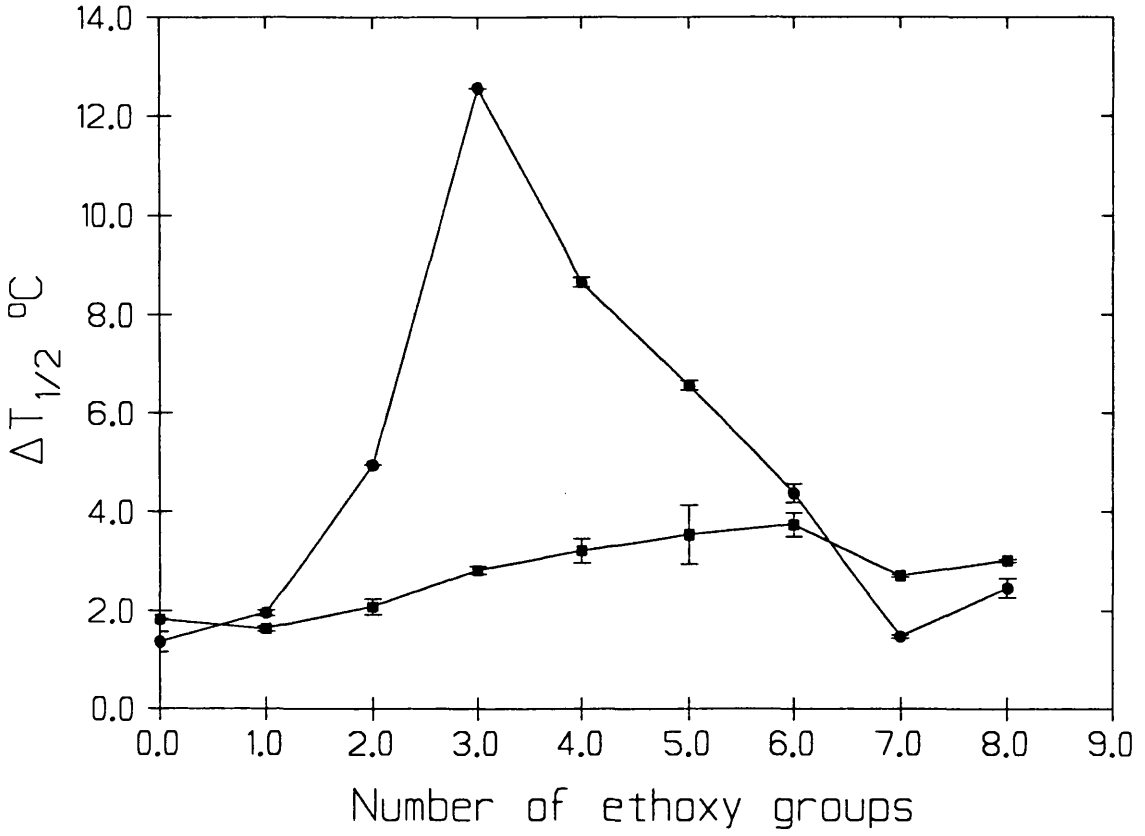

Figure 3.15 $\Delta T_{1/2}$ values for the gel-liquid crystalline phase transition of DSPC/$C_{12}E_n$ mixed vesicles plotted as a function of surfactant ethoxy chain length. 9 (■) and 50 (●) mole% surfactant. Mean±SD, n=4.

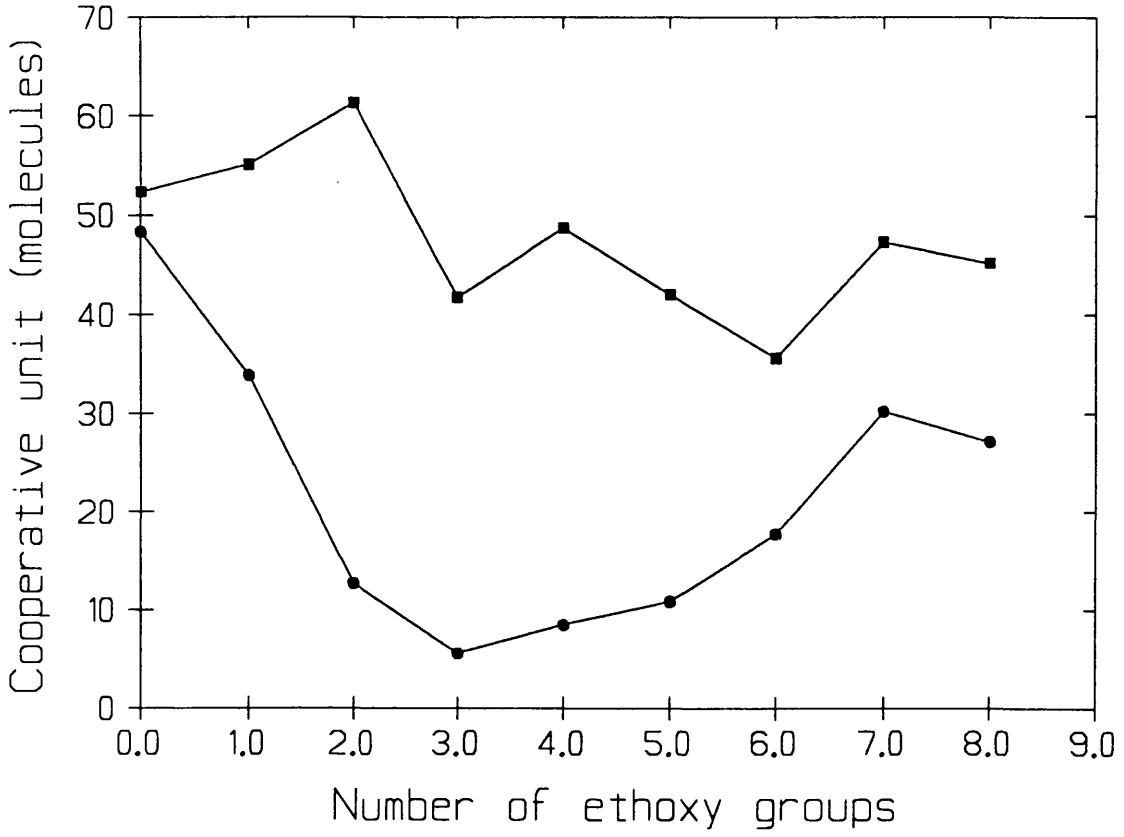

Figure 3.16 Size of the cooperative unit for the gel-liquid crystalline phase transition of DSPC/$C_{12}E_n$ mixed vesicles plotted as a function of surfactant ethoxy chain length. 9 (■), and 50 (●) mole% surfactant. Mean values.

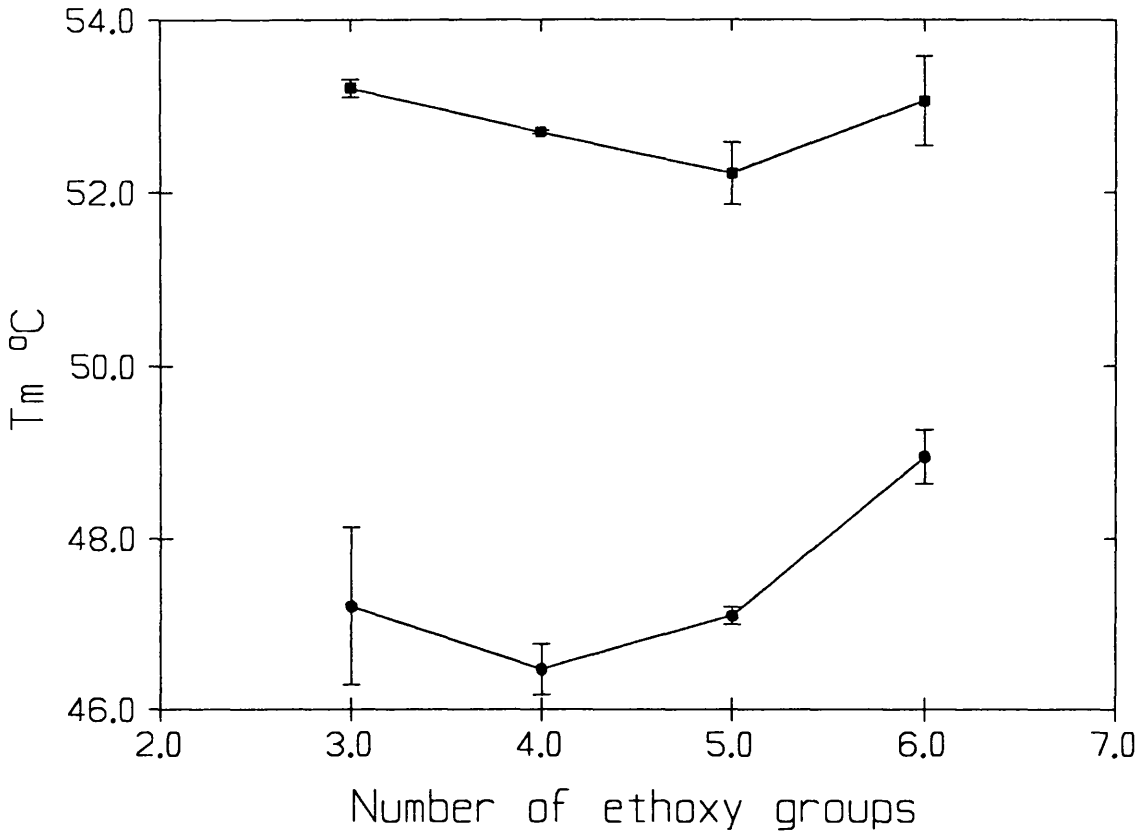

Figure 3.17 T_m values for the gel-liquid crystalline phase transition of DSPC/$C_{10}E_n$ mixed vesicles plotted as a function of surfactant ethoxy chain length. 9 (■), and 50 (●) mole% surfactant. Mean±SD, n=4.

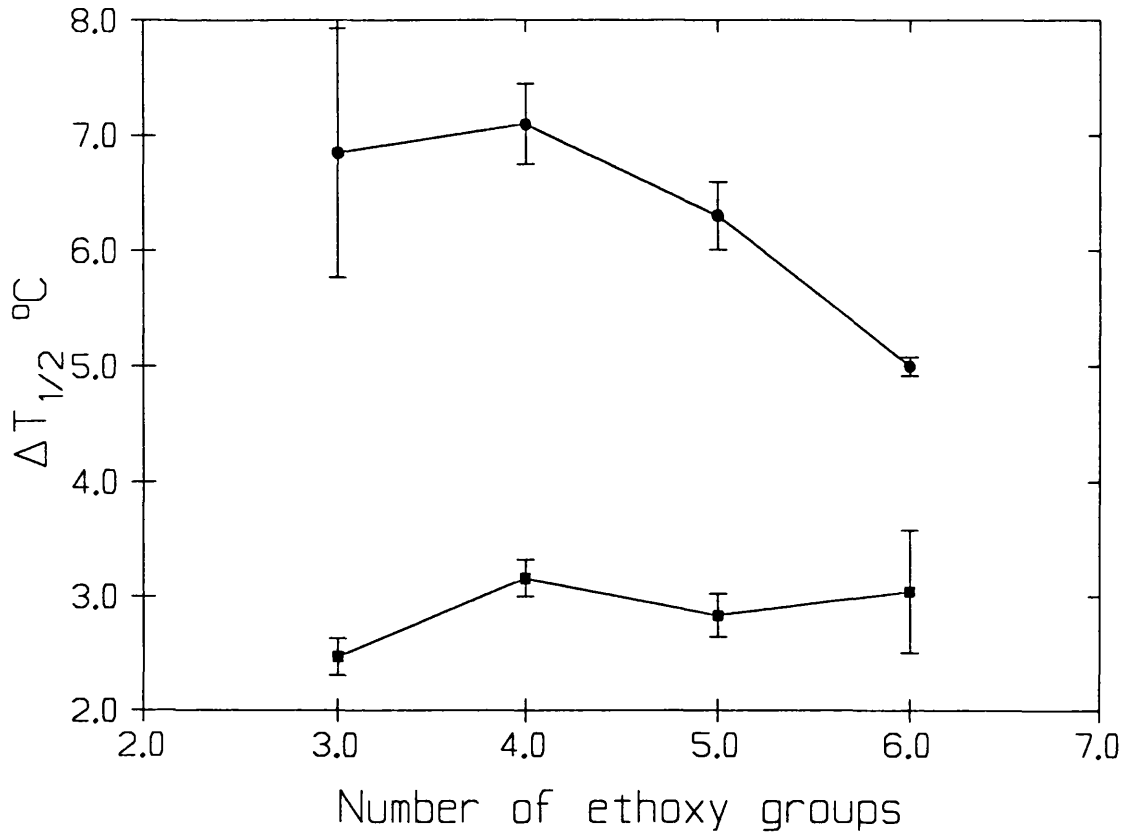

Figure 3.18 $\Delta T_{1/2}$ values for the gel-liquid crystalline phase transition of DSPC/$C_{10}E_n$ mixed vesicles plotted as a function of surfactant ethoxy chain length. 9 (■) and 50 (●) mole% surfactant. Mean±SD, n=4.

3.3.5 Effect of Decyl Ether Ethoxylates

Figures 3.17 and 3.18 show the effect of incorporation of 9 and 50 mole% $C_{10}E_3$-$C_{10}E_6$ upon the T_m and $\Delta T_{1/2}$ of the DSPC phase transition respectively. There was no significant difference between surfactants at 9 mole% surfactant. At 50 mole% $C_{10}E_4$ produced the greatest effect upon T_m and $\Delta T_{1/2}$ although the effect was not statistically different from the effects of $C_{10}E_3$ (t-test, $p<0.05$).

3.3.6 Effect of Azone, Brij 30 and Brij 36T

The T_m, $\Delta T_{1/2}$ ΔH_{cal} and calculated cooperative unit size of DSPC liposomes and mixed vescicles of DSPC with 9 and 50 mole% Azone and 50 mole% Brij series surfactants are given in Table 3.4.

3.3.7 Effect of Total Surfactant and DSPC Concentration

Table 3.5 gives the T_m, $\Delta T_{1/2}$ and ΔH_{cal} values for 1:1 molar mixtures of DSPC with $C_{12}E_3$ and $C_{12}E_7$ at concentrations of 0.126M and 0.0126M. No significant differences were observed in T_m or $\Delta T_{1/2}$ between the two concentrations for either surfactant (t-test, $p<0.05$). However for both $C_{12}E_3$ and $C_{12}E_7$ addition the ΔH_{cal} value was lower at 0.0126M total surfactant.

3.3.8 The Influence of Surfactant Hydrophile-lipophile Balance (HLB)

The compiled data for the effects of 3 surfactant series, NP2-NP15, $C_{12}E_0$-$C_{12}E_8$, $C_{10}E_3$-$C_{10}E_6$ and the Brij surfactants upon the DSPC T_m at 50 mole% surfactant is shown plotted as a function of surfactant ethoxy content (Figure 3.19) and calculated HLB values (Figure 3.20).

Surfactant	T_m(°C)	$\Delta T_{1/2}$(°C)	ΔH_{cal}	C U
DSPC only	54.34±0.37	1.51±0.23	44.69±10.18	52.8±28
9 mole% Azone	52.72±0.01	3.27±0.21	28.04±4.31	38.5
50 mole% Azone	41.48±0.03	6.47±0.53	23.38±6.63	21.7
50 mole% Brij 30	47.36±0.20	8.45±0.11	50.87±9.21	7.93
50 mole% Bjij 36T	48.18±0.11	3.43±0.11	46.37±1.69	21.56

Table 3.4 The effect of Azone, Brij 30 and Brij 36T upon the thermal characteristics of DSPC liposomes

Concentration	DSPC + $C_{12}E_3$		
	T_m(°C)	$\Delta T_{1/2}$(°C)	ΔH_{cal}
0.126M	38.98±1.06	11.01±0.47	43.09±1.20
0.0126M	38.75±0.02	10.00±1.37	35.39±3.46
	DSPC + $C_{12}E_7$		
	T_m(°C)	$\Delta T_{1/2}$(°C)	ΔH_{cal}
0.126M	45.76±0.69	2.54±0.24	47.24±2.01
0.0126	46.82±0.02	2.57±0.41	32.61±0.41

Table 3.5 The effect of surfactant/DSPC concentration upon the thermal characteristics of 1:1 molar mixes of DSPC/$C_{12}E_3$ and DSPC/$C_{12}E_7$ (mean±SD, n=4)

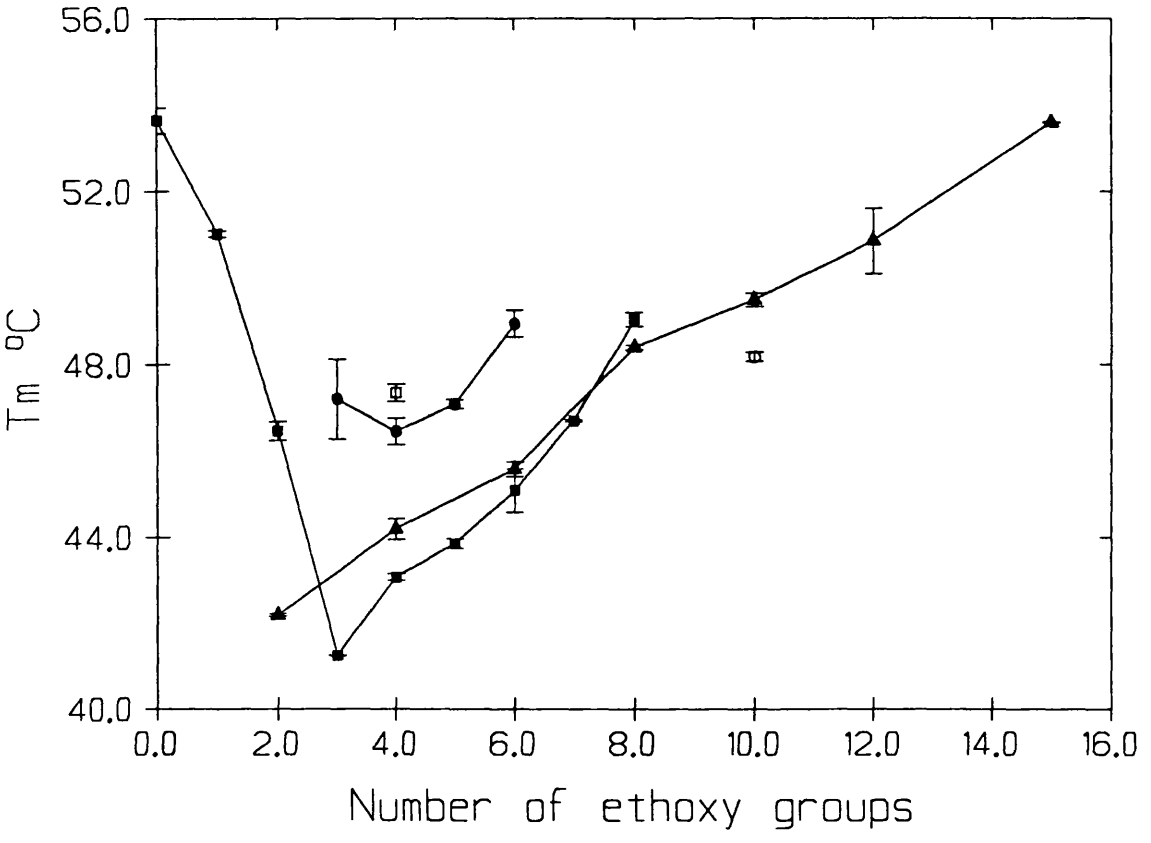

Figure 3.19 T_m values for the gel-liquid crystalline phase transition for DSPC/surfactant mixed vesicles plotted as a function of surfactant ethoxy chain length. NPX (▲), $C_{12}E_n$ (■), $C_{10}E_n$ (●), Brij 30 (□) and Brij 36T (○). Mean±SD, n=4.

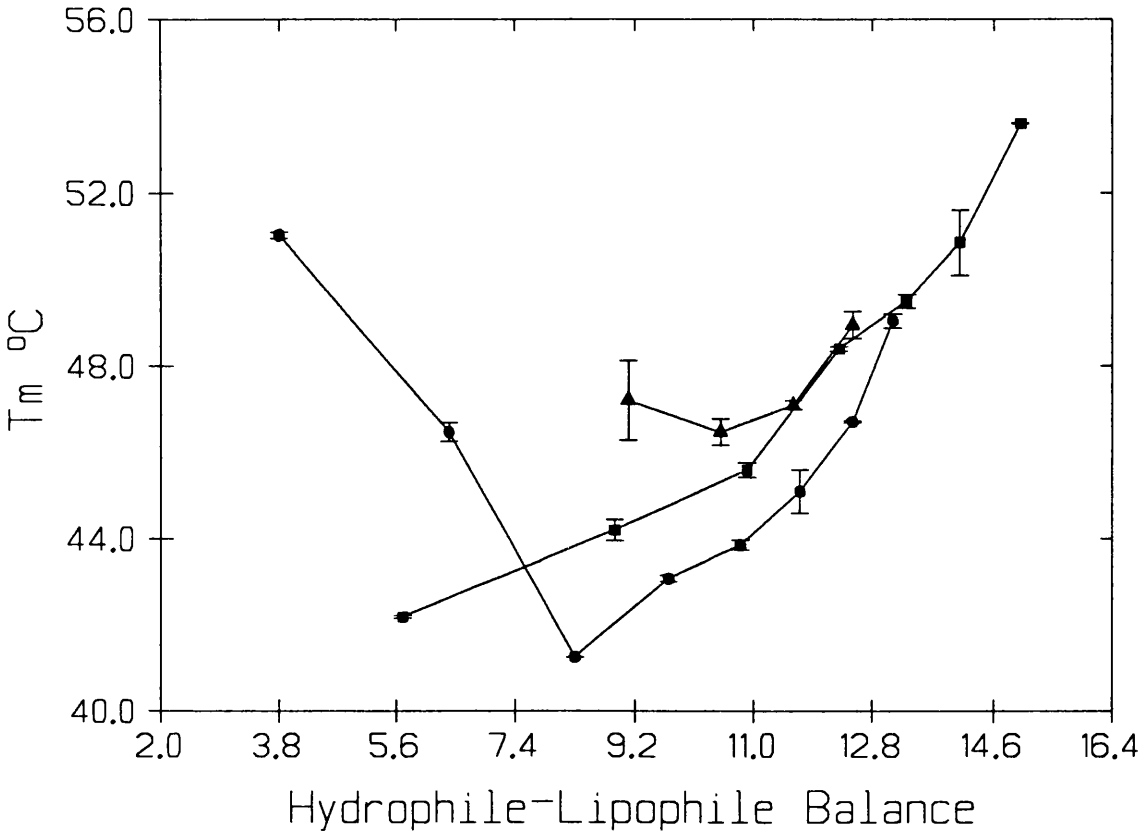

Figure 3.20 T_m values for the gel-liquid crystalline phase transition for DSPC/surfactant mixed vesicles plotted as a function of calculated surfactant hydrophile-lipophile balance. NPX (■), $C_{12}E_n$ (●), $C_{10}E_n$ (▲). Mean±SD, n=4.

3.3.9 Extracted Porcine Stratum Corneum Lipids

Solvent treatment of the stratum corneum (see 3.2.6) extracts the intercellular lipid. The solvent extracted material constituted 11.3±3.4% (n=5) by weight of the stratum corneum.

Hydration of the extracted lipids at 98% relative humidity, method 2 (see 3.2.7), caused an average of 0.12±0.07mg (n=10) of water per mg of dry lipid to be taken up by the sample.

Figure 3.21 shows a typical thermal transition profile for the heating of rehydrated porcine stratum corneum lipids. The lipids underwent a single broad transition with an average T_m of 56.0±1.87°C, a $\Delta T_{1/2}$ of 19.07±1.97°C and a ΔH_{cal} of 29.36±4.89 J g^{-1} hydrated lipid. These values are means and standard deviations of duplicate samples from five preparations.

Lipids hydrated by the addition of PBS pH 7.4 to produce 10%($^{w}/_{v}$) lipid mixtures produced similar shape transition profiles. No difference was observed in Tm for the two methods of hydration but the latter hydration with PBS produced lower $\Delta T_{1/2}$ (13.45±1.33°C) and ΔH_{cal} (24.52±0.51) values.

3.3.10 Effect of Dodecyl Ether Ethoxylates on Extracted Stratum Corneum Lipids

Individual lipid extractions showed some intersample variation in their thermal properties. Investigations of surfactant treatment, with a series of surfactants, were therefore carried out on a single batch of extracted lipid.

The addition of the dodecyl ether ethoxylates $C_{12}E_1$-$C_{12}E_7$ caused an increase in the percentage uptake of water upon hydration at 95% relative humidity (Table 3.6) and a decrease in transition T_m, $\Delta T_{1/2}$ and ΔH_{cal} with respect to extracted lipid in the absence of surfactant. The thermal transition data (n=2) is presented graphically as a function of surfactant ethoxy chain length in Figures 3.22, 3.23 and 3.24.

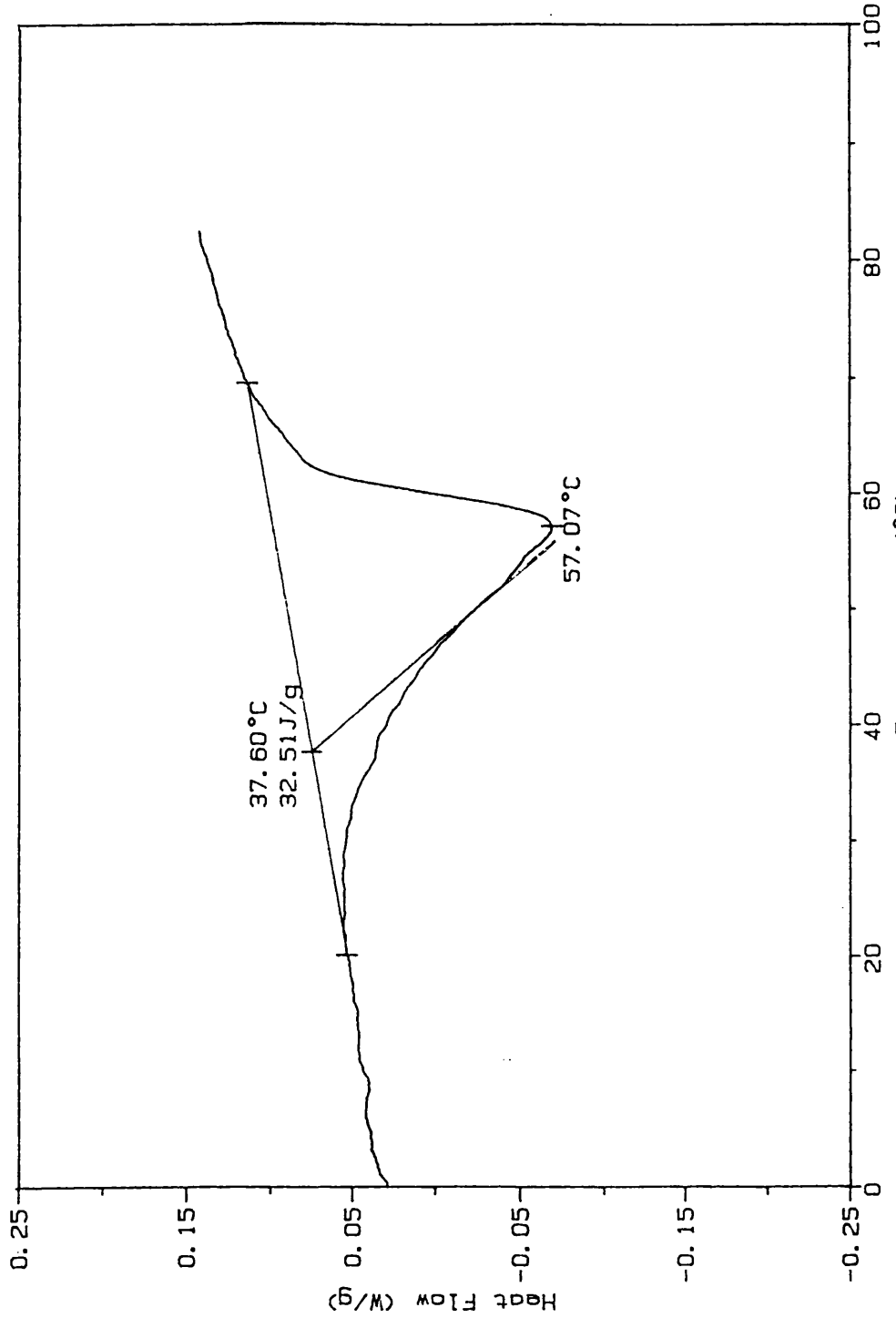

Figure 3.21 Typical DSC heating curve for rehydrated, extracted porcine stratum corneum lipids.

Surfactant	Hydration[a]
Lipid only	18.55±4.87
$C_{12}E_1$	23.05±1.48
$C_{12}E_2$	29.30±2.54
$C_{12}E_3$	31.25±0.64
$C_{12}E_4$	33.05±0.97
$C_{12}E_5$	28.25±0.07
$C_{12}E_6$	29.60±0.71
$C_{12}E_7$	29.25±1.76

[a] mg H_2O/mg dry lipid, Mean ± range, n=2

Table 3.6 The effect of surfactants on the hydration of extracted porcine stratum corneum lipid.

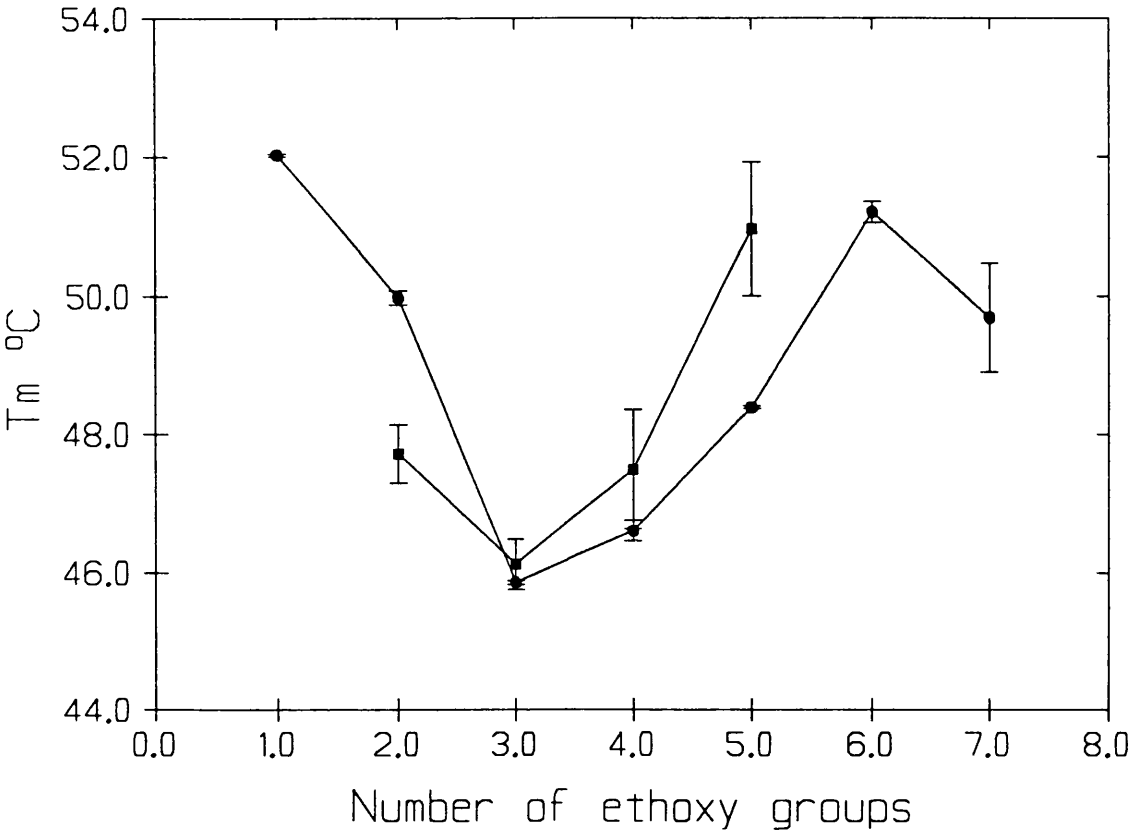

Figure 3.22 T_m values for the phase transition obtained with extracted porcine stratum corneum lipid/surfactant mixtures plotted as a function of surfactant ethoxy chain length for two lipid samples; A (●) and B (■). Mean±range, n=2

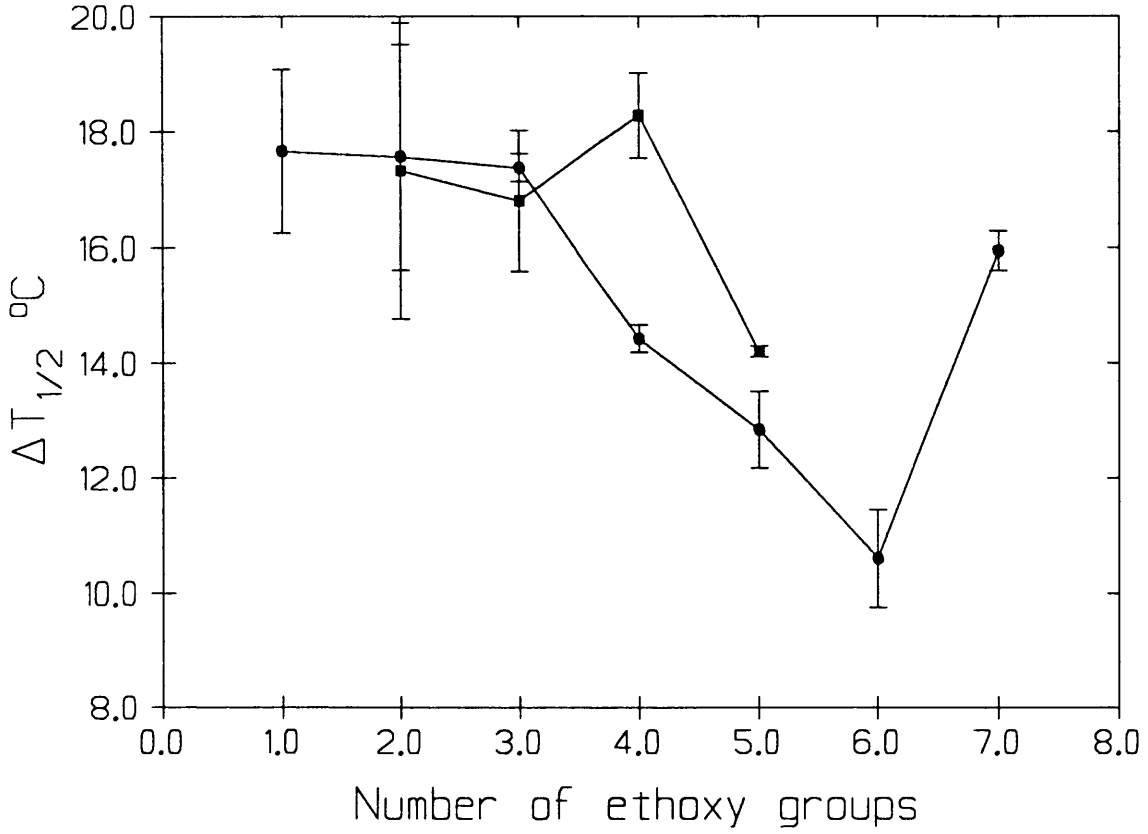

Figure 3.23 $\Delta T_{½}$ values for the phase transition obtained with extracted porcine stratum corneum lipid/surfactant mixtures plotted as a function of surfactant ethoxy chain length for two lipid samples; A (●) and B (■). Mean±range, n=2.

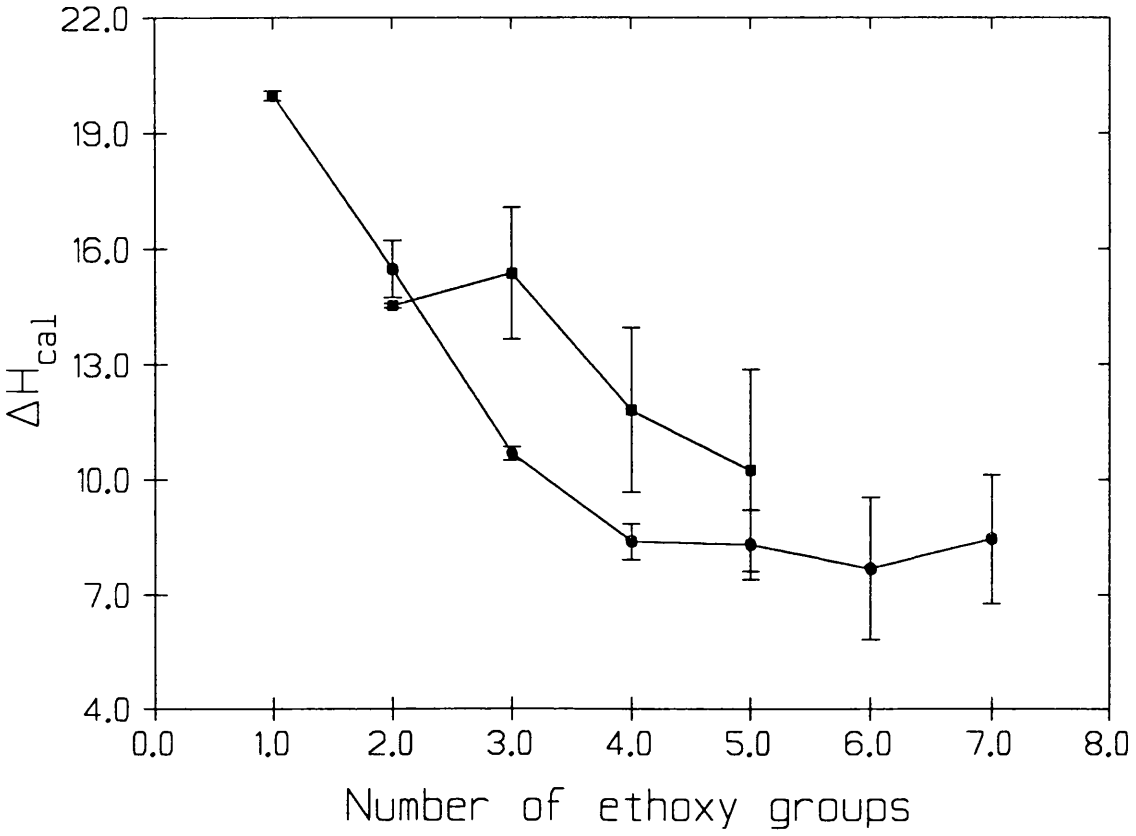

Figure 3.24 ΔH_{cal} values for the phase transition obtained with extracted porcine stratum corneum lipid/surfactant mixtures plotted as a function of surfactant ethoxy chain length for two lipid samples; A (●) and B (■). Mean±range, n=2

Over the series $C_{12}E_1$-$C_{12}E_7$ T_m reduced to a minimum with $C_{12}E_3$ incorporation and then rose again as ethoxy chain length increased (Figure 3.22). The $\Delta T_{½}$ and ΔH_{cal} values did not follow this pattern. As the ethoxy chain length of the surfactant increased both $\Delta T_{½}$ (Figure 3.23) and ΔH_{cal} (Figure 3.24) decreased for the whole series studied.

3.3.11 Isolated Stratum Corneum

Rehydration of the desiccated stratum corneum at 98% relative humidity caused a mass increase of 26.58±9.9% ($^{W}/_{W}$) (n=25) which corresponds to 0.26±0.1 mg of water being taken up per mg of dry tissue. Hexane washing had no effect on this rehydration.

Figure 3.25 shows a typical heating trace of hydrated human stratum corneum. Three endotherms were observed upon primary heating centered at 67.01±2.05°C, 78.41±3.51°C and 93.23±4.33°C (mean±SD, n=15). The corresponding ΔH_{cal} values were 1.17±0.34 J g^{-1}, 0.558±0.15 J g^{-1} and 1.29±0.40 J g^{-1} respectively.

Upon reheat of the sample over the same temperature range the third transition disappeared and the first two peaks combined to form a single biphasic peak (e.g. Figure 3.25). The two peak maxima of this transition were 62.74±1.44°C and 70.35±1.69°C. It was impossible to resolve the transition endotherms separately; the ΔH_{cal} value overall was 2.33±0.96 g^{-1} dry tissue.

Porcine stratum corneum showed similar transition profiles, upon primary heating, to human tissue (Figure 3.26). However the T_m and ΔH_{cal} values of the three peaks were different to human stratum corneum (Table 3.7). T_m was 5-10°C lower for the first and second peaks of porcine skin. The reheat of porcine stratum corneum produced a single endotherm with a T_m of 57.82±1.69°C and a ΔH_{cal} of 1.84±0.27 J g^{-1} (n=5). (Figure 3.26).

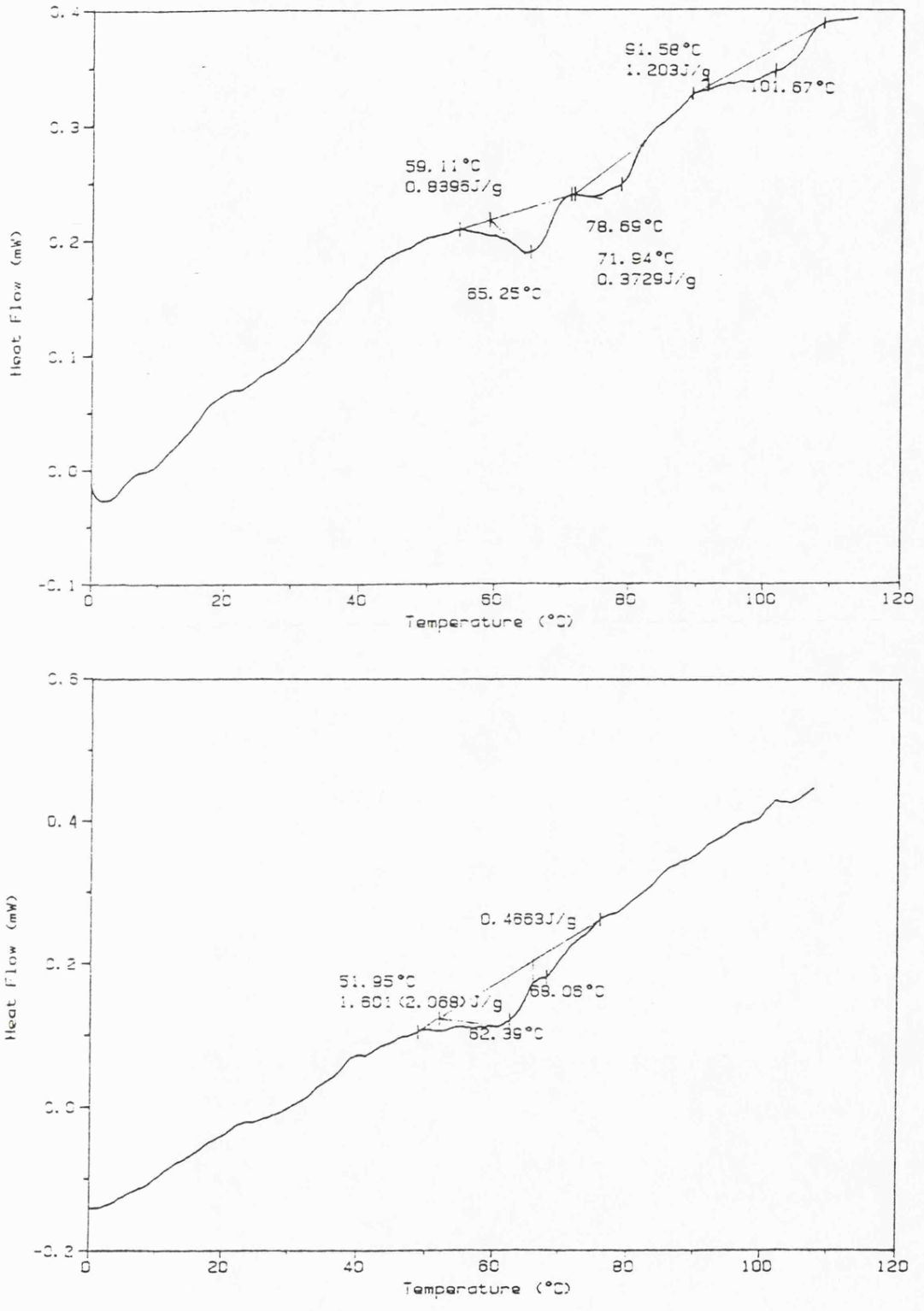

Figure 3.25 Typical heating curves for untreated, hydrated human stratum corneum. Primary heating (top) and reheat (bottom).

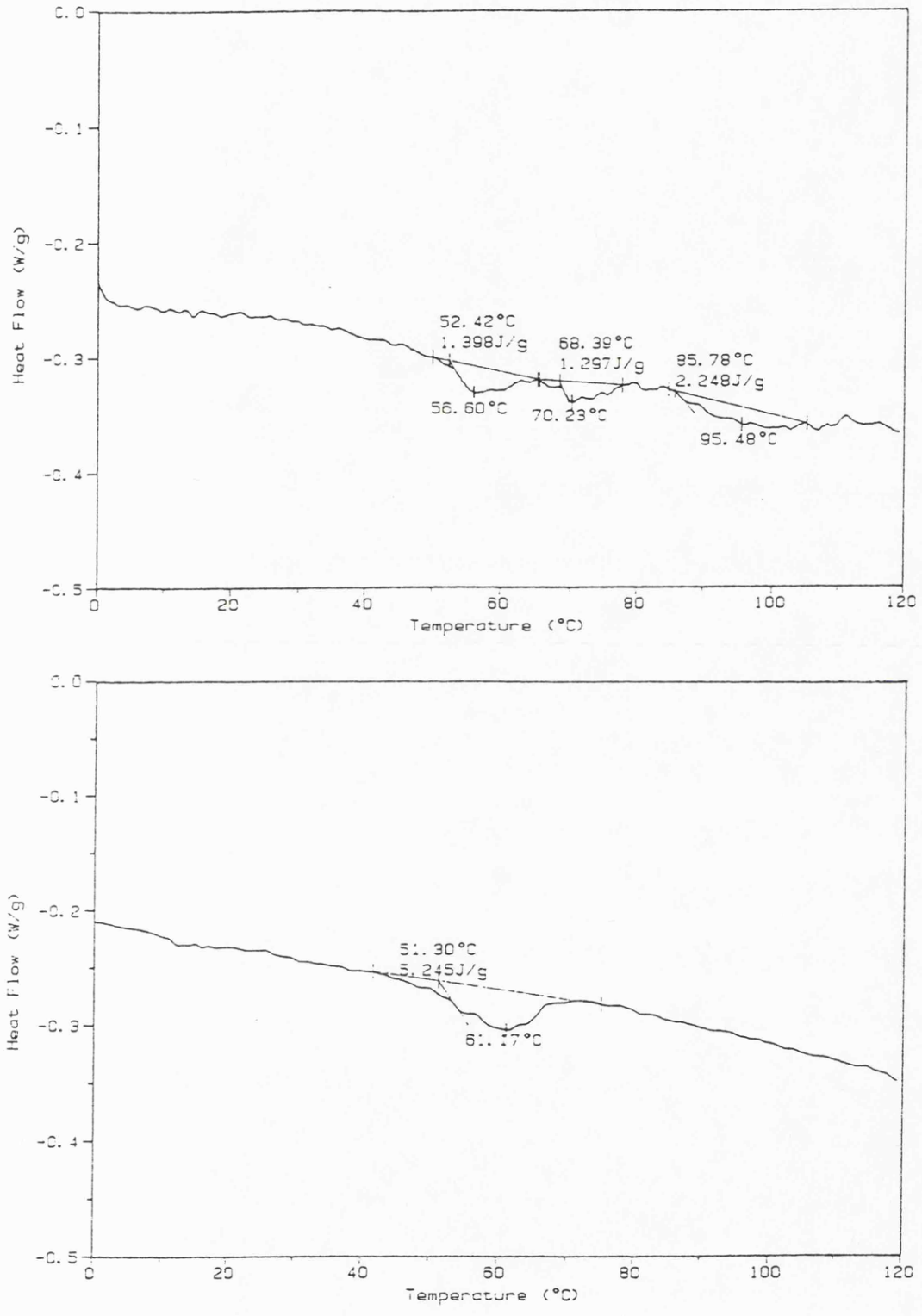

Figure 3.26 Typical heating curves for untreated, hydrated porcine ear stratum corneum. Primary heating (top) and reheat (bottom).

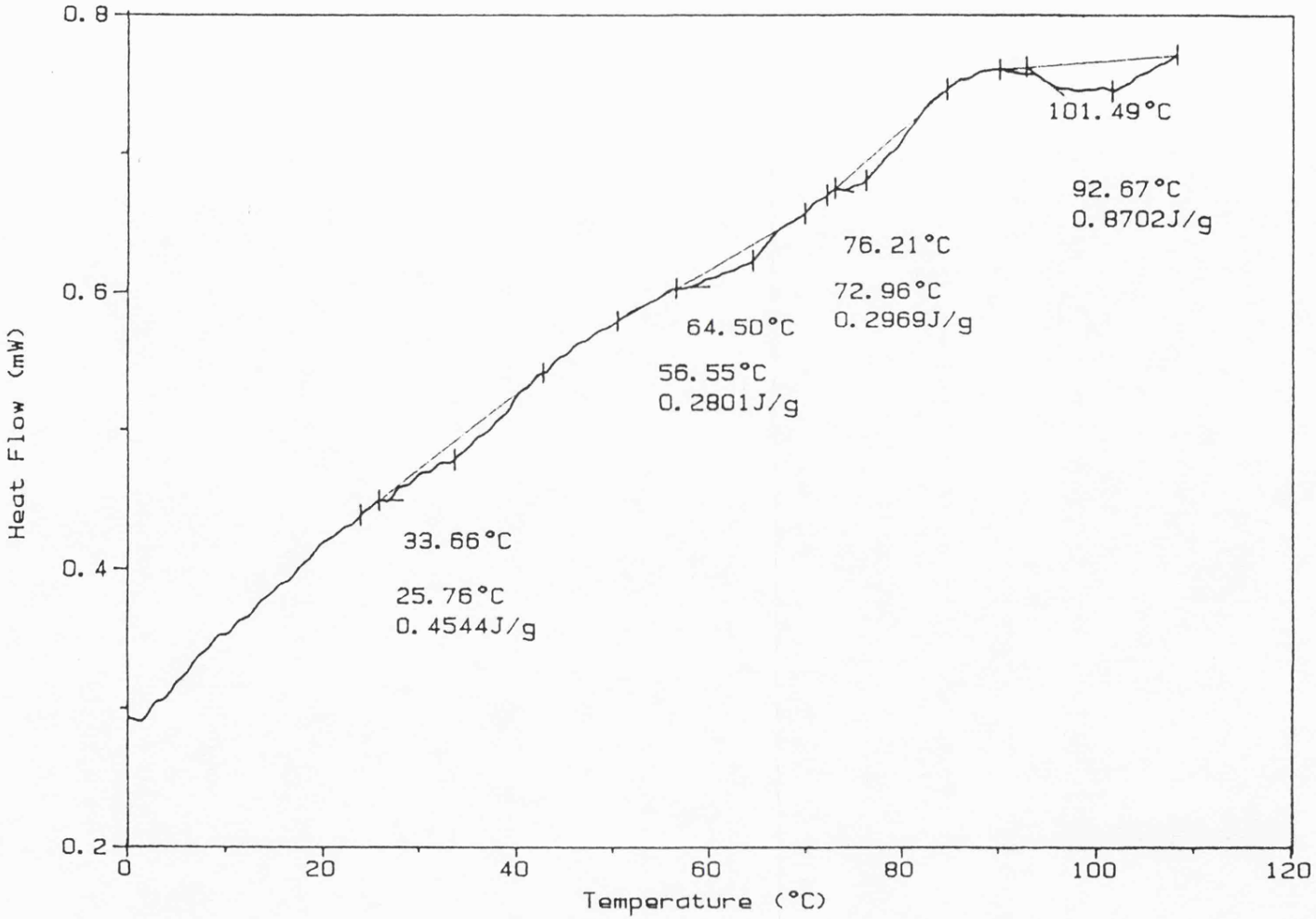

Figure 3.27 Typical heating curve for hydrated human stratum corneum treated with $C_{12}E_3$.

Species	Peak	T_m(°C)	ΔH_{cal}(J g^{-1})
Human	1	67.01±2.05	1.17±0.34
	2	78.41±3.51	0.558±0.15
	3	98.23±4.33	1.29±0.40
Porcine	1	56.55±0.41	0.407±0.2
	2	69.37±1.63	0.70±0.54
	3	96.80±5.91	1.22±0.43

Table 3.7 Transition temperatures and enthalpies for the primary heating of human and porcine stratum corneum (mean±SD, n > 15).

Treatment	Peak	T_m(°C)	ΔH_{cal}(J g^{-1})
Azone	1	64.59±0.09	0.494±0.08
	2	77.98±1.81	0.326±0.02
	3	98.83±2.6	1.203±0.32
$C_{12}E_3$	1	64.83±0.44	0.623±0.38
	2	77.86±2.86	0.401±0.14
	3	98.43±3.61	0.970±0.36
	?	33.51±0.16	0.450±0.04

Table 3.8 The effect of Azone and $C_{12}E_3$ upon thermal transitions in human stratum corneum (mean±SD n=4).

3.3.12 Effect of Surfactants Isolated Stratum Corneum

Addition of Azone to human stratum corneum had little effect upon T_m of the transition peaks but the first two peaks were flattened and had reduced ΔH_{cal} values. $C_{12}E_3$ also had this effect but it also produced a new peak centered at $33.51 \pm 0.16°C$ (Figure 3.27 and Table 3.8). The third peak was unaltered in each case.

3.4 DISCUSSION

Pure DSPC liposomes exhibited a typical sharp, highly cooperative melting endotherm with thermodynamic parameters in good agreement with literature values (94,96).

The pretransition peak has been reported to be associated with a change in polar head group organisation and possibly a change in the angle of the lipid acyl chains from a tilted to vertical conformation (97). The pretransition is very sensitive to "foreign" molecules and very low quantities of drugs (116), surfactants (117) and other lipids (104) cause it to disappear. These observations were confirmed in this study; all surfactants investigated caused the disappearance of the pretransition even at low concentrations (1.6 mole%).

Addition of surfactant had pronounced effects on the DSPC gel to liquid crystalline phase transition. Incorporation of surfactant into the lipid bilayers decreased T_m increased $\Delta T_{1/2}$ and in some cases decreased ΔH_{cal}. These changes are considered to reflect a decrease in the degree of crystallinity of the acyl chain packing and hence an increase in the fluidity of the lipid bilayers (97). Increase in $\Delta T_{1/2}$ can be explained by decrease in cooperativity of the melt endotherm which results in enlargement of the temperature range within which both fluid and gel phases coexist in the lamellae (118).

These phenomena have been observed for many systems. Phillips, Ladbrooke and Chapman (101), working with molecular mixtures of 1,2-diacyllecithins of differing acyl chain length, showed that when the difference in

hydrocarbon chain length of the two components was greater than or equal to four methylene groups, co-crystallisation of the mixtures does not occur and the lipids exhibit monotectic behaviour. The authors considered the decrease in T_m and increase in $\Delta T_{1/2}$ to be due to the more disordered liquid hydrocarbon chains of the lower melting point component causing an increase in the kinetic motion of the ordered chains of the higher melting point component.

Nonylphenyl, dodecyl and decyl radicals are all at least six methylene groups shorter than the stearyl chains of DSPC, assuming that only the hydrophobic part of the surfactant is embedded in the bilayer. The introduction of short acyl chains into a bilayer is known to have a disruptive effect on membrane structure (119) decreasing Van der Waals forces between terminal methylene groups of the normal bilayer components, and lowering the T_m of the transition.

Another effect to be considered is the action of the ethoxy chains of the surfactants upon the choline head groups of the DSPC bilayers. Disruption of headgroup packing would cause a decrease in T_m and an increase in $\Delta T_{1/2}$. However, a reduction in repulsive forces between charged choline head groups due to surfactant interaction would have the opposite effect (118). The latter effect is more usually associated with anionic surfactants than nonionic surfactants.

The effect of nonionic surfactants upon lipid bilayers is dependent upon the molecular ratio of detergent to lipid (120,121). The following sequence of events has been suggested for addition of increasing amounts of nonionic surfactants to bilayers of pure phospholipid (73).

As surfactant concentration increases, with constant phosphipid content, surfactant is incorporated into the lipid bilayer and causes changes in its physical properties. When the bilayers are saturated with surfactant, mixed micelles begin to form resulting in a lamellar-micellar phase change and complete solubilisation of the membrane. This sequence of events presupposes that the surfactant used is hydrophilic enough to form micelles in an aqueous medium.

The surfactant to lipid ratio at which mixed micelle formation and solubilisation occurs is dependent on both surfactant and target membrane structure. In most cases complete solubilisation begins at surfactant to lipid ratios between 0.8 and 3.0 for good solubilising surfactants (121); those with an HLB between 12.5-14.5 (73).

A typical nonionic surfactant in this HLB range and used in solubilisation studies is Triton X-100, (t-octylphenol decaether ethoxylate, OP10). For Triton X-100/DSPC systems mixed micelle formation begins at a mole ratio surfactant to lipid of one (120). For the surfactants and concentration ranges studied in this investigation little solubilisation of the membrane was likely to occur and the phospholipid/surfactant mixtures were thought to remain mostly in the lamellar phase.

As the surfactant structure affected its activity each surfactant in a series exhibited a slightly different concentration/activity profile. NP10 reduced T_m and increased $\Delta T_{1/2}$ indicating fluidisation of the bilayer (Figures 3.5 and 3.6). NP10 also caused a concentration dependent decrease in ΔH_{cal} (Figure 3.7). Similar behaviour was observed for the closely related surfactant Triton X-100 (OP10) acting on DPPC membranes (117). These authors concluded that the surfactant was penetrating the bilayer and withdrawing a portion of the lipid from participating in the transaction.

The less hydrophilic nonylphenyl, NP6, was a more potent membrane fluidiser, indicated by the greater reduction in T_m and greater increase in $\Delta T_{1/2}$ (Figures 3.5 and 3.6). NP6 however, did not cause any significant effect on transition enthalpy. The ability of the surfactant to penetrate the membrane, its partitioning behaviour and the capacity of the membrane for the surfactant will all affect the surfactants concentration/activity profile. It is thought that less NP10 entered the membrane or was tolerated by the membrane than NP6 as the fluidisation effects plateaued at about 40-50 mole% for NP10 but continued to increase up to 80 mole% for 9N6 (Figure 3.5 and 3.6).

For the whole nonylphenyl series these effects are reflected in the plots of T_m and $\Delta T_{1/2}$ of the DSPC phase transition as a function of average ethoxy chain length of the surfactant (Figures 3.8 and 3.9). As the number of ethylene oxide groups increased there was a decrease in the extent of the bilayer fluidisation. This was evident at 1%($^{W}/_{V}$) surfactant concentration but was greatly highlighted at the higher concentrations investigated, 5 and 10%($^{W}/_{V}$). Little effect was observed with NP15 whereas, in contrast, NP2 and NP1 were very potent membrane fluidisers.

These phenomena can be explained by the partitioning behaviour of the surfactants. For a given concentration of surfactant added to the liposomes, more of the low ethoxy content surfactant partitioned into the hydrophobic bilayer than the longer ethoxy chain molecules which were more soluble in the aqueous phase.

A point to be noted is that the concentration for the nonylphenyls was expressed in terms of percentage weight in volume. Therefore the numbers of molecules of low ethoxy content surfactants present were greater than for the longer ethoxy chain surfactants, due to the differences in average molecular weight. At 10%($^{W}/_{V}$) concentration approximately three times the number of NP2 molecules, with respect to NP15, molecules, would have been added to the system. There have been several other structure-activity studies upon the membrane perturbing effects of nonylphenyl ether ethoxylates.

The ability of the nonylphenyl ethoxylates to reduce the mobility of the protozoan *Tetrahymena elliotti*, presumed to be caused by the membrane activity of the surfactant, was found to decrease with increasing ethoxy chain length. (85). The maximum activity was seen with NP4 the lowest HLB surfactant studied in the series, despite its inability to micellize at ambient temperatures.

Similar findings were noted by Gadd and Curtis-Prior (86) who observed that spermicidal activity of the nonoxynols decreased with increasing hydrophilic chain length. Levin, (87) working with a large range of nonoxynols upon rat vaginal bioelectric activity found the most potent members of the series to be those

with eight or nine ethoxy groups. The activity was reduced at both higher and lower ethoxy chain lengths. These observations were explained in terms of solubility. The more hydrophilic surfactants were too water soluble to attain an effective intermembrane concentration whilst the more hydrophobic surfactants were so poorly water soluble that access to be cell membrane was restricted. With the co-deposition of surfactant and lipid used in this study there was no such restriction of access to the membrane. Thus the more potent fluidisation potential of hydrophobic surfactants could be observed. However, it was possible during hydration for the surfactant to partition out to form a separate oily or micellar phase.

Although the nonylphenols studied formed a homologous series each surfactant was polymeric with respect to ethoxy chain length (see 2.4). Thus any structure-activity relationship observed would be expected to be compromised by the heterogeneity of the materials in use. The Nikkol dodecyl ether ethoxylates were all of single ethoxy chain length (see 2.4) so eliminating ambiguities due to varying polydispersity of the surfactants. Nevertheless, the results obtained with the series $C_{12}E_0$-$C_{12}E_8$ did show broad similarities to the results from the nonylphenols. In general, the pure surfactants produced sharper structure-activity effects, as might be expected.

The series $C_{12}E_0$-$C_{12}E_8$ caused comparible concentration dependent effects to the nonylphenyls with respect to HLB of the surfactants. The effect of $C_{12}E_7$ on increases in membrane fluidity plateaued at a far lower concentration (20-40 mole%) than $C_{12}E_3$ (50-60 mole%) (Figures 3.10-3.12), this was similar to the situation observed for NP10 and NP6 (Figures 3.5 and 3.6). $C_{12}E_5$ showed behaviour intermediate between $C_{12}E_3$ and $C_{12}E_7$.

If these effects were dependant upon partitioning behaviour it would be expected that the lower HLB surfactants would show greater effects at all concentrations. At low concentrations up to 20 mole% (Figures 3.10 and 3.11) differences in fluidisation were not greater than experimental error. This point is

further illustrated in Figures 3.13 and 3.14. At 9 mole% surfactant no relationship between ethoxy chain length of the surfactant and membrane fluidising ability could be discerned, presumably too few molecules of any surfactant were present to have a distinctive effect upon the membrane.

At 50 mole% surfactant a far clearer relationship was seen. An optimum fluidisation effect was observed with $C_{12}E_3$, both higher and lower ethoxy chain lengths being less effective. This can be explained along the lines proposed by Levin (87) for the nonoxynols (see above), in terms of solubilities and partitioning behaviour.

Further observations of this type of phenomena were reported by Florence *et al* (63). This group studied several series of polymeric alkyl ether and ester ethoxylates, including the Brij 30 series ($C_{12}E_n$). All the surfactants showed a parabolic relationship between membrane activity and lipophilicity. From this information the authors postulated that "the depth of penetration of the hydrocarbon chain may not be equal in a homologous series varying in ethylene oxide chain length, leading to variation in biological activity. When the number of ethoxy groups is lower than optimum, low concentration limits monomer activity, also part of the ethoxy chain may penetrate into the membrane. When the ethoxy chain length is above optimum, high molecular area and decreased surface activity will result in less efficient membrane penetration". From all these considerations it can be understood that $C_{12}E_3$ has the right balance of partition coefficient, molar volume and the right depth of chain penetration to cause the greatest effect upon the DSPC membrane. During the current study it was observed that $C_{12}E_{0\text{-}2}$ molecules, which were not able to micellize, had a tendency to separate as oily droplets, indicating poor membrane incorporation.

A comparison of the effects of all three series of surfactants investigated with respect to both ethoxy chain length and HLB is presented in Figures 3.19 and 3.20. It can be seen that the lower HLB surfactants were the more potent membrane fluidisers, but the optimum ethoxy chain length and HLB was different for each

hydrophobic moiety. Such effects have been noted for the haemolytic effects of several classes of nonionic surfactants of the same HLB (122). Below an optimum HLB both the decanol and dodecanol based surfactants showed a decrease in membrane fluidisation. Such an effect did not occur in the nonylphenol series where concentration was expressed as percent $^{w}/_{v}$. This can be explained by two factors; a higher molar concentration of the low HLB surfactants was present with respect to the larger molecules and low HLB surfactants (NP1 and NP2) were polydisperse and therefore contained some higher ethoxylated molecules (2.4.4.1.1) which would have been more potent fluidisers.

The dodecyl ether ethoxylates were far more potent fluidisers of DSPC bilayers than the C_{10} equivalents. The potency of the C_{12} chain has been observed as the optimum chain length in studies upon several types of biological membrane (71,74,122,123). The reasons for this optimum potency have been debated. Schott (124) suggested the lauryl chain has the best balance between monomer concentration and penetratability of the membrane. Dominquez *et al* (125) postulated that the C_{12} chain can adopt a compact open cyclohexane structure that will allow the molecule to migrate deeper into the target membrane.

The industrial, polydisperse, counterparts of the Nikkol dodecyl ether ethoxylates are the Brij 30 surfactant series. Brij 30 (average $C_{12}E_4$) showed far less activity than pure $C_{12}E_4$ (Figure 3.19, Table 3.4). The sample of Brij 30 used had an average ethoxy chain length very close to that stated by the supplier (Table 2.4). However, the presence of other chain length molecules, (see 2.4.4.1.2) most of which are less active would mean a lower concentration of $C_{12}E_4$ present in the membrane. In addition longer chain micellar molecules present had the potential to solubilize shorter ethoxylates. Similarly, Brij 36T ($C_{12}E_{10}$) appeared more active than would be predicted from the trends observed. The sample of Brij 36T used in this study had an average ethoxy chain length of 7.85 ± 0.54, well below the expected value of E_{10}. As the surfactant contains many lower ethoxy chain length molecules its effectiveness as a fluidiser was increased.

Azone is a well documented permeation enhancer (126) and is known to fluidise lipid membranes (50,127). In the study Azone proved to be a potent membrane fluidiser significantly reducing T_m and increasing $\Delta T_{1/2}$ (t-test, $p<0.01$). At 50 mole% concentration very similar effects to $C_{12}E_3$ were observed on T_m and $\Delta T_{1/2}$ (Table 3.4). Azone has a C_{12} acyl chain and a low polarity headgroup thus its effects can be explained as surfactant properties. Azone probably has an effective HLB very similar to that of $C_{12}E_3$, and exerts similar effects on DSPC bilayers.

The storage of extracted stratum corneum lipids at 98% relative humidity resulted in $18.5\pm4.9\%(^{W}/_{W})$ hydration. This was lower but not significantly different (t-test, $p>0.05$) from the percentage hydration of whole stratum corneum ($26.58\pm9.9\%^{W}/_{W}$) which would be expected to take up more water due to hydration of the keratin bundles in the corneocytes. Both preparations had been stored over dry slica gel and vacuum dried and, therefore, should have been fully desiccated. Addition of surfactant increased the extent of hydration of the extracted lipids. No similar observation was made for surfactant treated whole stratum corneum. The ethoxy chains of the surfactants may help bind extra water into the lipid preparations.

The extracted skin lipids are unlikely to form discrete liposomes using these methods of hydration. However, liposomes can be prepared by other techniques (128). It is more likely that in the hydrated state used in this study the lipids will be present as lamellae in the L-α-liquid crystalline phase (129). This hydration is unlikely to be complete when the method of incubation at 98% relative humidity was used. This was confirmed by the slightly lower T_m and $\Delta T_{1/2}$ of lipids hydrated in excess PBS. T_m and $\Delta T_{1/2}$ are known to decrease with hydration down to a minimum at the fully hydrated state (97). The T_m of the melt of the extracted porcine lipids was in good agreement with results of previous studies on porcine skin (110). The ΔH_{cal} value for the transition was in good agreement with that obtained with extracted human stratum corneum lipids (129). As there was

intersample variation, structure-activity studies with the surfactants were carried out on a single lipid extract.

Addition of surfactant caused a decrease in T_m, $\Delta T_{1/2}$ and ΔH_{cal}. This would seem to conflict with previous results with DSPC where a decrease in T_m was accompanied by an increase in $\Delta T_{1/2}$, indicating membrane fluidisation. The $\Delta T_{1/2}$ value of untreated lipid was very large, spanning the maximum expected for a biological transition (95). Addition of surfactant is unlikely to increase this and in high enough concentration may have increased the cooperativity of the transition. The inclusion of the surfactants, which have a lower melting point, does however reduce T_m and can be seen to be fluidising the lipids. $C_{12}E_3$ induced the maximum decrease in Tm and can be thought of as the most potent fluidiser, in agreement with the DSPC studies.

The rehydration of dry whole stratum corneum at 98% relative humidity produced a large variation between samples. This has been observed by other investigators (79). The transition temperatures (T_m) for the three transition peaks observed for the primary heating of whole human stratum corneum were lower than those previously reported. (105,106). The large degree of sample variation that occurs with different skin sources may account for this. The behaviour of the samples upon reheating agreed with the literature results (105,106).

The behaviour of porcine stratum corneum was similar to human upon thermal analysis but with lower T_m values for the two lipid associated peaks (see 3.1.3). This was in agreement with a previously described study (110). For both types of tissue the ΔH_{cal} value of the reheat peak was approximatey equal to the ΔH_{cal} values of the two lipid associated peaks seen in the primary heating. This has been observed by other workers (107).

Goodman and Barry (107) found that addition of Azone removed the lipid assigned transitions. In this study the size of the transition was reduced but it was not completely removed. The difference may be explained by the different method used by Goodman and Barry who used Azone as an emulsion in 0.1% Tween 20,

thus allowing some possible extraction of intercellular lipids. In this study Azone was deposited on to the stratum corneum from a volatile solvent, extraction of lipid components therefore being minimised.

Boustra *et al* (111) found Azone in propylene glycol reduced ΔH_{cal} of the transitions in stratum corneum and reduced the T_m of the lipid peaks by about 15°C. In this study no significant decrease in T_m was observed however both Azone and $C_{12}E_3$ reduced the ΔH_{cal} of the lipid associated peaks. In a similar study to that of Boustra (111), Goodman and Barry (50) noted propylene glycol alone reduced T_m by about 10°C so again the difference between studies may be due to the method of application of enhancer. Addition of $C_{12}E_3$ to the stratum corneum produced a new peak at 33.51°C; the identity of this peak is unknown.

CHAPTER 4

MEASUREMENT OF LIPID BILAYER FLUIDISATION BY FLUORESCENCE POLARISATION SPECTROSCOPY

4.1 INTRODUCTION

4.1.1 Principles of Fluorescence Polarisation Spectroscopy (FPS)

The absorption of light by a molecule causes the electrons of that molecule to become excited and move to a higher electron orbital. The return of a paired electron to a lower energy state results in a fluorescent emission. Due to loss of energy in this process emission occurs at a longer wavelength relative to the absorption (130). Substances which display significant fluorescence, fluorophores, are generally those which possess delocalised electrons formally present in conjugated double bonds.

Upon excitation with polarised light the emission from fluorescent molecules is also polarised in the same plane as the excitation. If the fluorophore undergoes rotational motion during the fluorescent lifetime of the molecule, the time between absorption and subsequent emission of a photon, then depolarisation of the emission occurs. The degree of depolarisation, the anisotropy of the flurophore, is dependent upon the rate and extent of rotational diffusion of the molecule during the fluorescent lifetime. These motions of the molecule depend upon its size and shape and more so on the viscosity of the solvent. A change in solvent viscosity or in the viscosity of the microenvironment of the fluorophore will therefore result in a change in fluorescence anisotropy (131).

4.1.2 Measurement of Fluorescence Polarisation

The measurement of fluorescence polarisation or anisotropy is illustrated schematically in Figure 4.1. The sample is excited with vertically polarised light and the intensities of emissions are measured through polarisers orientated parallel to the plane of excitation i.e. vertically polarised (I_{VV}) and perpendicular to the plane of excitation ie. horizontally polarised (I_{VH}). From these measurements the polarisation anisotropy (r) can be defined as:-

$$r = \frac{I_{VV} - I_{VH}}{I_{VV} + 2I_{VH}} \qquad \text{Equation 4.1}$$

For completely polarised emissions which are observed with scattered light (1), $I_{VH} = 0$ and $r = 1.0$. For natural unpolarised light $I_{VV} = I_{VH}$ and $r = 0$.

The lower the viscosity of the solvent the higher the rate of rotation of the fluorophore, hence the larger the depolarisation and the lower the value of r.

Equation 4.1 assumes that the excited and emitted light is not affected by any polarisation of the optical components. This is unlikely, as both excitation and emission monochromators are likely to partially polarise the incident light. Therefore a correction has to be added to the equation to account for this (3). This correction factor, as described by Azumi and McGlynn (133), is calculated from the ratio:-

$$G = \frac{I_{HV}}{I_{HH}} \qquad \text{Equation 4.2}$$

i.e. horizontal excitation, emitted light measured in both vertical and horizontal planes. This leads to the corrected equation for anisotropy shown below.

$$r = \frac{I_{VV} - G.I_{VH}}{I_{VV} + 2.G.I_{VH}} \qquad \text{Equation 4.3}$$

4.1.3 Measurement of Fluorescence Polarisation in Membranes

Using FPS it is possible to obtain good estimations of membrane fluidity and the microviscosity of the membrane interior (134). The fluorescence anisotropy can be calculated from the polarisation characteristics of a hydrocarbon fluorescent probe embedded in the membrane. The anisotropy value will give an indication of the relative viscosity of the membrane interior and the microenvironment of the probe. This technique has been widely used in the study of membrane biophysics and biochemistry in both artificial model membranes (135,136) and naturally occurring cell membranes (137,138).

Below the gel-liquid crystalline phase transition of the membrane the motion of the probe will be constrained by the crystal packing of the lipid acyl chains and a

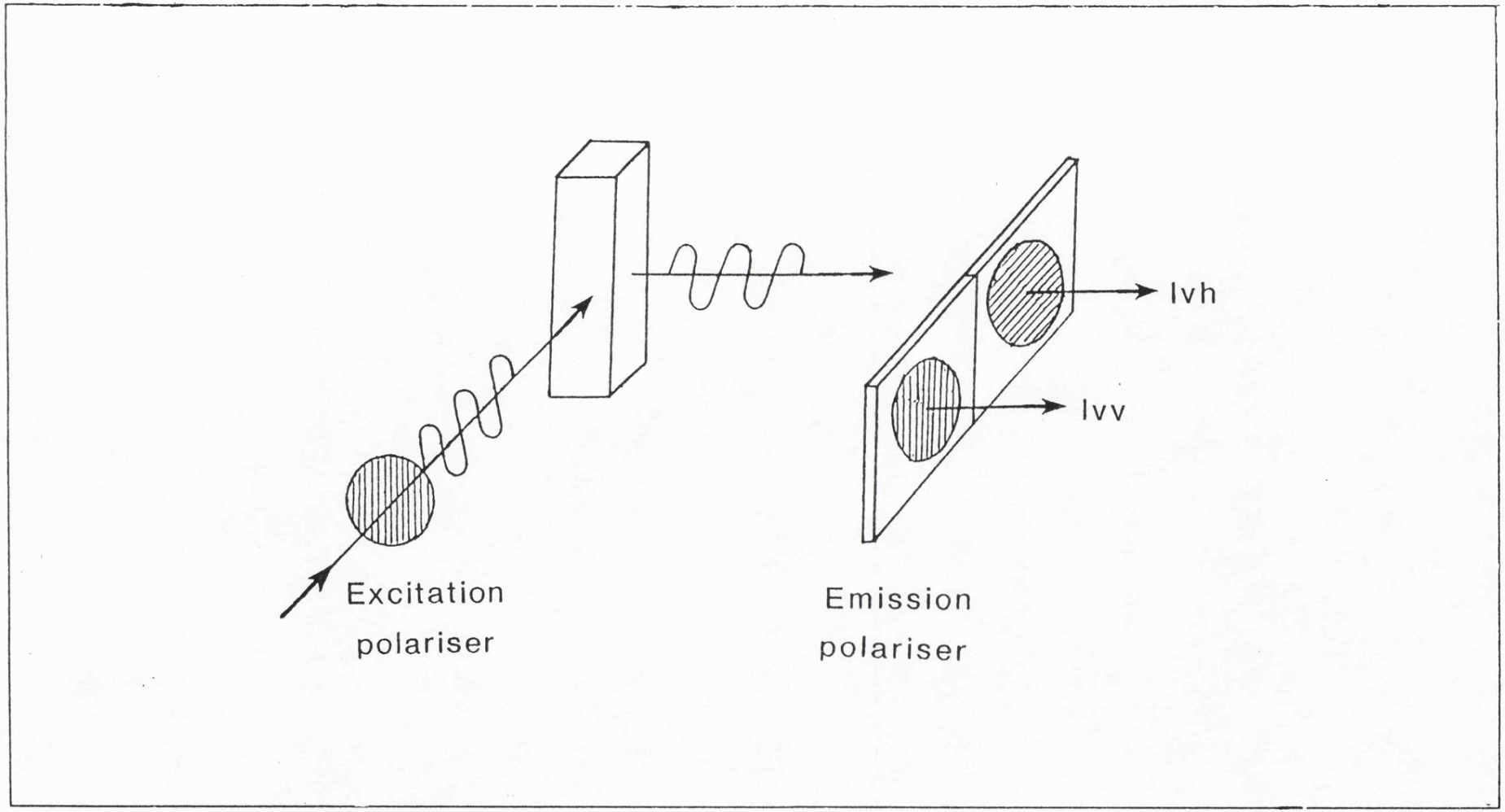

Figure 4.1 Schematic of the basic principle of the measurement of fluorescence polarisation. (see text in 4.1.2 for detail).

high anisotropy value will be obtained. It has been calculated that the maximum possible value of r that can be obtained for a probe in a membrane system is 0.4, any higher value than this must be due to light scattering (130).

If the membrane is heated, as temperature rises, the motion of the probe will gradually increase and concurrently r will decrease. At the phase transition the membrane fluidises, r will fall rapidly during the transition until reaching a constant, lower value in the liquid crystalline phase. This produces a sigmoidal curve for a plot of anisotropy (r) as a function of temperature over the phase transition range (139).

In this chapter the effect of the pure dodecyl ether ethoxylates $C_{12}E_1$-$C_{12}E_8$ upon the membrane fluidity of DSPC liposomes will be investigated by fluorescence polarisation measurements of some commonly used membrane probes.

4.2 METHODS

4.2.1 Preparation of Liposomes

DSPC multilamellar liposomes and DSPC/surfactant mixed vesicles were prepared as previously described (3.2.1, 3.2.2). Surfactant and DSPC were codeposited in all these studies. As this was a spectroscopic method a far lower concentration and far greater volume of liposome suspension was required than that used for DSC studies. For each sample 4ml of liposome suspension in pH 7.4 PBS was prepared in 4.5ml vials. In order to produce consistent size vesicles with a lower absorbance the dispersions were sonicated. A 3mm probe sonicator (Ultrasonics Ltd., Shipley, UK) was used at 50mw power for three minutes, without cooling, under helium, to produce smaller oligolamellar vesicles. The effect of liposome concentration and hence absorbance upon light scattering and associated depolarisation effects (140) was investigated over the DSPC concentration range 0.025-1mg ml^{-1} using cis-pna as the fluorescence probe. Samples were prepared by serial dilution and analysed by methods described in 4.2.3 at 25°C. From the

results obtained (Figure 4.3.1.) it was decided to use a final DSPC concentration of 0.05mg ml^{-1} ($6.34x10^{-5}M$) for all experiments.

4.2.2 Addition of Fluorescent Probes

The DSPC liposome and DSPC/surfactant vesicle suspensions were purged with helium to prevent oxidation of the probe molecules. The fluorescent probes, cis-pna, DPH, ANS and perylene (see 2.6) were added in 1μl of solvent, as detailed in Table 4.1, to experimental samples which had been heated to 65°C. The probes were dispersed by vortex mixing for 2-3 seconds. The hydrophobic probes rapidly partitioned into the vesicles which were above their phase transition temperature. Any probe which remains in the aqueous buffer shows negligible fluorescence with respect to the incorporated probe (141,142). Final probe concentrations and probe to DSPC ratios are given in Table 4.1. The probe:lipid ratio was kept low to avoid perturbation of the lipid packing by the probe. For experiments involving cis-pna 2,6 di-t-butyl-4-methyl phenol (BHT) was added as an antioxidant in a 1:1 ratio with cis-pna molecules.

For all experiments light scattering blanks were prepared. These were produced by addition of 1μl of solvent only, or, for cis-pna, 1μl of BHT in ethanol to the liposome suspensions.

4.2.3 Analysis of Samples by FPS

Fluorescence polarisation measurements were performed using a Shimadzu RF540 spectrofluorimeter fitted with a Shimadzu P/N 204-03290 fluorescence polariser (Shimadzu Ltd., Japan). The temperature in the cuvettes was controlled by a Howe temperature control unit (VA Howe, London UK) and the cuvette continually stirred with a magnetic stirrer. The instrument settings, slit widths, excitation and emission wavelengths, employed for each type of probe are detailed in Table 4.2.

Probe	Solvent	Final Conc^{n} (M)	Probe:Lipid
Cis-pna	Ethanol	2.2×10^{-7}	1:300
DPH	THF	5.07×10^{-7}	1:500
Perylene	Acetone	2.2×10^{-7}	1:300
ANS	Ethanol	5.07×10^{-7}	1:500

Table 4.1 The solvents used for adding fluorescent probes, the final probe concentrations in the cuvette and the probe:lipid ratios used in the FPS experiments

Probe	Wavelength	
	Excitation [a]	Emission [b]
Cis-pna	325	410
DPH	365	425
Perylene	413	470
ANS	366	460

[a] Slit width 5nm

[b] Slit width 20nm

Table 4.2 The instrument settings used with the four probes for FPS analysis.

Fluorescence intensities both parallel and perpendicular to vertically and horizontally excited light were measured for both experimental samples and light scattering blanks. Polarisation measurements were made either at 30°C or monitored over the temperature range 20-65°C with a heating rate not greater than 1°C $min.^{-1}$

4.2.4 Alignment of Polarisers

Accurate measurement of fluorescent anisotropies requires that the polarisers be precisely positioned in the vertical and horizontal orientations. A dilute suspension of glycogen in water (1mg ml^{-1}) was used to produce scattered light that is 100% polarised, r=1.0 (130). The excitation polariser was set to vertical and the angular alignment of the emission polariser adjusted so that a minimum intensity was observed. This was the horizontal position. The maximum intensity was the vertical position. Once these had been determined the horizontal and vertical positions for the excitation polarisers were determined in a similar fashion with the emission polariser set vertically.

4.2.5 Treatment of Results

The blank scattering readings were subtracted from the experimental values and the anisotropy function calculated from Equation 4.3. For samples examined over a temperature range, plots were constructed of anisotropy against temperature. A typical plot is shown in Figure 4.2. From tangents drawn to the baselines and transition slopes, transition onset temperature (T_c) and transition widths (T_w) were calculated as shown. Results given are means$\pm$SD. For measurements of T_c and T_w, n=4 whilst for determinations of r at 30°C $n > 6$.

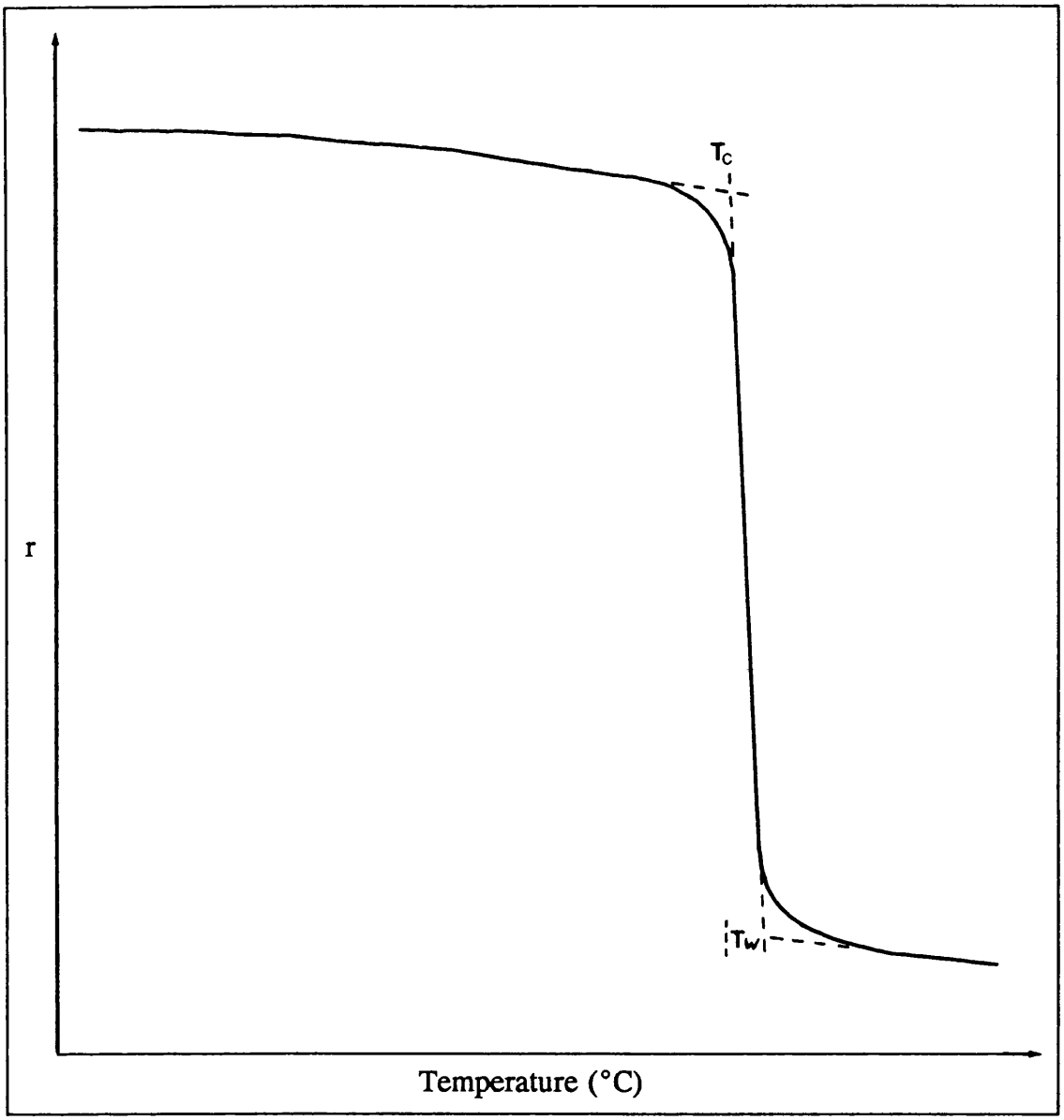

Figure 4.2 Fluorescent probe anistropy r, for a molecule incorperated into DSPC liposomes plotted as a function of temperature. From plots such as these it is possible to calculate the phase transition onset temperature T_c and the phase transition width T_w.

4.3 RESULTS

4.3.1 Effect of Sample Absorbance upon Polarisation

Figure 4.3 shows the observed anisotropies of cis-pna fluorescence in DSPC liposomes at 25°C plotted against the sample absorbance at 325nm. The observed anisotropy (r) remained constant at approximately 0.25 up to an absorbance of around 0.5 absorbance units. Above this absorbance a decrease in r was observed. This was consistent with the findings of Lentz *et al* (140) working with DPPC liposomes and DPH.

4.3.2 The Effect of Dodecyl Ether Ethoxylates upon DSPC Bilayer Fluidity Measured by Cis-pna Anisotropy

Pure DSPC liposomes showed a sharp decrease in probe anisotropy from 0.25 to 0.10 between 50.4 and 54.1°C corresponding to the large increase in fluidity at the gel-liquid crystalline melting transition. This gave values for T_c of 50.45 ± 0.07°C and $T_w = 3.67 \pm 0.6$°C. Addition of surfactant to the liposomes caused a broadening of T_w and a decrease in T_c, Figure 4.4. The traces shown are for liposomes with 50 mole% surfactant.

T_c and T_w were determined for mixed vesicles of DSPC/$C_{12}E_{1\text{-}8}$, containing 9, 33 and 50 mole% surfactant, this corresponds to 1:0.1, 1:0.5 and 1:1 lipid:surfactant ratios. T_c and T_w were plotted as a function of surfactant ethoxy chain length (Figures 4.5 and 4.6). At 9 mole% there was no significant change in T_c or T_w of the phase transition with any of the surfactants (t-test, $p < 0.05$). At 33 mole% surfactant a greater effect was seen upon both T_c and T_w. The decrease in T_c and increase in T_w, was greatest with the intermediate HLB surfactants $C_{12}E_3$-$C_{12}E_6$, the higher and lower HLB surfactants being less potent fluidisers. This was highlighted at 50 mole% surfactant. T_c decreased and T_w increased over the range $C_{12}E_1$-$C_{12}E_5$, the effect being maximal at $C_{12}E_5$ ($T_c = 35.7 \pm 1.4$°C, $T_w = 12.5 \pm 1.2$°C). From $C_{12}E_5$-$C_{12}E_8$ the reverse trend was observed.

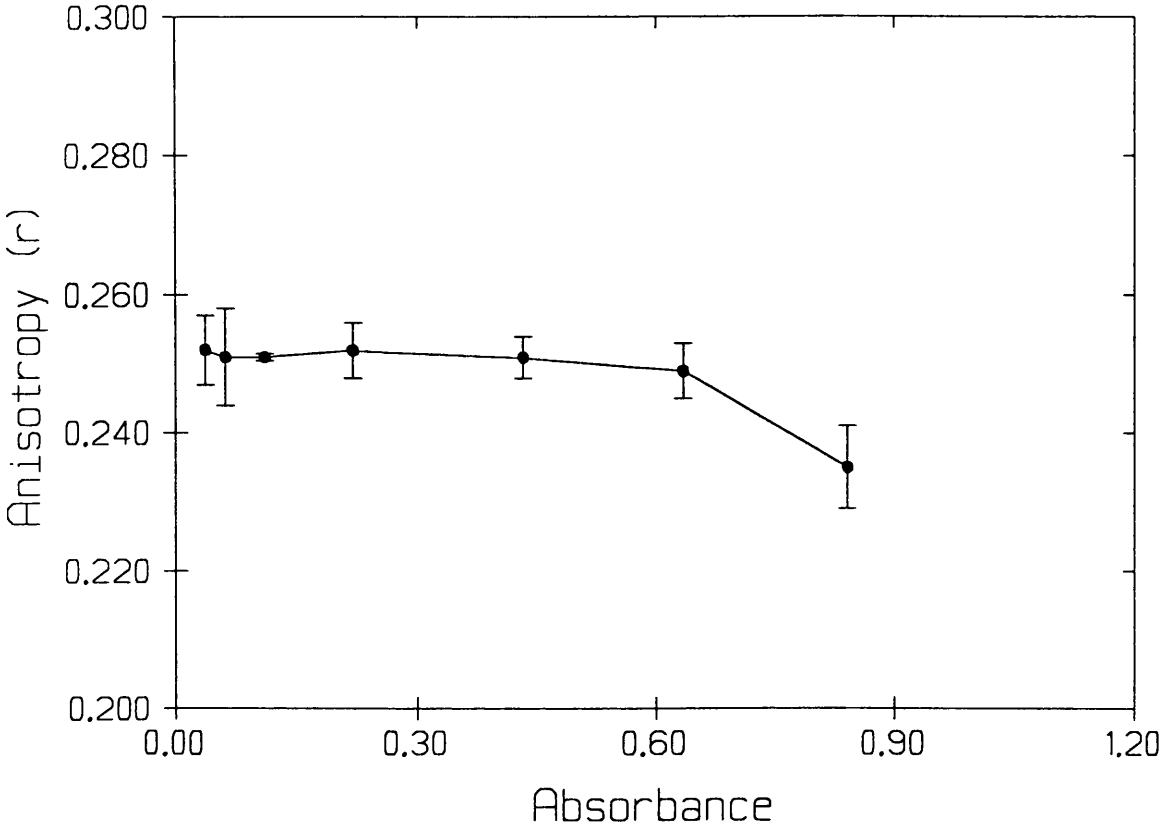

Figure 4.3 Observed anisotropy of cis-pna in DSPC liposomes at 25°C plotted as a function of the sample absorbance at 325nm.

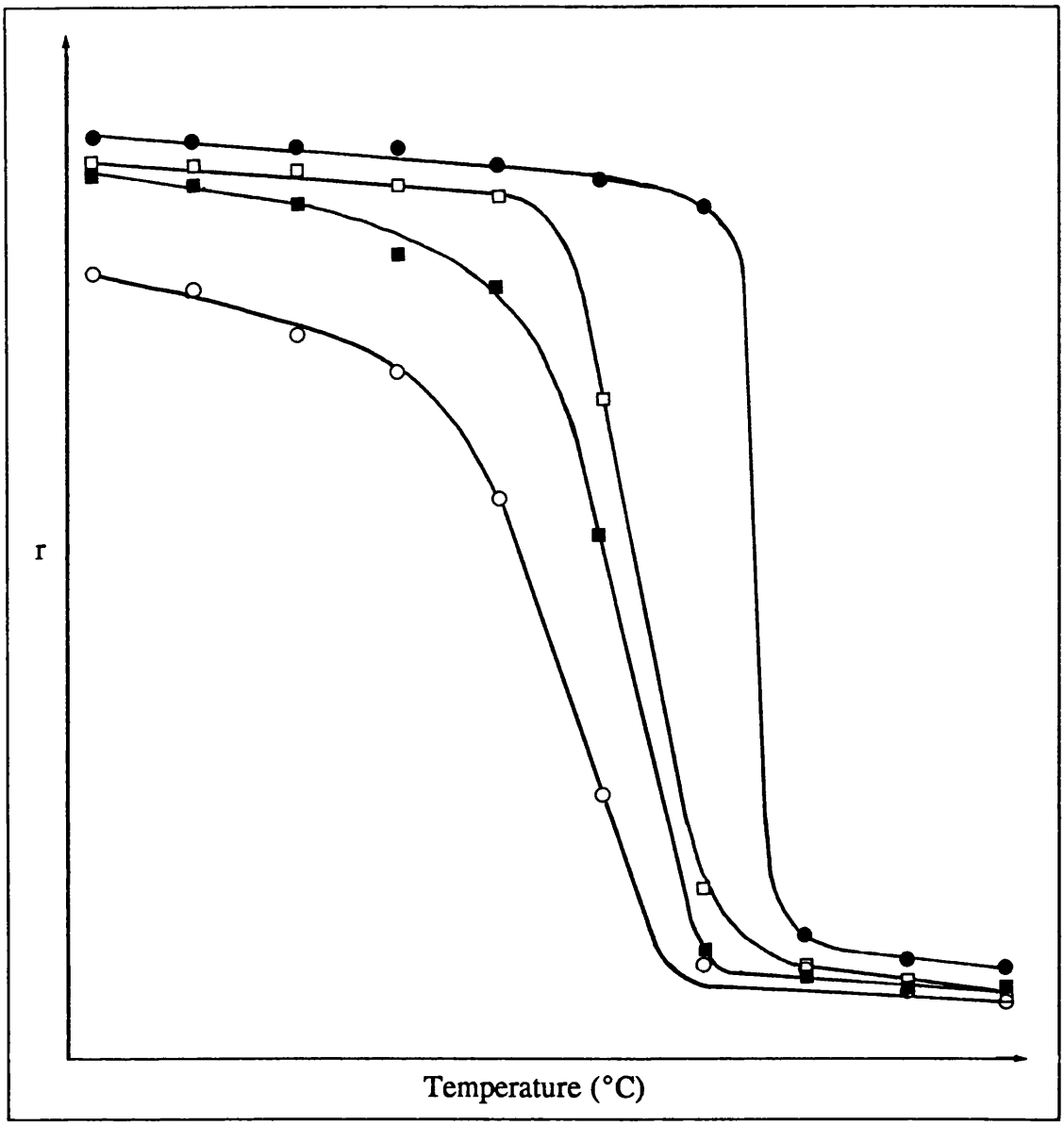

Figure 4.4 Typical FPS heating curves of pure DSPC and DSPC/surfactant vesicles incorporating 50 mole% surfactant. DSPC (●), $C_{12}E_3$ (■), $C_{12}E_5$ (○) and $C_{12}E_7$ (□).

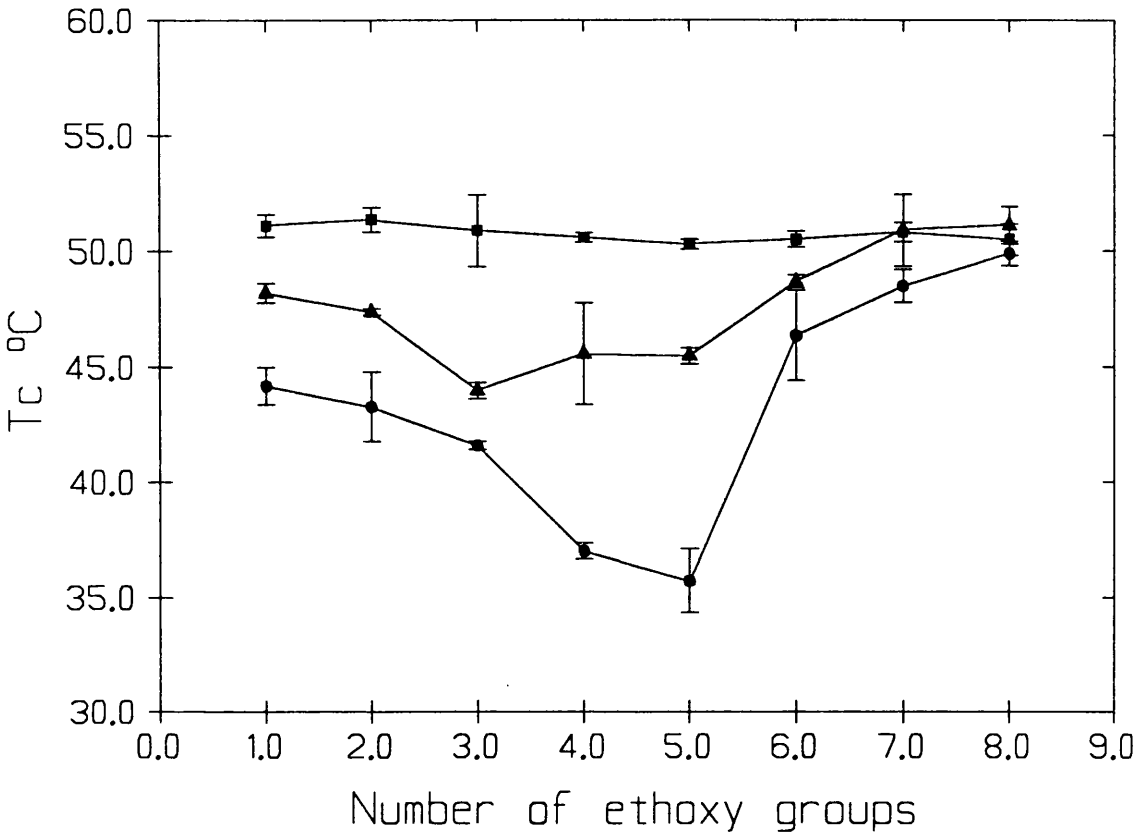

Figure 4.5 T_c values, using cis-pna as the probe, for the gel-liquid crystalline phase transition of DSPC/$C_{12}E_n$ mixed vesicles plotted as a function of surfactant ethoxy chain length. 9 (■), 33 (▲) and 50 (●) mole% surfactant. Mean±SD, n=4.

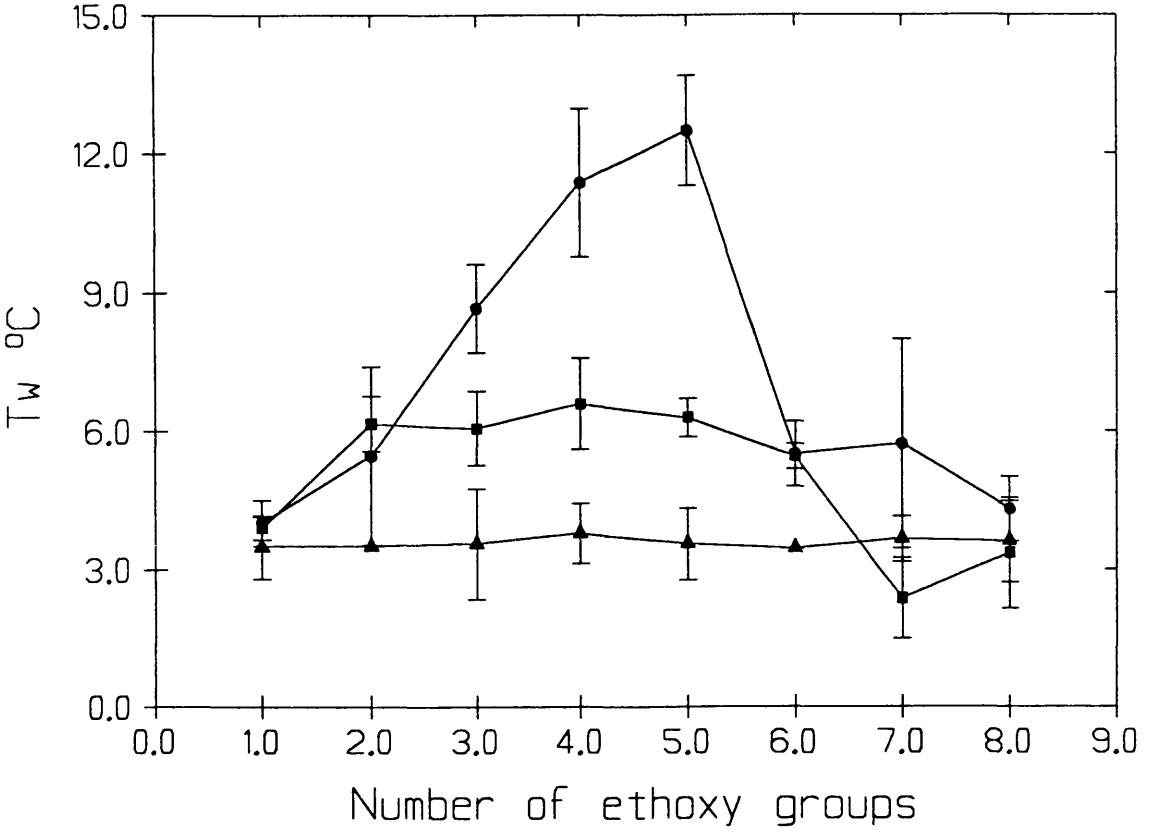

Figure 4.6 T_w values, using cis-pna as the probe, for the gel-liquid crystalline phase transition of DSPC/$C_{12}E_n$ mixed vesicles plotted as a function of surfactant ethoxy chain length. 9 (▲), 33 (■) and 50 (●) mole% surfactant. Mean±SD, n=4.

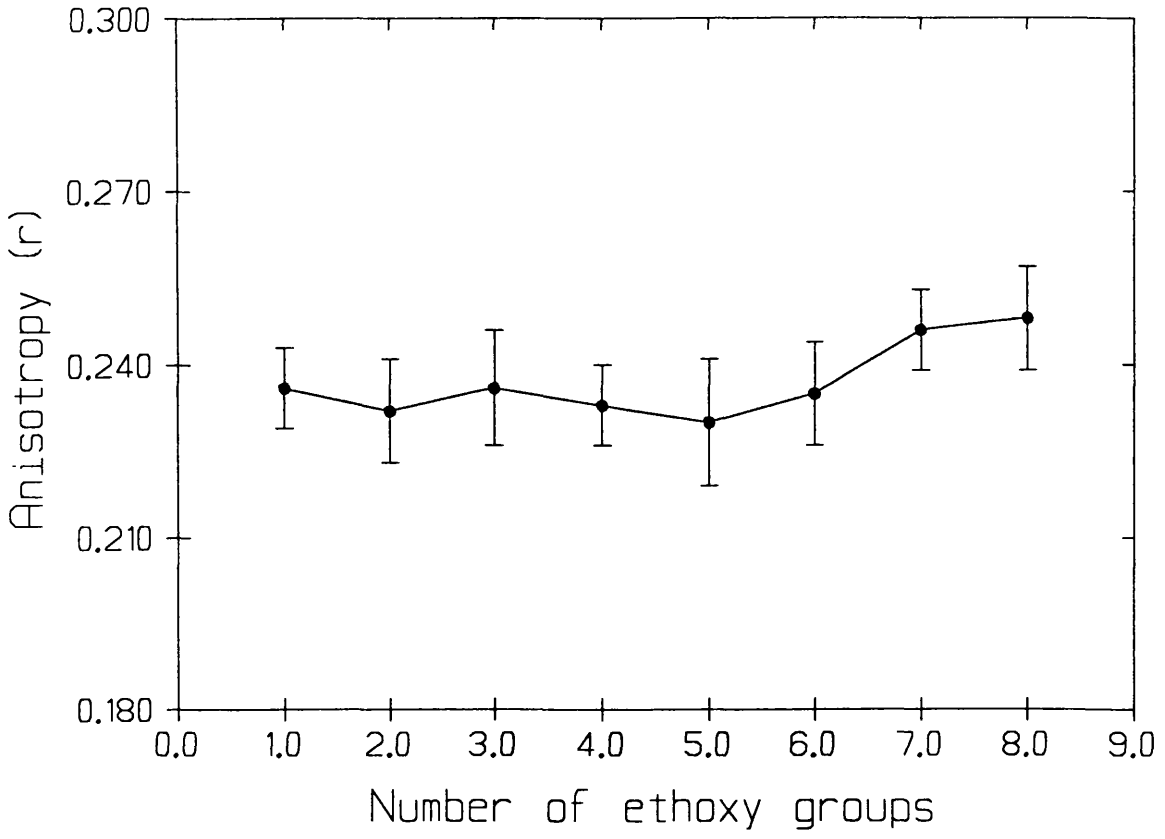

Figure 4.7 Cis-pna probe anistropy at 30°C in DSPC/$C_{12}E_n$ mixed vesicles containing 50 mole% surfactant plotted as a function of surfactant ethoxy chain length. Mean±SD, n=18.

There was a statistically significant difference (Students' t-test, $P<0.05$) between the values of T_c and T_w for $C_{12}E_{4-5}$ and the other surfactant treated vesicles.

Figure 4.7 shows cis-pna anisotropy, r, at 30°C plotted as a function of ethoxy chain length of the incorporated surfactant for DSPC liposomes containing 50 mole% surfactant.

Pure DSPC liposomes gave an r value at 30°C of 0.249 ± 0.005 (n=18). There was no significant difference in anisotropy between surfactants but $C_{12}E_4$ and $C_{12}E_5$ showed a significant decrease in r, with respect to pure DSPC liposomes.

4.3.3 The Effect of Dodecyl Ether Ethoxylates upon DSPC Bilayer Fluidity Measured by DPH Anisotropy

DSPC liposomes showed a sharp phase transition with a T_c of 50.5 ± 1.19°C and a T_w of 3.95 ± 1.27°C when measured by DPH anisotropy. Addition of surfactant again produced a reduction in T_c and an increase in T_w. Plots of T_c and T_w determined by DPH anisotropy, against the ethoxy chain length of incorporated surfactant are shown in Figures 4.8 and 4.9. Looking across the series $C_{12}E_1$-$C_{12}E_8$ T_c decreased and T_w increased from $C_{12}E_1$-$C_{12}E_4$. The maximum effect was observed with $C_{12}E_3$ and $C_{12}E_4$. From $C_{12}E_4$-$C_{12}E_8$ the trend was reversed, T_c increased and T_w decreased.

At 30°C in pure liposomes, DPH anisotropy had a value of 0.254 ± 0.007 (n=9). Addition of surfactant reduced the value of r. The change in r with ethoxy chain length of surfactant displayed similar patterns to those obtained for the plots of T_c against ethoxy chain length (Figure 4.10). A minimum value was obtained with liposomes containing $C_{12}E_4$. The r value of DPH in liposomes containing $C_{12}E_1$-$C_{12}E_3$ was higher than for DPH in liposomes containing $C_{12}E_4$-$C_{12}E_8$.

The effect of the addition of increasing concentrations of $C_{12}E_4$ to DSPC upon DPH anisotropy at 30°C is shown in Figure 4.11. Little effect on r was

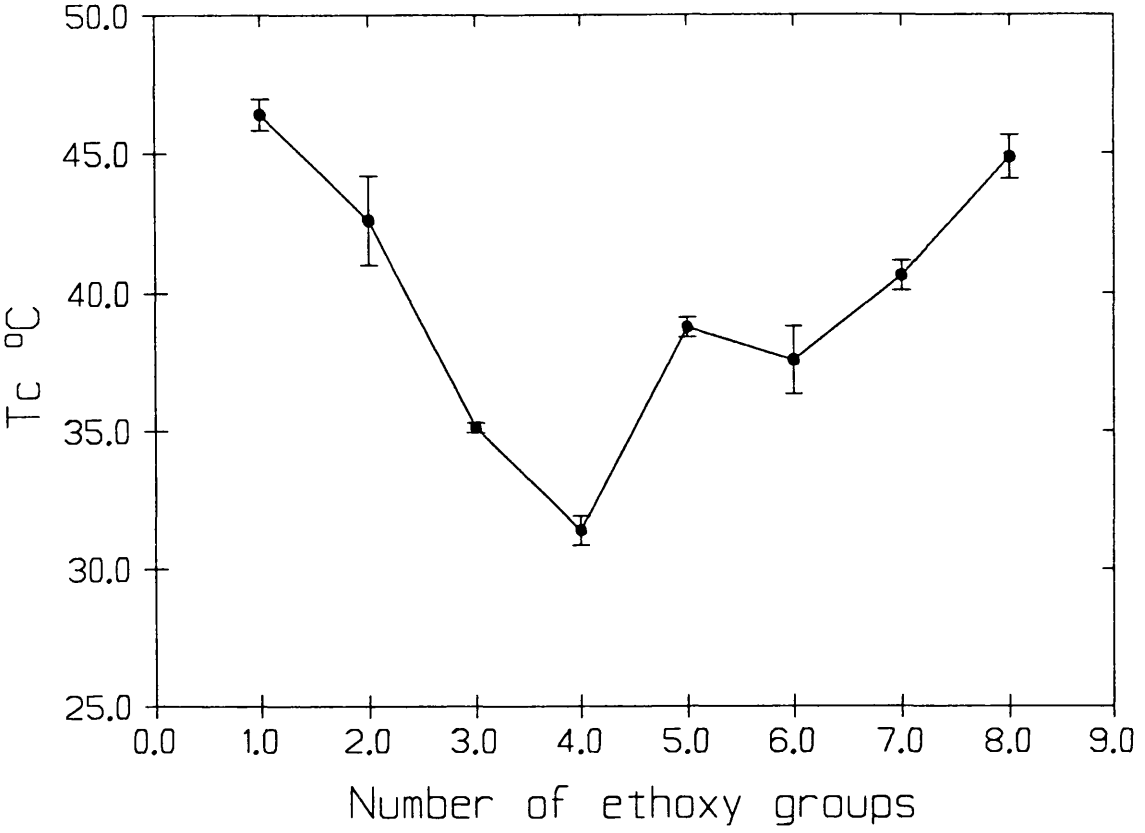

Figure 4.8 T_c values, using DPH as the probe, for the gel-liquid crystalline phase transition of DSPC/$C_{12}E_n$ mixed vesicles containing 50 mole% surfactant plotted as a function of surfactant ethoxy chain length. Mean±SD, n=4.

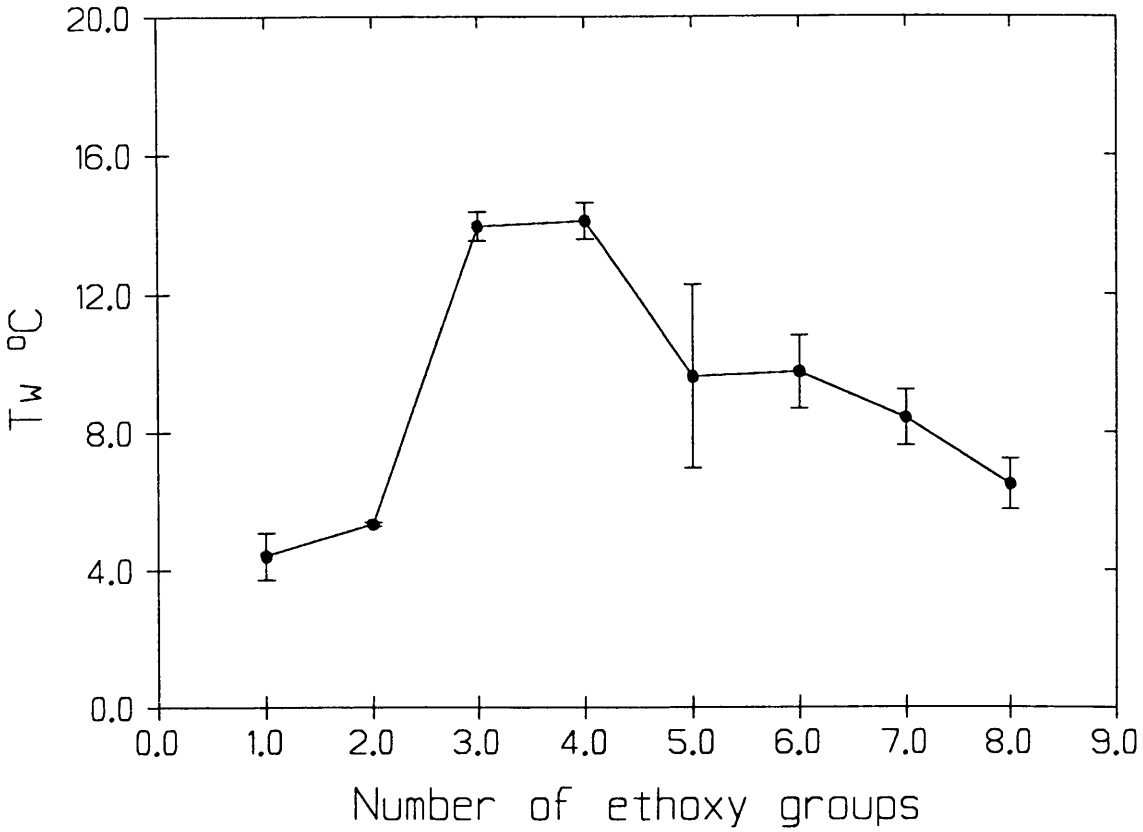

Figure 4.9 T_w values, using DPH as the probe, for the gel-liquid crystalline phase transition of DSPC/$C_{12}E_n$ mixed vesicles containing 50 mole% surfactant plotted as a function of surfactant ethoxy chain length. Mean$\pm$SD, n=4.

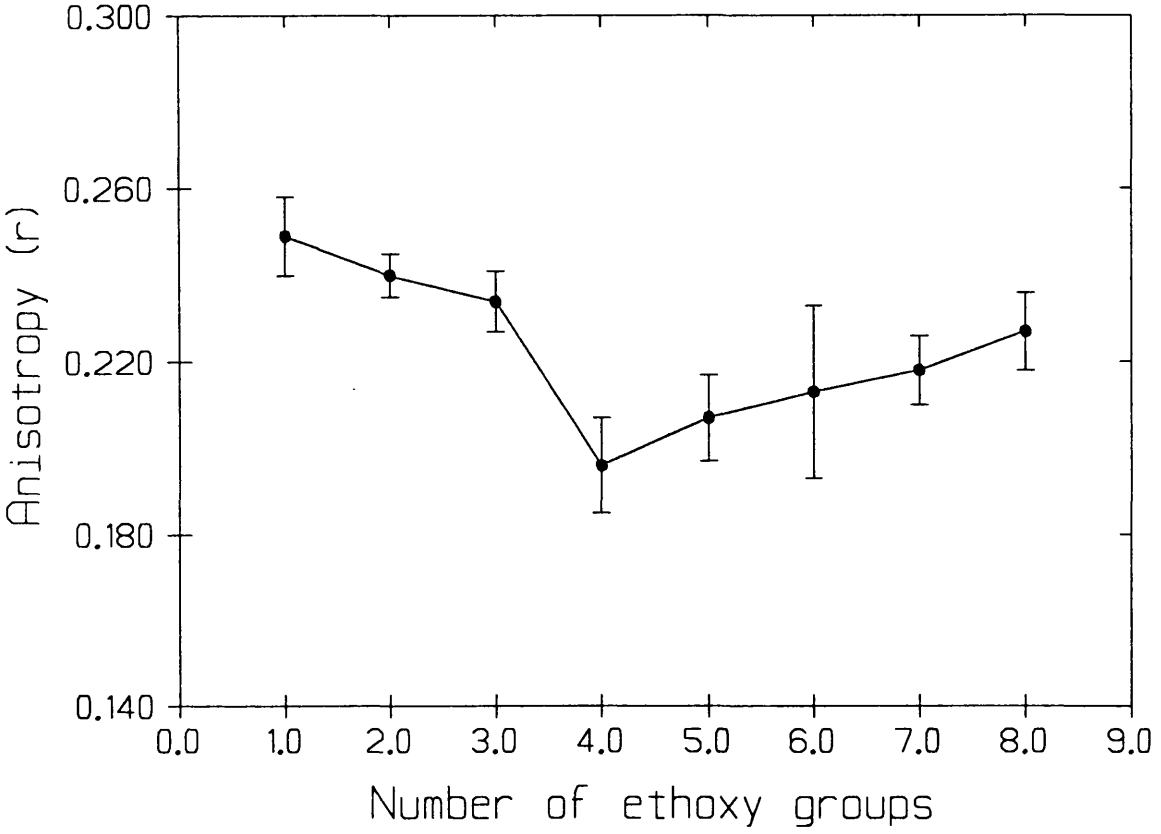

Figure 4.10 DPH probe anistropy at 30°C in DSPC/$C_{12}E_n$ mixed vesicles containing 50 mole% surfactant plotted as a function of surfactant ethoxy chain length. Mean±SD, n=9.

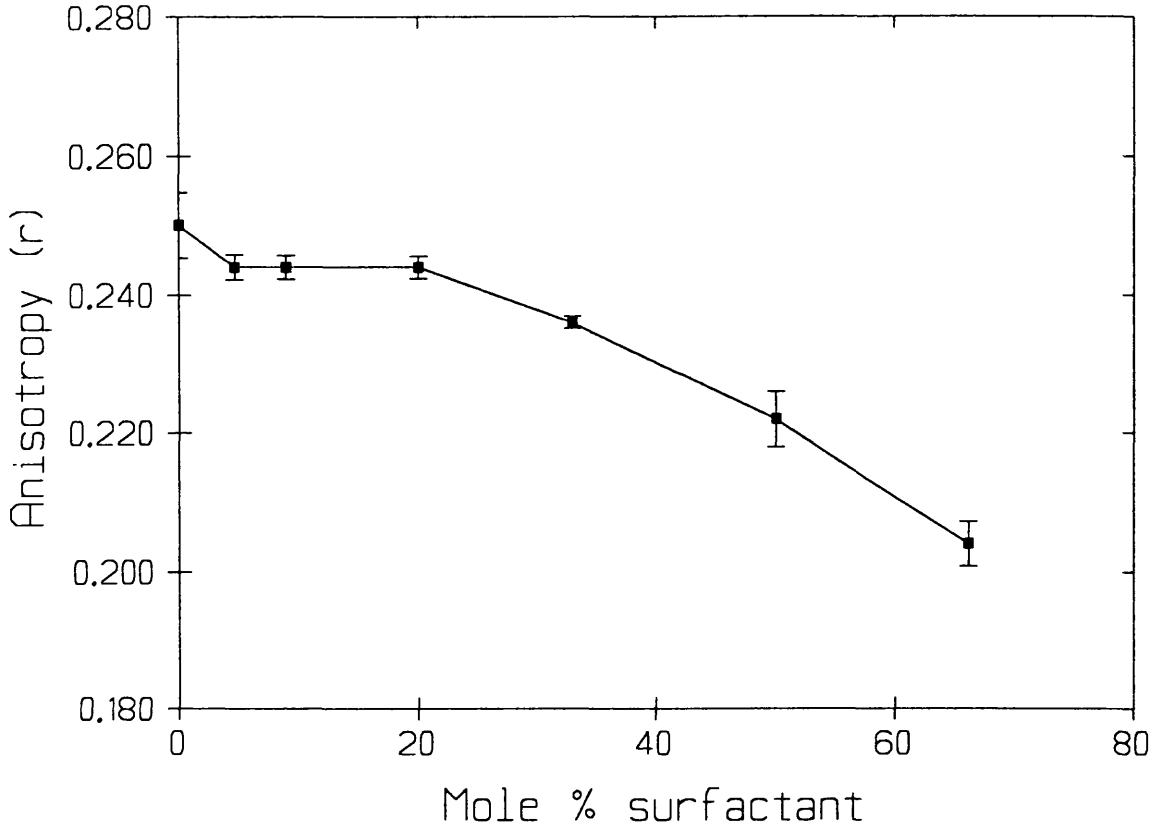

Figure 4.11 The effect of increasing mole percentage $C_{12}E_4$ upon the value of DPH probe anistropy at 30°C in DSPC/$C_{12}E_4$ mixed vesicles. Mean±SD, n=6.

observed up to 20 mole% $C_{12}E_4$. Increasing the surfactant concentration beyond this caused a linear decrease in r with surfactant concentration.

4.3.4 The Effect of Dodecyl Ether Ethoxylates Upon DSPC Bilayer Fluidity Measured by Perylene Anisotropy

The probe anisotropy of perylene in DSPC liposomes was far lower than for either DPH or cis-pna. At 20°C, an r value of about 0.11 was obtained. As temperature increased r dropped linearly to about 0.05 at 50°C. Between 50-55°C r fell to a value of approximately 0.01 and remained constant up to 65°C. This produced a flat sigmoidal curve of r against temperature, Figure 4.12. From this curve T_c was calculated to be 50.87±0.17°C and T_w 3.32±0.106°C.

T_c and T_w were calculated for liposomes incorporating 50 mole% surfactant. When plotted as a function of surfactant ethoxy chain length, T_c was seen to be lowered most by surfactants in the range $C_{12}E_2$-$C_{12}E_5$, $C_{12}E_1$ and $C_{12}E_6$-$C_{12}E_8$ were less potent (Figure 4.13). T_w was raised the most by $C_{12}E_5$. The other surfactants all had a similar less potent effect (Figure 4.14).

At 30°C the measured probe anisotropy of perylene in pure DSPC liposomes was 0.109±0.007. Addition of surfactant caused a decrease in r, Figure 4.15. As a function of added surfactant ethoxy chain length there was no significant difference between the effects of $C_{12}E_3$-$C_{12}E_8$, all of which lowered r to a value of about 0.06 (t-test, $p < 0.05$ in all cases). This was significantly different to the value obtained in pure DSPC (t-test, $p > 0.05$). $C_{12}E_1$ and $C_{12}E_2$ had less of an effect upon r at 30°C.

The effect of the addition of increasing concentrations of $C_{12}E_4$ to DSPC liposomes upon perylene anisotropy is shown in Figure 4.16. No effect was observed upon r up to 9 mole% surfactant, above which increasing surfactant concentration caused a linear decrease in r.

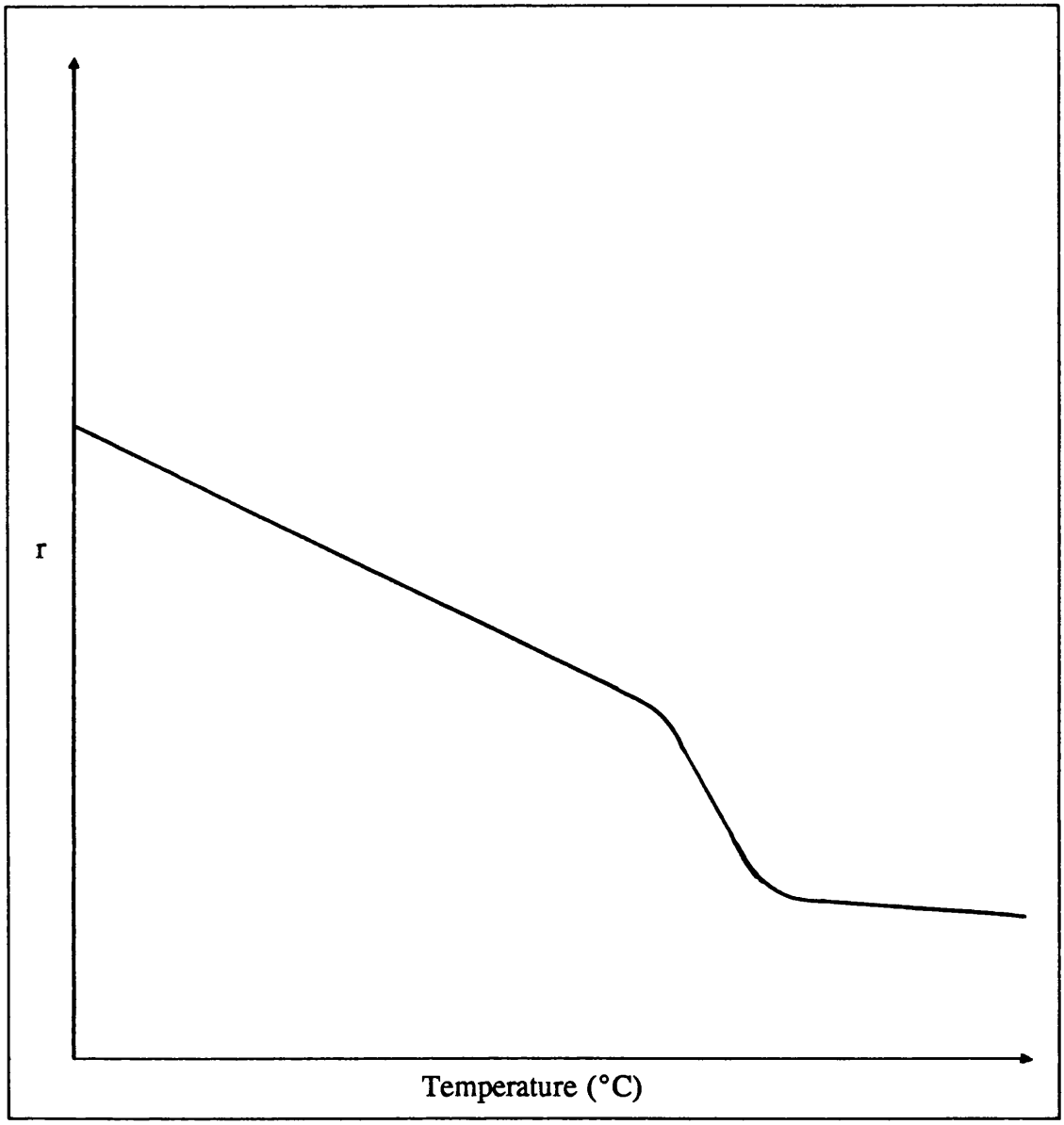

Figure 4.12 Probe anistropy r, plotted against temperature for perylene incorporated into DSPC liposomes.

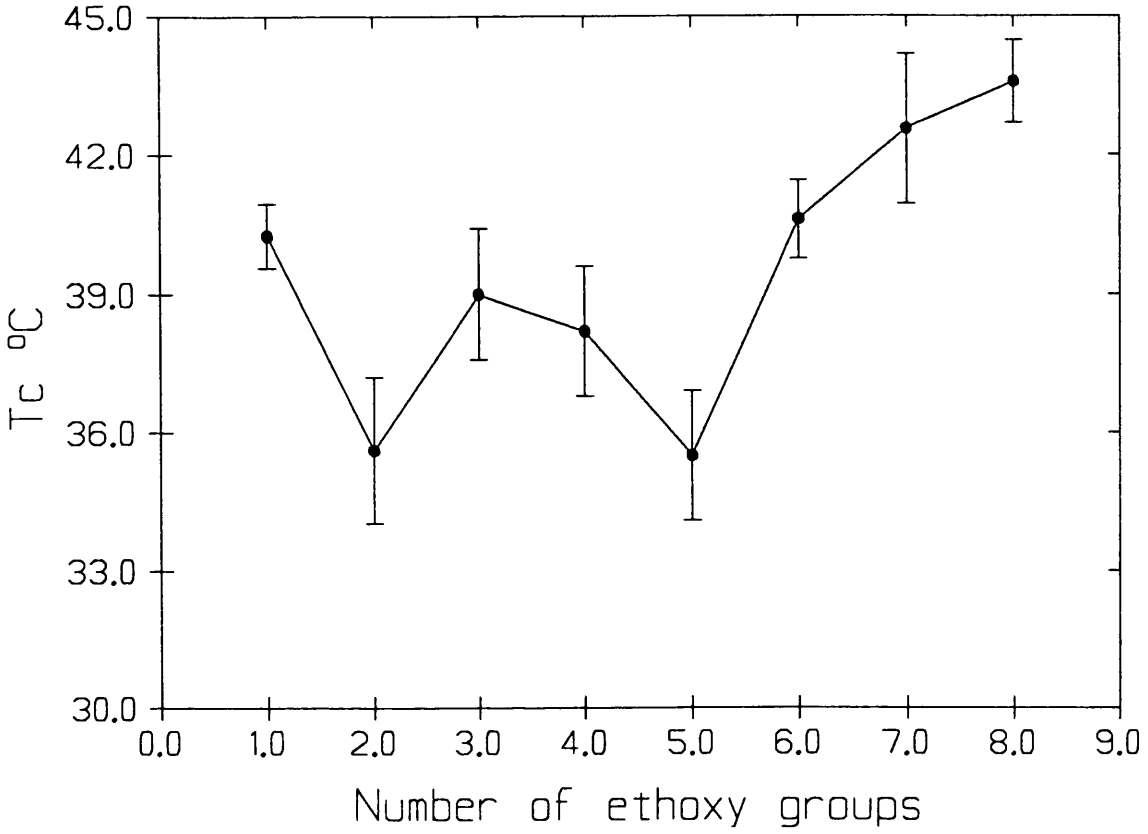

Figure 4.13 T_c values, using perylene as the probe, for the gel-liquid crystalline phase transition of DSPC/$C_{12}E_n$ mixed vesicles containing 50 mole% surfactant plotted as a function of surfactant ethoxy chain length. Mean±SD, n=4.

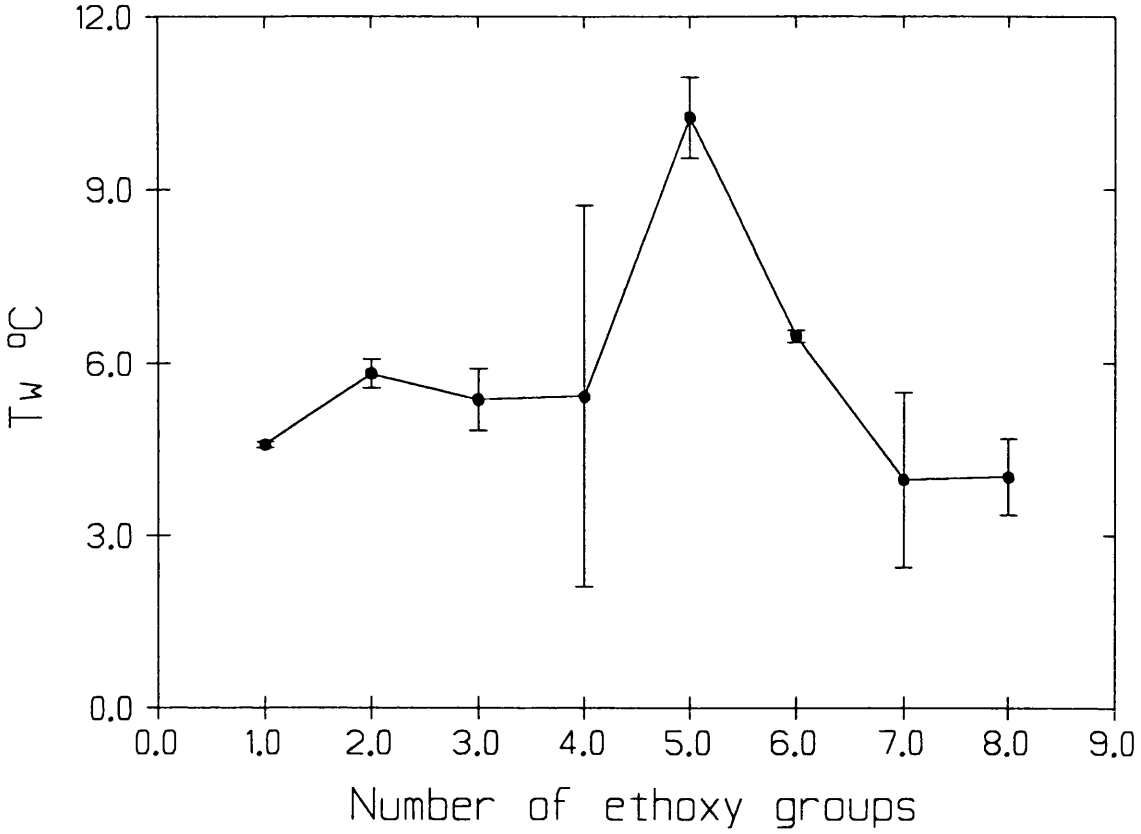

Figure 4.14 T_w values, using perylene as the probe, for the gel-liquid crystalline phase transition of DSPC/$C_{12}E_n$ mixed vesicles containing 50 mole% surfactant plotted as a function of surfactant ethoxy chain length. Mean$\pm$SD, n=4.

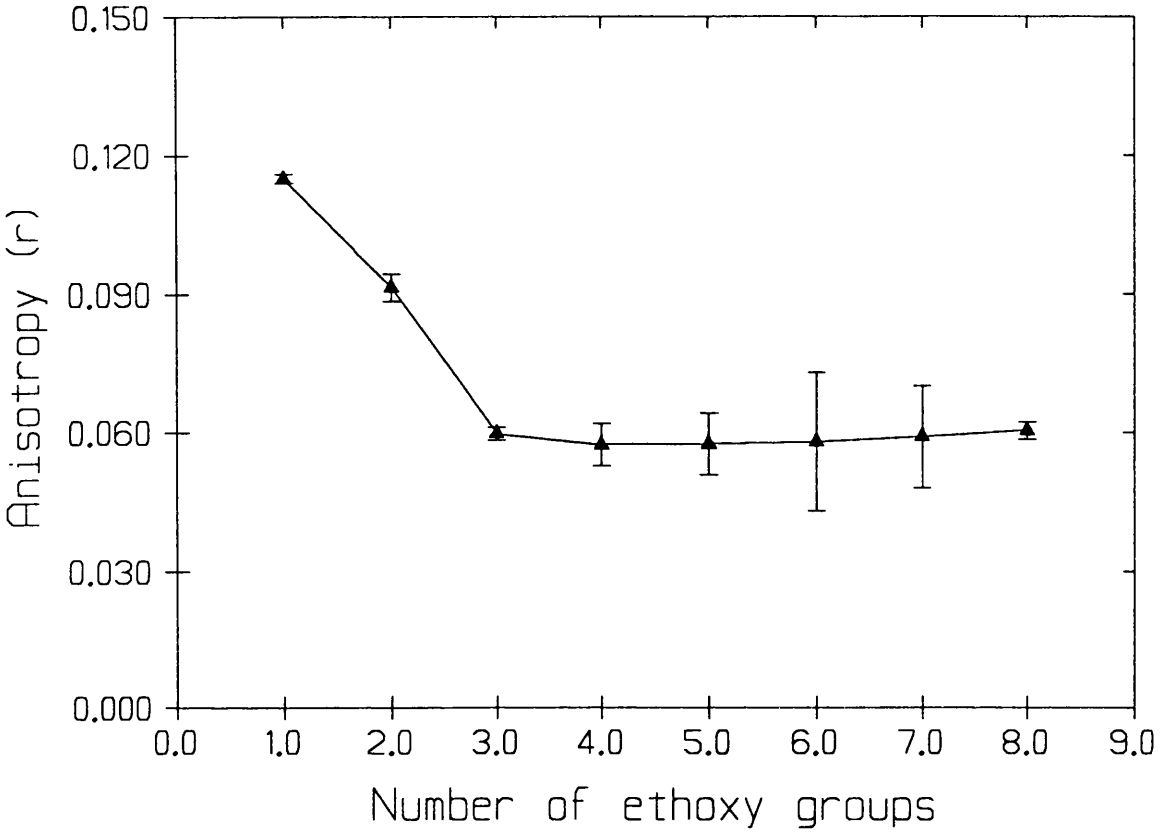

Figure 4.15 Perylene probe anistropy at 30°C in DSPC/$C_{12}E_n$ mixed vesicles containing 50 mole% surfactant plotted as a function of surfactant ethoxy chain length. Mean±SD, n=9.

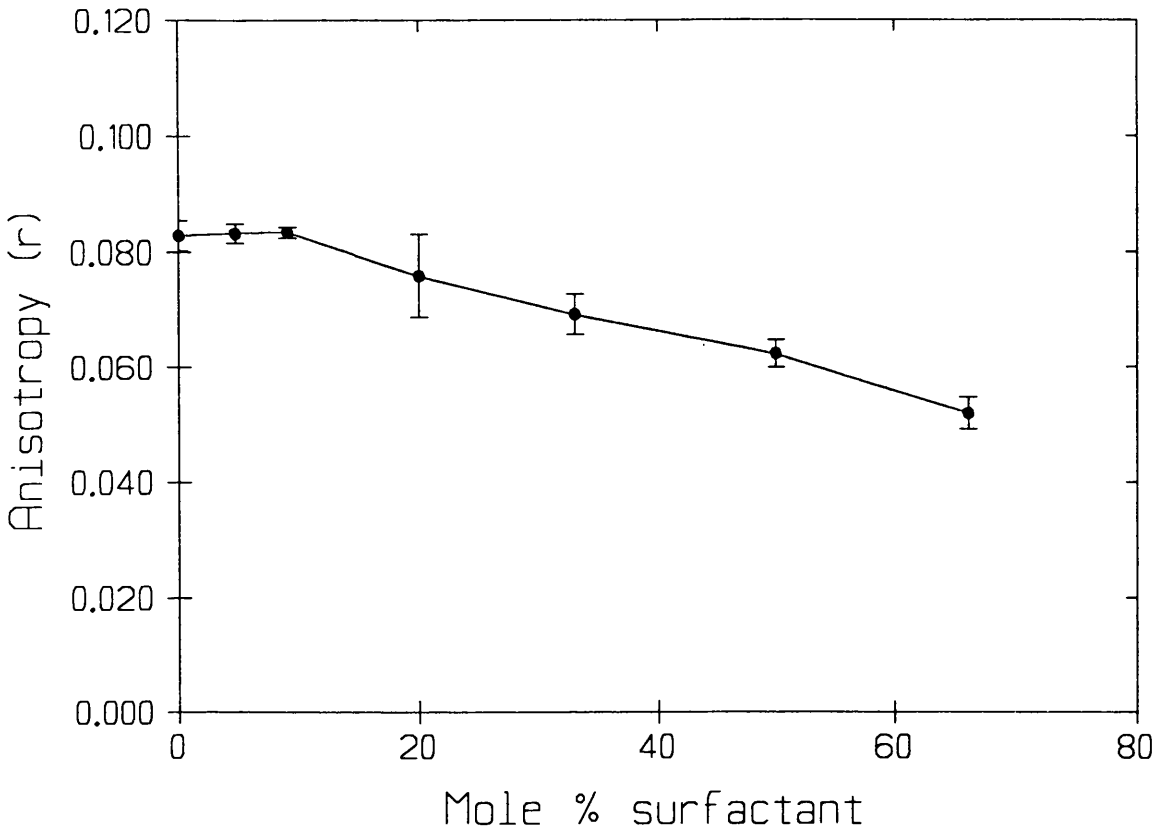

Figure 4.16 The effect of increasing mole percentage $C_{12}E_4$ upon the value of perylene probe anistropy at 30°C in DSPC/$C_{12}E_4$ mixed vesicles. Mean$\pm$SD, n=6.

4.3.5 The Effect of Dodecyl Ether Ethoxylates upon DSPC Bilayer Fluidity as measured by ANS Anisotropy

The probe polarisation anisotropy of ANS was measured only at 30°C. In pure DSPC liposomes a value of 0.159 ± 0.006 was obtained. Addition of $C_{12}E_1$-$C_{12}E_3$ to the liposomes caused no significant change in r (Figure 4.17). However, over the range $C_{12}E_4$-$C_{12}E_6$ there was a continual decrease in r, a minimum being reached with $C_{12}E_6$. Further increases in ethoxy chain length of the surfactant produced higher values of r. $C_{12}E_4$-$C_{12}E_7$ all produced a statistically significant decrease in r with respect to pure DSPC liposomes (t-test, $p > 0.05$).

4.3.6 The Effect of Azone on DSPC Bilayer Fluidity Measured by FPS

Table 4.3 shows the calculated T_c and T_w of the gel-liquid crystalline phase transition of DSPC liposomes containing 9, 33 and 50 mole% Azone by cis-pna FPS and 50 mole% Azone using DPH and perylene as probes. The table also shows the probe anisotropy, r, of the above stated systems and ANS anisotropy in DSPC liposomes containing 50 mole% Azone. At 9 mole% Azone no significant effect was observed. With 33 mole% Azone with cis-pna and 50 mole% Azone with all four probes T_c decreased and T_w increased. In the same systems, r at 30°C showed a significant decrease with respect to pure DSPC liposomes (t-test, $p > 0.01$).

4.4 DISCUSSION

The transition onset temperatures and transition widths of the gel-liquid crystalline phase transition of DSPC liposomes obtained with three probes cis-pna, DPH and perylene were all in close agreement with each other and reported literature values for both FPS (136,143) and other techniques (96). The transition widths calculated here were broader than the $\Delta T_{1/2}$ values observed for DSPC

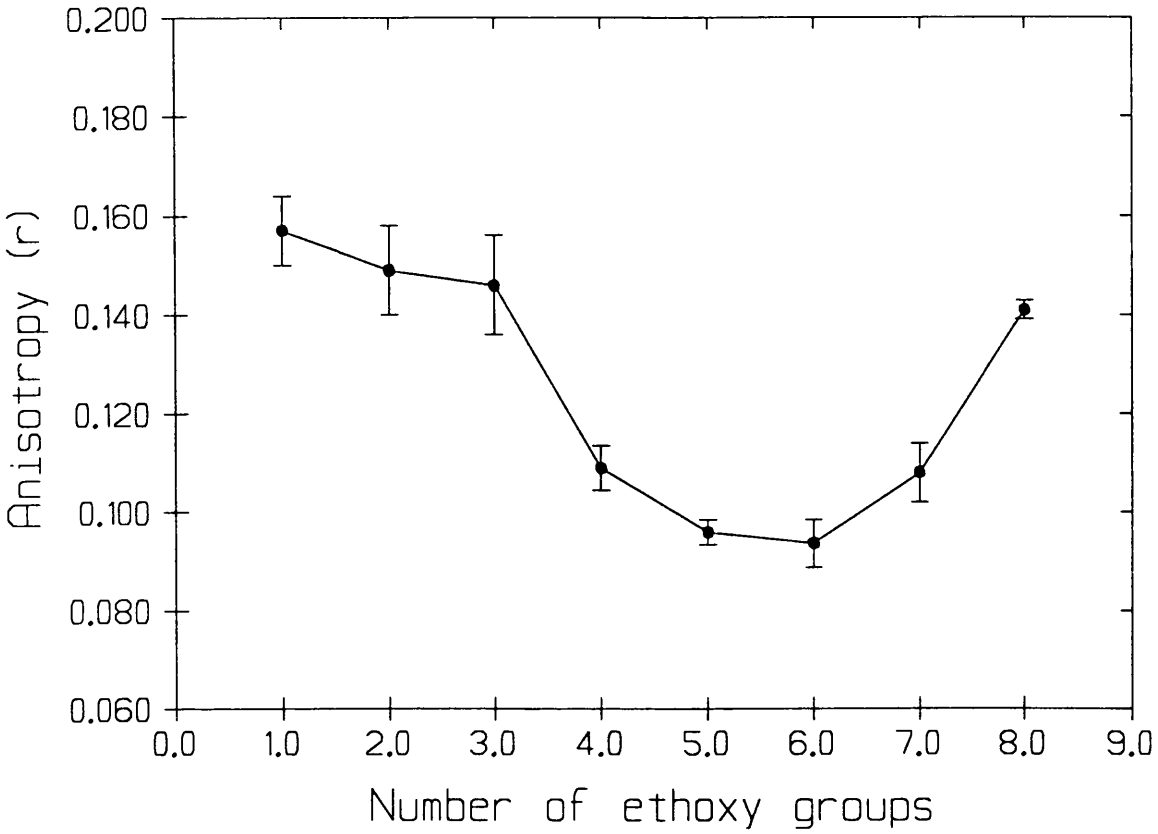

Figure 4.17 ANS probe anistropy at 30°C in DSPC/$C_{12}E_n$ mixed vesicles containing 50 mole% surfactant plotted as a function of surfactant ethoxy chain length. Mean±SD, n=9.

Probe	T_c (°C)	T_w (°C)	r @ 30°
Cis-pna [a]	49.1±0.14	4.52±0.03	0.252±0.013
[b]	43.3±2.03	7.00±1.20	0.232±0.005
[c]	39.9±2.50	8.80±1.50	0.226±0.013
DPH [c]	38.2±1.06	13.62±1.9	0.156±0.017
Perylene [c]	42.6±0.07	7.63±1.10	0.042±0.005
ANS [c]	-	-	0.123±0.002

Table 4.3. The effect of Azone on the T_c and T_w of DSPC liposomes and probe anisotropy, r, at 30°C measured by FPS with four fluorescent probes

[a] 9 mole% Azone

[b] 33 mole% Azone

[c] 50 mole% Azone

T_c and T_w (mean±SD, n=4)

r (mean±SD, n>6)

transitions measured by DSC (Chapter 3). The T_w values were calculated as the entire transition width incorporating the pretransition, whereas $\Delta T_{1/2}$ values were calculated as the peak width at half peak height. The r values obtained in gel and fluid phases of pure DSPC for cis-pna, DPH and perylene were in agreement with literature values (140,143).

The incorporation of dodecyl ether ethoxylate surfactants into the lipid bilayers reduced the phase transition temperature and increased the phase transition width. The changes in these parameters are indicative of disruption of the ordered packing of the lipid chains causing increased fluidity in the lipid bilayers and a reduction in the cooperativity of the melt (see discussion in Chapter 3).

Incorporation of surfactant also caused a reduction in the probe anisotropy (r). A mixture of long (C_{18}) and short (C_{12}) acyl chains does not pack in as tight a crystalline structure as pure lipid (119). The extent and strength of molecular interactions between lipid molecules and probe molecules would therefore be reduced in the surfactant treated systems. This allows the probes to undergo a greater amount of molecular rotation and translational motion thus reducing r with respect to its value in pure DSPC bilayers.

The relationship between the extent of bilayer fluidisation and surfactant structure could be expected to be equivalent in the presence of all four fluorescent probes used. However, the results indicated that this fluidisation caused different effects on the rotational motion of each probe.

The observed differences in the surfactant structure/bilayer fluidisation relationship between probes was thought to be dependent upon probe structure, probe location in the membrane and probe/lipid/surfactant interactions.

Due to their differences in structure each probe will occupy a different location and orientation in the bilayer. Cis-pna is C_{18} fatty acid and was expected to sit in the same plane of the membrane as the C_{18} chains of the DSPC molecules (141,144). DPH and perylene are both highly hydrophobic molecules and are used to probe the nonpolar membrane interior (136,145,146). ANS, however, has a

negatively charged sulphonate group attached to a hydrophobic naphthalene group. These two groups give the molecule an amphipathic nature so ANS is thought to adsorb at the bilayer polar/non polar interface and is regarded as a good probe for studying the headgroup vicinity of the membrane (145,147). This has been confirmed by X-ray diffraction studies of phospholipid membranes containing ANS (148). This information is summarised diagrammatically in Figure 4.18

When cis-pna was used as the probe, $C_{12}E_4$ and $C_{12}E_5$ showed the greatest degree of membrane fluidisation observed by all three considered parameters, T_c, T_w and r at 30°C. As cis-pna is located in the membrane plane similarly to a DSPC acyl chain it would be expected to behave similarly to DSPC molecules in response to perturbing agents such as heat or surfactant addition. The results obtained with this probe would therefore be expected to be in good correlation with those obtained in the previous chapter by DSC, where $C_{12}E_3$ was the optimum membrane fluidiser. The differences observed may have been related to the differences in surfactant and DSPC concentrations. For both DSC and FPS studies 1:1 lipid/surfactant ratios were used but for FPS the overall concentration was 2000 times lower than for DSC. This may have affected phase and partitioning behaviour of the surfactants emphasising the importance of phase ratio in the partitioning of surfactants into membranes. These concentration differences would be expected to effect the results with all probes studied. The interaction of the surfactant ethoxy chains with the cis-pna carboxyl group is another factor which may have caused a difference between the DSC and FPS results. Although there were significant differences in T_c and T_w as a function of structure, there was less variation in probe anisotropy at 30°C within the series of surfactants, although $C_{12}E_4$ and $C_{12}E_5$ treated liposomes were significantly more fluid than pure DSPC systems. These results suggest that the fluidity of the lipids in the gel-crystalline phase at 30°C, physiological skin temperature, will be increased by the presence of the surfactants, but the degree of change may not be as great as the change in T_c or T_w.

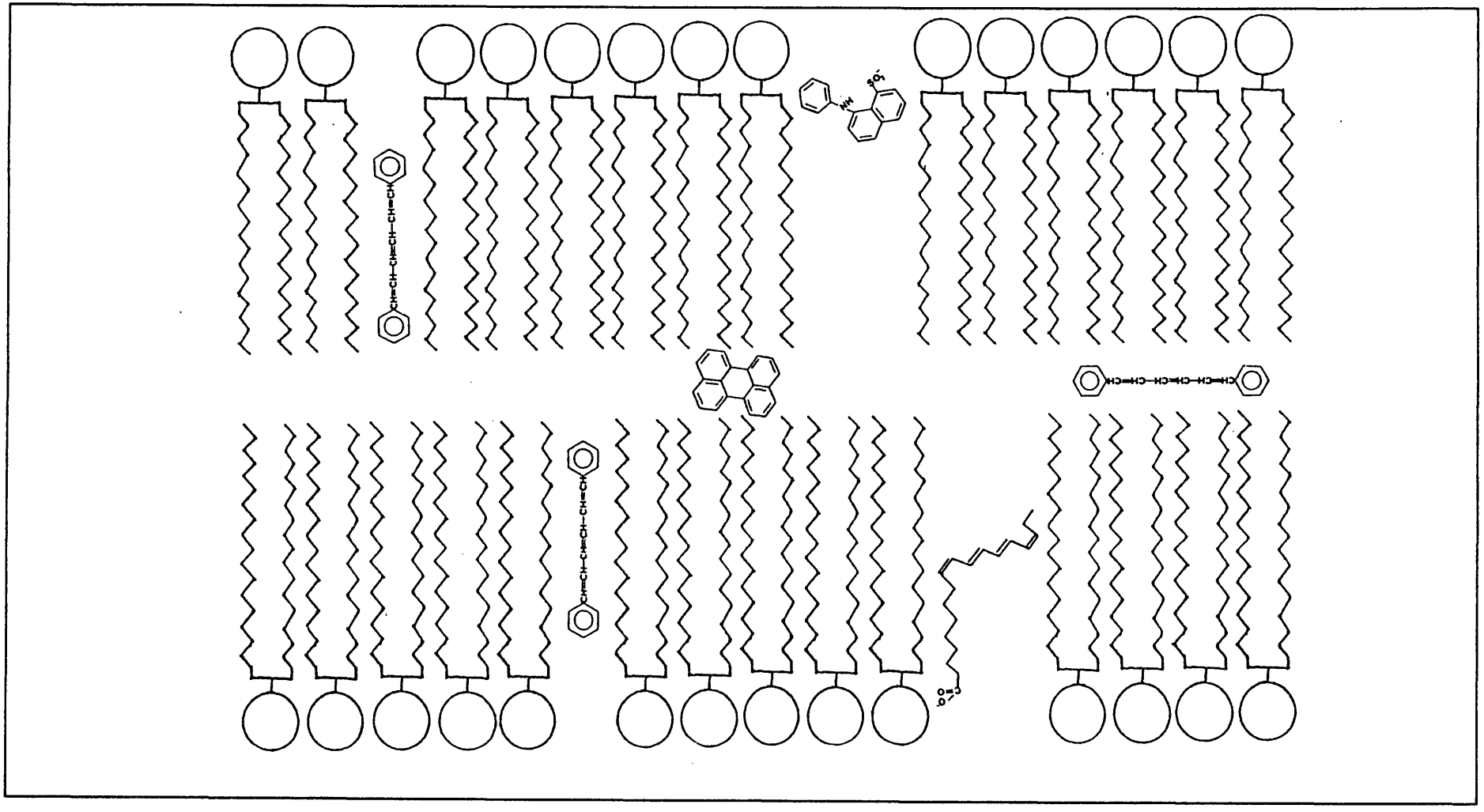

Figure 4.18 The suspected orientation and distribution of the fluorescent probes in a model lipid bilayer.

Using DPH as the probe $C_{12}E_3$ and $C_{12}E_4$ were the most potent membrane fluidisers, indicated by the change in T_c and T_w. When assessed by probe anisotropy at 30°C, $C_{12}E_4$ was judged to be the most potent fluidiser. The effect of the surfactants measured with perylene showed a more complicated relationships between structure and fluidisation. This may be due to the difficulties in the precise measurement of T_c and T_w with the flatter transition profiles obtained with perylene.

DPH and perylene might be expected to give similar results as they both probe the same microenvironment; the bilayer interior. However, with perylene a wider range of surfactants ($C_{12}E_2$-$C_{12}E_5$) was observed as effective fluidisers, when judged by T_c and T_w. Differences were also observed between the results obtained with perylene and DPH with respect to the concentration dependent change in anisotropy with added $C_{12}E_4$ to DSPC bilayers. Less $C_{12}E_4$ (9 mole%) was needed to invoke a decrease in the r value for perylene compared to the 20 mole% $C_{12}E_4$ required to invoke such a change in DPH anisotropy.

These effects may be associated with differences in probe location although both were expected to reside in the membrane interior. Perylene is thought to locate within the bilayers between the terminal methylene groups of the DSPC (145). The disc shaped, planar, perylene molecules do not easily fit into ordered crystalline systems. An increase in acyl chain flexibility as the acyl chain is transcended from head group to terminal methyl has been reported (149) which creates a slightly more fluid region in the bilayer centre. The region may act as a solvent for perylene molecules. DPH on the other hand, can be envisaged as a long rod shaped molecule (150). It is thought to be more evenly dispersed throughout the bilayer interior, both in the bilayer centre and between the acyl chains of the DSPC (136). The anisotropy observed is a mean of the anisotropic movements of all probe molecules in the membrane regardless of their location. The molecules near the bilayer interface will be more constrained than those deeper in the bilayer

interior. A fluidising compound may exert a graded effect upon fluidisation down the acyl chains into the bilayer.

In membranes containing two non-ideally mixing components, those with large differences in acyl chain length, lateral phase separation can occur (101). If the fluorescent probe molecule preferentially partitions into either a more fluid or more crystalline phase the measured anisotropy will be biased to that area of the membrane (139). Cis-pna and DPH have gel crystalline-liquid crystalline partition coefficients of 0.7 ± 0.2 (142) and 1.2 ± 0.2 (151) respectively and so will distribute fairly evenly between phases giving a good average viscosity. Perylene is thought to preferentially partition into more fluid phases (14,19) so may give lower than expected anisotropy values.

The effect of probe partitioning would have a greater effect on the total probe anisotropy (r) than on the determination of the phase transition parameters T_c and T_w. This may explain why the plots for T_c and T_w differ from those for r at 30°C, which was most notable with perylene. The values of r in liposomes containing $C_{12}E_7$ and $C_{12}E_8$ were much lower than expected (Figure 4.15) from the experiments of surfactant partitioning behaviour described earlier (3.4.). This could be explained by the probe becoming incorporated into surfactant micelles which may form with hydrophilic surfactants. Such micelles may produce a lower probe anisotropy than DSPC liposomes or DSPC/surfactant vesicles. Such effects were observed when r was measured for both DPH and perylene at 30°C in samples prepared without DSPC, i.e. surfactant only. (results not shown). The net effect observed would be a lower value of r, even though $C_{12}E_7$ and $C_{12}E_8$ may not alter the gel-liquid crystalline phase transition of DSPC.

When ANS was used as the probe the largest increase in membrane fluidity was obtained with the surfactant range $C_{12}E_4$-$C_{12}E_7$ with maximum fluidisation observed with $C_{12}E_6$. As with the other probes the very high and very low HLB surfactants had less effect.

The interaction of surfactants with the DSPC bilayer at the polar interface observed with ANS will be dependent upon the surfactant penetration of the bilayer and the interaction of the surfactant ethoxy chain with the polar head region of the DSPC and ANS probe. In phosphatidylcholine membranes the ANS binding site appears to be composed of four polar choline headgroups (147). Changes in the character of these sites due to perturbation by foreign molecules will result in reduced or altered binding of the ANS (147). The surfactant ethylene oxide chains may disrupt headgroup packing or the hydration sphere that would be bound around the polar groups. Surfactants in the range $C_{12}E_4$-$C_{12}E_7$ may have the most appropriate balance of partition coefficient and a long enough ethoxy chain length to cause disruption of the headgroup region.

CHAPTER 5

MEASUREMENT OF LIPID BILAYER FLUIDISATION BY ELECTRON SPIN RESONANCE SPECTROSCOPY

5.1 INTRODUCTION

5.1.1 Principles of Electron Spin Resonance Spectroscopy

Electron spin resonance spectroscopy (ESR) can be described as the study of molecules containing unpaired electrons by observing the magnetic field at which they come into resonance with monochromatic radiation (152).

The layout of a basic spectrometer is shown schematically in Figure 5.1. It consists of a microwave source (a Klystron), the sample cavity, a microwave detector and an electromagnet that produces fields that can be varied in the region of 0.3 Tesla (3 KGauss). Magnetic fields of about 0.3T correspond to produce resonance with an electromagnetic field of frequency of 9GHz and wavelength 3cm.

An ESR spectrum is obtained by monitoring the microwave absorption by a molecule as the magnetic field strength is changed. As only molecules that possess unpaired electrons will show spin resonance the technique is used to study free radicals or triplet states formed during reactions. ESR can also be used to study systems that do not possess suitable molecules by incorporation of stable radicals into these systems as probe molecules.

The most important feature of ESR spectra is their hyperfine structure, the splitting of individual resonance lines. The extent of hyperfine splitting observed for a particular molecule is determined primarily by the spin of the molecules nucleus. If the molecule has a nuclear spin of ½ two spin orientations are possible and two resonance positions will occur. The absorption spectrum will be split into two lines. The field separation between the two lines is known as the hyperfine splitting tensor which is termed A.

If the radical is based around a nitrogen atom, for example a nitroxide group, the ESR spectrum will be split into 3 lines of equal intensity as the ^{14}N nucleus has 3 possible spin orientations +1, 0 and -1. The hyperfine splitting tensors for a nitroxide radical are affected by the fact that the interactions with the applied magnetic field are anisotropic due to the axial symmetry of the π orbital electrons in the nitroxide radical. This is very relevant when the motion of the

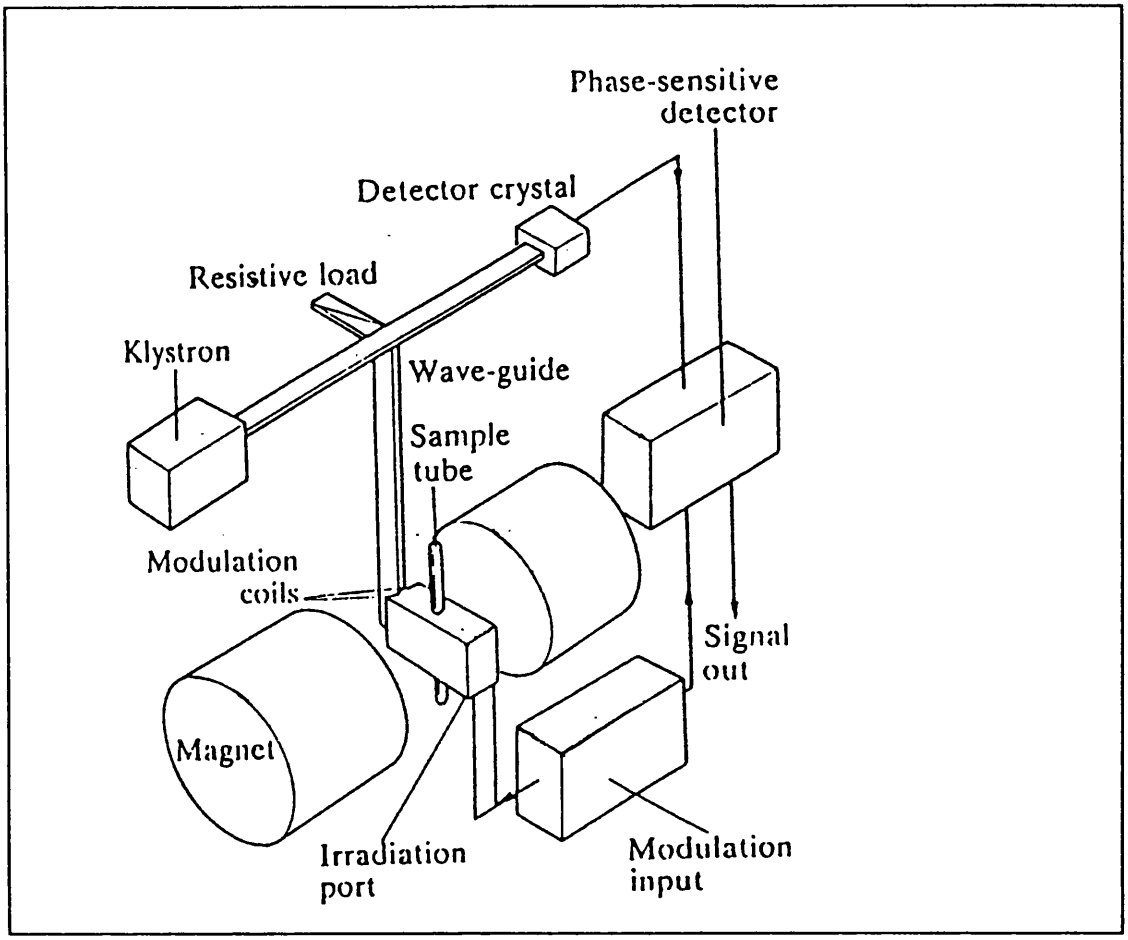

Figure 5.1 The basic layout of a typical electron spin resonance spectrometer.

probe is restricted in viscous solvents. Two characteristic hyperfine splittings can be determined from the ESR spectra. These are termed A_{II} and $A_{\perp}$ which are the hyperfine splitting generated when the magnetic field is parallel and perpendicular to the π orbital axis of the nitroxide bond respectively (153).

The viscosity of the medium surrounding the probe has an effect upon spectra. In a sample that contains probe molecules in all possible orientations in the absence of molecular motion, for example in a dispersion of crystalline powder, a complicated spectrum is produced (153). The contribution of all molecular orientations is added and the observed spectrum is of the type shown in Figure 5.2. This is known as a 'powder spectrum'. The distance between the low and high field peaks is a direct measure of $2A_{II}$ (154,155).

If the nitroxide radical is tumbling in solution all orientations are present but the resonance position will hop from one position to another as the molecule changes orientation in the magnetic field. This resonance exchange process leads to averaging of the hyperfine splitting tensors and intermediate values are obtained. The value of A_{II} will decrease and $A_{\perp}$ increase. As the rate of molecular tumbling increases the extent of the averaging will also increase. A typical ESR spectrum for a nitroxide radical present on a fatty acid chain (see 5.1.3) undergoing fast anisotropic motion in a comparatively fluid membrane is shown in Figure 5.3. Both A_{II} and $A_{\perp}$ can be measured directly from the spectrum.

5.1.2 The Order Parameter: A Measure of Probe Anisotropic Motion

As described previously, an increase in probe motion results in a decrease in A_{II} and an increase in $A_{\perp}$. Therefore the quantity A_{II}-$A_{\perp}$ reflects the degree of order of the spin label. This is often normalised relative to the maximum possible splitting measured from powder spectra of single crystals, to give a dimensionless quantity, the Order Parameter, S, where:

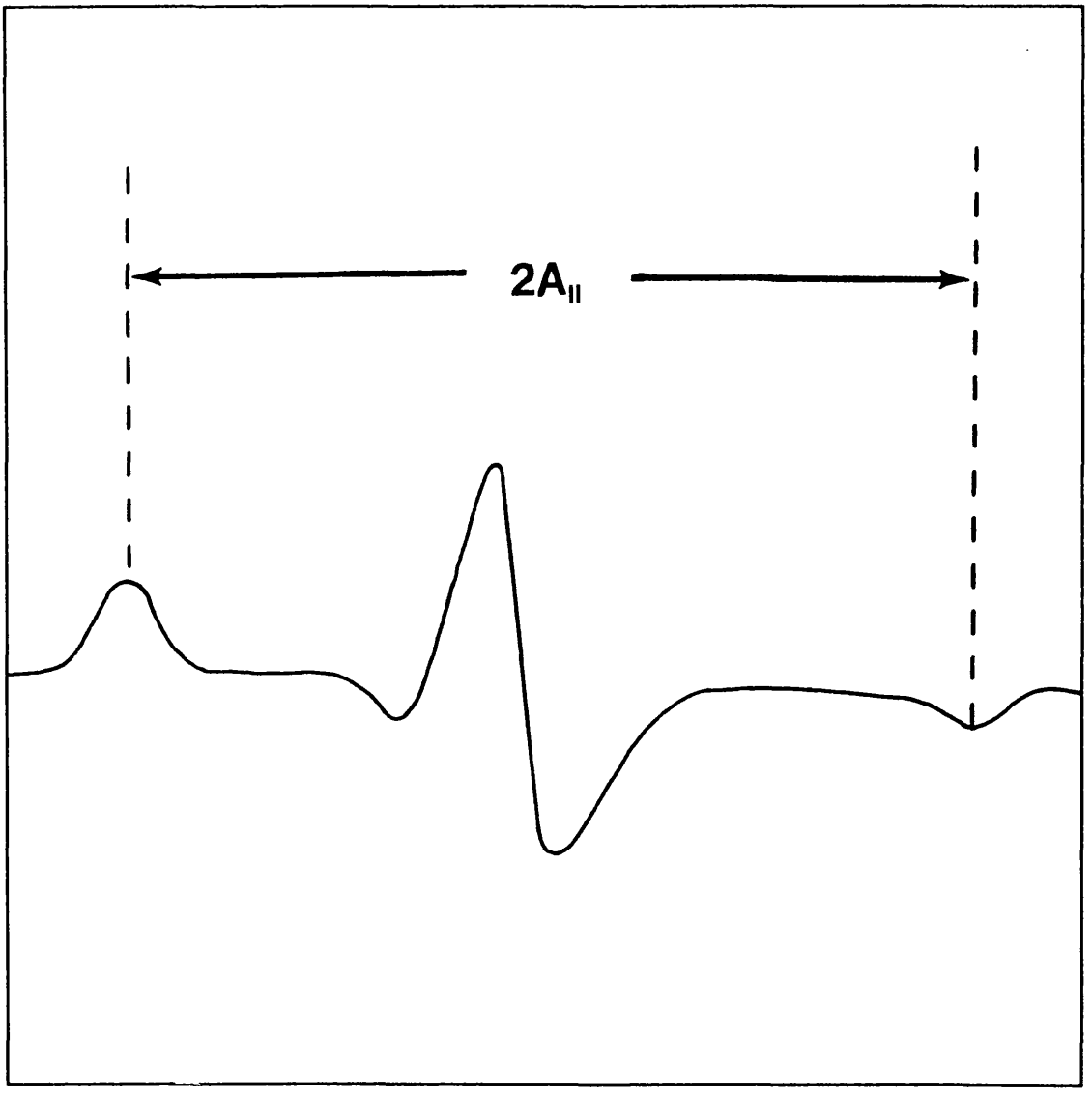

Figure 5.2 A typical ESR `powder spectrum'

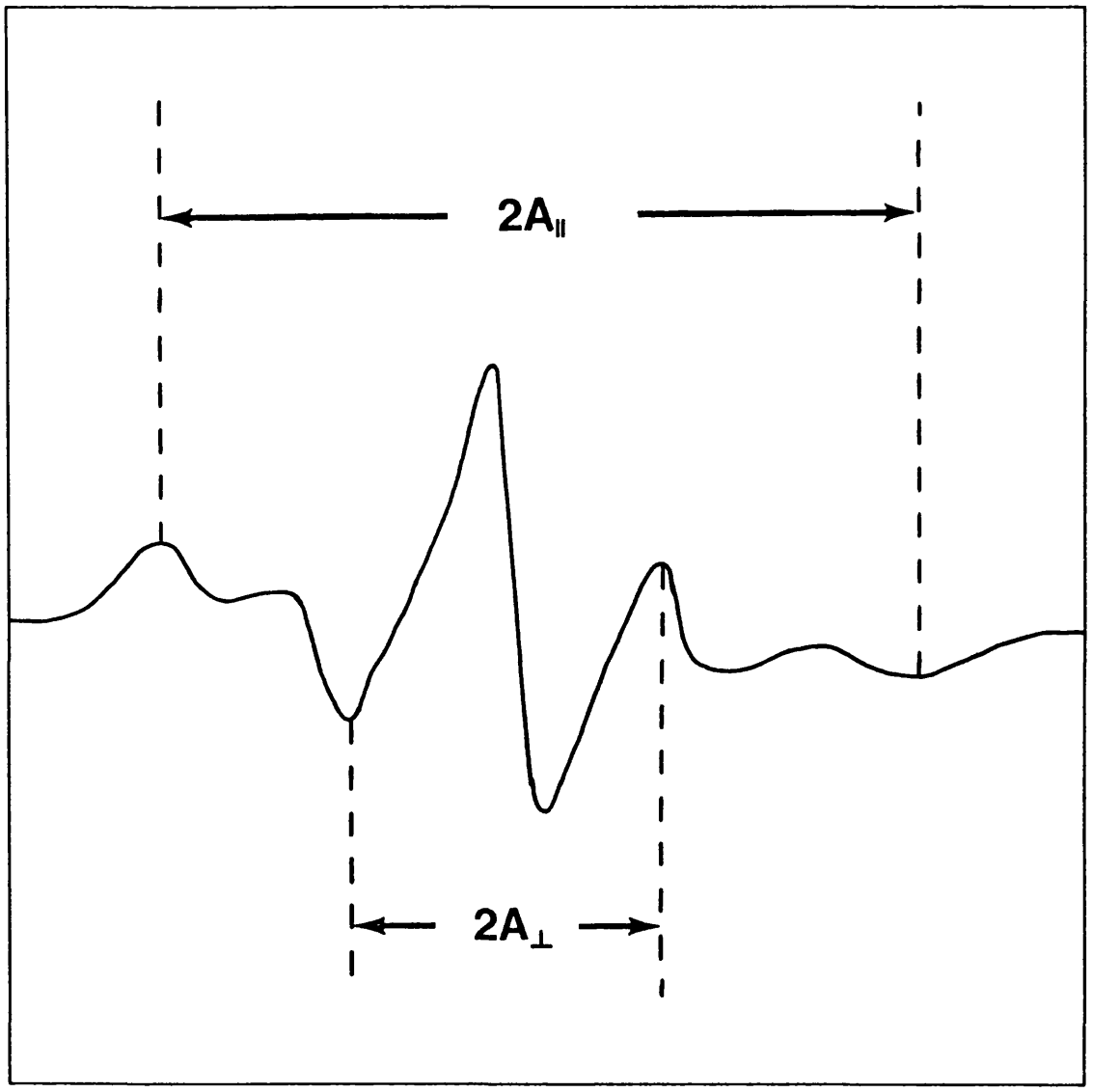

Figure 5.3 Typical ESR spectrum for a fatty acid nitroxide spin probe undergoing fast anisotropic motion in a fluid membrane.

$$S = \frac{A_{II} - A_{\perp}}{A_{zz}-(\frac{1}{2})(A_{xx}+A_{yy})} \qquad \text{Equation 5.1}$$

Where A_{zz}, A_{xx} and A_{yy} are the principle hyperfine splitting tensors corresponding to the molecular axes of the spin label. For nitroxides attached to the acyl chain of fatty acids (5.1.3) the Z axis is parallel to the long axis of the probe. A_{zz} is the limiting value of A_{II} and $(\frac{1}{2})(A_{xx}+A_{yy})$ is the limiting value of $A_{\perp}$.

The hyperfine splittings have been shown to depend on the polarity of the environment so a polarity normalisation term, a_o'/a_o, is introduced to Equation 5.1 to give the order parameter described by Hubbell and McConnell (155).

$$S = \frac{A_{II}-A_{\perp}}{A_{zz}-(\frac{1}{2})(A_{xx}+A_{yy})} \cdot \left(\frac{a_o'}{a_o}\right) \qquad \text{Equation 5.2}$$

where $a_o' = (1/3)\ A_{zz}+A_{xx}+A_{yy}$ and $a_o = (1/3)A_{II}+2A_{\perp}$.

The principle hyperfine splitting values required to calculate the order parameters have been previously determined for the fatty acid probe used in this study (5-doxyl-stearic acid) to be 32.9, 5.9 and 5.4 gauss for A_{zz}, A_{xx} and A_{yy} respectively (156). The relevant order parameter can thus be reduced to:

$$S = 0.5407.\ (A_{II}-A_{\perp})/a_o \qquad \text{Equation 5.3}$$

5.1.3 Anisotropic Motions of Nitroxide Probes in Membranes

A wide variety of nitroxide probes have been used in membrane studies. These range from simple molecules incorporating nitroxides such as TEMPO (157) to spin labelled fatty acids (154-156), phosphatidylcholines (149) and nitroxide labelled steroids (158,159). These more complicated molecules all contain the 2,2-dimethyl-N-oxyl-oxazolidine moeity which is normally abbreviated to 'doxyl'. The chemical structures of some of these probes are shown in Figure 5.4.

Fatty acid nitroxide probes have been used by many investigators to study membrane fluidity and structure (156,158-160). The fatty acids are assumed to sit in the bilayer with the changed carbonyl group anchored at the membrane surface. The position of the doxyl group on the acyl chain can be varied so different depths into the membrane can be probed. Using this approach it has been shown that the lipid acyl chains have a greater freedom of movement as the distance from the membrane surface increases, i.e. membranes are more fluid in their central core compared to just below the charged head groups (141,156).

5.1.4 Aim of the Investigation

In this study the nitroxide fatty acid probe 5-doxyl stearic acid (5-DS) Figure 5.4, will be used to evaluate the effect of the surfactants $C_{12}E_1$-$C_{12}E_8$ upon the membrane fluidity of DSPC liposomes. The same molecule will be used to probe the intercellular lipid bilayers of porcine stratum corneum *in-situ* to determine any effects the surfactants have upon the stratum corneum intercellular lipid fluidity.

5.2 METHODS

5.2.1 Preparation of DSPC Liposomes

For the ESR studies DSPC liposomes were prepared by an adaption of the method described previously (3.2.1). For ESR the final concentration of DSPC used was 0.08M (0.126M was used for the DSC studies). The nitroxide probe 5-DS was deposited into the glass vial from ethanol after the DSPC and surfactant had been deposited from chloroform. The amount of 5-DS added was kept to a minimum to avoid perturbation of the membrane by the probe. The 5-DS was used at a final concentration of 2.67×10^{-4}M, that is a molar ratio of DSPC:5-DS of 300:1.

For the ESR studies borate buffer pH 8.8 (2.2.3) was used rather than PBS pH 7.4 which was used in the DSC and FPS studies. A higher pH was chosen to ensure that all the carboxyl groups of the spin probes were ionised. In partially

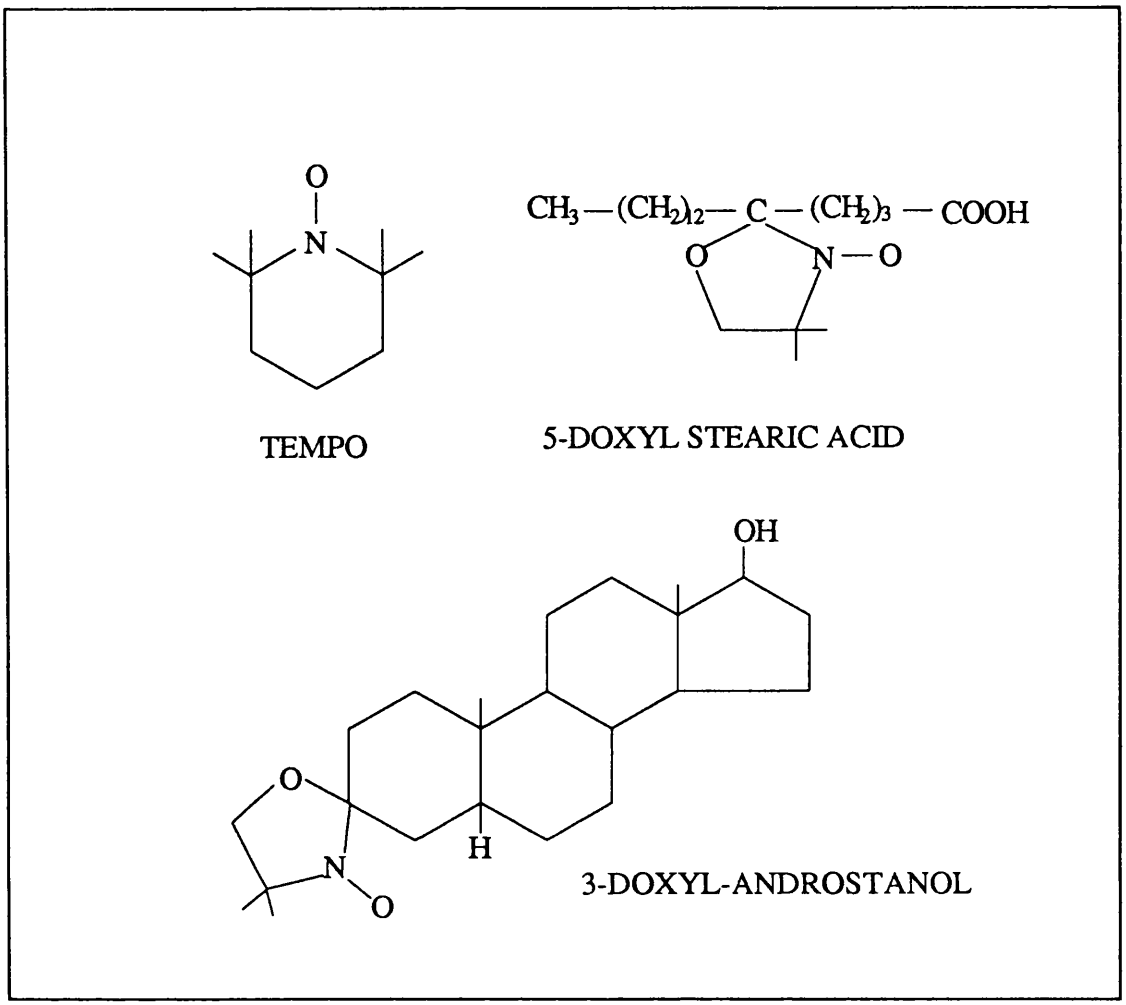

Figure 5.4 Typical nitroxide spin probes used in membrane investigations.

ionised mixtures of 5-DS in membranes it has been reported that the spectral trace can be complicated by two components of the spectrum which are suggested to relate to the $-COO^-$ and -COOH forms of the carboxyl group (158).

For analysis by ESR approximately 50μl of the 5-DS labelled liposomes were injected into 1mm bore quartz capillary tubes which had been sealed at one end with a flame.

5.2.2 Preparation of Stratum Corneum

Porcine ear stratum corneum was prepared and stored as described previously (3.2.4). For ESR spectroscopy pieces of stratum corneum of approximately 2.5cm^2 were cut and allowed to rehydrate at a relative humidity of 98% (see 3.2.5) for 24 hours. $1x10^{-8}$ moles of 5-DS was then deposited onto the stratum corneum surface from 20μl of absolute ethanol. For surfactant treated samples $2.2x10^{-6}$ moles of surfactant was deposited onto the stratum corneum surface from 20μl of acetone at the same time that the 5-DS was applied. The solvents were evaporated using a stream of dry nitrogen to leave a thin film of 5-DS and surfactant. For control samples 20μl of acetone only was applied to the skin. The surfactant and 5-DS were left for 24 hours at room temperature to penetrate into the skin. Excess surfactant and probe were then washed from the stratum corneum surface by immersing the sample in acetone at 0°C for 5 seconds and blotting dry on tissue. The samples were then carefully folded, rolled and placed into 2mm internal diameter quartz capillary tubes which had been sealed previously at one end in a flame.

5.2.3 Collection of ESR Spectra

All ESR spectra were collected using a Varian E3 spectrometer (Walton-on-Thames, UK). Normally samples were scanned over a 200 Gauss range centred at 3270 Gauss. The microwave frequency and power were approximately 9.18 GHz and 20mw respectively. All samples were analysed at 30$\pm$0.5°C. The temperature

in the cavity was controlled with a nitrogen-flow temperature regulation system the performance of which was monitored with a nickel/chromium-nickel/aluminium thermocouple attached to a digital display unit (RS Components, Corby, UK). All spectra were collected in duplicate.

5.2.4 Analysis of Spectra

The hyperfine splittings A_{II} and $A_{\perp}$ were measured directly from the ESR spectra obtained, as shown in Figure 5.2, allowing calculation of the order parameter, S, according to Equation 5.3.

RESULTS

5.3.1 Pure DSPC Liposomes

Figure 5.5 shows a typical ESR spectrum for 5-DS incorporated into DSPC liposomes at 30°C. The small bar represents a distance equal to 10 Gauss. The hyperfine splittings taken from spectra of replicate samples were 29.59 ± 1.18 and 9.35 ± 0.54 for A_{II} and $A_{\perp}$ respectively. The calculated value of S for the DSPC liposomes was 0.679 ± 0.026 (mean$\pm$SD, n=21).

Figure 5.6 shows that ESR spectra for 5-DS in DSPC liposomes with the incorporation of 50 mole% of dodecyl ether ethoxylates $C_{12}E_1$-$C_{12}E_8$. Addition of surfactant caused the spectra lines to narrow and become more pronounced. The presence of surfactant also altered the hyperfine splittings. A_{II} decreased and $A_{\perp}$ increased relative to the values obtained in pure DSPC liposomes. Both these changes in splitting tensors reduced the order parameter, S.

The values of S plotted against the ethoxy chain length of the dodecyl ether ethoxylate added to DSPC liposomes at 9, 33 and 50 mole% surfactant are shown in Figures 5.7, 5.8 and 5.9 respectively. At 9 mole% surfactant the addition of $C_{12}E_1$-$C_{12}E_3$ caused no significant change in the value of S with respect to its value in pure DSPC liposomes (t-test, $p < 0.05$). Incorporation of $C_{12}E_4$-$C_{12}E_8$ resulted in a decrease in S to approximately 0.55. $C_{12}E_7$ caused the greatest reduction in S

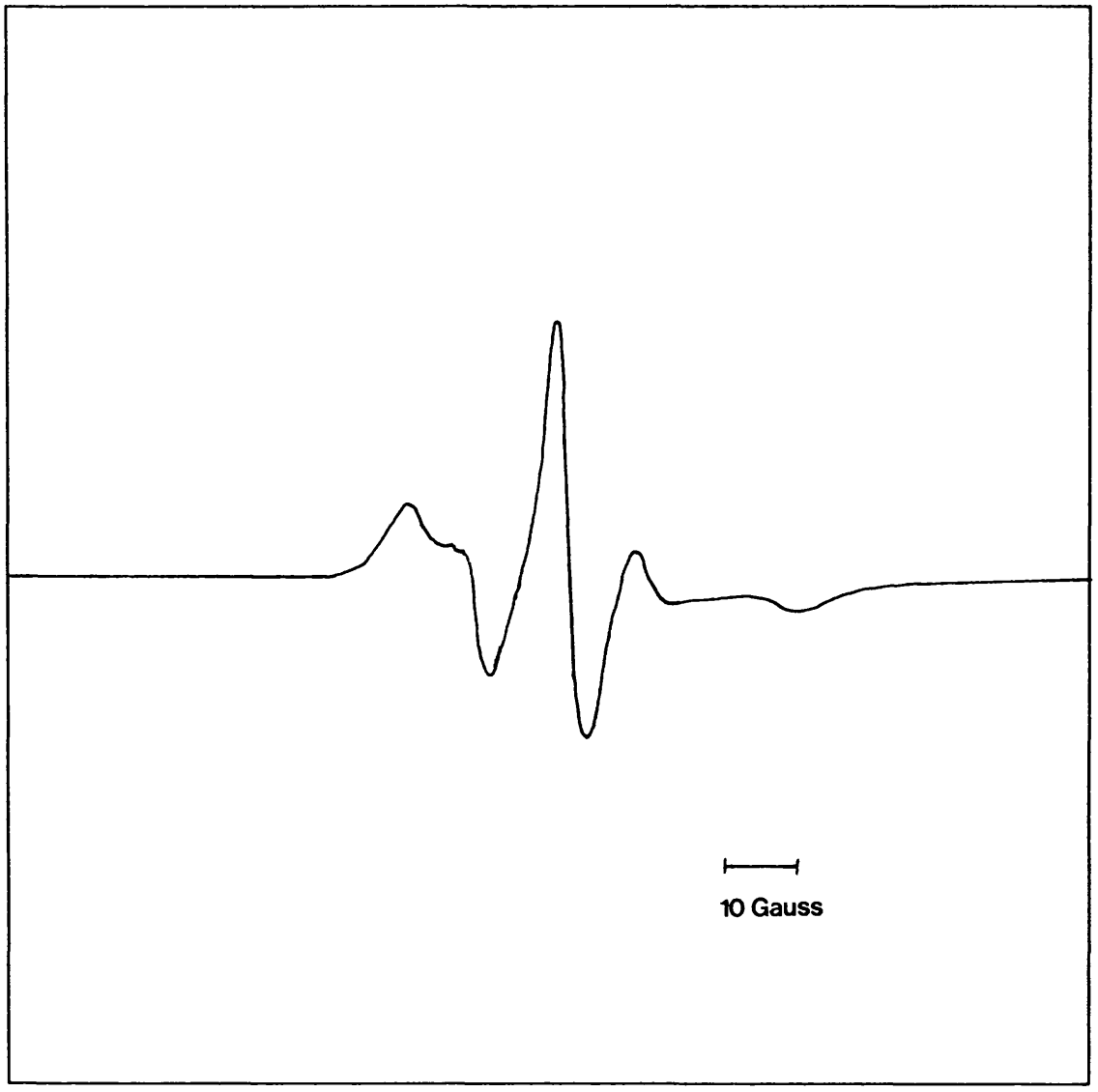

Figure 5.5 ESR spectrum for 5-DS incorporated into pure DSPC liposomes at 30°C.

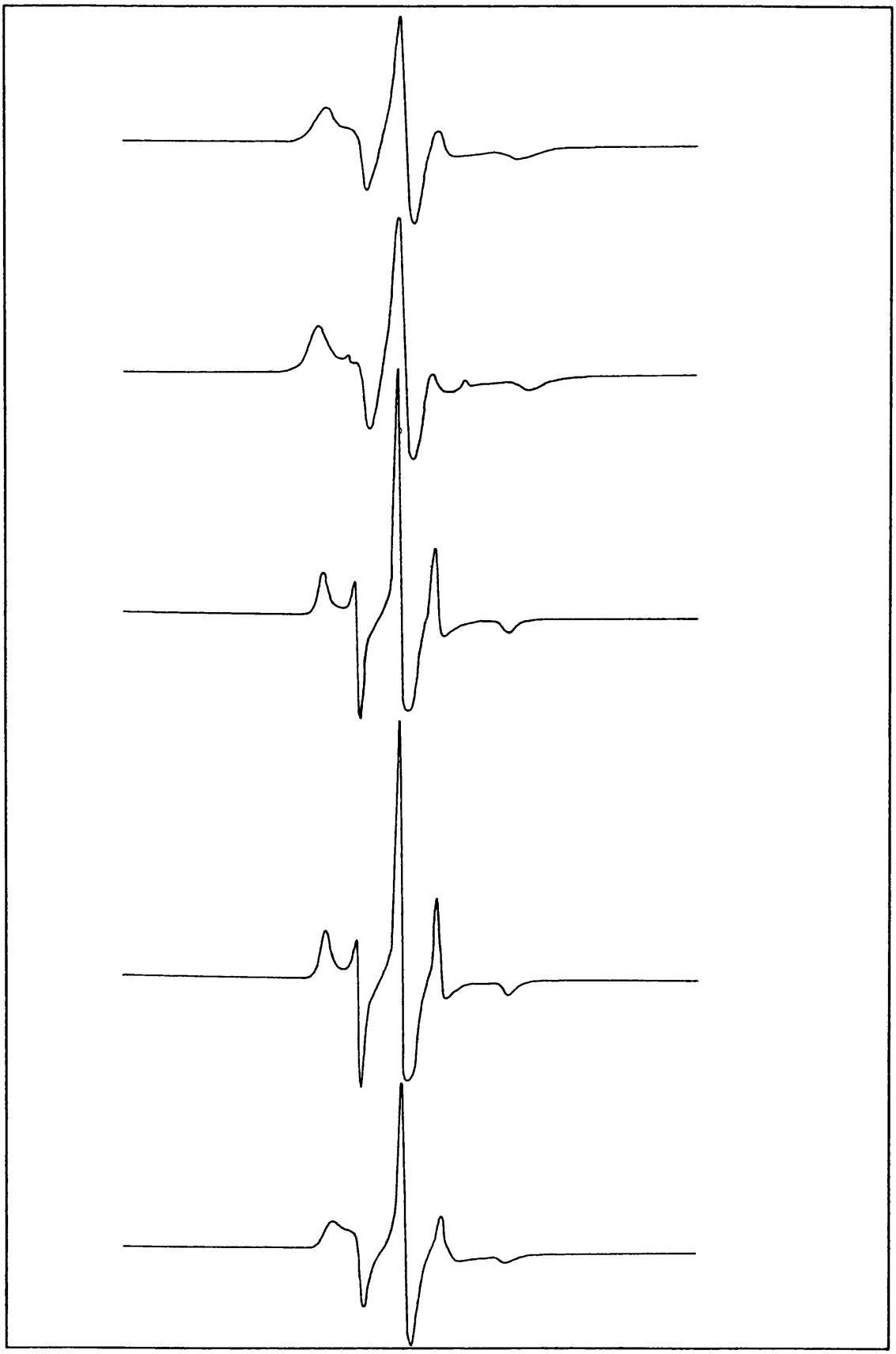

Figure 5.6 ESR spectra for 5-DS incorporated into DSPC/$C_{12}E_n$ mixed vesicles containing 50 mole% surfactant at 30°C. Top to bottom: DSPC, $C_{12}E_1$, $C_{12}E_3$, $C_{12}E_5$, $C_{12}E_7$.

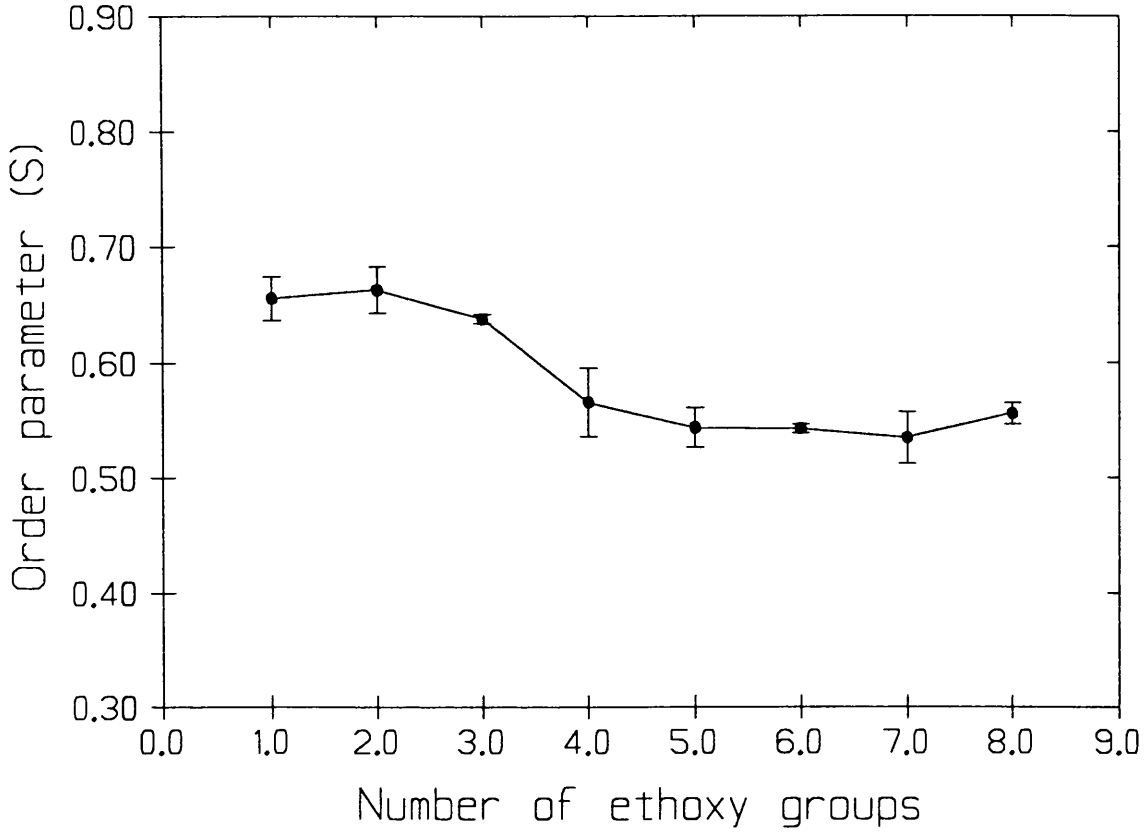

Figure 5.7 Values of S for 5-DS incorporated into DSPC/$C_{12}E_n$ mixed vesicles containing 9 mole% surfactant plotted as a function of surfactant ethoxy chain length. Measurements were made at 30°C. Points are mean$\pm$SD, n=4

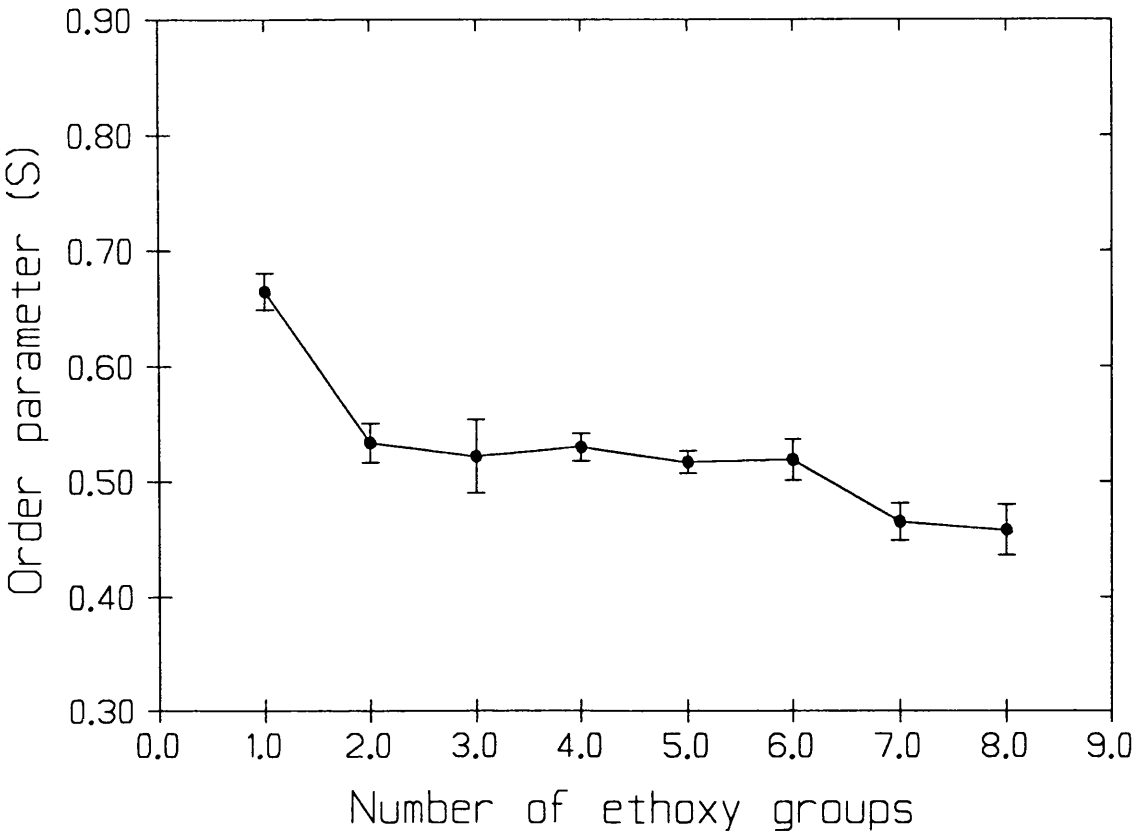

Figure 5.8 Values of S for 5-DS incorporated into DSPC/$C_{12}E_n$ mixed vesicles containing 33 mole% surfactant plotted as a function of surfactant ethoxy chain length. Measurements were made at 30°C. Points are mean$\pm$SD, n=4

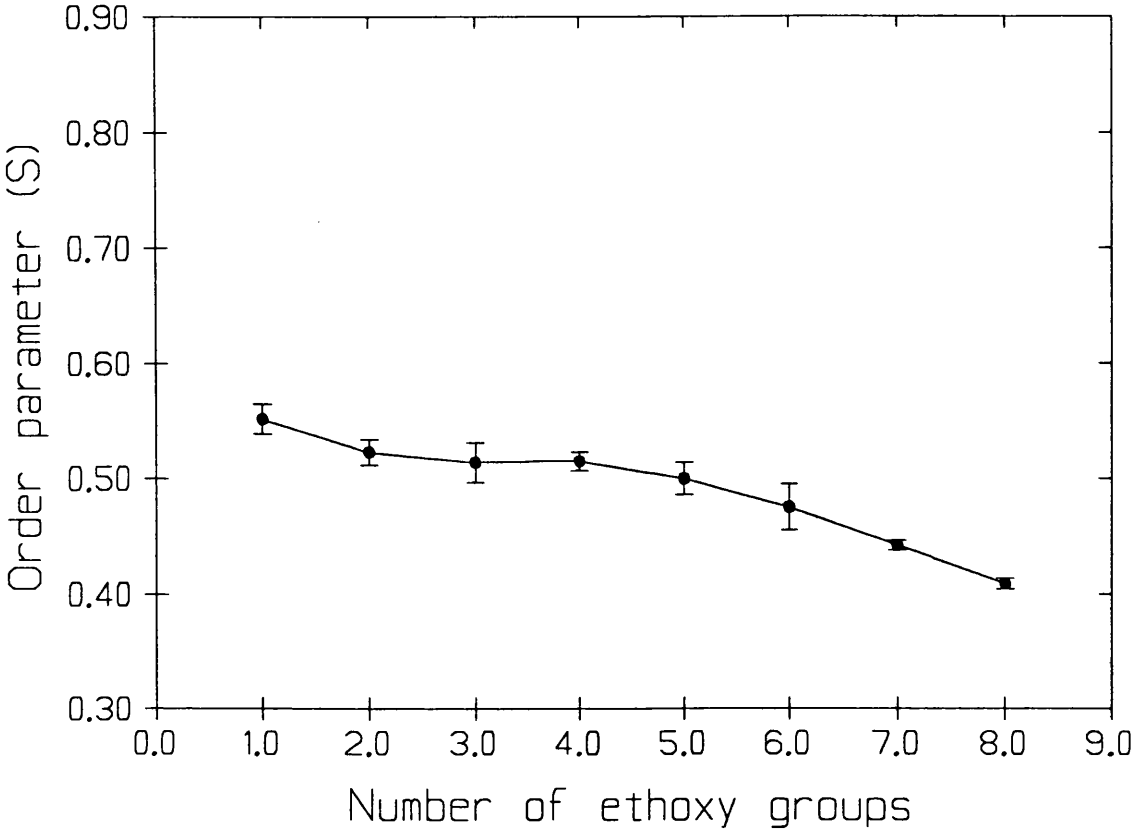

Figure 5.9 Values of S for 5-DS incorporated into DSPC/$C_{12}E_n$ mixed vesicles containing 50 mole% surfactant plotted as a function of surfactant ethoxy chain length. Measurements were made at 30°C. Points are mean$\pm$SD, n=4

however there were no statistical differences between the effects of $C_{12}E_4$-$C_{12}E_8$ inclusive (t-test, $p<0.05$). The addition of 33 mole% surfactant to the DSPC liposomes produced a large decrease in S with all ethoxy chain lengths except $C_{12}E_1$ which caused no significant change. $C_{12}E_2$-$C_{12}E_8$ all reduced S to a value of about 0.525. The longer ethoxy chains $C_{12}E_7$ and $C_{12}E_8$ produced greater changes in S to 0.468 and 0.465 respectively. A similar structure-activity relationship to that observed at 33 mole % surfactant was produced by the addition of 50 mole% surfactant to the DSPC liposomes. The value of S was reduced to a greater extent by the higher surfactant concentration. This was very noticeable for samples treated with $C_{12}E_1$. The results for all three concentrations are summarised in Figure 5.10 where the effect of each surfactant is expressed as mean percentage decrease in S with respect to the control value obtained in the absence of surfactant.

Figure 5.11 shows the effect of concentration of $C_{12}E_3$ upon the order parameter of 5-DS in DSPC liposomes. There was a slight decrease in S with the addition of up to 20 mole% $C_{12}E_3$. Increasing the concentration of $C_{12}E_3$ above this level caused the value of S to decrease more rapidly. At 50 mole% surfactant S had fallen to 0.528 ± 0.005. Further increase in surfactant concentration had little effect upon the value of S.

5.3.2 Isolated Stratum Corneum

A typical spectrum for 5-DS incorporated into hydrated porcine stratum corneum is shown in Figure 5.12. The spectra had very broad lines. The hyperfine splittings obtained from the spectra were 33.67 ± 0.48 and 10.86 ± 0.15 for A_{II} and $A_{\perp}$ respectively. For untreated stratum corneum the order parameter of the 5DS probe was calculated to be 0.667 ± 0.0015 (mean$\pm$sd, n=3).

Treatment with surfactant narrowed the spectral lines and reduced A_{II}. There was little change in the value of $A_{\perp}$. A typical spectrum for surfactant treated stratum corneum, in this case $C_{12}E_3$, is shown in Figure 5.13. The calculated order parameters of 5-DS incorporated into stratum corneum samples

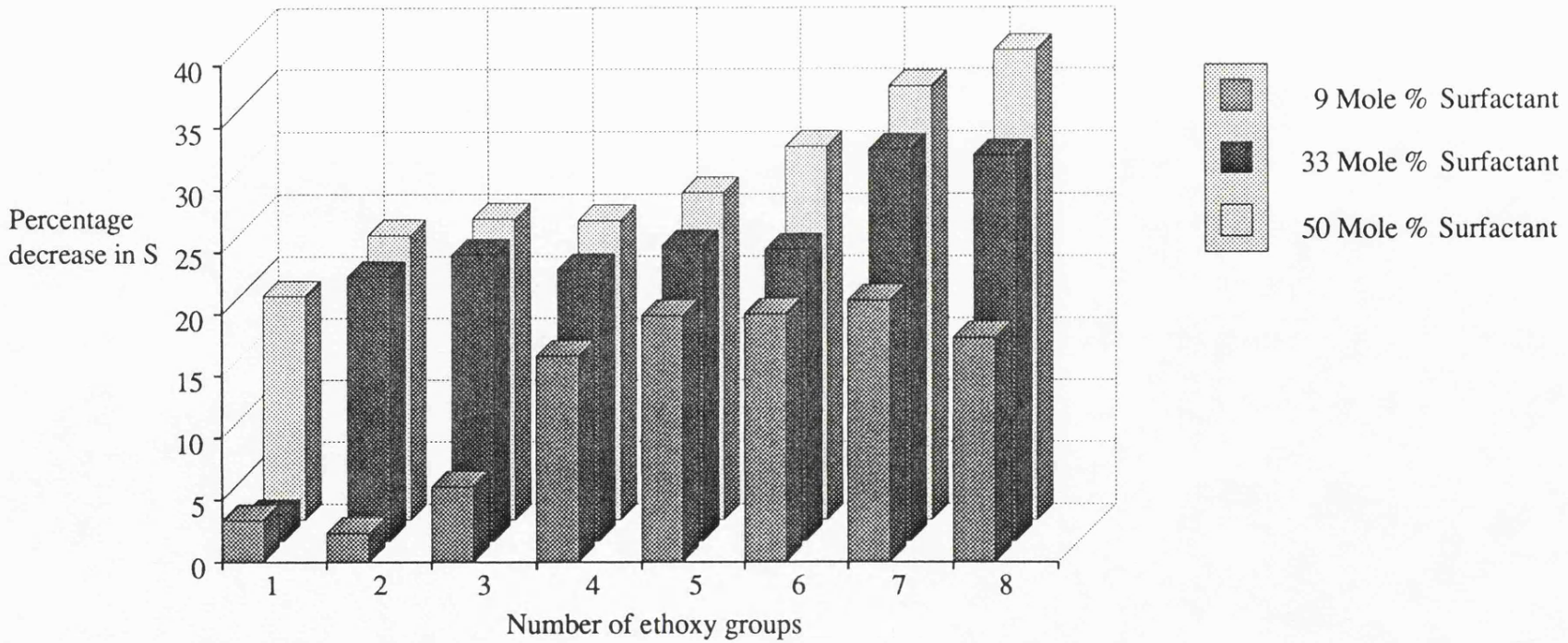

Figure 5.10 The percentage decrease in S for 5-DS incorporated into DSPC/$C_{12}E_n$ mixed vesicles containing 9, 33 and 50 mole% surfactant relative to pure DSPC liposomes plotted as a function of surfactant ethoxy chain length. Values shown are means of four observations.

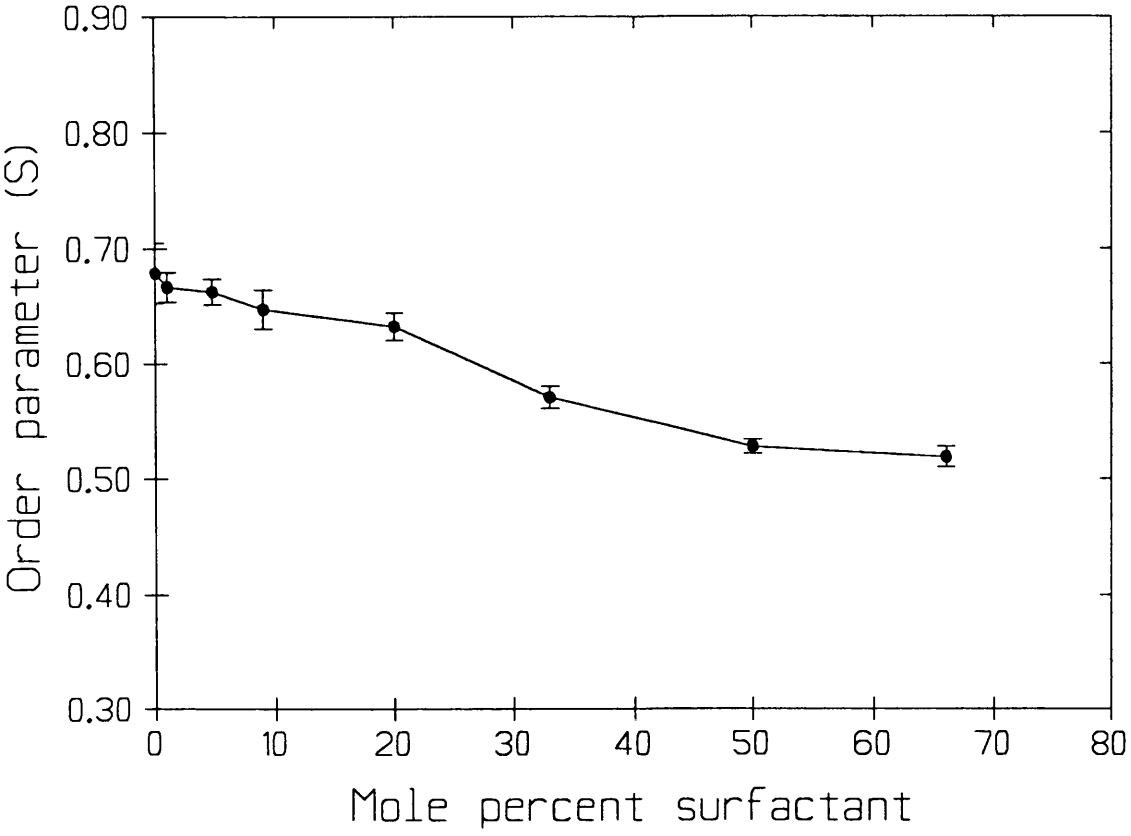

Figure 5.11 The effect of increasing surfactant concentration upon S for 5-DS in DSPC/$C_{12}E_3$ mixed vesicles at 30°C. Mean±SD, n=4.

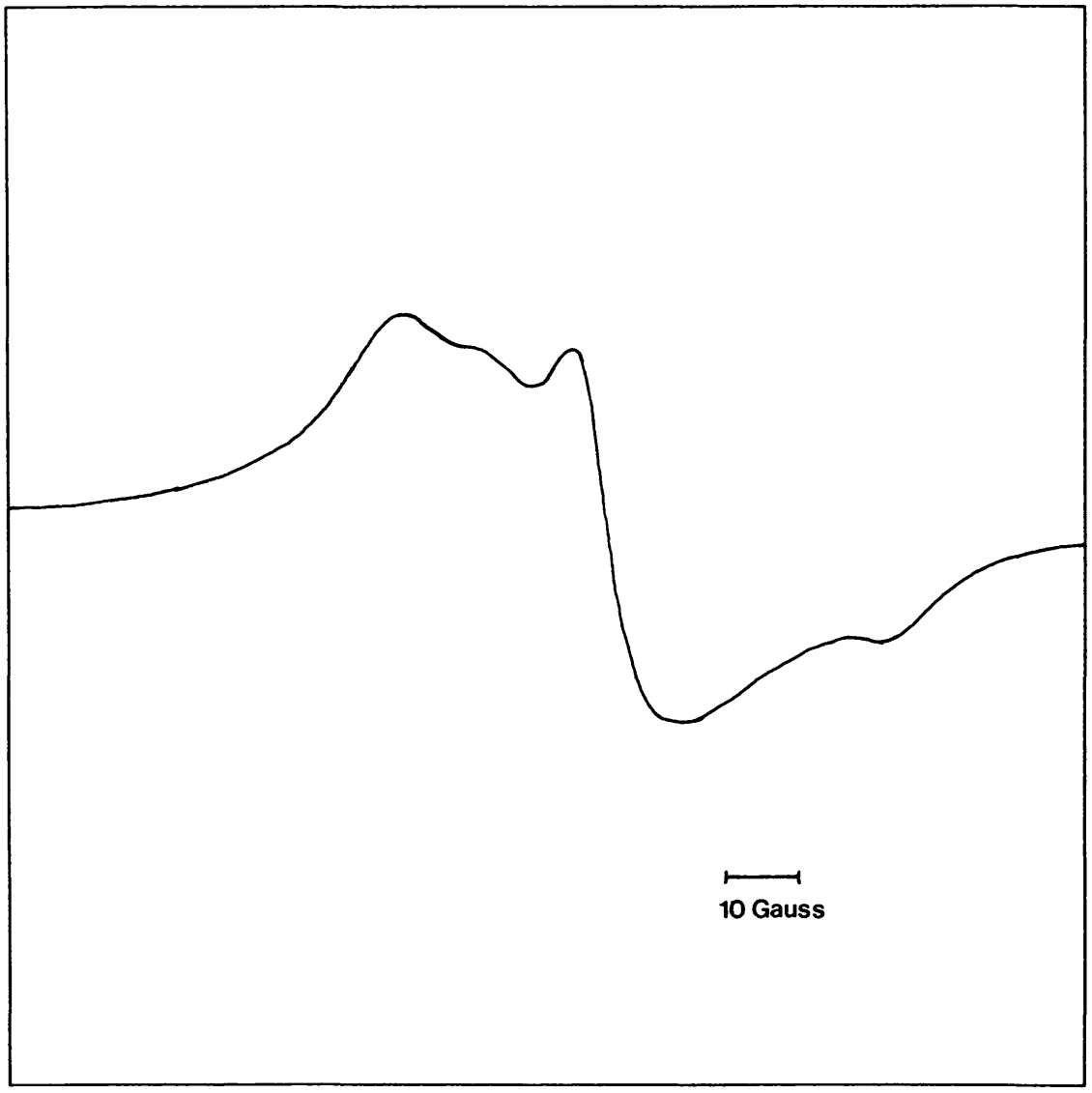

Figure 5.12 ESR spectrum for 5-DS incorporated into hydrated porcine stratum corneum at 30°C.

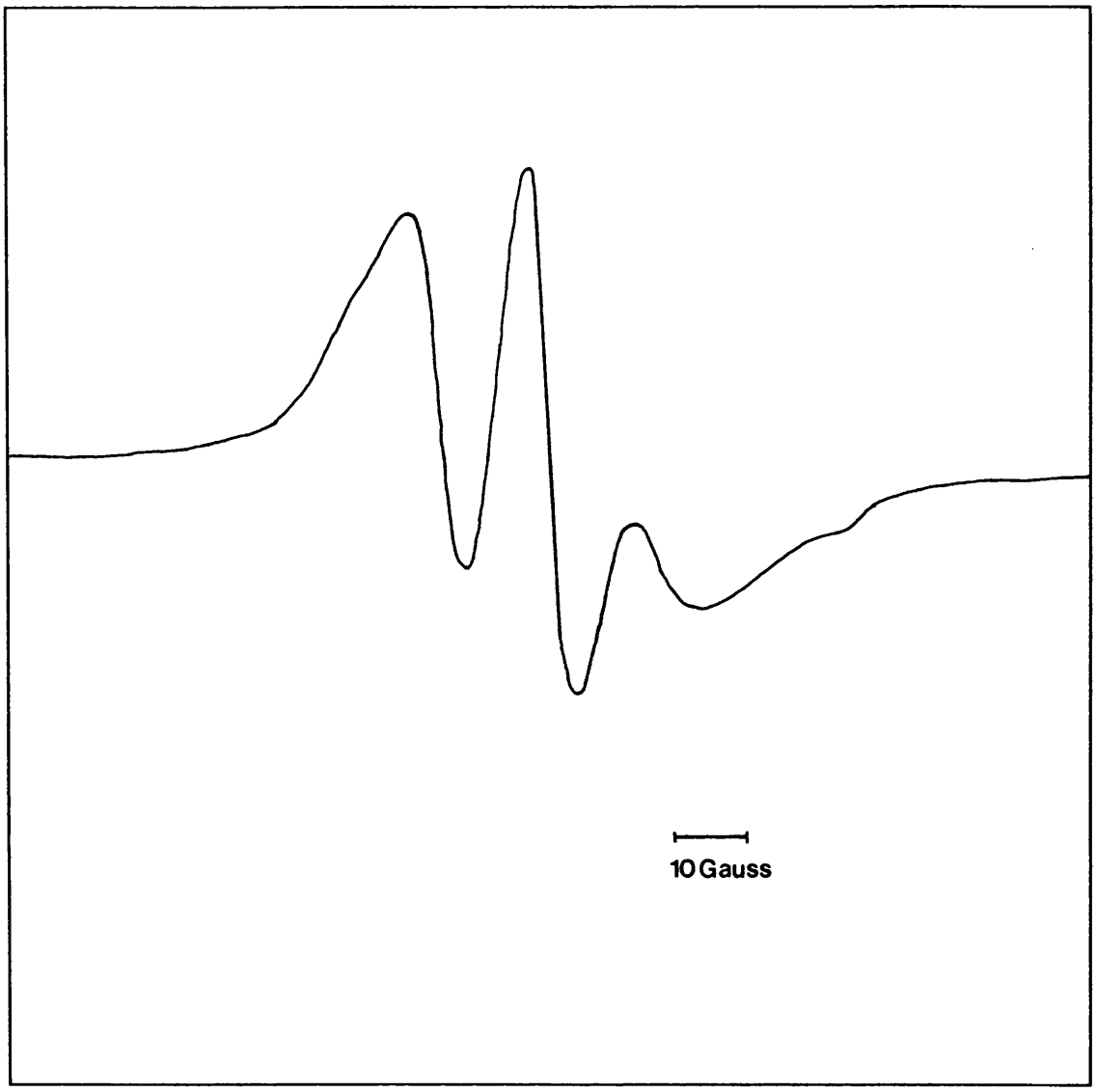

Figure 5.13 ESR spectrum for 5-DS incorporated into hydrated porcine stratum corneum treated with $C_{12}E_3$ at 30°C.

treated with $C_{12}E_0$-$C_{12}E_8$ are shown in Figure 5.14 plotted as a function of surfactant ethoxy chain length. All surfactants reduced S to between 0.565 and 0.610, a significant decrease in the order parameter with respect to untreated stratum corneum (t-test, $p<0.05$). However there were no significant differences in the values of S obtained with the different surfactant (t-test, $p>0.05$).

5.4 DISCUSSION

The ESR spectra observed were normal for nitroxide fatty acid probes undergoing anisotropic motion in membranes. Each sample gave highly reproducible spectra, less than a 3% change in hyperfine splittings being observed between repeated spectra. A greater variation was observed between samples. This indicated that the majority of experimental variation occurred during sample preparation and not in the measurement of the spectra.

The spectra observed for 5-DS in pure DSPC liposomes at 30°C were typical for this type of probe in a relatively immobile state. Similar spectra have been reported by several other investigators working with 5-DS and similar probe molecules (161-163). At 30°C pure DSPC membranes were in a gel crystalline state with the lipid acyl chains packed in an ordered fashion. The probe molecule would therefore have been highly constrained and would have undergone little movement. The hyperfine splittings obtained in pure DSPC liposmes were in accordance with previously reported values for 5-DS in gel phase lipids. Marsh *et al* (157) studied 5-DS in DPPC liposomes. At temperatures below the gel-liquid crystalline phase transition a value of approximately 30.4 Gauss was obtained for A_{II}. Above the phase transition temperature, when the lipid is in a liquid crystalline phase this value was reduced to 26.8 Gauss.

In this present study an order parameter of 0.679 ± 0.54 was determined for 5-DS in DSPC liposomes. This was typical for this probe in gel phase lipids (154,155,164). Addition of surfactant to the DSPC liposomes caused a reduction in

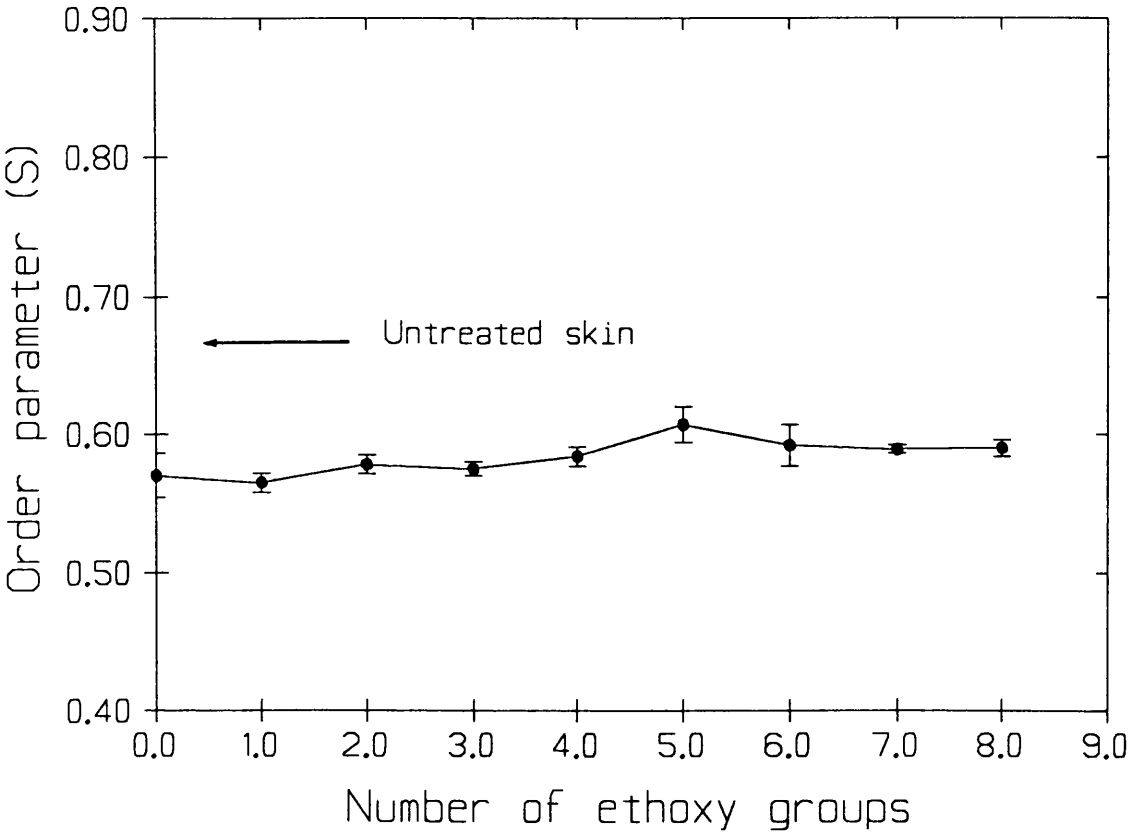

Figure 5.14 Values of S for 5-DS incorporated into porcine stratum corneum treated with $C_{12}E_n$ plotted as a function of surfactant ethoxy chain length. Measurements were made at 30°C. Points are mean±SD, n=4

the order parameter of 5-DS in the liposomes at 30°C. This was mainly due to large decreases in the value of A_{II}.

The change in the A_{II} was accompanied by a narrowing of the spectral lines. Both of these effects have been reported to be associated with an increase in the rate of rotation of the probe molecule around its long molecular axis (162,165). The value of $A_{\perp}$ also increased with the addition of surfactant. This was due to increased averaging of the hyperfine splitting (see 5.1.1) and probably an increase in the freedom of motion of the probe. Increased values of S indicate more molecular wobble of the probe, i.e. an increase in the angle of movement of which the probe can undertake around the molecular long axis as the probe sits in the bilayer (162). The changes in lipid packing caused by the surfactants and the manner in which surfactants act upon membranes has been discussed previously (see 3.4 and 4.4).

The decrease in order parameter indicated that addition of surfactant to the DSPC bilayers caused a decrease in the order of packing of the lipids i.e. fluidisation of the bilayers. This allowed the increased motion discussed above. Similar results were obtained with Brij 36T ($C_{12}E_{10}$) and oleic acid by Gay *et al* (163).

The effect of the surfactant upon the bilayers in this ESR study is in agreement with the findings of the DSC and FPS studies reported in Chapters 3 and 4 in that the surfactants caused bilayer fluidisation, however a different structure-activity relationship was indicated by the nitroxide probe. When analysed by DSC the most potent surfactant for fluidisation of DSPC bilayers when present at a concentration of 50 mole% was $C_{12}E_3$. When analysed by FPS the structure-activity relationships regarding apparent bilayer fluidisation in the 1:1 surfactant lipid systems were dependent upon the fluorescent probe structure. The position of the probe in the bilayer was of consequence in these studies. DPH which sits in the membrane interior was affected to the greatest extent by $C_{12}E_4$, whilst ANS a 'headgroup' probe was affected more by the higher ethoxy chain length molecules

around $C_{12}E_6$. Cis-pna is a C_{18} fatty acid and would therefore be expected to sit in the membrane in a similar orientation to 5-DS and produce results in parity with 5-DS with respect to surfactant efficacy. This however was not the case, with cis-pna $C_{12}E_5$ was shown to be the most potent membrane fluidiser in terms of reducing T_c, with increasing T_w and reducing probe anisotropy r. In the ESR study the 5-DS order parameter decreased with surfactant ethoxy chain length, $C_{12}E_7$ and $C_{12}E_8$ were observed as the most potent membrane fluidisers amongst the surfactant series above 33 mole% surfactant.

The difference in the results of the FPS and ESR experiments was thought most likely to be due to the differences in structure of the probes. 5-DS is reported to detect changes in fluidity in the membrane just below the polar head groups of the molecules (149,163). This is due to the position of the doxyl group upon the acyl chain. The fluidity changes reported by cis-pna may have been affected by changes in the order of acyl chain packing deeper in the membrane. The longer ethoxy chain surfactants $C_{12}E_6$-$C_{12}E_8$ may have caused greater disruption in packing of the polar headgroups than $C_{12}E_4$-$C_{12}E_5$. The relative increase in membrane fluidity caused by $C_{12}E_6$-$C_{12}E_8$ would thus be greater when observed with 5-DS than with cis-pna. This theory would in part be supported by the results observed for the FPS of ANS, a headgroup probe when the surfactants with longer ethoxy chain lengths were seen as relatively effective membrane fluidisers.

As suggested in the discussion of the FPS studies (see 4.4) the membrane probe may partition into areas of localised fluidity caused by phase separation in the membrane. The probe could have also become incorporated into surfactant micelles with the micellising surfactants which would be a more fluid environment. These possibilities have to be considered when comparing the results from the FPS and ESR studies with those obtained by DSC.

The spectra observed for 5-DS incorporated into the extracellular lipid lamellae of the stratum corneum show the probe to be highly immobile in the membrane. The spectral line widths were very broad and a relatively high value of

S (0.667±0.00015) was obtained from the hyperfine splittings. These parameters indicated that the acyl chains of the lipids in the intercellular lamellae were highly ordered and tightly packed. The shape of the ESR spectra and the value of S were in close agreement with a similar study upon 5-DS in human stratum corneum by Gay *et al* (166). It should be noted that different formulae were used for the calculation of the order parameter in the two studies. Recalculation of the results of this study according to the equation used by Gay *et al* show the two values of S, one in porcine and the other human stratum corneum, to be extremely close.

Treatment of the stratum corneum with surfactant greatly changed the ESR spectra. The spectral lines narrowed and became more pronounced. The value of S decreased, mainly due to a decrease in A_{II}. These changes indicated increased molecular motion of the probe and fluidisation of the lipid bilayers as discussed previously for DSPC liposomes. All the surfactants produced a decrease in the order parameter to values between 0.565 and 0.610. This was a decrease in S of between 8.6 and 15.4 percent of the value obtained in untreated stratum corneum. There were no significant differences between the effects of the different surfactants. This decrease in S observed was in parity with results obtained by Gay *et al* (166). They reported a 14.7% decrease in the value of S for 5-DS in human stratum corneum that had been treated with Brij 36T ($C_{12}E_{10}$). The investigators concluded that the Brij 36T caused bilayer fluidisation in the skin.

The results from the liposome and stratum corneum studies did show some correlation with respect to surfactant treatment. It is not east to make direct comparisons between the two techniques. In the liposome studies both the degree of fluidisation and structure-activity relationship changed with the concentration of added surfactant. In the stratum corneum studies it was unknown how much surfactant would have penetrated into the lipid lamellae. It is likely the surfactants would have penetrated the stratum corneum at different rates. The molecules with shorter ethoxy chain lengths were expected to permeate the skin more readily than the hydrophilic molecules (32). After 24 hours there would be more of the lower

HLB molecules present in the lipid bilayers of the skin preparation than longer chain molecules. In the liposome studies the same amount was added for each surfactant, although it is unknown exactly how much partitions into the membrane. The higher efficacy of $C_{12}E_6$-$C_{12}E_8$ observed in DSPC bilayers (Figures 5.3.4, 5.3.5) may be counteracted in the stratum corneum investigations by the relatively poor permeation of these surfactants. This is assuming that the 5-DS probe sits in the membranes at the same position in both preparations, as this would have bearing on the structure-activity relationship.

Studies using ESR in stratum corneum have great potential for investigating percutaneous absorption of drugs and the relative efficacy of penetration enhancers. The rate of molecular movement in the stratum corneum can be measured for any molecule with unpaired spin or a spin label moiety attached to it. It may be possible to synthesize spin labelled analogues of drug with potential for transdermal delivery. The molecular movement, which is related to ease of diffusion through the membrane, could be easily measured by ESR. The effect of any potential penetration enhancers upon this molecular motion could be quickly screened.

CHAPTER 6

MEASUREMENT OF THE PENETRATION ENHANCEMENT OF STEROIDS BY *IN-VITRO* PERMEATION STUDIES

6.1 INTRODUCTION

In order to assess the potency of penetration enhancers it is ultimately necessary to measure the percutaneous absorption of drug compounds in the presence and absence of the enhancing agent.

These experiments ideally would be carried out *in-vivo* using human volunteers, plasma drug concentrations being assayed over a period of time. Several studies of this type have been carried out using radiolabelled material (30) when excreted label was used as a measure of percutaneous absorption, due to the very low plasma concentrations achieved. Human *in-vivo* experiments, however, may have ethical, financial and toxicological problems. An alternative is the use of animal models *in-vivo*. These may cause extra problems due to skin differences between the animal and man, and will still suffer from the biological variability and complex biological factors which are difficult to control in all *in-vivo* studies (see Chapter 1).

Many of the problems of variability, and high cost can be avoided by the use of *in-vitro* techniques using excised skin. In *in-vitro* experiments there is an assumption that the non viable stratum corneum functions as the major permeability barrier in both living and dead skin. Human skin would be the ideal choice for *in-vitro* studies, however, a regular, consistent supply of good human skin is often hard to obtain so animal models are often used. Porcine skin has been shown to be one of the best models for human skin (see chapter 1).

Many different techniques have been used for *in-vitro* studies of percutaneous absorption. To assess the relative potency of the surfactant series $C_{12}E_0$-$C_{12}E_8$ as penetration enhancers, the permeation of the steroids oestradiol (OE), hydrocortisone (HC), oestrone (OT) and progesterone (PG) through porcine ear skin was determined in the presence and absence of each surfactant. It was decided to use a 'finite dose' technique in which both the permeant and the enhancer were deposited as a thin film onto the skin surface from a volatile solvent. This technique has been used in similar studies (59). It was thought these methods would

as far as possible avoid complication of the data due to complex vehicle/drug, vehicle/skin interactions.

6.2 METHODS

6.2.1 Preparation of Thin Skin Membranes for Permeation Experiments.

Porcine ear skin was obtained and stored as described previously (2.1). For the preparation of membranes for permeation studies samples were allowed to thaw slowly at room temperature. Circular discs were then punched out of the skin using a sharpened number 16 cork borer. This produced discs of whole skin approximately 2.6cm diameter. These discs were then placed stratum corneum down onto aluminium plates which had been cooled to -70°C. All subcutaneous fat and most of the dermis was removed from the sample to leave a preparation comprising of the epidermis and a thin layer of dermis. The whole preparation was 0.8mm thick. The prepared membranes were then washed in distilled water and blotted with tissue paper to remove residual water from the skin surface.

6.2.2 Diffusion Experiments

The prepared skin membranes were mounted into glass, horizontal, static diffusion cells, stratum corneum uppermost, as shown in Figure 6.1. The receptor compartment was filled with a known volume (approximately 4.5ml) 20% ($^{V}/_{V}$) ethanol in pH 7.4 PBS. Ethanol was added to the receptor fluid in order to increase the solubility of the steroids in this phase and thus maintain sink conditions.

The ^{14}C labelled steroids were prepared in acetone as described in Chapter 2. For application to the skin 20μl of the steroid solution was pipetted onto the skin surface. The solution was spread evenly over the skin by agitation and repeated pipetting. The acetone was then evaporated under a gentle stream of nitrogen gas. For each cell 0.1μCi of steroid were applied to the skin this corresponded to 98μg total steroid of OE and 130μg of HC. For OT and PG 0.2μl of steroid were applied corresponding to 194μg and 226μg respectively.

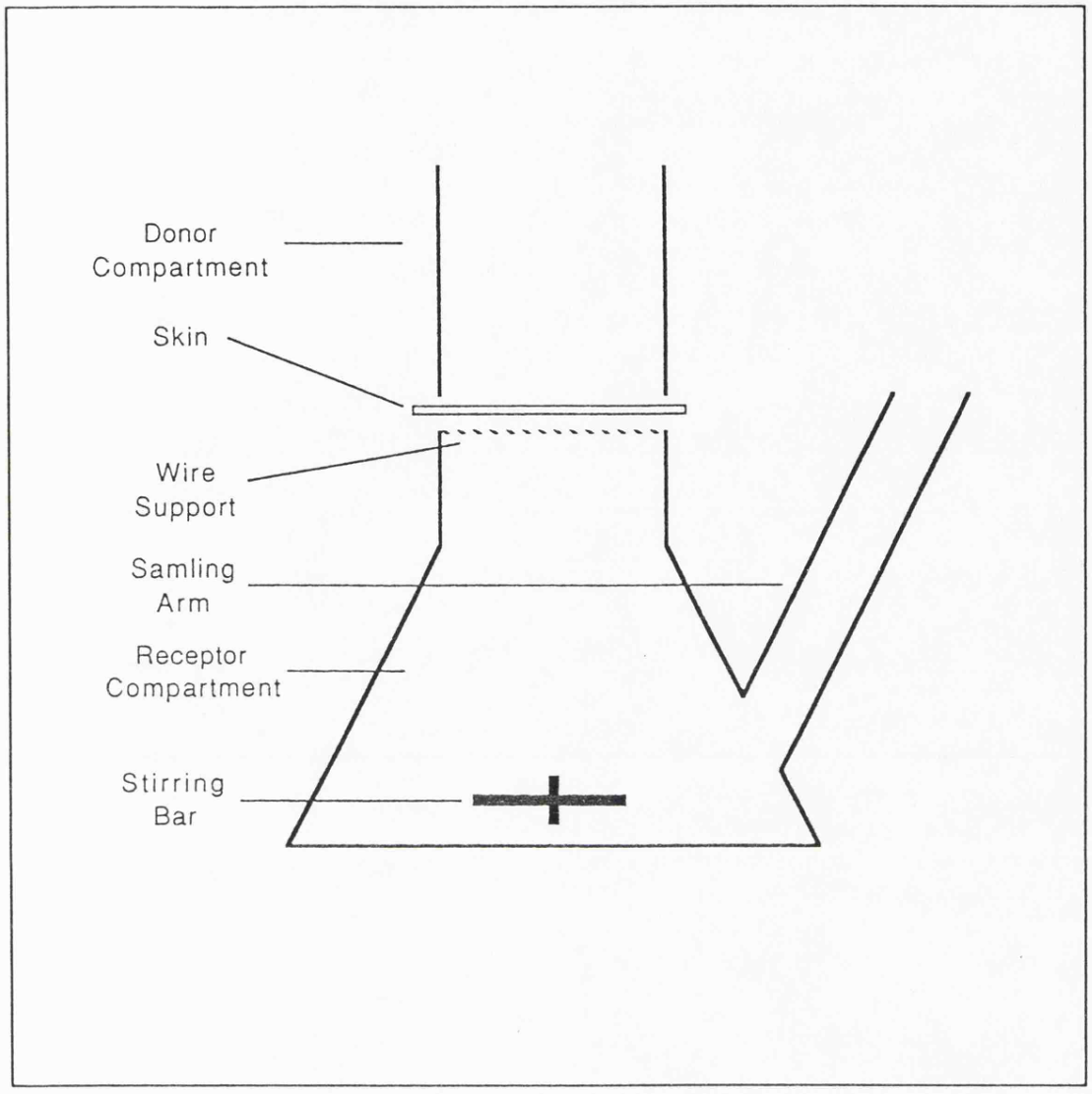

Figure 6.1 Schematic diagram of skin mounted in a horizontal diffusion cell.

The surfactant was applied in 20μl of acetone by the same method and at the same time as the steroid so as to codeposit the surfactant and steroid on the skin surface. For each experiment $2.2x10^{-6}$ moles of surfactant were applied to the skin except where stated. This corresponded to 0.8mg of $C_{12}E_4$. For control experiments in the absence of enhancer, 20μl of acetone was pipetted with the drug onto the skin surface.

The cells were mounted over underwater magnetic stirrers in a water bath at 32°C. This produced a skin surface temperature of 30$\pm$1°C. The skin surface was left open to the laboratory atmosphere. The receptor fluid was constantly stirred to prevent the development of static layers under the skin. 1ml samples were taken from the receptor fluid periodically over 90-100 hours. The samples were replaced with 1ml of fresh prewarmed ethanolic PBS. The samples collected were analysed by liquid scintillation counting.

6.2.3 Construction of a Quench Calibration Curve

In order to calculate the mass of steroid in the receptor fluid it was necessary to obtain the radioactive count in terms of disintegrations per minute (dpm). The LKB Rackbeta II used had an inbuilt dpm package which utilised the channels ratio method of quench correction with an external standard. In order to use this package a quench calibration curve was constructed by the 'hat-trick' method (LKB Wallac, Sweden) in which quenching agent, (carbon tetrachloride) was continuously added to a volume of scintillant containing a radioactive sample, via a filter paper wick whilst the sample was repeatedly counted. The dpm package then interpolated a calibration curve using a spline function from which a counting efficiency was obtained from the calculated channel ratio. The curve obtained and used in the experiments is shown in Figure 6.2

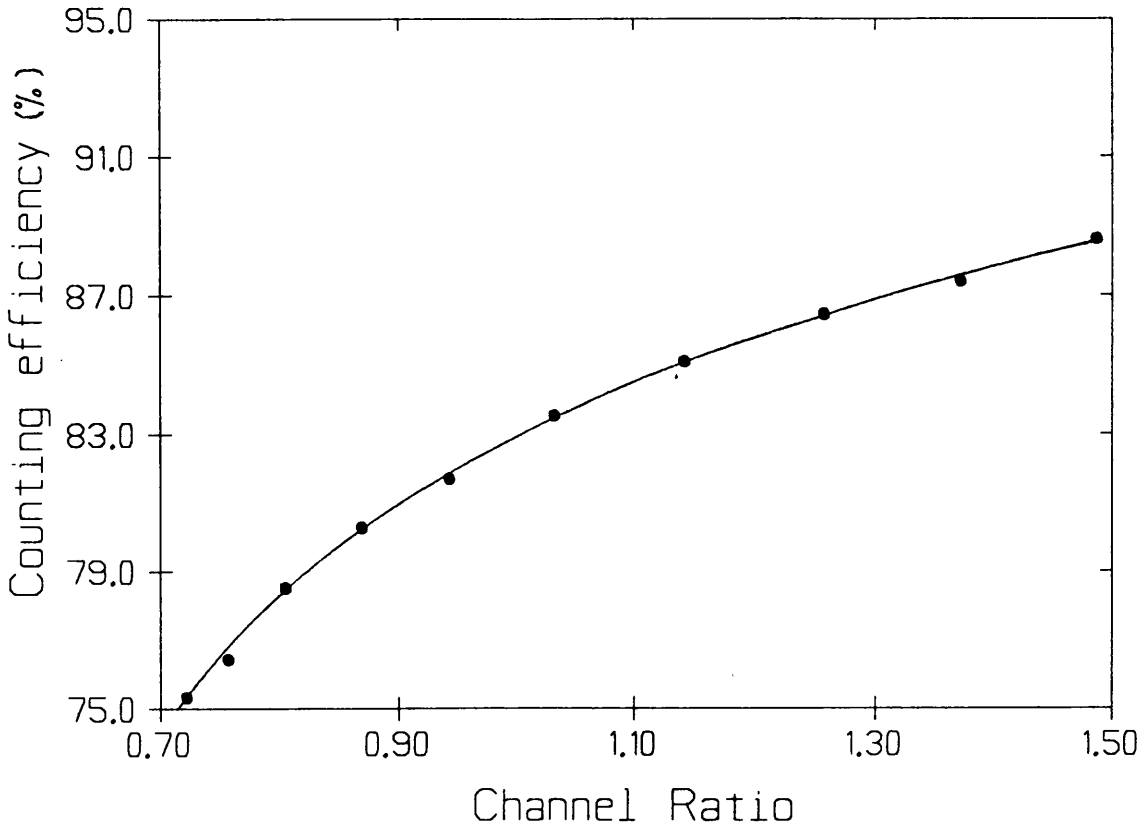

Figure 6.2 Quench calibration curve for ^{14}C in 10ml Optiphase scintillation cocktail.

6.2.4 Liquid Scintillation Counting of Samples

Each 1ml sample taken from the diffusion experiments was pipetted into a 20ml plastic scintillation vial, 9ml of scintillation cocktail (Optiphase; Pharmacia Sweden) was added to the sample and the vial shaken to produce a single phase. The samples were then counted for 180 seconds using a LKB 'Rackbeta II' (Pharmacia) liquid scintillation counter.

6.2.5 Calculation of Results

For each diffusion cell the cumulative mass of steroid in μg penetrating unit area of skin was calculated, corrections being made for dilutions used at sampling. These calculated values were plotted against time. From these plots the mass of steroid that had permeated through the skin after 24, 48, 60 and 72 hours was determined. The effectiveness of each surfactant as a penetration enhancing agent was determined by comparing the mass of steroid that penetrated surfactant treated skin to that for untreated skin. This can be defined as the enhancement ratio (ER) such that:

$$ER_t = \frac{\text{(Mass of steroid penetrating surfactant treated skin in time t)}}{\text{(Mass of steroid penetrating untreated skin at time t)}}$$

where t is the time from initial drug-skin contact.

Pseudo steady state flux in terms of μg $cm^{-2}hr^{-1}$ was obtained from linear portions of the plots after the effect of acetone deposition had subsided; generally after 30 hours. For surfactant-enhanced hydrocortisone penetration it was not possible to calculate this flux value due to non-linearity which is discussed below (6.4).

6.3 RESULTS

6.3.1 Counting Efficiency

For all four ^{14}C steroids a channels ratio of approximately 1.35 was obtained. From the quench correction curve this showed the counting efficiency to be around 86%.

6.3.2 Permeation of Oestradiol

Figure 6.3 shows a typical permeation profile for oestradiol through pig ear skin in the absence of surfactant. There was little or no lag time before the appearance of OE in the receptor fluid. The initial flux over the first 30 hours was 0.0206 ± 0.005 (mean$\pm$SD, n=6) $\mu g\ cm^{-2}hr^{-1}$. Flux decreased over the next 10 hours to $0.0135 \pm 0.004 \mu g\ cm^{-2}\ hr^{-1}$ after 40 hours and remained constant at this value until termination of the experiment. The amount of OE that penetrated the skin after 24, 48, 60 and 72 hours was 0.57 ± 0.026, 1.06 ± 0.055, 1.22 ± 0.095 and $1.39 \pm 0.125\ \mu g\ cm^{-2}$ respectively.

Application of surfactant to the skin greatly increased the mass of OE penetrating the skin. Figure 6.4 shows permeation profiles for OE penetration through pig skin in the presence of $C_{12}E_1$, $C_{12}E_3$, $C_{12}E_5$ and $C_{12}E_7$. All the surfactants produced a similar shape permeation profile over the time course of the experiment with the exception of $C_{12}E_0$, which caused a profile similar in shape to unenhanced permeation. $C_{12}E_1$ and $C_{12}E_2$ which showed some reduction in the rate of enhanced flux after 45 hours.

The extent of penetration enhancement was highly dependent upon the ethoxy chain length of the surfactant. Figure 6.5 shows the cumulative amounts of OE permeated after 24 hours plotted against the ethoxy chain length of the surfactant. The points shown are mean and standard deviation of four observations. As ethoxy chain length of surfactant increased from $C_{12}E_0$-$C_{12}E_3$ the amount of OE permeated also increased to a maximum with $C_{12}E_3$ treated skin. $C_{12}E_3$ increased the OE penetration to $6.3 \pm 1.4 \mu g\ cm^{-2}$ after 24 hours. Further increases in ethoxy

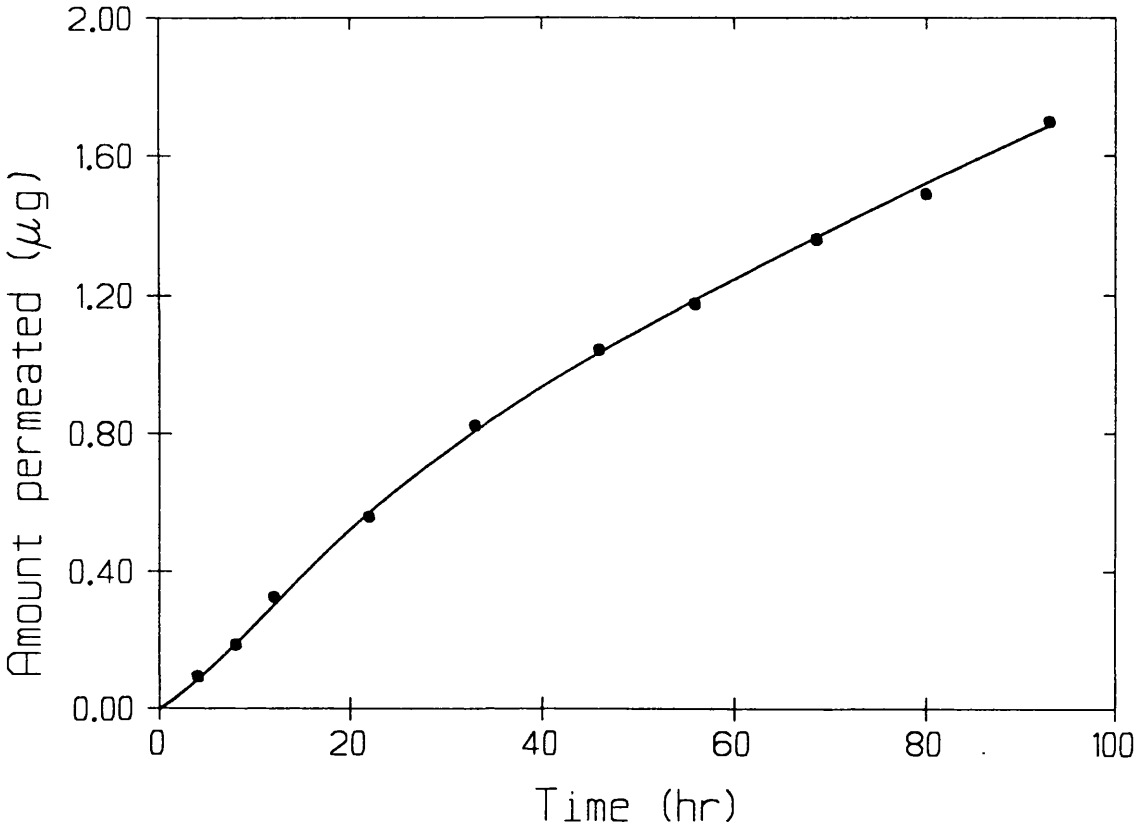

Figure 6.3 Typical permeation profile for oestradiol through unit area of porcine ear skin in the absence of surfactant enhancer.

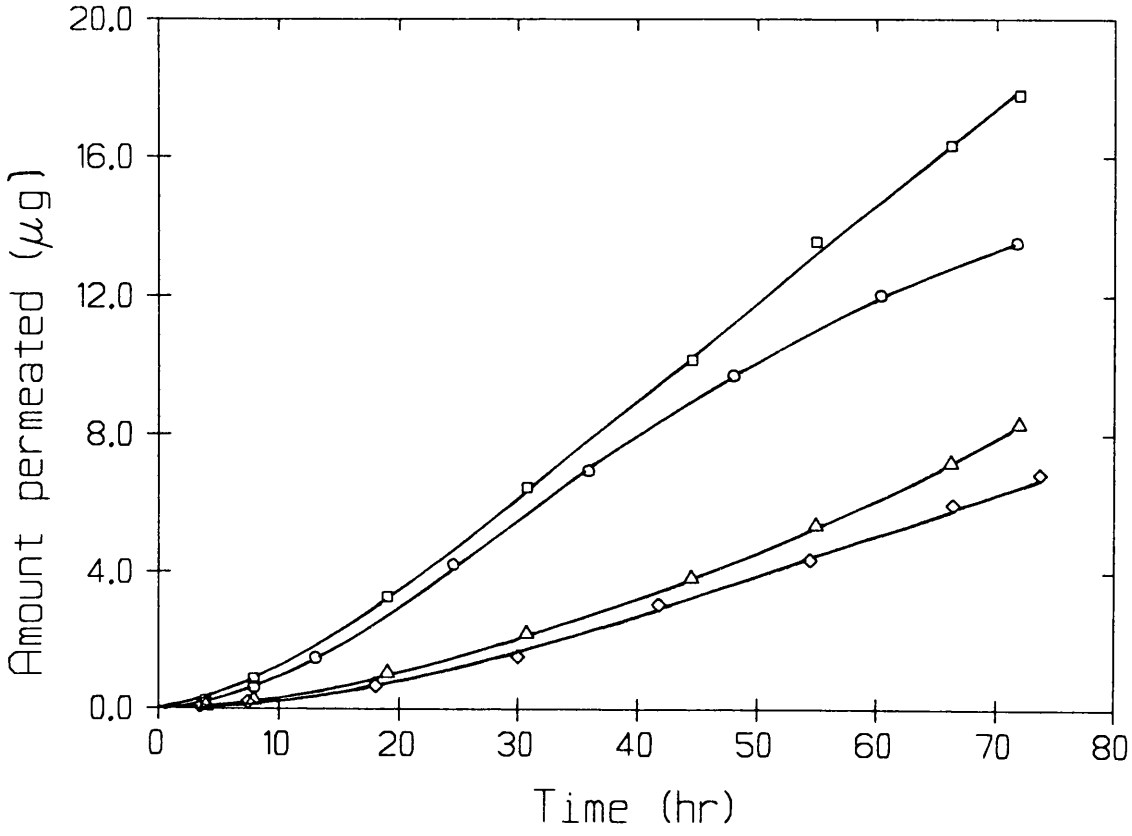

Figure 6.4 Permeation profiles for the penetration of oestradiol through 1 cm^{-2} of porcine ear skin in the presence of $C_{12}E_1$ (○), $C_{12}E_3$ (□), $C_{12}E_5$ (△) and $C_{12}E_7$ (◇).

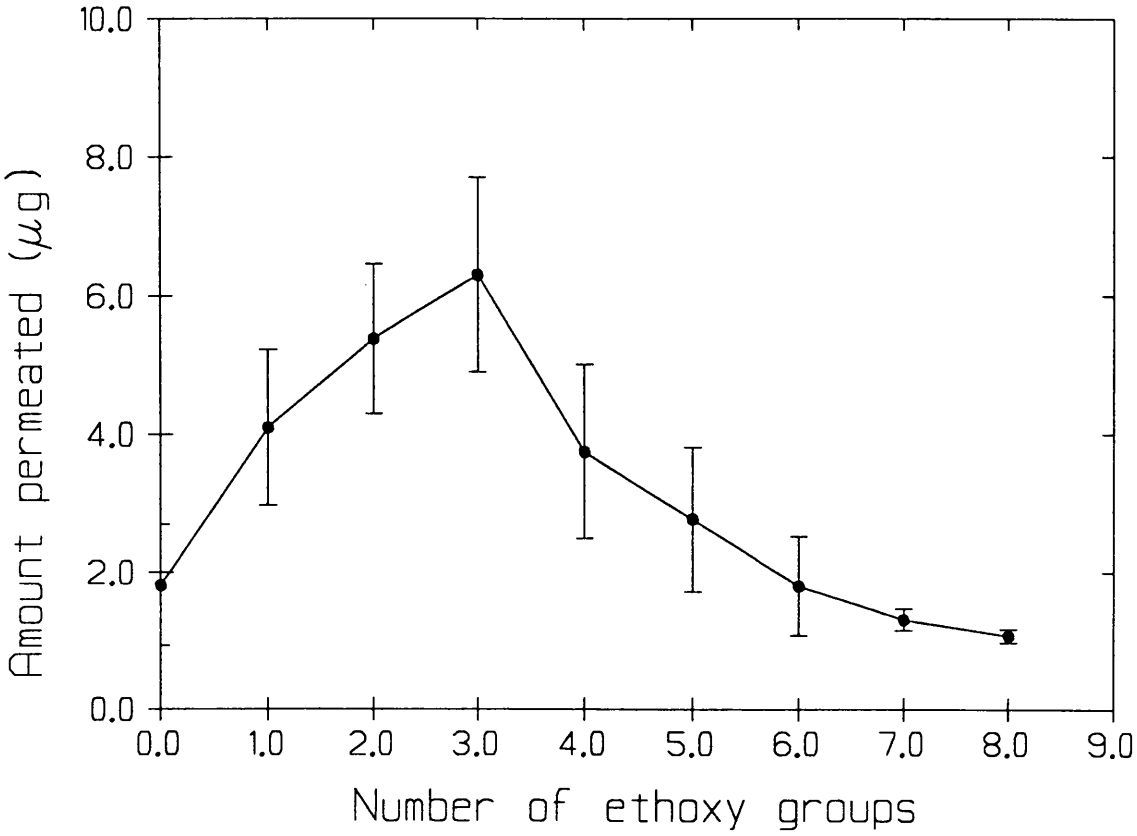

Figure 6.5 Cumulative mass of oestradiol that permeated 1 cm^{-2} of surfactant treated skin after 24 hours plotted as a function of the surfactant ethoxy chain length. Mean$\pm$SD, n=4

chain length of the surfactants from $C_{12}E_3$-$C_{12}E_8$ reversed this trend, the amount of OE that penetrated the skin decreased with surfactant ethoxy chain length.

Figure 6.6 shows the mean cumulative OE permeation for unenhanced skin and skin treated with surfactant for four skin samples at 24, 48, 60 and 72 hours. Time is plotted on the z-axis into the plot. The structure-activity relationship observed after 24 hours became more distinct as time of penetration increased, 22.82 ± 5.31 μg cm^{-2} of OE having penetrated $C_{12}E_3$ treated skin after 72 hours.

Figure 6.7 shows calculated pseudo steady state flux values for surfactant treated skin. The points shown are mean and standard deviation for four skin samples. All fluxes were calculated by linear regression of permeation profiles between 40-80 hours. All had linear correlation coefficients (r) >0.95.

6.3.3 Permeation of Hydrocortisone

A typical plot for cumulative hydrocortisone permeation through pig skin in the absence of surfactant, is shown in Figure 6.8. The permeation of HC showed little to no lag time under the conditions used, radioactive material was detected in the receptor fluid after two hours.

HC flux was at a maximum immediately after the lag period and then decreased continually with time until approximately 40 hours when a pseudo-steady state flux of 0.008 ± 0.0012 μg $cm^{-2}hr^{-1}$ was reached. This rate of permeation remained unaltered until the end of the experiment. The amount of HC that penetrated the skin after 24, 48, 60 and 72 hours was 0.73 ± 0.53, 0.99 ± 0.62, 1.09 ± 0.65 and 1.19 ± 0.68 μg cm^{-2} respectively.

Application of all surfactants investigated to the skin increased the penetration of HC through the skin. The effect observed was highly dependent upon the surfactant ethoxy chain length. Figures 6.9 and 6.10 show the permeation profiles for HC through skin in the presence of $C_{12}E_0$-$C_{12}E_8$ respectively. The relationship between the mass of steroid that permeated the skin and time, the permeation profile, was different for each surfactant. As the number of ethylene

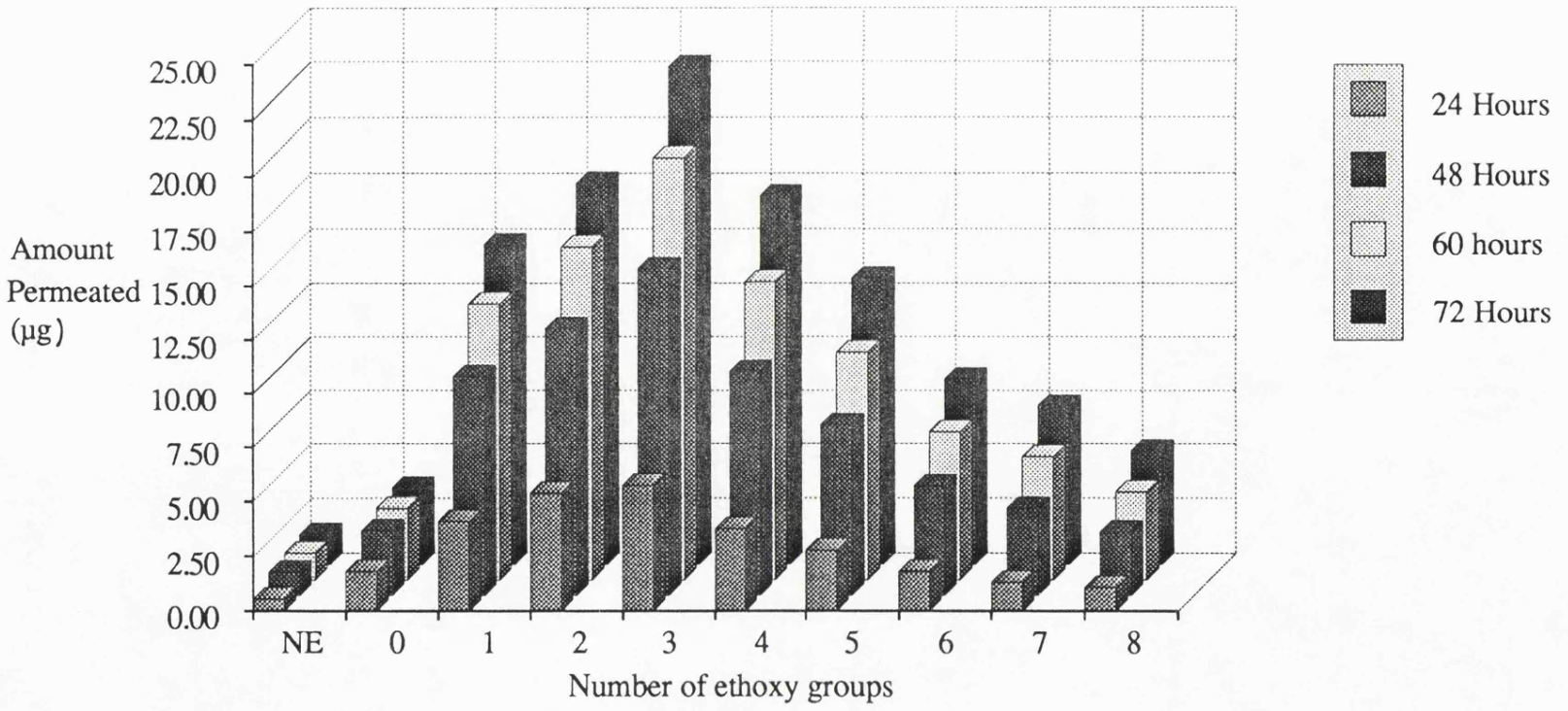

Figure 6.6 Cumulative amounts of oestradiol that permeated surfactant treated skin after 24, 48, 60 and 72 hours plotted against surfactant ethoxy chain length. Values shown are means, n=4

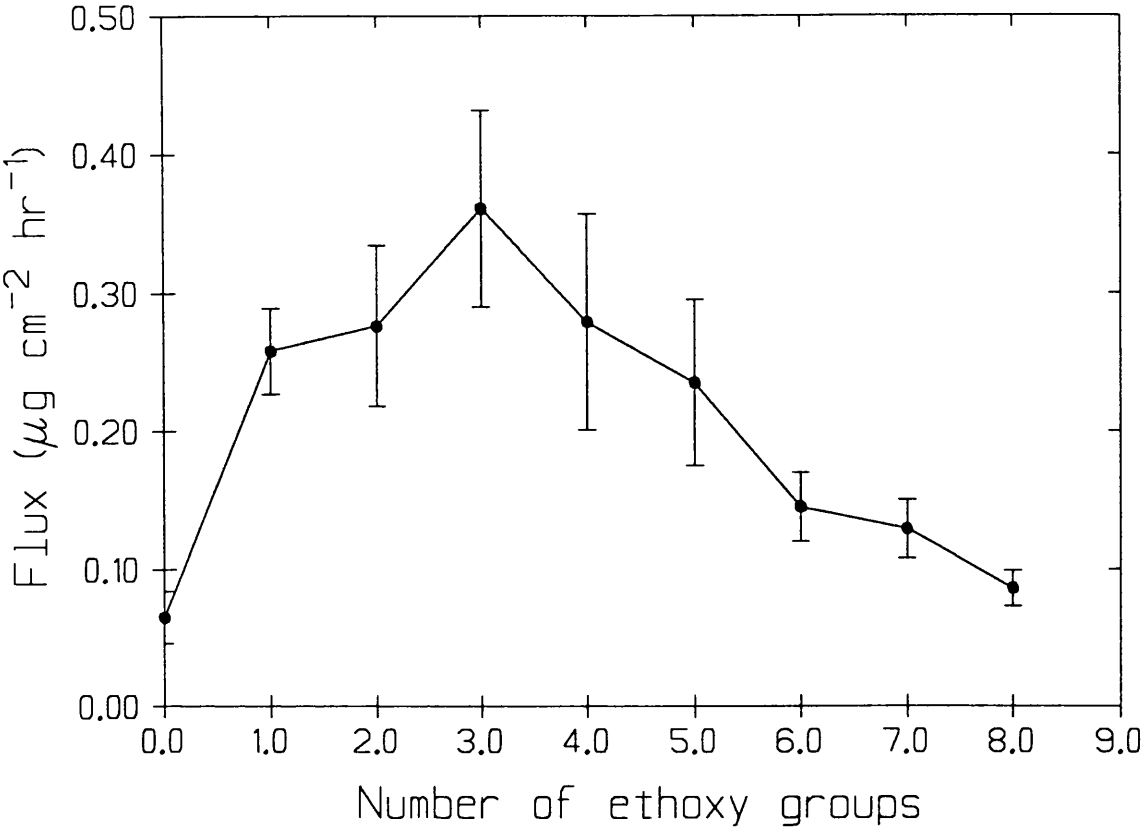

Figure 6.7 Calculated pseudo steady state flux values for the permeation of oestradiol through surfactant treated skin plotted as a function of surfactant ethoxy chain length. Mean±SD, n=4

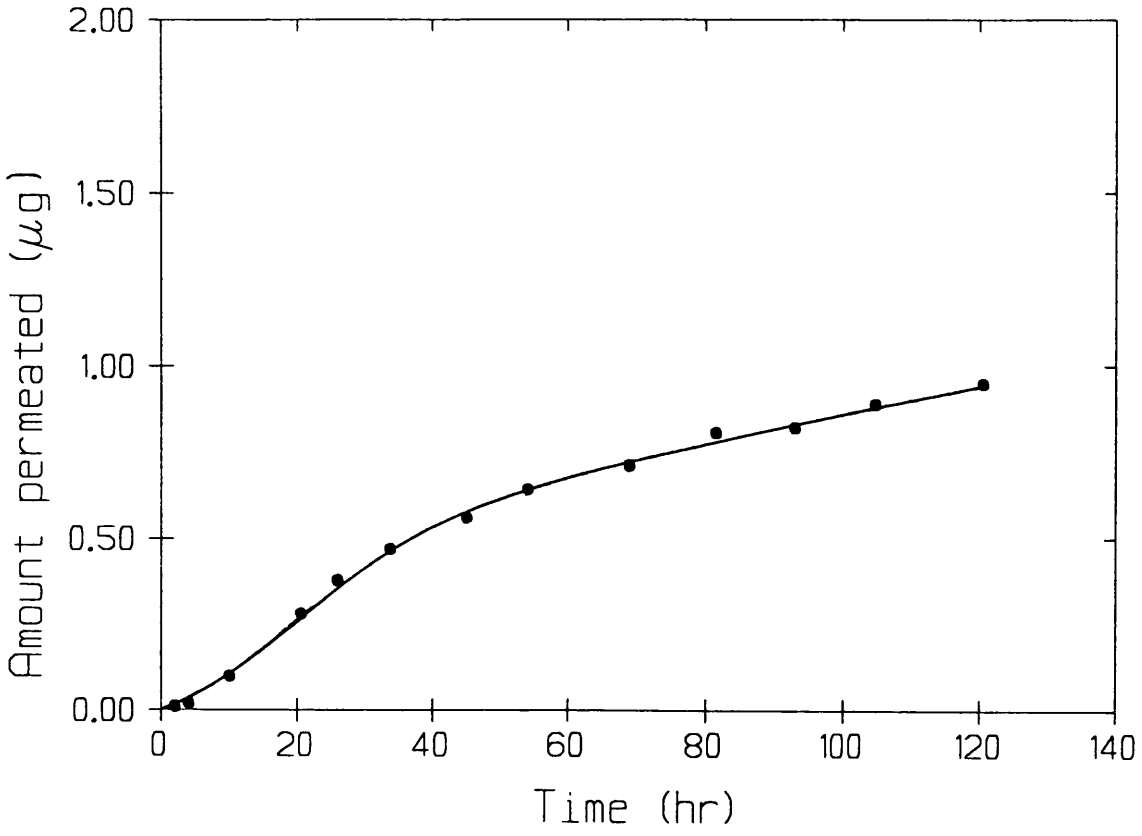

Figure 6.8 Typical permeation profile for the penetration of hydrocortisone through 1 cm^{-2} of porcine ear skin in the absence of surfactant enhancer.

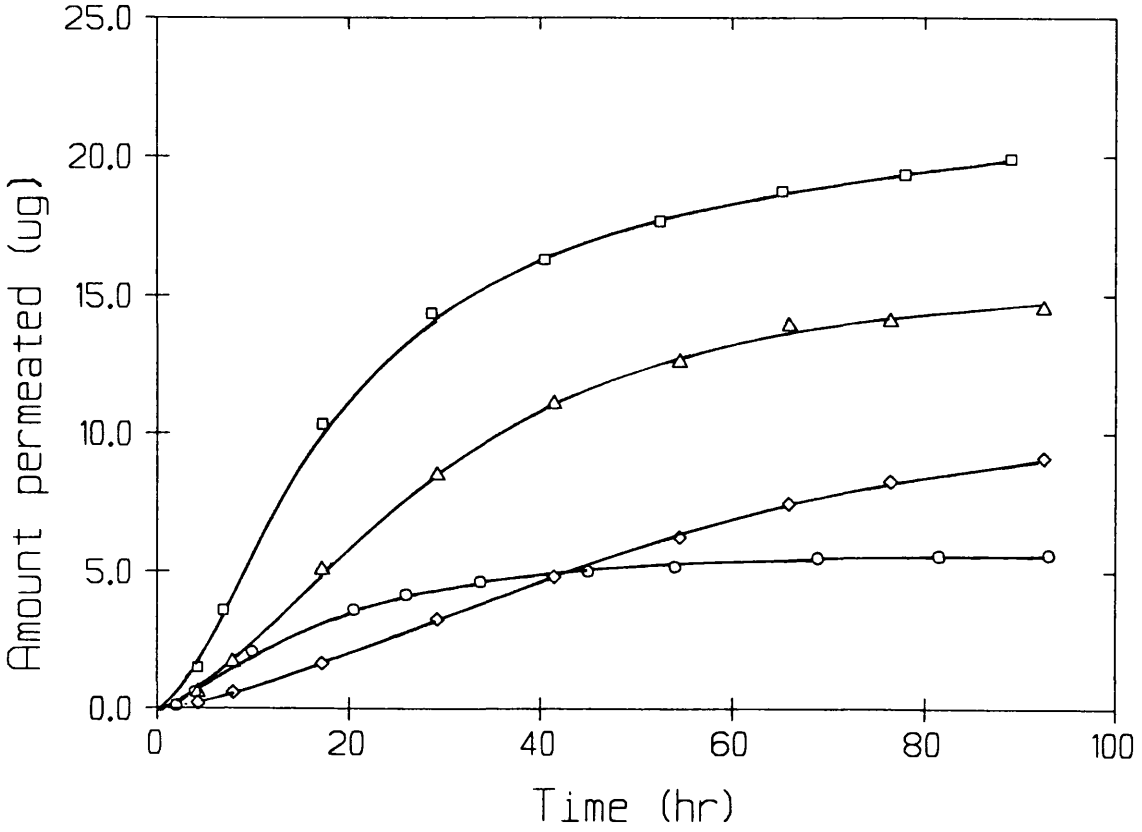

Figure 6.9 Permeation profiles for the penetration of hydrocortisone through 1 cm^{-2} of porcine ear skin in the presence of $C_{12}E_1$ (○), $C_{12}E_3$ (□), $C_{12}E_5$ (△) and $C_{12}E_7$ (◇).

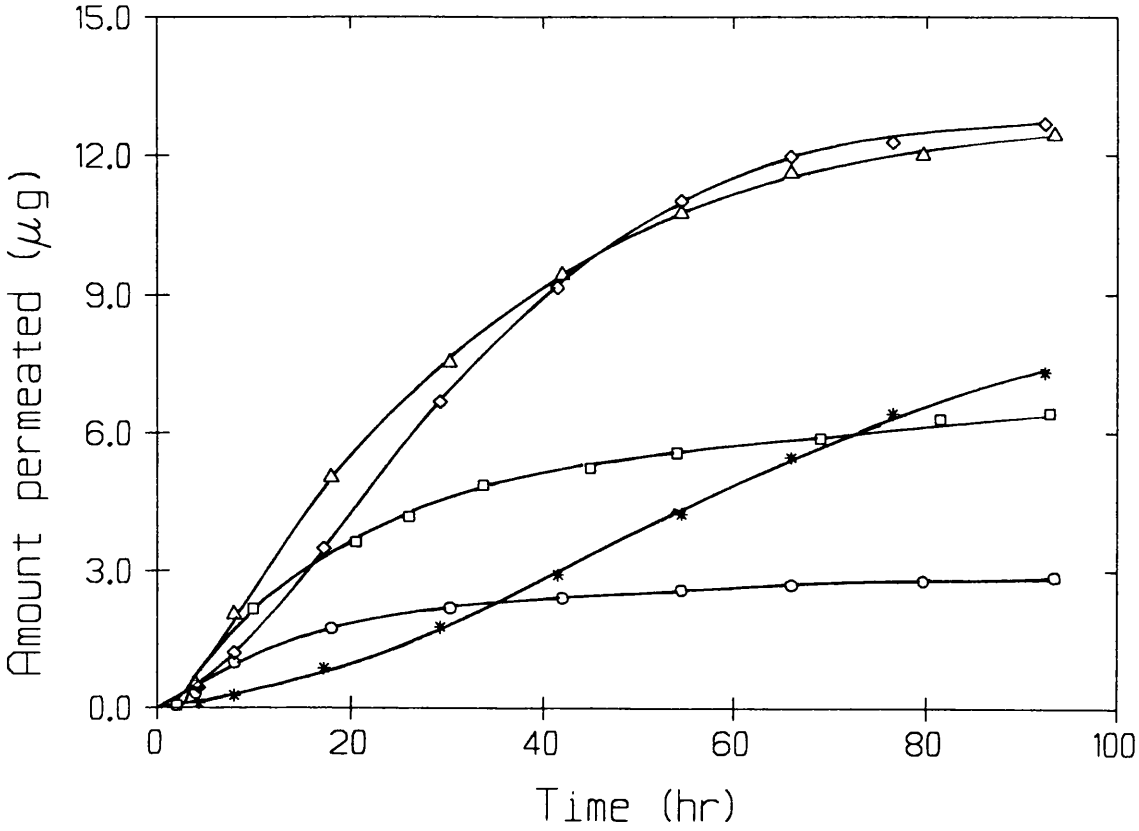

Figure 6.10 Permeation profiles for the penetration of hydrocortisone through 1 cm^{-2} of porcine ear skin in the presence of $C_{12}E_0$ (○), $C_{12}E_2$ (□), $C_{12}E_4$ (△) $C_{12}E_6$ (◇) and $C_{12}E_8$ (✱).

oxide groups per molecule increased from $C_{12}E_0$-$C_{12}E_8$ the time taken to reach maximum hydrocortisone flux increased. In addition the duration of the surfactant induced enhanced flux lengthened. For example $C_{12}E_1$ caused maximum flux of HC across the skin to be reached after 4 hours, this maximum rate was maintained until 10 hours after steroid application. The HC flux then decreased continually to a level almost equal to the untreated skin after 40 hours. However, with $C_{12}E_8$ maximum flux was not reached until 40 hours after application and was maintained until the end of the experiment. These effects influenced the amount of drug penetrating the skin with time. This is illustrated in Figure 6.11. The bar graph shows the mean mass of HC, (n=3) that permeated the skin after 24, 48, 60 and 72 hours plotted against surfactant ethoxy chain length on the x-axis; time is plotted on the z-axis into the page. Considering the graphs as a function of increasing ethoxy chain length over the range $C_{12}E_0$-$C_{12}E_8$; at 24 hours there was a sharp rise in the mass of HC penetrated to a maximum at $C_{12}E_3$ and then an equally sharp decline to a minimum with $C_{12}E_8$. As time of permeation increased the effects of longer ethoxy chain enhancers became more pronounced. After 72 hours there was little difference between the amount of HC penetration with $C_{12}E_3$, $C_{12}E_4$ and $C_{12}E_5$ and only slightly less permeated with $C_{12}E_6$-$C_{12}E_8$. The amount of HC permeated in the presence of $C_{12}E_0$-$C_{12}E_2$ had increased only slightly after 24 hours. These values are summarised in Figure 6.12, which shows the amount of HC permeated after 72 hours plotted against surfactant ethoxy chain length. The points are mean $\pm$ standard deviation for 3 skin samples.

Figure 6.13 shows the effect of the application of increasing amounts of $C_{12}E_3$ upon the permeation of HC through porcine ear skin. As the mass of surfactant applied to the skin increased so did the mass of hydrocortisone penetrating the skin. The initial rates of flux were very similar for all amounts of $C_{12}E_3$ up to 4.4×10^{-6} moles but the duration of the period of maximum flux lengthened with increased amounts of $C_{12}E_3$. With the two largest amounts of surfactant applied, the initial flux is reduced with respect to the application of

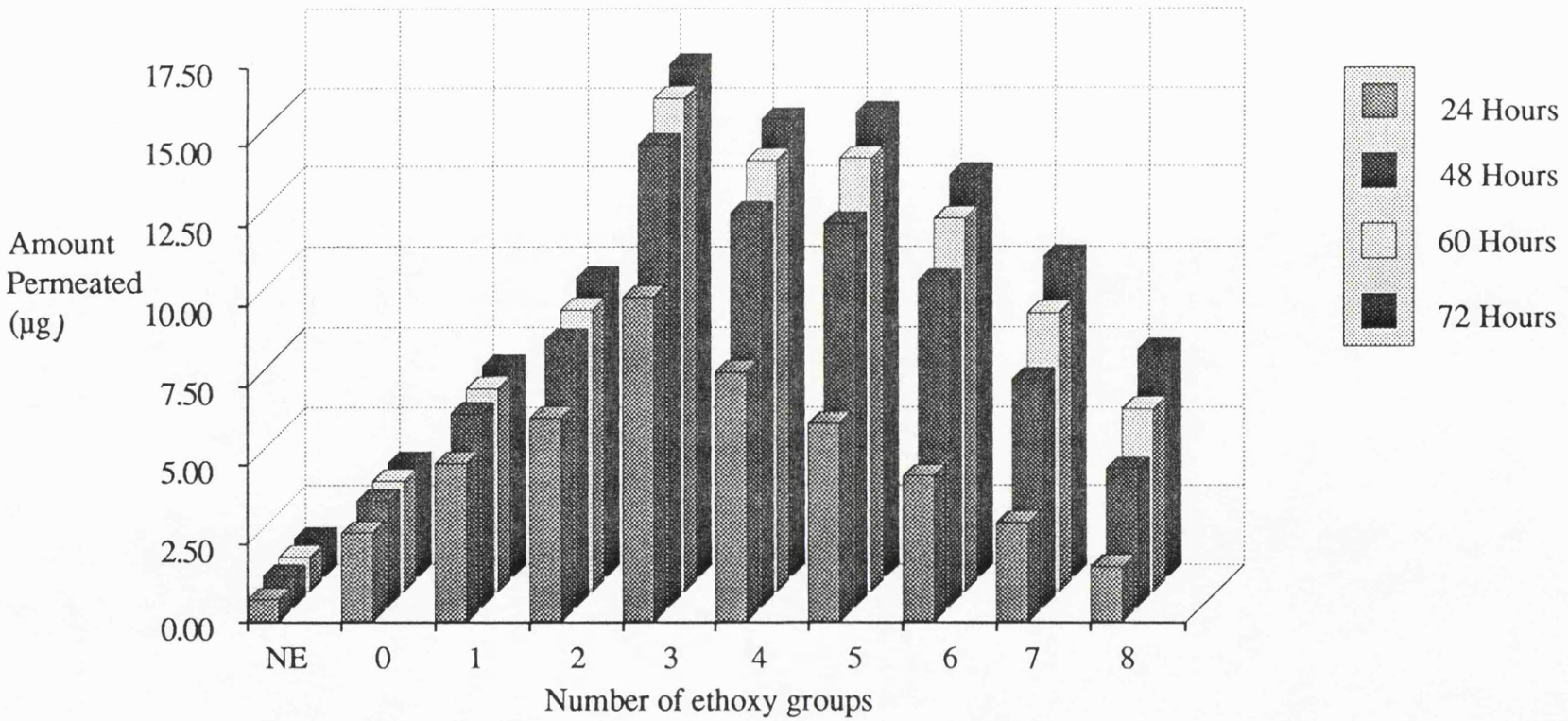

Figure 6.11 Cumulative mass of hydrocortisone that permeated surfactant treated skin after 24, 48, 60 and 72 hours plotted against surfactant ethoxy chain length. Values shown are means, n=3

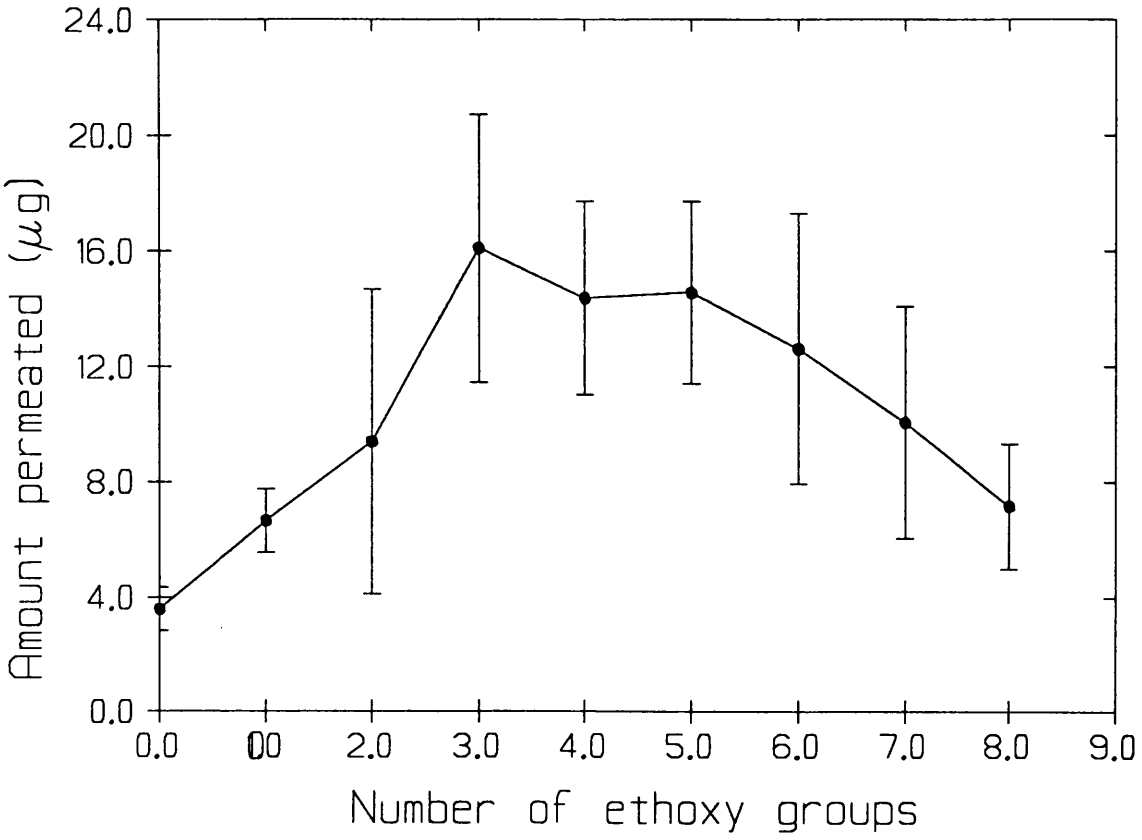

Figure 6.12 Cumulative mass of hydrocortisone that permeated 1 cm^{-2} of surfactant treated skin after 72 hours plotted as a function of the surfactant ethoxy chain length. Mean±SD, n=3

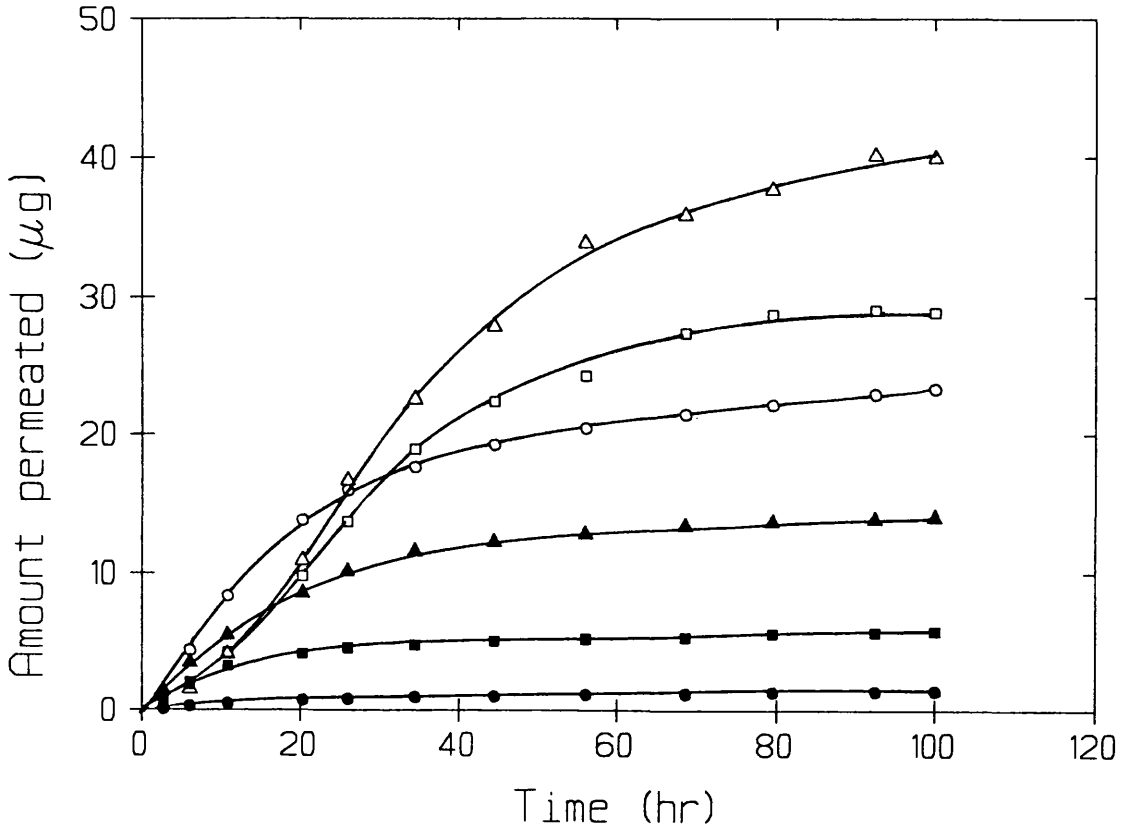

Figure 6.13 The effect of application of increasing amounts of $C_{12}E_3$ upon the permeation of hydrocortisone through 1 cm^{-2} of porcine ear skin. 0.55 (●) 1.1 (▲), 2.2 (■), 4.4 (○), 8.8 (□) and 17.6 (△) moles $x10^{-6}$ $C_{12}E_3$.

$4.4x10^{-6}$ moles, and the amount of steroid penetrating the skin did not exceed the amount that permeated with less surfactant until 35 hours after application.

6.3.4 Oestrone and Progesterone Permeation

Figure 6.14 and 6.15 show the respective permeation profiles for oestrone and progesterone penetration through porcine ear skin with and without application of $C_{12}E_3$. The points shown are mean and standard deviation of 3 skin samples.

The pseudo steady state flux values, the amount of steroid that permeated the skin at 24, 48, 60 and 72 hours and the enhancement ratios calculated from these values are given in Tables 6.1 and 6.2.

6.4 DISCUSSION

There has been a considerable volume of work published by many authors on the permeation of steroids through skin. It is difficult however to make direct comparisons to other researchers work as invariably different investigations have used different methods, different skin preparations and different species of animal skins. In making reference to other work in this field, the limitations involved in extrapolating between systems must be taken into account.

The permeation of the four steroids used in this study through porcine skin, without enhancement, all produced a similar shaped penetration profile with time. The rate of penetration of each steroid was however different. In each case there was short lag time ($\leq$8hr) before maximum flux was reached. Other works have quoted longer lag times for steroid diffusion through the skin, especially in the case of the more polar steroid HC (35). This may indicate that initial flux is controlled by "shunt pathway" diffusion for the polar steroids (29) or may be a consequence of the method of steroid application. A small fraction of the acetone solution applied to the skin could penetrate the appendages before evaporation of the solvent. Any steroid deposited directly over the appendages would also penetrate the skin rapidly. This initial rapid rate would be expected quickly to become insignificant with

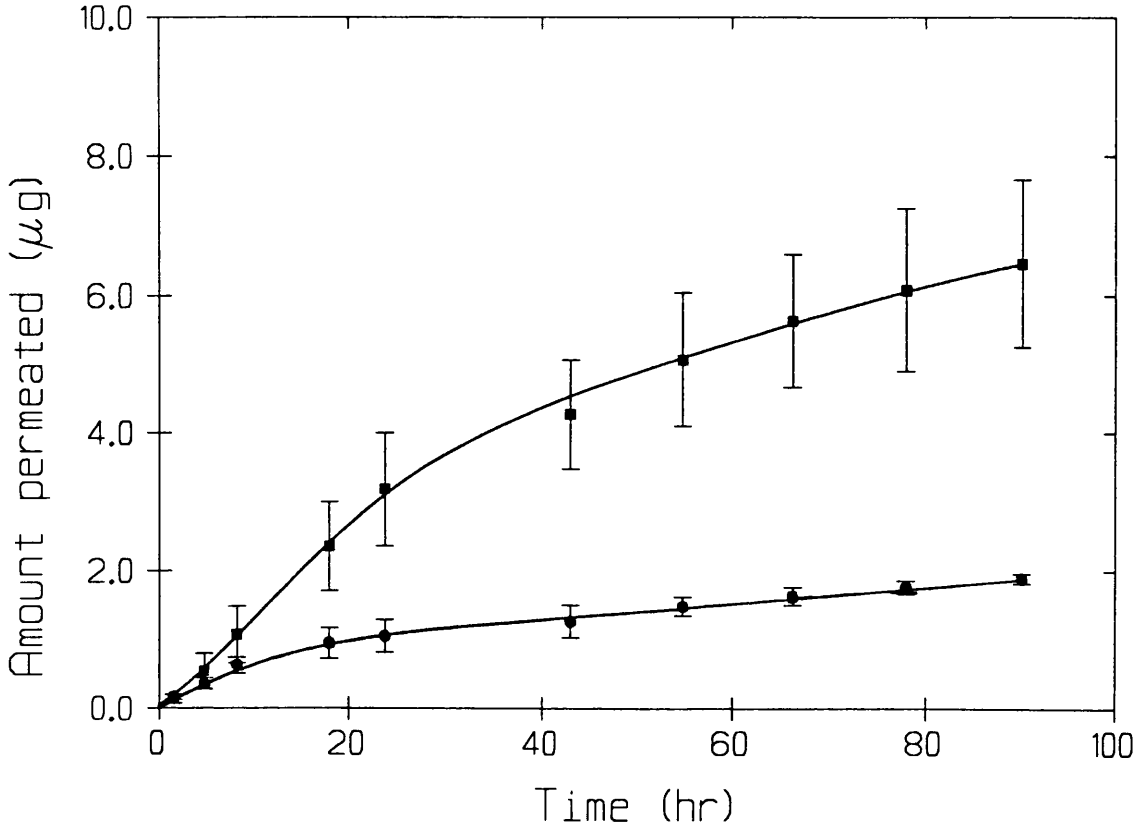

Figure 6.14 Permeation profiles for the penetration of oestrone through 1 cm^{-2} of porcine ear skin in the absence (●) and presence (■) of $C_{12}E_3$. Mean±SD, n=3.

System	Flux	Mass permeated per cm^{-2} of skin at time t (μg)			
	($\mu g\ cm^{-2}\ hr^{-1}$)	24hr	48hr	60hr	72hr
NE	0.0126±0.0026	1.09±0.21	1.39±0.15	1.53±0.13	1.70±0.132
$+C_{12}E_3$	0.053±0.005	2.90±0.72	4.67±0.84	5.31±0.91	5.86±1.00
ER	4.21*	2.66	3.35	3.47	3.45

* Flux $+C_{12}E_3$/flux NE, NE=No Enhancer

Table 6.1 The flux, mass permeated at 24, 48, 60, and 72 hours and enhancement ratios (ER) for oestrone permeation through porcine skin in the presence and absence of $C_{12}E_3$ (mean±SD, n=3)

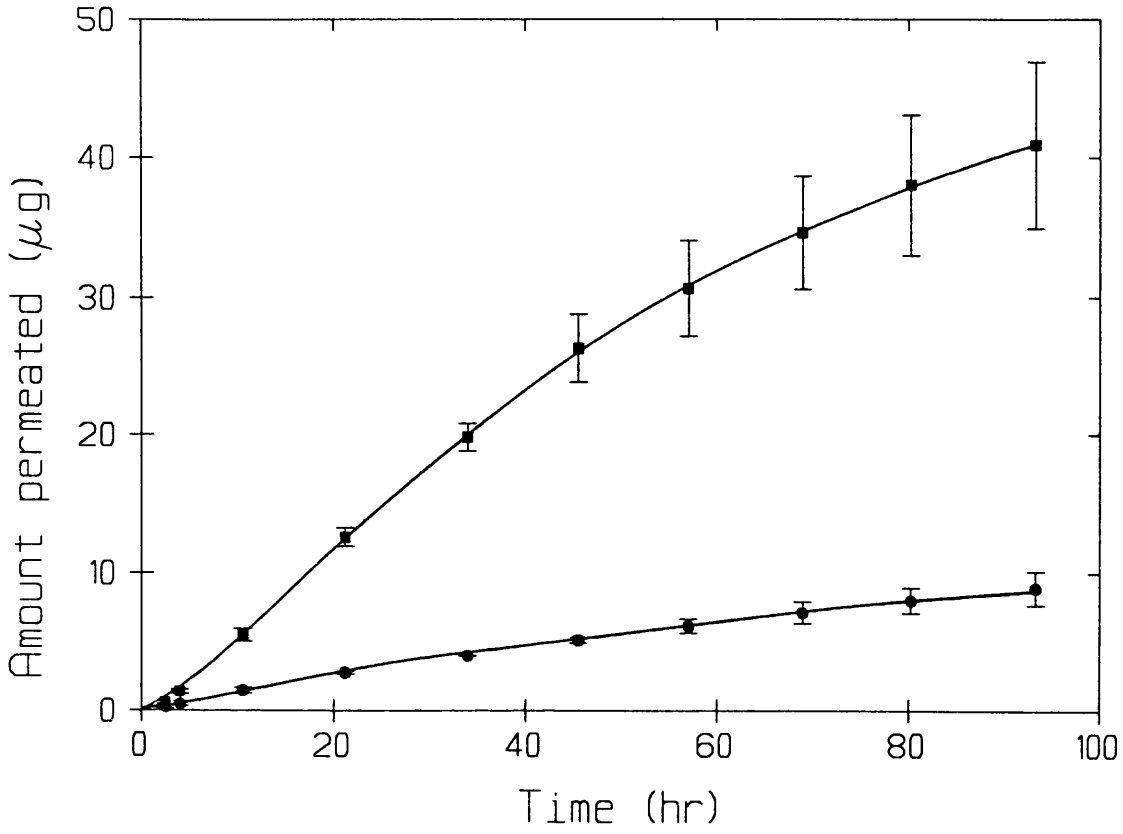

Figure 6.15 Permeation profiles for the penetration of progesterone through 1 cm^{-2} of porcine ear skin in the absence (●) and presence (■) of $C_{12}E_3$. Mean±SD, n=3.

System	Flux	Mass permeated per cm^{-2} of skin at time t (μg)			
	($\mu g\ cm^{-2}\ hr^{-1}$)	24hr	48hr	60hr	72hr
NE	0.087±0.02	3.03±0.06	5.32±0.25	6.34±0.50	7.33±0.79
$+C_{12}E_3$	0.574±0.06	14.37±0.80	26.8±2.77	31.6±3.46	35.62±4.15
ER	6.6*	4.74	5.03	4.98	4.86

* Flux $+C_{12}E_3$/flux NE, NE=No Enhancer

Table 6.2 The flux, mass permeated at 24, 48, 60, and 72 hours and enhancement ratios (ER) for progesterone permeation through porcine skin in the presence and absence of $C_{12}E_3$ (mean±SD, n=3)

respect to permeation through the whole stratum corneum due to effective depletion of the drug within the appendages. Lateral diffusion in the dry steroid film would be negligible.

After the initial burst of steroid flux across the skin the flux constantly decreased over the next 30 hours to a pseudo steady state level after approximately 40 hours which continued until the end of the experiment. These observations can be explained by the shunt route flux described above and the evaporation of acetone from the skin surface. After application of the steroid in acetone the solvent remains visable on the skin for approximately two minutes. As acetone evaporated the steroid would be deposited as a film on the skin surface.

In the initial moments of contact the steroid is in solution and the flux into the skin would be determined by the stratum corneum/acetone partition coefficient. As solvent evaporated the chemical potential of the steroids increased. At the saturation point of the steroid in acetone, the driving force for partitioning into the skin was maximal. The optimal partitioning continued until the acetone completely evaporated leaving solid steroid on the skin. The initial burst of penetrant partitioning into the skin provided a peak flux, this was also likely to cause the build up of a reservoir of steroid in the stratum corneum. The reservoir effect in steroid percutaneous absorption is a well documented phenomenon (167). The decrease in flux following the initial maximum was probably due to the depletion of this resevoir and as dissolution of the penetrant from the deposited film became the rate limiting step in the percutaneous absorption of the steroid.

This theory is supported by the fact that application of 20μl of acetone to a film of hydrocortisone on the skin surface after 40 hr caused a second burst of steroid flux through the skin presumably by redissolving the steroid and increasing the partitioning of drug into the skin (results not shown).

The use of acetone as a vehicle to deposit drug on the skin surface has been demonstrated to have damaging effects upon the permeability barrier in hairless mouse skin (168). The same study showed however, that human cadaver skin was

not significantly affected by the solvent. As porcine stratum corneum is more similar in nature to human than hairless mouse skin, it was thought unlikely that acetone would damage porcine skin preparations, especially as the amount used (11.4 μl cm^{-2}) was significantly less than the 160 μl cm^{-2} used by Bond and Barry in the above mentioned investigation.

The pseudo steady state flux values calculated for all four steroids, without enhancement, were made between 40-80 hr after drug application, this was after the initial acetone affected drug flux had subsided. Table 6.3 gives the compiled data for the fluxes of the four steroids used. The rate of penetration of the steroids decreased in the order progesterone > oestradiol = oestrone = hydrocortisone (t-test, $p > 0.01$). This order would be expected from human stratum corneum/water partition coefficients calculated by Scheuplein *et al* (35). These values of 104, 46, 46 and 7 for PG, OE, OT and HC respectively would be expected to give an estimation of the expected penetration of the steroids into the skin. The same investigation calculated permeability constants (kp) from aqueous solutions and also maximum obtainable fluxes from saturated aqueous solutions for the four steroids used in this study through human cadaver skin. The kp values obtained were 3600, 1500, 300 and 3 cm $hr^{-1}x10^{-6}$ for OT, PG, OE and HC respectively, a different order to this study. The calculated maximum fluxes gave a different picture again, with PG, OT, HC and OE producing values of 0.0128, 0.046, 0.0008 and 0.00034μg $cm^{-2}hr^{-1}$ respecitvely. These latter flux values are between 2 and 10 fold less than the flux values obtained in this work with the exception of oestradiol which showed a 40 fold greater permeability in this study with respect to the calculations of Scheuplein *et al.*

In an *in-vivo* study upon steroid permeation through human forearm skin, Feldman and Maibach (30) found similar amounts of PG and OE penetrated the skin whilst far less HC permeated through the skin from the same dose and time of permeation.

Steroid	Flux
	(μg $cm^{-2}hr^{-1}$)
Oestradiol	0.0135±0.004
Hydrocortisone	0.008±0.0012
Oestrone	0.0126±0.0026
Progesterone	0.087±0.02

Table 6.3 Pseudo steady-state fluxes of oestradiol, hydrocortisone, oestrone and progesterone through porcine ear skin. (mean±SD, n>3)

Barry and Bennet (58) stated fluxes of 0.0237 ± 0.0063 $\mu g\ cm^{-2}\ hr^{-1}$ for HC and 0.0467 ± 0.0089 $\mu g\ cm^{-2}\ hr^{-1}$ for PG through human epidermis, using an acetone deposition method similar to this study. Using similar methods and conditions Goodman and Barry (59) quoted an average flux of $0.025 \mu g cm^{-2} hr^{-1}$ for OE this included the 'acetone burst'. These three values are similar to those obtained in this work. Moelgaard and Hoelgaard (169) found OE deposited as a film from ethanol to have a steady state flux of 0.011 ± 0.004 $\mu g\ cm^{-2}\ hr^{-1}$ through human skin which is the same as obtained in this investigation. Ponec and Polano (170) investigated the permeation of hydrocortisone from an ethanolic solution through human skin. They did not calculate a flux value, but quoted that $7.45 \mu g$ of HC permeated the skin in 72 hours compared to 1.19 ± 0.68 μg in this study.

All nine surfactants caused some increase in the amount of steroid penetrating the skin. In the case of HC permeation, there was a difference in the amount of enhancement and shape of the permeation profiles between the members of the surfactant series. As the length of the ethylene oxide chain increased so did the time to reach maximum flux and the duration of action in the skin. The low ethoxylated molecules showed permeation profiles with a rapid initial flux reducing with time to a constant rate of steroid permeation. This shape of permeation curve would be consistent with drug depletion from the skin surface or from an initially set up reservoir, decrease in the thermodynamic activity of the steroid, steadily increasing resistance to penetration in the skin or reduction in enhancement effects due to surfactant depletion.

The last of these suggestions was the most likely cause of this profile shape. Increasing the amount of surfactant ($C_{12}E_3$) on the skin surface did not alter the rate of the initial maximum flux but did increase the duration of the period of maximum flux of HC (see Figure 6.13).

If it is assumed that the surfactant has to be present in the stratum corneum to exert an enhancement effect, it could be concluded from these results that the low HLB surfactants rapidly permeate through the skin and effectively deplete the

amount of enhancer. As the length of the ethoxy chain increased, the rate of surfactant depletion decreased and with $C_{12}E_7$ and $C_{12}E_8$ maximum flux is observed until the termination of the experiment. As the maximum flux is reached more slowly with the longer ethoxy chain lengths, it may suggest that as the ethoxy chain length of the surfactant increased, the rate of permeation of the surfactant molecules across the skin decreased. The low HLB molecules would thus exert a rapid but short lived action and the higher HLB molecules would give a slower but more prolonged action.

This suggestion is consistant with the findings of Nishiyama *et al* (32) who studied the permeation of dodecyl ether ethoxylates in the range $C_{12}E_0$-$C_{12}E_{10}$ across hairless mouse skin *in-vivo*. They found $C_{12}E_0$ to have the highest rate of absorption of 0.12 μmole $cm^{-2}hr^{-1}$ (22.32 μg $cm^{-2}hr^{-1}$). A comparable rate through pig skin would mean all the applied surfactant would permeate through the skin in only 18 hours, it is however likely that pig skin is less permeable than hairless mouse skin. As ethoxy chain length of the surfactant increased the rate of percutaneous absorption decreased $C_{12}E_1$ and $C_{12}E_{2.6}$ (average ethoxy chain length) had similar flux values of 0.097 μmole $cm^{-2}hr^{-1}$. This would mean complete absorption of the $2.2x10^{-6}$ moles of surfactant in approximately 22.7 hours. A flux value of 0.0075 μmole $cm^{-2}hr^{-1}$ was reported for $C_{12}E_{10}$, would take 293 hours to completely permeate $2.2x10^{-6}$ moles through the skin. The authors also found that there was almost no lag before $C_{12}E_0$ penetrated the skin and as ethoxy chain length of the surfactants increased, so did the time to reach the maximum rate of permeation. Similar findings were made by Black and Howes (62) who reported the permeation of $C_{12}E_3$ and $C_{12}E_6$ to be far greater than that of $C_{12}E_{10}$ through rat skin *in-vitro*.

The presence of surfactant on the skin surface may also have affected the availability of the drug for percutaneous absorption. After evaporation of the acetone the steroid will be present in a crystalline form. In order to diffuse into the skin the drug would have to dissolve in either the sebum or directly into the stratum

corneum lipids. There may have been limited contact between available steroid and the skin surface. The steroid crystals may have dissolved in the film of surfactant present on the skin surface. This would have increased the effective contact between the steroid and skin surface relative to crystalline drug. Surfactant depletion due to their penetration through the skin would result in recrystallisation of the steroid and therefore a decrease in the extent of the improved contact. These effects would have been dependant upon the solubility of the steroid in the surfactant and the rate of depletion of surfactant from the skin surface. As there was only an initial 1:7 molar ratio of drug to surfactant present upon the skin surface it is expected that most of the drug would not have dissolved. The thermodynamic activity of the steroid would not have been reduced by the surfactant. $C_{12}E_5$-$C_{12}E_8$ may have kept the steroid in solution for a longer period of time than the shorter ethoxy chain molecules, but these may have been better solvents for the steriod. The extent these effects had upon the drug penetration rate is unknown.

The surfactant depletion effects were very prominent in the enhancement of HC penetration but for OE with the exception of $C_{12}E_0$ there was little difference in the shapes of the permeation profiles between surfactants. This can be seen more clearly by looking at the enhancement ratios (ER) at 24, 48, 60 and 72 hours for OE and HC, Figures 6.16 and 6.17 respectively. In the studies with HC there is a decrease in ER with time for the surfactant range $C_{12}E_0$-$C_{12}E_3$, an increase in ER up to 48 hours and then a decrease for $C_{12}E_4$, an increase up to 60 hours then a decrease for $C_{12}E_5$ and $C_{12}E_6$ and a continual increase in ER with time for $C_{12}E_7$ and $C_{12}E_8$. For OE enhancement a continual increase in ER with time is seen for all surfactants except $C_{12}E_0$ which shows a continual decrease, however the extent of the increase in ER with $C_{12}E_1$ and $C_{12}E_2$ is smaller after 60 and 72 hours compared with higher HLB surfactants.

The enhanced permeation of both oestrone and progesterone by $C_{12}E_3$ showed no real signs of surfactant depletion with respect to the situation with HC.

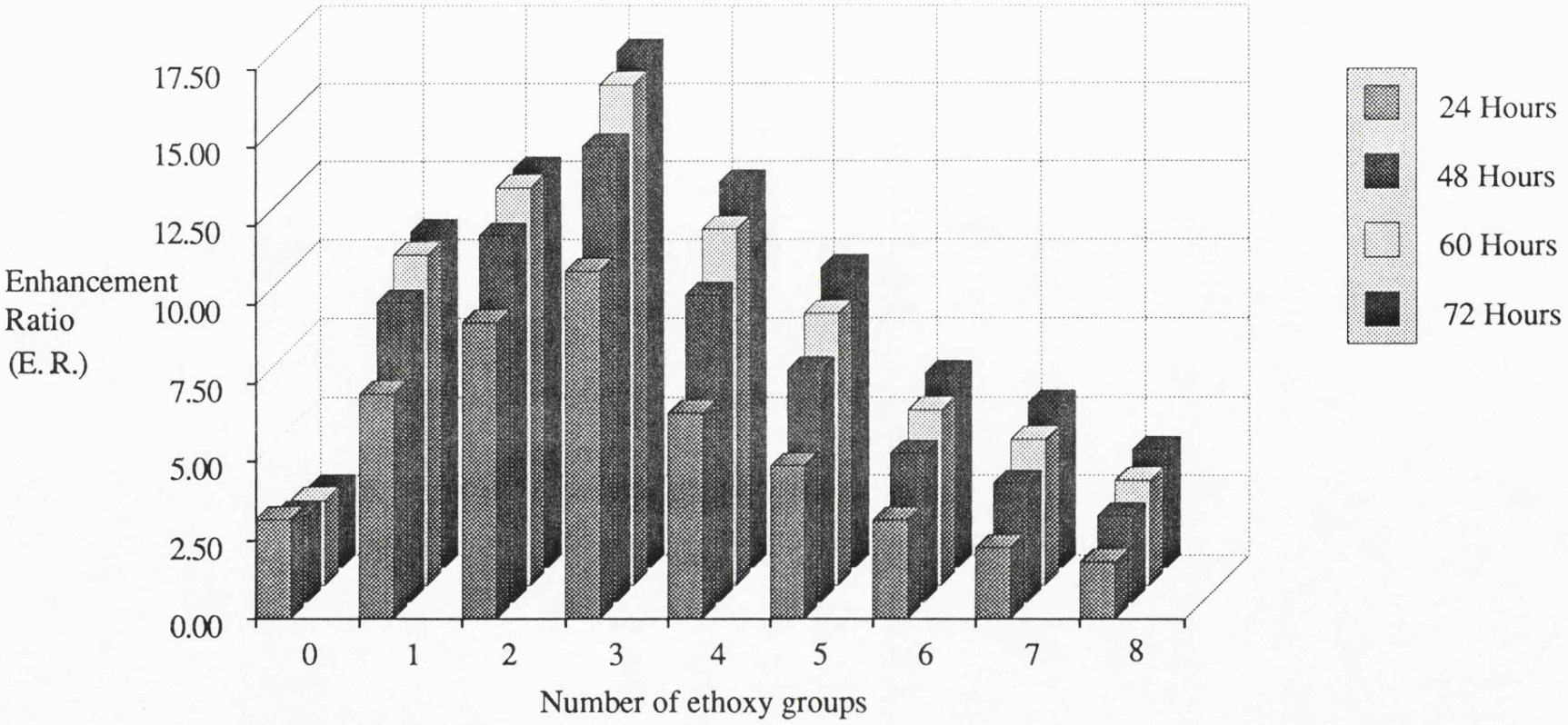

Figure 6.16 Calculated enhancement ratios (ER) for oestradiol permeation through porcine ear skin at 24, 48, 60 and 72 hours. Values are means, n=4.

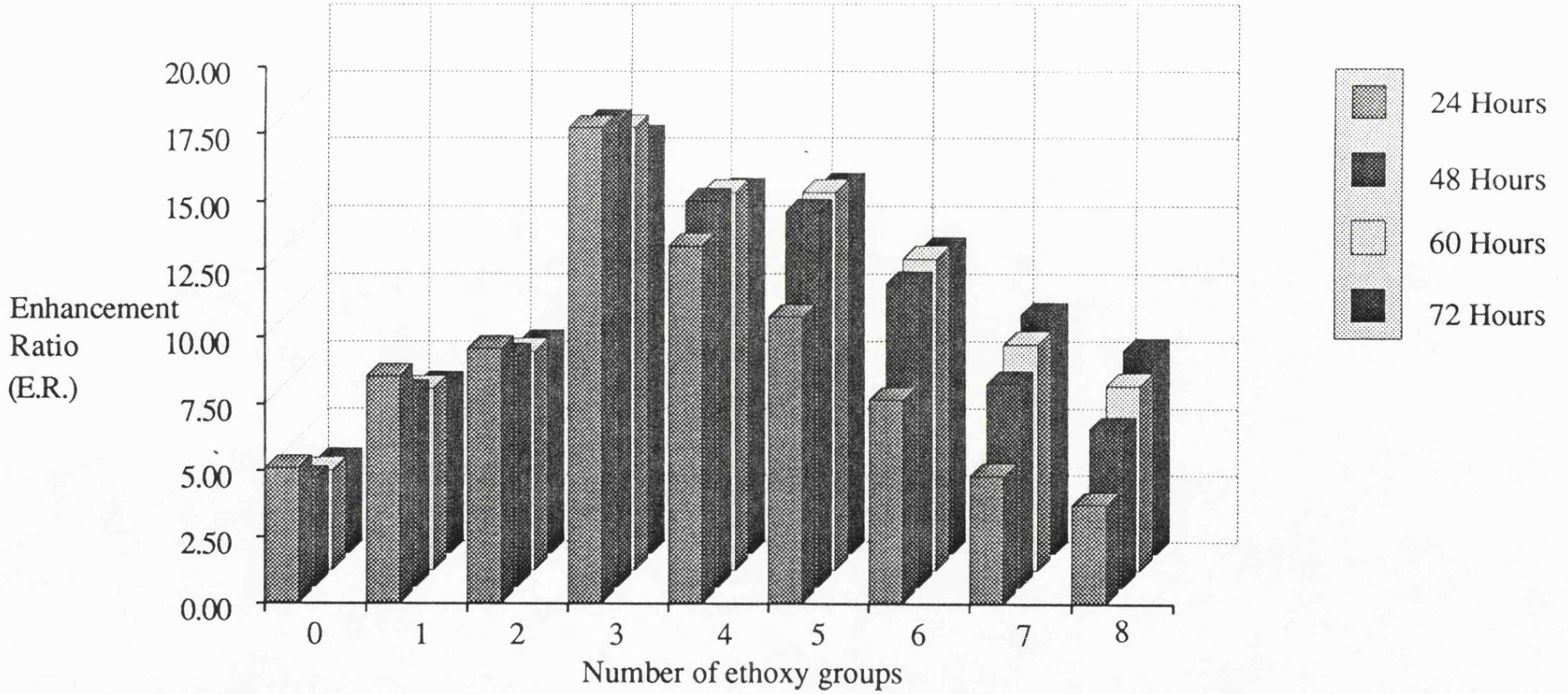

Figure 6.17 Calculated enhancement ratios (ER) for hydrocortisone permeation through porcine ear skin at 24, 48, 60 and 72 hours. Values are means, n=4.

This suggests that the enhancement of the more lipophilic molecules PG, OT and OE may have occurred at either a different site of action, by a different mode of action or with a different concentration dependance with respect to the more hydrophilic HC.

For both OE and HC maximum penetration enhancement was observed with $C_{12}E_3$ however the extent of enhancement by this surfactant differed for the two steroids as did the relative effects of the other members of the surfactant series. $C_{12}E_3$ produced an ER_{24} of 11.0 for OE permeation and 17.7 for HC penetration. These ratios altered with time to produce ER_{72} values of 16.4 and 15.5 for OE and HC respectively. The ER_{24} for OT and PG were 2.7 and 4.7, after 72 hours (ER_{72}) then had become 3.4 and 4.9 respectively. This made the order of enhancement of the four steroids by $C_{12}E_3$ HC>OE>PG=OT at 24 hours and at 72 hr OE=HC>PG=OT (t-test, $p>0.05$).

Figures 6.16 and 6.17 also show the distribution of enhancement ratios around the maximum value obtained with $C_{12}E_3$. For OE and HC this distribution differs to a great extent. For OE the ER_{24} showed a skew to the low ethoxy content molecules, $C_{12}E_1$ and $C_{12}E_2$ were more potent enhancers than $C_{12}E_4$ and $C_{12}E_5$. After 72 hours this skew has evened up and the ER_{72} were similar for $C_{12}E_2/C_{12}E_4$ and $C_{12}E_1/C_{12}E_5$. $C_{12}E_0$ and $C_{12}E_6$-$C_{12}E_8$ gave far lower ER values.

For HC the distribution around $C_{12}E_3$ is skewed towards the more hydrophilic surfactants at 24 hours and this relationship became accentuated with time, $C_{12}E_4$-$C_{12}E_6$ all show significantly greater enhancement ratios than $C_{12}E_1$ and $C_{12}E_2$ after 72 hours (t-test, $p>0.05$). These results again pointed to different sites or mechanisms of enhancement for OE and HC. Theories of these mechanisms of permeation enhancement and correlation to the physical studies with surfactant with model membranes and stratum corneum will be discussed in the next chapter.

CHAPTER 7

CONCLUSIONS

7.1 Effects of Nonionic Surfactants on Lipid Bilayer Fluidity

The effects of a homologous series of nonionic surfactants upon the fluidity of lipid bilayers were studied using three different biophysical techniques, DSC, FPS and ESR in order to obtain quantitative structure-activity relationships. The three techniques all produced different results in terms of the structure-activity relationship observed showing that the choice of method of analysis is important in studies such as these. These differences observed in the results, however, provided additional information on the mechanisms of action of bilayer fluidisation by the surfactants.

Consider the effects of the series of pure dodecyl ether ethoxylates $C_{12}E_0$-$C_{12}E_8$ upon the fluidity of DSPC bilayers at a concentration of 50 mole% surfactant. When analysed by DSC it was observed that the most potent fluidiser in the series was $C_{12}E_3$. Different results were obtained using the other techniques of analysis. A large amount of information was obtained from the FPS studies with four different probe molecules. The relative efficacy of the surfactants was dependent upon the probe molecule structure and its location in the membrane. DPH and perylene both sit in the bilayer hydrophobic core. For these two probes the most effective fluidisers lay in the range $C_{12}E_2$-$C_{12}E_4$. However, when ANS was used as the probe the most effective fluidisers were seen to be in the range $C_{12}E_5$-$C_{12}E_7$, the surfactants of shorter ethoxy chain length being less effective. ANS is known to probe the bilayer headgroup region. Cis-pna can be seen to span the whole bilayer as it sits in the same orientation as DSPC molecules. The most potent fluidisers amongst the surfactant series for this probe was $C_{12}E_4$-$C_{12}E_5$. In the ESR studies the most potent effect upon 5-DS was observed with the surfactants with long ethoxy chains $C_{12}E_6$-$C_{12}E_7$. The possible differences between results observed with cis-pna and 5-DS were discussed in Chapter 5.

A possible explanation for these results can be built from the information obtained in these investigations. It would appear that the very low HLB surfactants

$C_{12}E_0$ and $C_{12}E_1$ have little effect on any part of the membrane. These molecules may be impeded by restricted access to the membrane. The short ethoxy chain length surfactants $C_{12}E_2$-$C_{12}E_4$ exert their greatest degree of action on the bilayer core fluidising the lipid acyl chains. This was observed with DPH and perylene in the FPS study and in the DSC investigation where the changes observed in T_m and $\Delta T_{½}$ relate to the gel-liquid crystalline phase transition which is mainly associated with melting of the lipid acyl chains. The longer ethoxy chain length molecules exert their effects more at the bilayer surface. This may be on the packing of the polar headgroups themselves or on the hydration sphere surrounding the polar groups. This was shown by the results with ANS and to some extent 5-DS where the reporting group is near to the bilayer surface. The mobility of cis-pna would be expected to be effected by events at both the nonpolar core and hydrophillic headgroup. The relative potency of the intermediate surfactant $C_{12}E_5$ and the little difference observed across the series in reducing the probe anisotropy, r, at 30°C may reflect the spanning of the two regions of the bilayer by this probe.

It was suggested in Chapter 3 and in other studies of the effects of series of nonionics upon membranes (63,85-87) that the observed structure-activity relationships can be explained in terms of the surfactants membrane partition coefficient. However if the relative effects were solely due to this all regions would be fluidised to the same extent by each surfactant, other factors must therefore influence the surfactant action. Florence *et al* (63) postulated that the depth of alkyl chain penetration into the membrane may be affected by the length of the ethoxy chain on the hydrophobic group (see 3.4). This theory would seem to be supported by this work although further investigation is required.

7.2 Permeation Enhancement by Nonionic Surfactants

As described previously (1.5.4.3) there have been several reports of nonionic surfactants increasing percutaneous absorption. In this investigation all the surfactants amongst the homologous series $C_{12}E_0$-$C_{12}E_8$ caused some increase in the percutaneous absorption of both a relatively polar compound (hydrocortisone) and a

nonpolar compound (oestradiol). The structure activity relationships for the enhancement of permeation by $C_{12}E_0$-$C_{12}E_8$ was different for the two permeants.

The ways in which enhancers may act to increase the absorption of compounds through the skin have been discussed earlier in this thesis (1.5.2). The enhancer may act to increase the thermodynamic activity or availability of the permeant at the skin surface. The enhancer may act as a cosolvent for the drug compound in the skin so increasing its partitioning into the stratum corneum, or the enhancer may act by decreasing the diffusional resistance of the skin to drug diffusion.

Oestradiol is a fairly hydrophobic compound and as such would be expected to permeate the stratum corneum mainly through the core of the bilayers of the intercellular lipid lamellae. From the physiochemical studies it was shown that the best fluidisers of this region of the bilayer were surfactants in the range $C_{12}E_2$-$C_{12}E_4$. Optimum enhancement of OE permeation was obtained using $C_{12}E_3$ as the enhancer. This correlation between the two studies suggests that the surfactants acted by fluidising the bilayer core of the lipid lamellae allowing increased diffusion of OE through the stratum corneum. A similar mechanism of action has been postulated for the enhancers Azone and oleic acid. (54). In a more recent paper Ongpipattanakul *et al* (171) suggested that oleic acid may act by a mechanism related to phase separation. Having permeated into the stratum corneum the more fluid oleyl chains of the oleic acid may exist as separate domains in the lipids providing areas of decreased resistance to permeation. Phase behaviour such as this is well documented for phospholipids (172). It is possible that the dodecyl ether ethoxylates may act as enhancers by a similar mechanism.

$C_{12}E_3$ was also noted as the optimum enhancer amongst the series of surfactants for HC permeation. HC is a relatively polar compound, as discussed in Chapter one the major route for the penetration of polar compounds is probably by partitioning into and diffusing through the aqueous regions between the lipid bilayer headgroups (1.3.1). However, it is unlikely that the aqueous regions would form a

continuous channel through the stratum corneum. The channels are likely to be blocked by lipid membranes as the intercellular lamellae fold around the corneocytes. In order to move from one aqueous region to the next, polar compounds would have to partition across a lipophilic membrane. This partitioning may be the rate limiting step in the diffusion of polar drugs through the stratum corneum. Fluidisation of the membranes would decrease the extent of the barrier allowing increased partitioning of polar compounds across the membrane and therefore increased permeation. $C_{12}E_3$ being amongst the optimum fluidisers of lipid bilayers will have the highest degree of efficacy upon this process and hence be the optimum enhancer for HC as well as OE. These suggestions are comparible to those postulated for the action of Azone on polar drugs (28).

The longer ethoxy chain length surfactants $C_{12}E_4$-$C_{12}E_7$ also demonstrated high levels of permeation enhancement for HC with respect to those seen for OE. The physiochemical studies showed these surfactants affected the upper part of lipid bilayers and the polar headgroups. The long ethoxy chains may disrupt the hydration sphere around the polar headgroup increasing the amount of "free" water. The chains may also help to increase the extent of bilayer hydration (an effect noted in the hydration of extracted porcine skin lipid/surfactant mixtures) swelling the aqueous phase. Both these effects would increase the aqueous volume available for polar drugs to partition into and so increase their rate of permeation through the skin. An increase in aqueous volume would not affect the diffusion of nonpolar drugs, hence the lack of efficacy of the higher HLB surfactants upon OE permeation. These suggested possible modes of action of the surfactants as permeation enhancers for polar and nonpolar durgs are summarised in Figure 7.1.

The duration of effect of the surfactants upon increased penetration was different for the two steroids investigated. For HC there was a marked 'depletion' effect noted with surfactants of ethylene oxide chain length of <4 units. For OE permeation this depletion was only noticible for surfactants smaller than $C_{12}E_2$. In Chapter 6 it was suggested that the differential rate of permeation of the surfactants

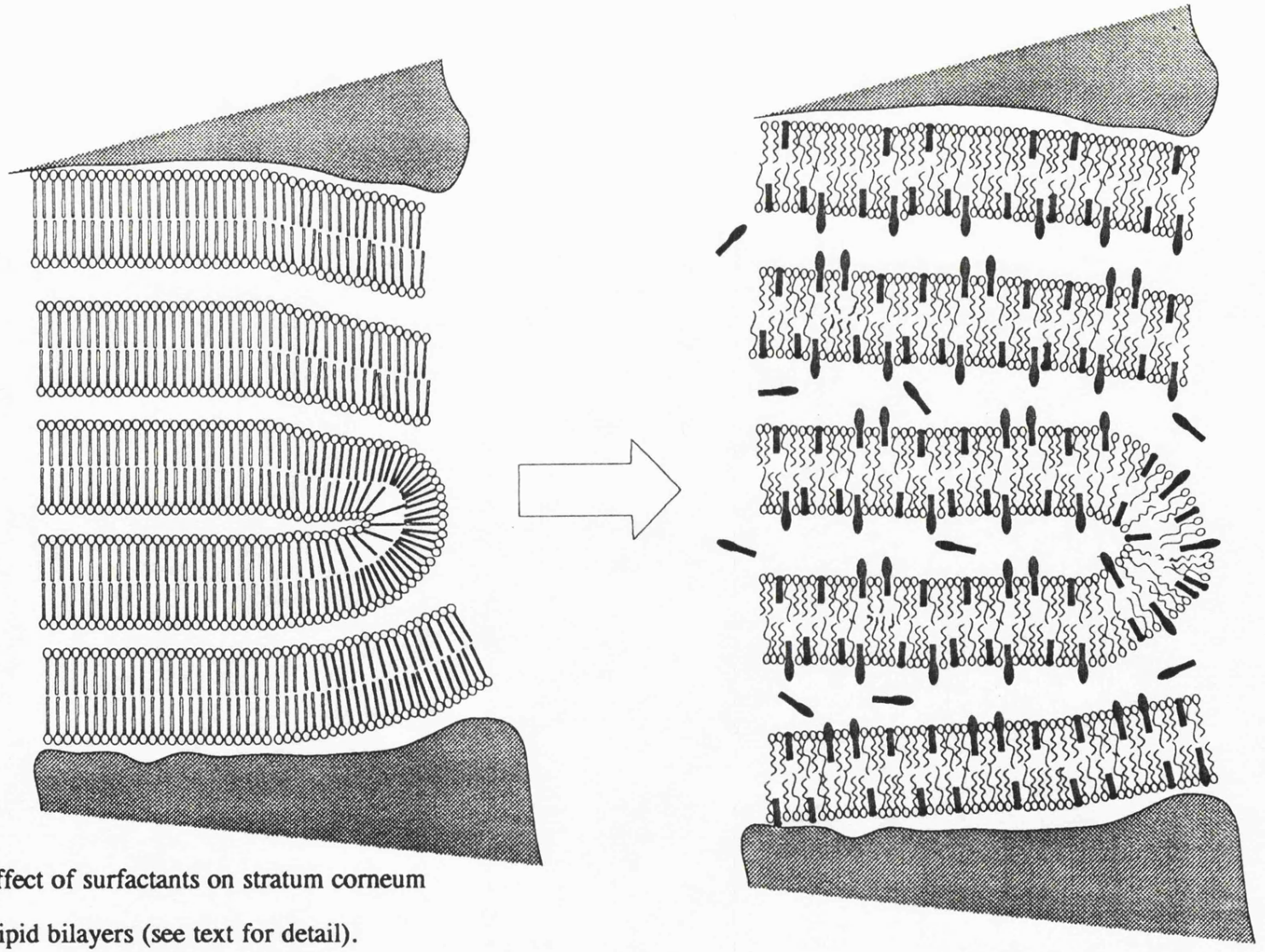

Figure 7.1 Effect of surfactants on stratum corneum lipid bilayers (see text for detail).

was linked to the extent of the depletion and hence tailing of the extent of enhancement. The difference observed between OE and HC enhancement would suggest that the surfactants ($\approx C_{12}E_3$) need to be present in a higher concentration to produce their maximum enhancement for HC than for OE. The increase in fluidisation necessary to allow increased partitioning of polar compounds across a membrane may be greater than that needed to allow the diffusion of a molecule along the membrane. As shown in the DSC, FPS and ESR studies fluidisation was proportional to surfactant concentration.

Surfactants are also known to have effects on the keratin of the stratum corneum (79,125,173). Little attention has been paid to this possible action of the surfactants in this thesis. The involvement of surfactant/protein interaction cannot therefore be ruled out. However, little or no change was observed in the keratin associated transition in the DSC analysis of $C_{12}E_3$ treated stratum corneum whereas the lipid associated peaks were significantly altered. The close relationship observed between permeation enhancement and lipid bilayer fluidisation would suggest that the skin lipids and not the keratin of the corneocytes are the major site of action of the surfactants.

Another effect not fully investigated is the interaction between the surfactant and the deposited steroid on the skin surface. The form of the drug on the skin and the extent to which it is solubilised by the surfactants may play a role in the increased steroid permeation observed.

7.3 The Suitability of Physiochemical Studies as a Screen for Potential Penetration Enhancers

Several indirect methods were used in this study to obtain information about the penetration enhancing activity of surfactants, i.e. not simple permeation experiments. Each method provided different information and entailed different degrees of complexity in their procedure. The suitability of each of these methods

DSC, FPS and ESR to act as quick screens for potential penetration enhancers is discussed below.

Two types of analysis were investigated. Those that used model lipid membranes made of DSPC and those that used isolated stratum corneum. The production and analysis of DSPC/enhancer vesicles for analysis by DSC was the simplest and quickest method investigated. This procedure also did not involve the purchase of expensive probe molecules. The results obtained from the DSC studies were in good agreement with the permeation studies with respect to the structure-activity relationship produced, however, the different efficacy of the compounds with respect to polar and nonpolar permeants was not observed. The methodology of the FPS and ESR studies with liposomes was slightly more complex than that used for DSC. The results obtained here were highly probe dependant, surface probes giving different results to probes of the membrane core. If polar and nonpolar drugs do penetrate the skin via different regions of the extracellular lipid lamellae then the choice of probe used could by varied depending upon the drug being formulated for transdermal delivery. A fluorescent or nitroxide labelled molecule that resembled the drug concerned may be an answer to this, although labelling may alter the physiochemical characteristics of the compound.

The preparation of isolated stratum corneum for DSC and ESR studies is relatively complex and time comsuming, FPS cannot easily be carried out on intact skin samples. DSC of stratum corneum has been shown to provide large amounts of information with respect to the effect of enhancers upon the skin (50). However, in studies with a range of enhancers the extent of the effects observed by DSC does not correlate well to *in-vitro* permeation results (174). The use of ESR spectroscopy upon isolated stratum corneum incorporating a nitroxide probe based upon a drug molecule has good potential for use as a screen for enhancers. The procedure is more complex than DSC but direct information can be obtained concerning the probe (drug) mobility in the skin at physiological temperatures. This technique would be usable for all types of drug if spin analogues could be produced,

however, as stated above the labelling may alter the physiochemical properties of the drug molecule and effect its distribution in the skin.

One further point to consider in this discussion is the availability of equipment for these screens. Most pharmaceutical research and development laboratories either poccesses or have access to DSC, however, few have either a fluorescence polarisation spectrometer or an ESR spectrometer.

7.4 Suggestions for Further Work

During the course of this study several questions have arisen concerning the effect of surfactants upon DSPC liposomes, skin and enhancement of percutaneous absorption. Listed below are some of these points and suggestions for futher investigations and continuation of this work.

In the studies using DSPC liposomes as model membrane systems one of the suggested reasons for the difference in efficacy of the surfactants was the partitioning behavior of the surfactants into the liposomes. This would effect the concentration of surfactant present in the membrane. Alkyl ether ethoxylates are very difficult to assay quantitatively. However, by the use of radiolabelled surfactant molecules it would be possible to easily determine liposome/water partition coefficients and assay the actual concentration of the surfactant in the membrane. It would also be possible to determine stratum corneum/water partition coefficients for the surfactants.

In the discussion to the *in-vitro* permeation studies it was suggested that the shape of the permeation profiles observed with hydrocortisone was due to depletion of surfactant from either the skin surface or the active site in the skin. The measurement of the permeation rates of the surfactants through the skin would determine whether this theory was correct. Again due to the difficulty of analysis of these surfactants these experiments would require radiolabelled molecules. By using ^{14}C labelled surfactant and ^{3}H labelled drug or vice-versa it would also be possible to measure the coflux of these molecules.

The interaction of the surfactant with the drug and the physical state of the drug upon the skin surface was not determined in this study. Measurement of the solubility of the permeants in the surfactant may yield information concerning this question.

It was suggested that the surfactants, especially those with longer ethoxy chains, may increase the extent of hydration of the stratum corneum and in particular the amount of free water present. It may be possible to assess this using two thermal analysis techniques, DSC and thermogravimetric analysis (TGA). In conjunction with this study it may be possible to observe any swelling of the lipid bilayers, due to increased hydration, by small angle X-ray scattering measurements

Further work needs to be undertaken with ESR spectrometery. Determining the mobility of labelled model drug compounds in the stratum corneum *in-situ* may yield information concerning mechanisms of action of penetration enhancers and routes of drug permeation through the skin. By the use of a variety of different probe molecules it may also be possible to determine the site of action of the different members of the surfactant series and other enhancers in the skin.

Finally the use of DSPC liposomes has provided useful information concerning the effects of surfactants in lipid bilayers. However, the acyl chains of the extracellular lipid lamellae in the skin are far longer than the C_{18} chains of DSPC. It may be worth repeating some of the experiments undertaken in this thesis upon either longer acyl chain phospholipid membranes or liposomes produced from extracted skin lipids.

REFERENCES

1. Dressman J.B., Ridout G, and Guy R.H.; Transdermal drug delivery systems. In Comprehensive Medicinal Chemistry Vol 5. Biopharmaceutics. Taylor J.B. (ed) Pergamon Press, Oxford. (1990) pp645-657

2. Shaw J.E. and Chandrasekaran S.K.; Transdermal therapeutic systems. In Drug Absorption. Prescott L.F. and Nimmo W.S. (eds) MTP Press Ltd, Lancaster. (1981) pp 186-193

3. Barry B.W., Dermatological Formulations, Marcell Dekker, New York and Basel. (1983)

4. Wilkes G.L., Brown I.A. and Wildnauer R.H., The Biomechanical Properties of Skin. *CRC Critical Review of Bioengineering* 453-495 (1973)

5. Ryan T.J.; Dermal Vasculature. In Methods in Skin Research, Skerrow, D. and Skerrow, C.J. (eds), Wiley and Sons, London. (1985) pp 527-558

6. Odland G.F. and Reed T.H.; Epidermis. In Ultrastructure of Normal and Abnormal Skin, Zelickson, A. (ed), Lea and Febiger, Philadelphia (1967) pp 54-75

7. Matoltsy A.G. and Parakkal P.F.; Keratinization. In Ultrastructure of Normal and Abnormal Skin, Zelickson, A. (ed), Lea and Febiger, Philadelphia (1967) pp 76-104

8. Christophers E.; Cellular architecture of the stratum corneum. *J. Invest. Dermatol.* **56,** 165-169 (1971)

9. Elias P.M.; Epidermal Lipids, Membranes, and Keratinization. *Int. J. Dermatol.* **20,** 1-19 (1981)

10. Lampe M.A., Williams M.C. and Elias P.M.; Human epidermal lipids: characterization and modulations during differentiation. *J. Lipid Research.* **24,** 131-140 (1983)

11. Lampe M.A., Burlingame A.L., Whitney J.A., Williams M.L., Brown B.E., Roitman E. and Elias P.M.; Human stratum corneum lipids: characterization and regional variations. *J. Lipid Research.* **24,** 120-130 (1983)

12. Bowser P.A. and White R.J.; Isolation, barrier properties and lipid analysis of stratum compactum, a discrete region of the stratum corneum. *Br. J. Dermatol.* **112,** 1-14 (1985)

13. Elias P.M., Goerke J. and Friend D.S.; Mammalian epidermal barrier layer lipids: composition and influence on structure. *J. Invest. Dermatol.* **69,** 535-546 (1977)

14. Wertz P.W. and Downing D.T.; Ceramides of pig epidermis: structure determination. *J. Lipid Research.* **24,** 759-765 (1983)

15. Gray G.M., White R.J., Williams R.H. and Yardley H.J.; Lipid composition of the superficial stratum corneum cells of pig epidermis. *Br. J. Dermatol.* **106,** 59-63 (1982)

16. Swartzendruber D.C., Wertz P.W., Kitko D.J., Madison K.C. and Downing D.T.; Molecular models of the intercellular lipid lamellae in mammalian stratum corneum. *J. Invest. Dermatol.* **92,** 251-257 (1989)

17. Wertz P.W., Swartzendruber D.C. and Downing D.T.; The role of the corneocyte lipid envelope in the struture and function of the barrier layer. In Prediction of Percutaneous Penetration, Scott R.C., Guy R.H. and Hadgraft J. (eds), IBC Technical Services, London, (1990) pp 405-411

18. Scheuplien R.J. and Blank I.H.; Permeability of the skin. *Physiol. Rev.* **51,** 702-747 (1971)

19. Elias P.M. and Friend D.S.; The permeability barrier in mammalian epidermis. *J. Cell Biol.* **65,** 180-191 (1975)

20. Bowser P.A., White R.J. and Nugteren D.H.; Location and nature of the epidermal permeability barrier. *Int. J. Cosmet. Sci.* **8,** 125-134 (1986)

21. Wertz P.W. and Downing D.T.; Glycolipids in mammalian epidermis: structure and function in the water barrier. *Science* **217,** 1261-1262 (1982)

22. Landmann L.; Epidermal permeability barrier: transformation of lamellar granule-disks into intercellular sheets by a membrane-fusion process, a freeze-fracture study. *J. Invest. Dermatol.* **87,** 202-209 (1986)

23. Elias P.M.; Lipids and the epidermal permeability barrier. *Arch. Dermatol. Res.* **270,** 95-117 (1981)

24. Scheuplien R.J.; Mechanism of percutaneous absorption. *J. Invest. Dermatol.* **45,** 334-346 (1965)

25. Elias P.M., Cooper E.R., Korc A. and Brown B.E.; Percutaneous transport in relation to stratum corneum structure and lipid composition. *J. Invest. Dermatol.* **76,** 297-301 (1981)

26. de Haan F.H.N., Boddé H.E., de Bruijn W.C., Ginsel L.A. and Junginger H.E.; Visualizing drug transport across stratum corneum: cryotechniques, vapour fixation, autoradiography. *Int. J. Pharm.* **56,** 75-86 (1989)

27. Boddé H.E., Kruithof M.A.M., Brussee J. and Koerten H.K.; Visualisation of normal and enhanced $HgCl_2$ transport through human skin in vitro. *Int. J. Pharm.* **53,** 13-24 (1989)

28. Boddé H.E., Tiemessen H.L.G.M., Mollee H., de Hann F.H.N. and Junginger H.E.; Modelling percutaneous drug transport in vitro: the interplay between water, flux enhancers and skin lipids. In Prediction of Percutaneous Penetration, Scott R.C., Guy R.H. and Hadgraft J. (eds), IBC Technical Services, London, (1990) pp 93-109

29. Scheuplien R.J.; Properties of the skin as a membrane. *Advances in Biology of the Skin* **12,** 125-152 (1972)

30. Feldmann R.J. and Maibach H.I.; Percutaneous penetration of steriods in man. *J. Invest. Dermatol.* **52,** 89-94 (1969)

31. Feldmann R.J. and Maibach H.I.; Absorption of some organic compounds through the skin in man. *J. Invest. Dermatol.* **54,** 339-404 (1970)

32. Nishiyama T., Iwata Y., Nakajima K. and Mitsui T.; *In-vivo* percutaneous absorption of polyoxyethylene lauryl ether surfactants in hairless mice. *J. Soc. Cosmet. Chem.* **34,** 263-271 (1983)

33. Wester R.C., Noonan P.K. and Maibach H.I.; Percutaneous absorption of hydrocortisone increases with long term administration: in vivo studies in the rhesus monkey. *Arch. Dermatol.* **116,** 186-188 (1980)

34. McKenzie A.W. and Stoughton R.B.; Methods for comparing percutaneous absorption of steriods. *Arch. Dermatol.* **86,** 608-610 (1962)

35. Scheuplien R.J., Blank I.H., Brauner G.J. and MacFarlane D.J.; Percutaneous absorption of steriods. *J. Invest. Dermatol.* **52,** 63-70 (1969)

36. Franz T.J.; Percutaneous absorption. On the relevance of in vitro data. *J. Invest. Dermatol.* **64,** 190-195 (1975)

37. Cooper E.R.; Increased skin permeability for lipophilic molecules. *J. Pharm. Sci.* **73,** 1153-1156 (1984)

38. Scott R.C.; Percutaneous absorption. In vivo: in vitro comparisons. In Pharmacology of the Skin. Vol 1. Shroot B., Schaefer H., Valbone. (eds) S. Karger, Basel, (1987) pp 103-110

39. Bronaugh R.L. and Stewart R.F.; Methods for in vitro percutaneous absorption studies III: hydrophobic compounds. *J. Pharm. Sci.* **73,** 1255-1258 (1984)

40. Jones S.J., Greenway M.J. and Orr N.A.; The influence of receptor fluid on in vitro percutaneous penetration. *Int. J. Pharm.* **53,** 43-46 (1989)

41. Bartek M.J., LaBudde J.A. and Maibach H.I.; Skin permeability in vivo: comparison in rat, rabbit pig and man. *J. Invest. Dermatol.* **58,** 114-123 (1972)

42. Bronaugh R.L., Stewart R.F. and Congdon E.R.; Methods for in vitro percutaneous absorption studies II. Animal models for human skin. *Toxicology and Applied Pharmacology.* **62,** 481-488

43. Marzulli F.N., Brown D.W.C. and Maibach H.I.; Techniques for studying skin penetration. *Toxicology and Applied Pharmacology.* **Suppl. 3,** 76-83 (1969)

44. Wester R.C. and Maibach H.I.; In vivo animal models for percutaneous absorption. In Percutaneous Absorption, Bronaugh R.L. and Maibach H.I. (eds), Marcel Dekker, New York and Basel, (1985) pp 251-266

45. Walker M., Dugard P.H. and Scott R.C.; Absorption through human and laboratory animal skins: in vitro comparisons. *Acta. Suecica. Pharma.* **20,** 52-53 (1983)

46. Scott R.C., Walker M. and Dugard P.H.; In vitro percutaneous absorption experiments: A technique for the production of intact epidermal membranes from rat skin. *J. Soc. Cosmet. Chem. 37,* 35-41 (1986)

47. Bhatti A.S., Scott R.C. and Dyer A.; In vitro percutaneous absorption: Pig epidermal membrane as a model for human skin. *J. Pharm. Pharmacol.* **40 (suppl),** 45p (1988)

48. Gray M.G. and White R.J.; Glycosphingolipids and ceramides in human and pig epidermis. *J. Invest. Dermatol.* **70,** 336-341 (1978)

49. Boustra J.; Personnal Communication.

50. Goodman M. and Barry B.W.; Action of penetration enhancers on human stratum corneum as assessed by differential scanning calorimetery. In Percutaneous Absorption. Vol. II, Bronaugh R. and Maibach H.I.(eds) Marcel Dekker, New York (1987) pp 567-593

51. Golden G.M., McKie J.E. and Potts R.O.; The role of stratum corneum lipid fluidity in transdermal drug flux. *J Pharm. Sci.* **76,** 25-28 (1987)

52. Knutson K., Potts R.O., Guzak D.B. Golden G.M., McKie J.E., Lambert W.J. and Higuchi W.I.; Macro- and molecular physical chemical considerations in understanding drug transport in the stratum corneum. In Advances in drug delivery systems, Anderson J.W. and Kim S.W. (eds) Elsevier Scientific, New York (1986) pp 67-87

53. Guy R.H., Mak V.H.W., Bommannan D. and Potts R.O.; Percutaneous penetration enhancers: mode of action. In Prediction of Percutaneous Penetration, Scott R.C., Guy R.H. and Hadgraft J. (eds), IBC Technical Services, London, (1990) pp 213-223

54. Barry B.W.; Mode of action of penetration enhancers in human skin. *J. Controlled Rel.* **6,** 85-97 (1987)

55. Feldmann R.J. and Maibach H.I.; Penetration of ^{14}C-hydrocortisone through normal skin: the effect of stripping and occlusion. *Arch. Dermatol.* **91,** 661-666 (1965)

56. Behl C.R., Flynn G.L., Kurihara T., Harper N., Smith W., Higuchi W.I., Ho N.F.H. and Pierson H.L.; Hydration and percutaneous absorption I. Influence of hydration on alkanol permeation through hairless mouse skin. *J. Invest. Dermatol.* **75,** 346-352 (1980)

57. Scheuplein R.J. and Ross L.; Effects of surfactants and solvents on the permeability of the epidermis. *J. Soc. Cosmet. Chem.* **21,** 853-873 (1970)

58. Barry B.W. and Bennett S.L.; Effect of penetration enhancers on the permeation of mannitol, hydrocortisone and progesterone through human skin. *J. Pharm. Pharmacol.* **39,** 533-546 (1987)

59. Goodman M. and Barry B.W.; Lipid-protien-partitioning (LPP) theory of skin enhancer activity: finite dose technique. *Int. J. Pharm.* **57,** 29-40 (1989)

60. Walters K.A.; Penetration enhancers and their use in transdermal therapeutic systems. In Transdermal Drug Delivery, Guy R.H. and Hadgraft J. (eds) Marcel Dekker, New York and Basel, (1989) pp 197-246

61. Van der Valk P.G.M., Nater J.P. and Bleumink E.; Skin irritancy of surfactants as assessed by water vapour loss measurements. *J. Invest. Dermatol.* **82,** 291-293 (1984)

62. Black J.G. and Howes D.; Skin penetration of chemically related detergents. *J. Soc. Cosmet. Chem.* **30,** 157-165 (1979)

63. Florence A.T., Tucker I.G. and Walters K.A.; Interactions of nonionic alkyl and aryl ethers with membranes and other biological systems. In Structure/performance relationships in surfactants (ACS symposium series, vol.253). Rosen M J (ed). American Chemical Society, Washington, D C (1984), pp 189-207.

64. Shahi V. and Zatz J.L.; Effect of formulation factors on penetration of hydrocortisone through mouse skin. *J. Pharm. Sci.* **67,** 789-792 (1978)

65. Sarpotdar P.P. and Zatz J.L.; Percutaneous absorption; enhancement by nonionic surfactants. *Drug Dev. Ind. Pharm.* **12,** 1625-1647 (1986)

66. Sarpotdar P.P. and Zatz J.L.; Evaluation of penetration enhancement of lidocaine by nonionic surfactants through hairless mouse skin in-vitro. *J. Pharm. Sci.* **75,** 176-181 (1986)

67. Shen W-W., Danti A.G. and Bruscato F.N.; Effect of nonionic surfactants on percutaneous absorption of salicylic acid and sodium salicylate in the presence of dimethyl sulphoxide. *J. Pharm. Sci.* **65,** 1780-1783 (1976)

68. Hwang C-C. and Danti A.G.; Percutaneous absorption of flufenamic acid in rabbits: effect of dimethyl sulphoxide and various nonionic surfactants. *J. Pharm. Sci.* **72,** 857-860 (1983)

69. Aguiar A.J. and Weiner M.A.; Percutaneous absorption studies of chloramphenicol solutions. *J. Pharm. Sci.* **58,** 210-215 (1969)

70. Mezei M. and Ryan K.J.; Effect of surfactants on epidermal permeability in rabbits. *J. Pharm. Sci.* **61,** 1329-1331 (1972)

71. Aungst B.J., Rogers N.J. and Shefter E.; Enhancement of naloxone penetration through human skin in-vitro using fatty acids, fatty alcohols, surfactants, sulfoxides and amides. *Int. J. Pharm.* **33,** 225-234 (1986)

72. Chowhan Z.T. and Pritchard R.; Effect of surfactants on percutaneous absorption of naproxen I. Comparisons of rabbit, rat and human excised skin. *J. Pharm. Sci.* **67,** 1272-1274 (1978)

73. Helenius A. and Simons K.; Solubilisation of membranes by detergents. *Biochim. Biophys. Acta.* **415,** 29-79 (1975)

74. Walters K.A., Walker M. and Olejink O.; Nonionic surfactant effects on skin permeability characteristics. *J. Pharm. Pharmacol.* **40,** 525-529 (1988)

75. Dalvi U.G. and Zatz J.L.; Effect of nonionic surfactants on penetration of dissolved benzocaine through hairless mouse skin. *J. Soc. Cosmet. Chem.* **32,** 87-94 (1981)

76. Eagle S.C., Barry B.W. and Scott R.C.; Inhibition of the damaging activity of divalent anionic surfactants on human skin. In Prediction of Percutaneous Penetration, Scott R.C., Guy R.H. and Hadgraft J. (eds), IBC Technical Services, London, (1990) pp 417-425

77. Walters K.A. and Olejink O.; Effects of nonionic surfactants on the hairless mouse skin penetration of methyl nicotinate. *J. Pharm. Pharmacol.* **35 (suppl),** 81P (1983)

78. Ashton P., Hadgraft J., Brain K.R., Millar A. and Walters K.A.; Surfactant effects in topical drug availability. *Int. J. Pharm.* **41,** 189-195 (1988)

79. Ashton P.; Surfactant effects in percutaneous absorption. PhD Thesis, Univ. of Wales (1988)

80. Tiemessen H.L.G.M.; Nonionic surfactant systems for transdermal drug delivery. PhD Thesis, Leiden (1989)

81. Kadir R., Stemper D., Liron Z. and Cohen S.; Penetration of theophylline and adenosine into excised human skin from binary and tertiary vehicles: effect of a nonionic surfactant. *J. Pharm. Sci.* **78,** 149-153 (1989)

82. Mahjour M., Mauser B.E. and Fawzi M.B.; Skin permeation enhancement effects of linoleic acid and Azone on narcotic analgesics. *Int. J. Pharm.* **56,** 1-11 (1989)

83. Sugibayasi K., Hosaya K-I., Morimoto Y. and Higuchi W.I.; Effect of the absorption enhancer Azone on the transport of 5-fluorouracil across hairless rat skin. *J. Pharm. Pharmacol. 37,* 578-588 (1985)

84. Touitou E.; Transdermal delivery of anxioltics: in vitro skin permeation of midazolam malate and diazepam. *Int. J. Pharm. 33,* 37-43 (1986)

85. Baillie A.J., Assadi-A. and Florence A.T.; Influence of nonionic surfactant structure on motility inhibition of *Tetrahymena elliotti* as a model for surfactant-membrane interactions. *Int. J. Pharm.* **53,** 241-248 (1989)

86. Gadd A.L. and Curtis-Prior P.B.; A modified transmembrane migration method for evaluating spermicidal potency of some nonoxynol compounds. *J. Pharm. Pharmacol.* **40,** 215-216 (1988)

87. Levin R.J.; Structure/activity relationships of a homologous series of surfactants (nonylphenoxypolyethoxyethanols) on the rat vaginal bioelectric activity over the oetrous cycle. *Pharmacol. and Toxicol.* **62,** 131-134 (1988)

88. Clark W.M. and Lubs H.A.; The colorimetric determination of hydrogen ion concentration and its applications in bacteriology. *J. Bacteriol.* **2,** 1-34 (1917)

89. McDonald C. and Robinson B.;The quantitative analysis of alkyl polyoxyethylene glycol monoethers with mass spectrometrey and proton magnetic resonance spectroscopy in combination. *J. Pharm. Pharmacol.* **22,** 727-728 (1970)

90. Flanagan P.W., Greff R.A. and Smith H.F.; Applications of high resolution nuclear magnetic resonance spectrometery to the identification and quantitative analysis of nonionic surfactants. *Analytical Chemistry.* **35,** 1283-1285 (1963)

91. Crutchfield M.M., Irani R.R. and Yoder J.T.; Quantitative applications of high-resolution proton magnetic resonance measurements in the characterization of detergent chemicals. *J. American Oil Chem. Soc.* **41,** 129-132 (1964)

92. McKenzie R.C.; Differential thermal analysis and differential scanning calorimetery. Similarities and differences. *Anal. Proc.* **17,** 217-220 (1980)

93. Brown M.E.;Introduction to thermal analysis. Chapman and Hall, New York. (1988)

94. Marbery S. and Sturtevant J.M.; High-sensitivity differential scanning calorimetery in the study of biomembranes and related systems. In Methods in Membrane Biology, vol.9, Korn E.D. (ed) Plenum Press, New York and London. (1978) pp237-274

95. McElhaney R.N.; The use of differential scanning calorimetery and differential thermal analysis in studies of model and biological membranes. *Chem. Phys. Lipids.* **30,** 229-259 (1982)

96. Hinz H-J. and Sturtevant J. M.; Caliometeric studies of dilute aqueous suspensions of bilayers formed from synthetic L-α-lecithins. *J. Biol. Chem.* **247,** 6071-6075 (1972)

97. Chapman D.; Phase transitions and fluidity characteristics of lipids and cell membranes. *Quart. Rev. Biophys.* **8,** 185-235 (1975)

98. Chapman D., Williams R.M. and Ladbrooke B.D.; Physical studies of phospholipids VI. Thermotropic mesomorphism of some 1,2 diacyl-phosphatidylcholines (lecithins). *Chem. Phys. Lipids.* **1,** 445-475 (1967)

99. Chapman D., Urbina J. and Keough K.M.W.; Biomembrane phase transitions. Studies of lipid-water mixtures using differential scanning calorimetery. *J. Biol. Chem.***249,** 2512-2521 (1974)

100. Marbery S. and Sturtevant J.M.; Investigation of phase transitions of lipids and lipid mixtures by high sensitivity differential scanning calorimetery. *Prot. Natl. Acad. Sci.* **73,** 3862-3866 (1976)

101. Phillips M.C., Ladbrooke B.D. and Chapman D.; Molecular interactions in mixed lecithin systems. *Biochim. Biophys. Acta.* **196,** 35-44 (1970)

102. Keough K.M.W. and Davies P.J.; Gel-liquid crystalline phase transitions in water dispersions of saturated mixed acid phosphatidylcholines. *Biochemistry.* **18,** 1453-1459 (1979)

103. Jain M.J. and Wu N.M.; Effect of small molecules on the dipalmitoyl lecithin liposomal bilayer III. Phase transition in lipid bilayer. *J. Membrane Biol.* **34,**157-201 (1977)

104. Ladbrooke B.D. and Chapman D.; Thermal analysis of lipids, protiens and biological membranes. A review and summary of some recent studies. *Chem. Phys. Lipids.* **3,** 304-356 (1969)

105. Van Duzee B.F.; Thermal analysis of human stratum corneum. *J. Invst. Dermatol.* **65,** 404-408 (1975)

106. Golden G.M., Guzek D.B., Harris R.R., McKie J.E. and Potts R.O.; Lipid thermotropic transitions in human stratum corneum. *J. Invest. Dermatol.* **86,** 255-259 (1986)

107. Goodman M. and Barry B.W., Differential scanning calorimetery of human stratum corneum: effect of penetration enhancers Azone and dimethyl sulphoxide. *Anal. Proc.* **23,** 397-398 (1986)

108. Swartzendruber D.C., Wertz P.W., Madison K.C. and Downing D.T.; Evidence that the corneocyte has a chemically bound lipid envelope. *J. Invest. Dermatol.* **88,** 709-713 (1987)

109. Rehfield S.J. and Elias P.M.;, Mammalian stratum corneum contains physiologic lipid thermal transitions. *J. Invest. Dermatol.* **79,** 1-3 (1982)

110. Golden G.M., Guzek D.B., Kennedy A.H., McKie J.E. and Potts R.O.; Stratum corneum lipid phase transitions and water barrier properties. *Biochemistry.* **26,** 2382-2388 (1987)

111. Boustra J.A., Peschier L.J.C., Brusse J. and Boddé H.E.; Effect of N-alkyl-azocycloheptan-2-ones including Azone on the thermal behaviour of stratum corneum. *Int. J. Pharm.* **52,** 47-54 (1989)

112. Bangham A.D.; Diffusion of univalent ions across the lamellae of swollen phospholipids. *J. Mol. Biol.* **13,** 238-252 (1965)

113. Klingman A.M. and Christophers E.; Preparation of isolated sheets of human stratum corneum. *Arch. Dermatol.* **88,** 70-73 (1963)

114. CRC Handbook of Chemistry and Physics, 60th Edition, Weast R.C. (ed) CRC Press, Florida. (1980)

115. Bligh E.G. and Dyer W.J.; A rapid method of total lipid extraction and purification. *Canad. J. Biochem. Physiol. 37,* 911-917 (1959)

116. Carter B.R., Chapman D., Hawes S.M. ans Saville J.; Lipid phase transitions and drug interactions. *Biochim. Biophys. Acta.* **363,** 54-69 (1974)

117. Alonso A. and Goni F.M.; Effect of Detergents and Fusogenic lipids on phospholipid phase transitions. *J. Membrane. Biol.* **71,** 183-187 (1983)

118. Elaisz A.W., Chapman D. and Ewing D.F.;*Biochim. Biophys. Acta.* **448,** 220-230 (1976)

119. Small D.M.; Lateral chain packing in lipids and membranes. *J. Lipid Res.* **25,** 1490-1500 (1984)

120. Dennis E.A.; Formation and characterisation of mixed micelles of the nonionic surfactant Triton X-100 with egg, dipalmitoyl and dimyristoyl phosphatidylcholine. *Arch. Biochem. Biophys.* **165,** 764-773 (1974)

121. Lichtenberg D., Robson R.J. and Dennis E.A.; Solubilization of phospholipids by detergents. Structural and kinetic aspects. *Biochim. Biophys. Acta.* **737,** 285-304 (1983)

122. Zaslavsky B.Y., Ossipov N.N., Krivich V.S., Baholdina L.P. and Rogozhin S.V.; Action of surface-active agents on biological membranes II. Hemolytic activity of nonionic surfactants. *Biochim. Biophys. Acta.* **507,** 1-7 (1978)

123. Walters K.A., Dughard P.H. and Florence A.T.; Nonionic surfactants and gastric mucosal transport of paraquat. *J. Pharm. Pharmacol.* **33,** 207-213 (1981)

124. Schott H.; Effect of chain length in homologous series of anionic surfactants on irritant action and toxicity. *J. Pharm. Sci.* **62,** 341-343 (1973)

125. Dominguez J.G., Parra J.L., Infante M.R., Peljero C.M., Balaguer F. and Sastre T.; A new approach to the theory of adsorption and permeability of surfactants on keratinic proteins: the specific behaviour of certain hydrophobic chains. *J. Soc. Cosmet. Chem.* **28,** 165-182 (1977)

126. Stoughton R.B.; Enhanced percutaneous penetration with 1-dodecyl-azacycloheptan-2-one. *Arch. Dermatol.* **118,** 474-477 (1982)

127. Beastall J.C., Hadgraft J. and Washington C.; Mechanism of action of Azone as a penetration enhancer: lipid bilayer fluidity and transition temperature effects. *Int. J. Pharm.* **43,** 207-213 (1988)

128. Wertz P.W., Abraham W., Landmann L and Downing D.T.; Preparation of liposomes from stratum corneum lipids. *J. Invest. Dermatol.* **87,** 582-584 (1986)

129. White R.J.; PhD Thesis CNAA, London (1985)

130. Lakowicz J.R.; Principles of fluorescence spectroscopy. Pelum Press, New York and London. (1983)

131. Weber G.; Rotational brownian motion and polarization of the fluorescence of solutions. *Advances in Protein Chem.* **8,** 415-459 (1953)

132. Chen R.F. and Bowman R.L.; Fluorescence polarisation; measurement with ultraviolet polarising filters in a spectrofluorimeter. *Science.* **147,** 729-732 (1965)

133. Azumi T. and McGlynn S.P.; Polarisation of the luminescence of phenanthrene. *J. Chem Phys.* **37,** 2413-2420 (1962)

134. Shinitzky M., Dianoux A.C., Gitler C. and Weber G.; Microviscosity and order in the hydrocarbon region of micelles and membranes determined with fluorescence probes I. Synthetic membranes. *Biochemistry.* **10,** 2106-2113 (1971)

135. Cogan U., Shinitzky M., Weber G. and Nishida T.; Microviscosity and order in the hydrocarbon region of phospholipid and phospholipid-cholesterol dispersions determined with fluorescencent probes. *Biochemistry.* **12,** 521-528 (1973)

136. Lentz B. R., Barenholz Y. and Tompson T. E.; Fluorescence depolarisation studies of phase transitions and fluidity in phospholipid bilayers. 1. Single component phosphatidylcholine liposomes. *Biochemistry.* **15,** 4521-4537 (1976)

137. Vanderkooi J.M. and Chance B.; Temperature sensitivity of fluorescent probes in the presence of model membranes and mitrochondria. *FEBS Letts.* **33,** 23-26 (1972)

138. Rudy B. and Gitler C.; Microviscosity of the cell membrane. *Biochim. Biophys. Acta.* **228,** 131-136 (1972)

139. Klein R.A.; Thermodynamics and membrane processes. *Quart. Rev. Biophys.* **15,** 667-757 (1982)

140. Lentz B. R., Moore B. M. and Barrow D. A.; Light scattering effects in the measurement of membrane microviscosity with diphenylhexatriene. *Biophysical Journal.* **25,** 489-494 (1979)

141. Sklar L. A., Hudson B. S. and Simoni R. D.; Conjugated polyene fatty acids as fluorescent probes: synthetic phospholipid membrane studies. *Biochemistry.* **16,** 819-828 (1977)

142. Sklar L. A., Miljanich G. P. and Dratz E. A.; Phospholipid lateral phase separation and the partition of cis-parinaric and trans-parinaric acid amongst aqueous, solid lipid and fluid lipid phases. *Biochemistry.* **18,** 1707-1716 (1979)

143. Rujanavech C., Henderson P. A. and Silvert D. F.; Influence of sterol structure on phospholipid phase behavior as detected by parinaric acid fluorescence spectroscopy. *J. Biol. Chem.* **261,** 7204-7214 (1986)

144. Andersen H.C.; Probes of membrane structure. *Ann. Rev. Biochem.* **47,** 359-383 (1978)

145. Jacobson K. and Wobschall D.; Rotation of fluorescent probes localised within lipid bilayer membranes. *Chem. Phys. Lipids.* **12,** 117-131 (1974)

146. Azzi A.; The application of fluorescent probes in membrane studies. *Quart. Rev. Biophysics.* **8,** 237-316 (1975)

147. Haynes D.H. and Staerk H.J.; 1-Anilino-8-naphthalene sulphonate; a fluorescent probe of membrane surface structure, composition and mobility. *J. Membrane Biol.* **17,** 313-319 (1974)

148. Lesslauer W., Cain J. and Blasic J.K.; On the localisation of 1-anilino-8-naphthalene sulphonate in lipid model systems. An X-ray diffraction study. *Biochim. Biophys. Acta.* **241,** 547-566 (1971)

149. Mc Connell H.M. and McFarland B.G.; The flexibility gradient in biological membranes. *Ann. NY Acad. Sci.* **195,** 207-217 (1978)

150. Shinitzky M. and Barenholz Y.; Dynamics in the hydrocarbon layer in liposomes of lecithin and sphingomyelin containing dicetylphosphate. *J. Biol. Chem.* **249,** 2652-2657 (1974)

151. Florine-Casteel K. and Feigenson G.W.; On the use of partition coefficients to characterise the distribution of fluorescent membrane probes between coexisting gel and fluid lipid phases; an analysis of the partition behavior of 1,6-diphenyl-1,3,5-hexatriene. *Biochim. Biophys. Acta.* **941,** 102-106 (1988)

152. Atkins P.W.; Determination of molecular structure; resonance techniques. In Physical Chemistry 3rd edition, W H Freeman and company, New York (1986) pp 496-500.

153. Devaux P.F. and Davoust J.; Physical aspects of the spin labelling technique. In ESR and NMR of paramagnetic species in biological and related systems. Bertini I. and Drago R.S. (eds). D. Ridel Publishing Company, Dordrecht, Holland. (1979) pp381-397

154. Schreier-Muccillo S., Marsh D., Dugas H., Schneider H. and Smith I.C.P.; A spin probe study of the influence of cholesterol on motion and orientation of phospholipids in multibilayers and vesicles. *Chem. Phys. Lipids.* **10,** 11-27 (1973)

155. Hubbell W.L. and McConnell H.M.; Molecular motion in spin labelled phospholipids and membranes. *J. Am. Chem. Soc.* **93,** 314-326 (1971)

156. Jost P., Libertini L.J., Herbert V.C. and Griffith O.H.; Lipid spin labels in lecithin multibilayers. A study of motion along fatty acid chains. *J. Mol. Biol.* **59,** 77-98 (1971)

157. Marsh D., Watts A. and Knowles P.F.; Cooperativity of the phase transition in single and multibilayer lipid vesicles. *Biochim. Biophys. Acta.* **465,** 500-514 (1977)

158. Sanson A., Ptak M., Rigaud J.L. and Gary-Bobo C.M.; An ESR study of the anchoring of spin labelled stearic acid in lecithin multibilayers. *Chem. Phys. Lipids.* **17,** 435-444 (1976)

159. Seelig J.; Spin label studies of oriented smectic liquid crystals (A model system for bilayer membranes). *J. Amer. Chem. Soc.* **92,** 3881-3887 (1970)

160. Hubbell W.L. and McConnell H.M.; Orientation and motion of amphiphilic spin labels in membranes. *Proc. Natl. Acad. Sci.* **64,** 21-27 (1969)

161. Oldfield E. and Chapman D.; Effects of cholesterol and cholesterol derivatives on hydrocarbon chain mobility in lipids. *Biochem. Biophys. Res. Comm.* **43,** 610-616 (1971)

162. Schreier S., Polnaszek C.F. and Smith I.C.P.; Spin labels in membranes. Problems in practice. *Biochim. Biophys. Acta.* **515,** 346-375 (1978)

163. Gay C.L., Murphy T.M., Hadgraft J., Kellaway I.W., Evans J.C. and Rowlands C.C.; An electron spin resonance study of skin penetration enhancers. *Int. J. Pharm.* **49,** 39-45 (1989)

164. Pates R.D., Watts A. and Marsh D.; Lipid-protein interactions in frog rod outer segment disc membranes. Characterisation by spin labels. *Biochim. Biophys. Acta.* **814,** 389-397 (1985)

165. Marsh D.; Molecular motion in phospholipid bilayers in the gel phase; long axis rotation. *Biochemistry.* **19,** 1632-1637 (1980)

166. Gay C.L., Hadgraft J., Kellaway I.W., Evans J.C. and Rowlands C.C.; The effect of skin penetration enhancers on human stratum corneum lipids: an electron spin resonance study. In Prediction of Percutaneous Penetration, Scott R.C., Guy R.H. and Hadgraft J. (eds), IBC Technical Services, London, (1990) pp 322-332

167. Vickers C.H.F.; Existence of resevior in the stratum corneum. Experimental proof. *Arch. Dermatol.* **88,** 20-23 (1963)

168. Bond J.R. and Barry B.W.;Damaging effect of acetone on the permeability barrier of hairless mouse skin compared with that of human skin. *Int. J. Pharm.* **41,** 91-93 (1988)

169. Mollgaard B. and Hoelgaard A.;. Permeation of estradiol through the skin-effect of vehicles. *Int. J. Pharm.* **15,** 185-197 (1983)

170. Ponec M. and Polano M.K.; Penetration of various corticosteroids through epidermis in vitro. *Arch. Dermatol. Res.* **265,** 101-104 (1979)

171. Ongpipattankul B., Burnette R.R., Potts R.O. and Francoeur M.L.; Evidence that oleic acid exists in a separate phase within stratum corneum lipids. *Pharm. Res.* **8,** 350-354 (1991)

172. Shimshick E.J., Kleeman W., Hubbell W.L. and McConnell H.M.; Lateral phase separations in membranes. *J. Supramol. Struct.* **23,** 285-295 (1973)

173. Breuer M.M.; The interactions between surfactants and keratinous tissues. *J. Soc. Cosmet. Chem.* **30,** 41-64 (1979)

174. Williams A.C. Personnal Communication